UNIVERSITY OF SOUTHAMPTON

FACULTY OF ENGINEERING, SCIENCE AND MATHEMATICS

SCHOOL OF ELECTRONICS AND COMPUTER SCIENCE

Iterative Downlink Multi-User MIMO Systems

by

Chun-Yi Wei

A thesis submitted in partial fulfilment of the requirements for the award of Doctor of Philosophy at the University of Southampton

May 2008

SUPERVISOR:

Professor Lajos Hanzo

University of Southampton

Southampton SO17 1BJ

United Kingdom

© Chun-Yi Wei 2008

Dedicated to my parents

UNIVERSITY OF SOUTHAMPTON

ABSTRACT

Faculty of Engineering, Science and Mathematics

School of Electronics and Computer Science

Doctor of Philosophy

Iterative Downlink Multi-User MIMO Systems

by Chun-Yi Wei

In this treatise, we explore diverse multi-user transmission techniques and joint detection-decoding schemes designed for downlink multi-user transmissions, while maintaining a low complexity, a high throughput and a high integrity.

More specifically, in Chapter 2 we will introduce various Multi-User Transmission (MUT) techniques for the Space Division Multiple Access Down-Link (DL-SDMA) employing the sophisticated linear Spatio-Temporal Pre-processing (STP) schemes, which are capable of eliminating the multi-user interference at the Base Station (BS) and increase the transmission integrity at the Mobile Stations (MS). Additionally, we will design signal detection techniques for the DL-SDMA system, which achieves a near-Maximum Likelihood (ML) performance at a fraction of the ML detector's complexity.

In Chapter 3 we extend our research to a joint iterative detection and decoding based DL-SDMA system. We will first introduce the iterative detection aided DL-SDMA system, which is capable of operating in the so-called rank-deficient scenario, where the number of transmit antennas is higher than the number of receive antennas and hence the system-matrix becomes non-invertible. Furthermore we will introduce a precoder aided iterative DL-SDMA system, which is designed with the aid of Extrinsic Information Transfer (EXIT) charts and has an improved iterative decoding gain. Finally, we will characterize the impact of imperfect Channel State Information (CSI) on the proposed iterative DL-SDMA and introduce sophisticated IrRegular Convolutional Codes (IRCC) for improving the integrity of the iterative DL-SDMA system.

In order to reduce the complexity of the iterative receivers, in Chapter 4 we will introduce a novel detection algorithm, which is referred to as the Irregular Generic Detection (IrGD) algorithm. The IrGD has a tunable complexity and it was particularly designed for reducing the complexity of the iterative decoding aided system. Furthermore, we will demonstrate the impact of imperfect CSI with the aid of EXIT charts. In addition, we will introduce an EXIT-Chart Optimized CSI Quantizer (ECO-CQ) for the iterative DL-SDMA system, which is capable of reducing CSI-related feedback overhead.

In Chapter 5 we will introduce an advanced space-time signaling technique aided MUT designed for the DL-SDMA system, which results in an improved capacity. Furthermore, we will propose a low-complexity Irregular Sphere Detection (IrSD) scheme designed for approaching the capacity DL-SDMA systems, which is capable of maintaining a near-ML performance. Additionally, we will characterize our pilot assisted channel prediction aided DL-SDMA system using limited CSI feedback.

Declaration of Authorship

I, **Chun-Yi Wei**, declare that the thesis entitled **Iterative Downlink Multi-User MIMO Systems** and the work presented in the thesis are both my own, and have been generated by me as the result of my own original research. I confirm that:

- this work was done wholly or mainly while in candidature for a research degree at this University;
- where any part of this thesis has previously been submitted for a degree or any other qualification at this University or any other institution, this has been clearly stated;
- where I have consulted the published work of others, this is always clearly attributed;
- where I have quoted from the work of others, the source is always given. With the exception of such quotations, this thesis is entirely my own work;
- I have acknowledged all main sources of help;
- where the thesis is based on work done by myself jointly with others, I have made clear exactly what was done by others and what I have contributed myself;
- parts of this work have been published.

Signed : Chun-Yi Wei

Date : 30 May 2008

Acknowledgement

I would like to take this opportunity to express my deep gratitude to Professor Lajos Hanzo, whose exceptional supervision and support enabled this work. His generous investment of time and energy as well as perpetual enthusiasm deserve my uttermost acknowledgement.

I would like also to thank staff members and colleagues in the Communications Research Group, namely Prof. Sheng Chen, Dr. Lie Liang Yang, Dr. Soon X Ng, Dr. Yosef Akhtman, Dr. Andreas Wolfgang, Dr. Rob Maunder, and many others, too numerous to mention here.

Finally, my personal thanks are my dear parents, who have supported me all these years unconditionally. My special thanks go to my adorable girlfriend Vega, who has been painting the colourful pictures in my life ever since we met.

List of Publications

Journal articles:

1. C.-Y. Wei, L. Wang and L. Hanzo, "Irregular Sphere Detection in Full-diversity and High-rate Downlink SDMA systems, in *IEEE Transactions on Vehicular Technology*, submitted in March 2008.

2. C.-Y. Wei, J. Akhtman, S. X. Ng and L. Hanzo, "Iterative Near-Maximum-Likelihood Detection in Rank-Deficient Downlink SDMA Systems," in *IEEE Transactions on Vehicular Technology*, vol. 57, pp. 653 - 657, January 2008.

Conference papers:

1. C.-Y. Wei, L. Wang and L. Hanzo, "Irregular Sphere Detection Aided Downlink SDMA Systems Using Linear Dispersion Codes, in *Proceedings of the 2008 IEEE Global Telecommunications Conference*, submitted in March 2008.

2. C.-Y. Wei, D. Yang, L.L. Yang and L. Hanzo, "Iterative Detection Aided Downlink SDMA Systems Using Quantized Channel Impulse Response, in *Proceedings of the 2008 IEEE 68th Vehicular Technology Conference, VTC 2008-Fall*, Calgary, Canada, submitted in February 2008.

3. C.-Y. Wei and L. Hanzo, "Irregular Generic Detection Aided Iterative Downlink SDMA Systems, in *Proceedings of the 2008 IEEE 67th Vehicular Technology Conference, VTC 2008-Spring*, Marina Bay, Singapore, 2008, in press.

4. C.-Y. Wei, J. Wang, and L. Hanzo, "EXIT Chart Aided Irregular Convolutional Code Design for Iterative Downlink SDMA Systems Using Imperfect Channel State Information," in *Proceedings of the 2007 IEEE Workshop on Signal Processing Systems*, Shanghai, China, pp. 105 - 110, October 2007.

5. C.-Y. Wei, T. Nguyen, N. Wu, J. Akhtman, L.-L. Yang, and L. Hanzo, "Luby Transform Coding Aided Iterative Detection for Downlink SDMA Systems," in *Proceedings of the 2007 IEEE Workshop on Signal Processing Systems*, Shanghai, China, pp. 397 - 402, October 2007.

6. J. Akhtman, C.-Y. Wei, and L. Hanzo, "Reduced-Complexity Maximum-Likelihood Detection in Downlink SDMA systems," in *Proceedings of the 2006 IEEE 64th Vehicular Technology Conference, VTC 2006-Fall*, pp. 1834-1836, Montréal, Canada, September 2006.

Contents

List of Symbols

A^{T}	Matrix/vector transpose
A^{H}	Matrix/vector hermitian adjoint, *i.e.* complex conjugate transpose
A^{*}	Matrix/vector/scalar complex conjugate
A^{-1}	Matrix inverse
$\mathtt{tr}\,(A)$	Trace of matrix, *i.e.* the sum of its diagonal elements
$\mathtt{E}\{\cdot\}$	Expectation of a random variable
$\|\cdot\|^2$	Second order norm
$\mathbb{H}\{\cdot\}$	The entropy of a random variable
$\mathbb{I}\{\cdot\}$	The mutual information of a random variable
$\mathfrak{C}$	The achievable capacity of the system
$\mathtt{P}\,(\cdot)$	Probability density function
$p\,(\cdot)$	Probability of a random variable
N_0	Gaussian noise variance
M	Number of transmit antennas
N	Number of receive antennas
K	Number of users
L_k	Number of independent data streams transmitted to the k-th user
N_k	Number of receive antennas for the k-th user
$\boldsymbol{H}^{(k)}$	The channel matrix of the k-th user
$\boldsymbol{T}^{(k)}$	The Spatio-Temporal Pre-processing (STP) matrix for the k-th user
$\mathbf{s}^{(k)}$	The transmitted signal of the k-th user
$\boldsymbol{r}^{(k)}$	The received signal of the k-th user

$\mathcal{L}$	Log Likelihood Ratio (LLR) value
$\mathcal{M}$	Set of M-PSK/M-QAM constellation phasors
$\mathcal{M}_c$	$\mathcal{M}_c$ denotes the set of $\mathcal{M}$ complex-valued constellation points of the modulation scheme employed
I	Number of iterations
$\check{\mathbf{s}}$	The candidate of the signal vector
$\hat{\mathbf{s}}$	The estimated signal vector
$\mathbf{s}$	The supervector of transmit signal
$\mathbf{H}$	The hyper channel matrix
$\mathbf{T}$	The Spatio-Temporal Pre-processing (STP) hyper-matrix
$\mathbf{r}$	The received signal's hyper-vector
L_s	The normalized system load
$\sigma^2_{ST-CIRR}$	The estimation error variance of the Spatio-Temporal Channel Impulse Response at the Receivers (ST-CIRR)
$\sigma^2_{ST-CIRT}$	The prediction error variance of the Spatio-Temporal Channel Impulse Response at the Transmitters (ST-CIRT)
$\mathcal{L}^{Dec}_{apr}$	The *a priori* LLRs produced by the channel decoders
$\mathcal{L}^{Dec}_{apt}$	The *a posteriori*LLRs produced by the channel decoders
$\mathcal{L}^{Dec}_{ex}$	The extrinsic LLRs produced by the channel decoders
$\mathcal{L}^{Det}_{apt}$	The *a posteriori* LLRs produced by the detectors
$\mathcal{L}^{P}_{apr}$	The *a priori* LLRs produced by the precoders
$\mathcal{L}^{P}_{apt}$	The *a posteriori* LLRs produced by the precoders
$\mathcal{L}^{P}_{ex}$	The extrinsic LLRs produced by the precoders
α	The weighting vector of the Irregular Generic Detector (IrGD)
r_{gd}	The normalized complexity ratio of the generic detector
q	The number of ST-CIRT quantization bits
T_d	The number of the data symbol intervals in each transmission frame
T_p	The number of the pilot symbol intervals in each transmission frame
T_q	The number of the feedback symbol intervals in each transmission frame
f_D	The normalized Doppler frequency

Λ	The normalized feedback overhead
R_Λ	The normalized feedback overhead reduction ratio
Q	The number of data symbols carried by a LDC symbol
T	The number of symbol intervals of a LDC symbol
$\mathcal{X}$	The linear dispersion matrix
Γ_o	The overall normalized system load
Γ_s	The normalized Spatial-Domain (SD) load
Γ_t	The normalized Time-Domain (TD) load
N_{cand}	The number of detection candidates in Sphere Detection
$\bar{h}_{i,j}$	The quantized ST-CIRT between the i-th receive and j-th transmit antenna
$\hat{h}_{i,j}$	The predicted ST-CIRT between the i-th receive and j-th transmit antenna
$\tilde{h}_{i,j}$	The estimated ST-CIRT between the i-th receive and j-th transmit antenna
$h_{i,j}$	The sampled ST-CIRT between the i-th receive and j-th transmit antenna

Chapter 1

Introduction

1.1 State-of-the-art and Trends

There is an increasing demand for high-rate wireless multimedia communication systems. Advanced wireless systems employing multiple transmit and receive antennas [1] are capable of providing a high bandwidth efficiency, hence they are attractive in the context of forthcoming wireless applications, such as Long-Term-Evolution (LTE) project [2] and in the IEEE 802.11 standard family [3].

The capacity of Multiple Input and Multiple Output (MIMO) systems increases linearly with the number of antennas employed [4].[1] Hence MIMOs are capable of supporting the high data-rates required by the emerging Wireless Internet. However the teletraffic demands of the Uplink (UL) and Downlink (DL) may be rather different, where the DL-rate has to be typically higher for the sake of supporting file download for example. This is one of the justifications for studying the DL of Space Division Multiple Access (SDMA) systems in this thesis. Secondly, the UL of SDMA systems has been documented in more detail in the literature [5]. Thirdly, the separation of multiple DL users' streams is more challenging than in the UL, because the UL MSs typically have rather different Channel Impulse Responses (CIRs) owing to their geographic separation, while for the DL this is not necessarily the case, because all the DL signals emanate from the BS and hence their CIRs are similar.

Hence the design of efficient DL transmitters and receivers is of paramount importance, as we will demonstrate throughout this thesis. Powerful iterative detection aided, soft-information assisted

[1] More explicitly, the capacity of the MIMO system equipped with M transmit antennas and N receive antennas is proportional to the value of $\min\{M, N\}$.

receivers capable of achieving a near-capacity performance will be designed, as motivated by [6].

1.2 Multiple Input and Multiple Output

MIMO systems employing multiple antennas at both the transmitter and receiver exhibit a substantially higher spectral efficiency than their conventional single-antenna aided counterparts [1]. The family of MIMO systems can be divided into four main classes.

Beamforming Beamforming is an angularly selective technique, which is widely employed for mitigating the effects of multiuser interference with the aid of multiple-antennas [7]. The ability of suppressing the co-channel interference allows the beamforming assisted system to support multiple users within the same bandwidth or same time-slot [5]. When used for transmissions, this technique can also be considered as a transmit pre-processing or Multi-User Transmission (MUT) technique, which requires the accurate knowledge of the CIR experienced by the remote receiver. It is also feasible to jointly design the transmitter and receiver for maximizing the achievable beamforming gain, for example, using Singular Value Decomposition (SVD) in order to decompose the multiple-antenna aided system into a number of parallel single-antenna systems. This technique is also often referred to as eigen-beamforming [8].

Spatial Diversity In this type of MIMO systems, we achieve diversity gain by generating extra copies of the transmit signal with the aid of multiple antennas using either transmit or receive diversity. Transmit diversity is achieved by sending extra copies of the data signals from multiple transmit antennas, while receive diversity is obtained by receiving the data signals from multiple receive antennas. The extra copies of the transmitted signals allow us to recover the original signal, despite being subjected to hostile fading channels. In [9, 10], the family of space-time coding techniques capable of achieving both transmit and receive diversity has been investigated. The knowledge of the CIR encountered by each MIMO element is required at the receivers of this type of MIMO systems.

Space Division Multiplexing (SDM) In SDM aided MIMO systems, we achieve a high data rate by transmitting independent data streams from the different transmit antennas [11]. In other words, the independent data streams are spatially multiplexed. In order to separate the independent data streams, SDM detectors, optimized using the Minimum Mean Squared Error (MMSE) or the Maximum-Likelihood (ML) criterion may be employed at the receivers of this type of MIMO systems. A

successful example of this type of the MIMO systems is the well-known Vertical Bell Laboratories Layered Space-Time Architecture (V-BLAST) [12]. In order to detect the signals, accurate knowledge of the CIR is required at the receiver of SDM-MIMO systems.

Space Division Multiple Access (SDMA) SDMA exploits the unique, user-specific "spatial signature" of the individual users for differentiating them [5]. In analogy to the conventional Code Division Multiple Access (CDMA), which differentiates the users by assigning them a unique spreading code, SDMA systems utilize the CIRs as the users' signatures.

In SDMA systems, there is a significant difference between the up-link and downlink, which is the ability of coordination between users. In the SDMA UL, the signals are transmitted from the Mobile Stations (MSs), while the Base Station (BS) equipped with multiple receive antennas employs a Multi-User Detector (MUD) for jointly detecting the users' signals. On the other hand, in the downlink of SDMA systems, the signal is transmitted from the BS to the MSs. In the absence of coordination between the MSs, each MS detects its own signal separately, while the other users' signals are considered as the undesired interference imposed on the desired user's signal.

The MUD techniques employed in the UL of SDMA systems have been well-documented in the literature [5, 13]. For rich scattering environments, the MIMO channel matrix may become near-orthogonal [14]. Therefore, in SDMA UL systems, the users' spatial signatures may be considered to be independent of each other. In this case low-complexity linear MUDs, such as the MMSE may achieve an adequate performance. However, in realistic shadow-faded environment the orthogonality of the MIMO channel matrix may not be guaranteed. In this scenario more powerful MUDs are required. In [5, 13], various non-linear MUDs have been advocated and detailed, such as the Successive Interference Cancellation (SIC) detector, the Parallel Interference Cancellation (PIC) aided MUD and the Maximum-Likelihood (ML) detector. By definition, the ML detector maximizes the probability of correct decisions at the cost of the highest complexity.

When the number of users and transmitter antennas is increased, the complexity of the non-linear MUD, especially that of the ML detector increases exponentially. Clearly, there is a tradeoff between the affordable complexity and the achievable performance. Hence our design objective is to achieve a near-ML performance at a fraction of its complexity.

The concept of Sphere Decoding (SD) employed for computing the ML estimates of the modulated symbols transmitted simultaneously from multiple antennas was first proposed by Damen *et al.* in [15]. The complex-valued version of the SD was proposed by Hochwald and Brink in [16] for

employment in multi-level modulations. An improved version of Complex Sphere Decoding (CSD) was presented by Pham *et al.* [17]. In [18], a new class sphere decoding, referred to as Optimized Hierarchy aided Reduced Search Algorithm (OHRSA) was advocated, which will be further detailed in Chapter 2.

Another powerful class of guided-random detection algorithms is constituted by Genetic Algorithm (GA) aided MUDs [19,20] and Markov Chain Monte Carlo (MCMC) aided MUDs [21].

In Figure 1.1, we portray the family-tree of the prominent SDMA detectors.

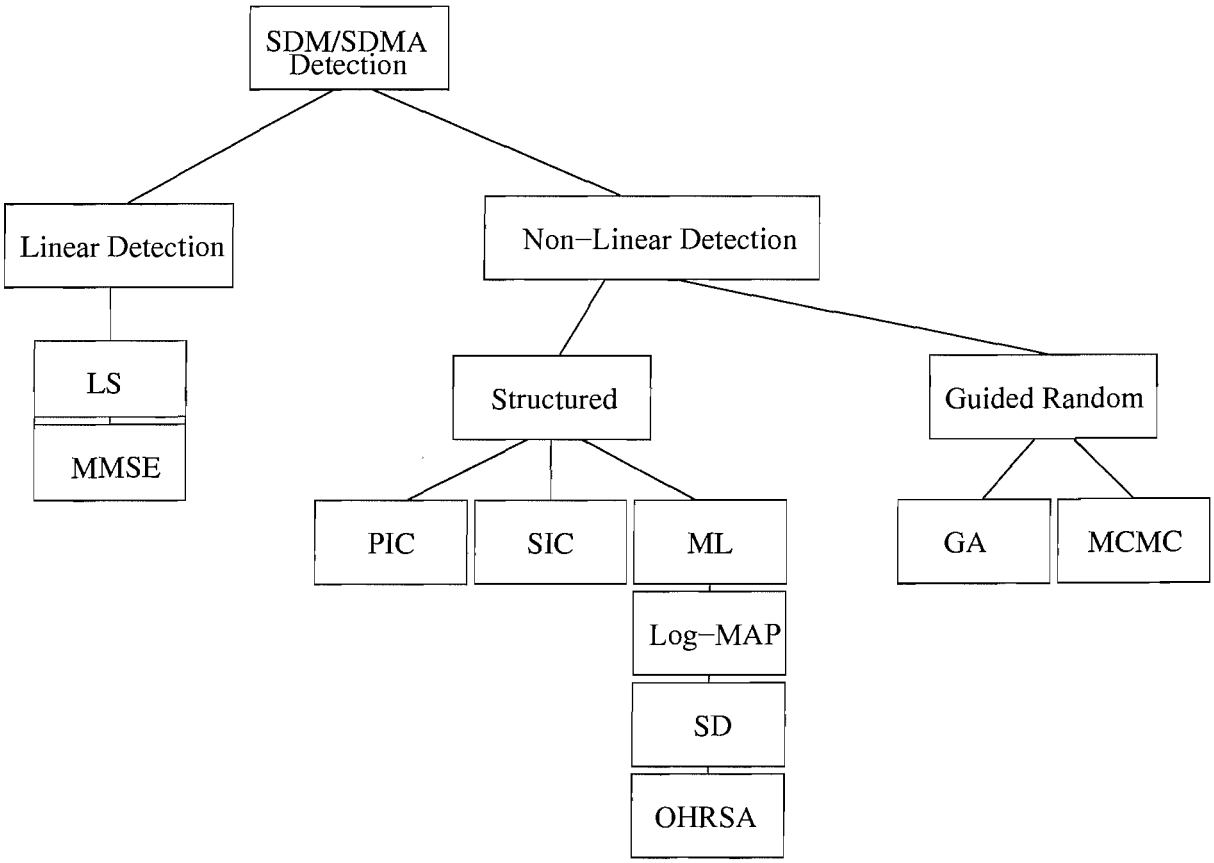

Figure 1.1: The family of SDM/SDMA detectors

In 1993, Berrou introduced the concept of iterative decoding in [6], where a concatenated code can be decoded at a moderate computational cost, while approaching the channel's capacity. Following Berrou's work, the turbo-detection principle has been further developed for channel equalization [22], MUD [5], channel estimation [23], synchronization [24], etc. In [25], Wang and Poor extended the conventional MMSE MUD to a Soft-In Soft-Ouput (SISO) MMSE MUD. In [26], van Zelst *et al.* proposed an iterative decoder for the BLAST system. In [27], Vikalo *et al.* proposed a SISO SD for MIMO systems, which can be readily adopted to MUD in the UL of SDMA systems. Wolfgang *et*

al. [28] discussed a SISO turbo space-time equalizer using the OHRSA detector of [18].

In our future discourse we focus our attention on the detection techniques of SDM/SDMA systems. In Table 1.1, we list the major contributions on the detection techniques employed in SDM/SDMA systems, while in Table 1.2 we list the major contributions on iterative detection.

Table 1.1: Major MUD contributions designed for SDM/SDMA systems

[5] Hanzo *et al.*, 2003	Detailed discussions of prominent MUDs designed for the UL of SDMA systems are provided, including SIC, PIC and ML MUDs. The generation of soft-bits in MUDs combined with soft-in soft-out based channel coders was detailed.
[15] Damen *et al.*, 2003	Sphere Decoding (SD) invoked for computing the ML estimates of the modulated symbols transmitted simultaneously from multiple transmit antenna.
[16] Hochwald and ten Brink, 2003	A SD technique having a reduced computational complexity due to using a limited number of SD candidates to attain a near-ML performance.
[29,30] Wong *et al.*, 2004	An advanced SD technique, designed for supporting rank-deficient MIMO systems.
[31,32] Cui and Tellambura, 2004	An advanced SD technique, referred to as multistage sphere decoding, which was proposed for supporting high-order modulation schemes.
[17] Pham *et al.*, 2004	An advanced extension of the CSD technique was proposed.
[18,20] Akhtman *et al.*, 2007	The Optimized Hierarchy aided Reduced Search Algorithm (OHRSA) aided log-MAP detector was proposed, which is capable of operating in rank-deficient scenarios.
[19,20] Jiang *et al.*, 2007	Nonlinear hybrid MUD scheme based on a novel soft-information assisted Genetic Algorithm (GA) was proposed for a Turbo Convolutional (TC) coded SDM aided Orthogonal Frequency Division Multiplexing (OFDM) system.

Table 1.2: Major contributions on iterative MUDs designed for SDM/SDMA systems

[25] Wang and Poor, 1999	The classic MMSE MUD was extended to a soft-input soft-output (SISO) MMSE MUD.
[26] van Zelst *et al.*, 2001	Iterative decoding was proposed for the BLAST system.
[33] Tüchler *et al.*, 2002	Minimum mean squared error equalization using a priori information was proposed.
[27] Vikalo *et al.*, 2004	A SISO SD assisted by iterative decoding was proposed for MIMO systems.
[28] Wolfgang *et al.*, 2006	A SISO OHRSA MUD was designed for single-carrier MIMO systems.

1.3 Downlink Space Division Multiple Access

In the DownLink of Space Division Multiple Access (DL-SDMA) all users' signals will contribute the composite multiuser received signal of the desired user, imposing substantial Multi-User Interference (MUI). The strategy to eliminate MUI is to invoke pre-processing at the BS's transmitter by assuming that the CIRs experienced by the MSs are quantized and reported back to the BS, which hence exploits this user-signature, for example in the form SVD-aided MUT.

Zero-Forcing aided Multi-User Transmission (ZF-MUT) is the simplest MUT technique designed for mitigating the MUI in a DL-SDMA system [13]. A more general version of the ZF-MUT referred to as Block Diagonalization (BD) was introduced in [34]. A similar approach based on SVD was advocated by Choi and Murch in [35]. The above-mentioned pre-processing techniques constitute linear Spatio-Temporal Pre-processing (STP). A well-known example of non-linear STP is constituted by Dirty Paper Coding (DPC) proposed by Costa [36], demonstrating that DPC is capable of approaching the maximum achievable capacity. An alternative non-linear STP technique, referred to as vector-precoding [37], was proposed in [38, 39]. In Figure 1.2, we portray the family-tree of spatio-temporal pre-processing of MUT (STP-MUT) techniques.

Unlike the SDMA UL, which has been well documented in the literature, the SDMA DL is less well characterized at the time of writing. In Table 1.3, we list the major contributions related to the design of DL-SDMA systems.

Hence in this treatise we embark on the design of DL-SDMA systems, which strike an attractive balance between the achievable system performance and the implementational complexity imposed.

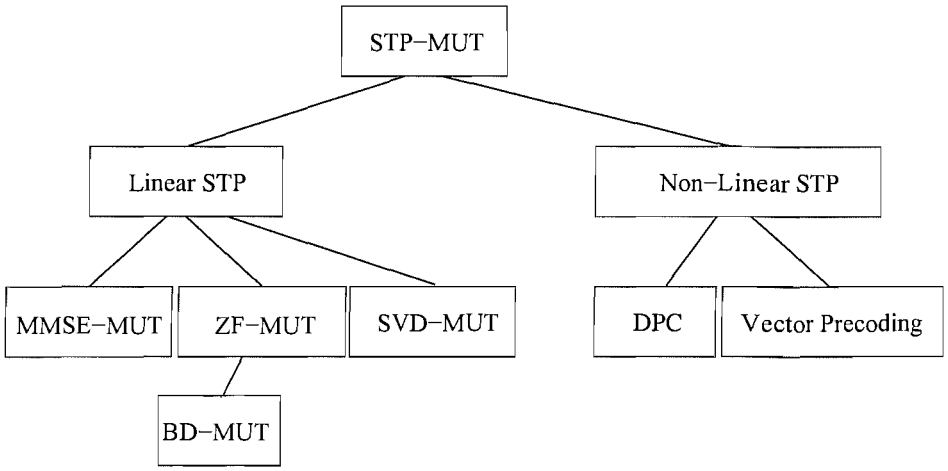

Figure 1.2: The family-tree of STP-MUT techniques

Table 1.3: Major contributions in DL-SDMA systems

[13] Vandenameele *et al.*, 2001	The concept of SDMA with employing different MUD strategies and the relationship between up-link and down-link SDMA systems was investigated using ZF-MUT based DL-SDMA systems. A single-receive antenna was used by the MS.
[40] Wong *et al.*, 2003	A joint transmitter-receiver design was proposed to eliminate the MUI in the downlink by employing a pair of pre- and post-processor.
[41] Tenenbaum *et al.*, 2004	Optimal transmit-receive linear processing based on the MMSE criterion was proposed.
[34] Spencer *et al.*, 2004	Block Diagonalization (BD) was proposed as a general form of ZF-MUT scheme, which is capable of supporting multiple receive antennas for each MS in DL-SDMA systems.
[35] Choi and Murch, 2004	A SVD based decomposition approach was proposed for DL-SDMA systems, which is reminiscent of the BD technique. However, the system model was generalised for an unequal number of transmit and receive antennas.

1.4 Outline and Contributions

Against the background provided in Sections 1.2 and 1.3, in Section 2.1, we will investigate various MUT techniques designed for DL-SDMA systems. In Section 2.2 we will characterize the DL-SDMA system's performance in conjunction with different detection techniques, such as the OHRSA aided ML detector. The corresponding results were published in [42].

In Chapter 3, we extend our research documented in Chapter 2 to a joint iterative detection and decoding based DL-SDMA system, which contains the following novel contributions:

- The iterative DL-SDMA system was proposed [43], which is capable of operating in the so-called rank-deficient scenario, where the number of transmit antennas is higher than the number of receive antennas and hence the system-matrix becomes non-invertible. The convergence behaviour of the iterative decoding aided DL-SDMA systems is improved by integrating it with a unity-rate precoder designed with the aid of Extrinsic Information Transfer (EXIT) charts.
- The impact of imperfect Channel State Information (CSI) on the precoded iterative DL-SDMA [43] was investigated using EXIT charts [44]. Sophisticated IrRegular Convolutional Codes (IRCC) were integrated with the iterative detection aided DL-SDMA system.

In Chapter 4 we further exploited EXIT charts to assist us in the design of iterative DL-SDMA system and proposed the novel concept of irregular iterative detection aided DL-SDMA systems, which relied on the following novel contributions:

- In order to reduce the complexity of our iterative receivers, we proposed the novel Irregular Generic Detection (IrGD) concept, where appropriately selected received signal segments are detected by different constituent detectors in the interest of reducing the overall system complexity and/or improving the attainable performance. The corresponding results were published in [45].
- The achievable performance of iterative DL-SDMA systems employing imperfect Spatio-Temporal Channel Impulse Response available at the Transmitters (ST-CIRT) imposed by the finite-accuracy CSI feedback was investigated. We proposed an algorithm, which assists us in exploring the CSI overhead required for achieving an infinitesimally low BER. We refer to the CSI quantization employing this algorithm as the EXIT-Chart Optimized CSI Quantizer (ECO-CQ), which was disseminated in [46].

The novel contributions of Chapter 5 are as follows:

- In Section 5.1 we improved the achievable capacity of the DL-SDMA systems by proposing a Linear Dispersion Coding (LDC) [47] aided MUT, which exhibits an improved achievable capacity and an increased degree of diversity, hence supporting a high data throughput.
- By extending the previously proposed IrGD concept of Section 4.2, we derived the Irregular Sphere Detection (IrSD) philosophy in Section 5.2, which was constructed by using the novel Center-Shifting aided K-best Sphere Detector (KSD-CS).
- In Section 5.3 we proposed and characterized a pilot assisted channel prediction aided LDC-MUT DL-SDMA system using limited CSI feedback.

The corresponding results of Chapter 5 were published in [48, 49].

Our conclusions provided in Chapter 6 highlight our major findings and elucidate the logical connection between chapters, leading to a number of future research ideas.

1.5 Assumptions and Channel Models

In this treatise, the following simplifying assumptions are stipulated, in order to facilitate our discussions. We will outline these assumptions in the following paragraphs.

Narrowband flat-fading channel model The wireless communication channel considered is assumed to be an $(M \times N)$-element non-dispersive MIMO channel, where M transmit and N receive antennas are employed [1], although in practice the dispersion often exceeds the bit duration of high-rate systems.

Uncorrelated channel statistics In SDMA systems, an antenna element spacing in excess of 10λ would be necessary to ensure that the transmitted signals of different antennas experience independent fading [50]. In SDMA UL systems this condition is easier to satisfy than in the DL, since the transmitted signals arrive at the receiver from a number of geographically dispersed MSs. On the other hand, in SDMA DL systems, the size of the BS limits both the number of antenna elements as well as their affordable maximum spacing, which in turn imposes correlation on the fading profiles of the antennas. Therefore, the number of users supported will be limited by the number of transmit antennas accommodated at the BS. In order to be able to use the CIRs as their unique user-specific signature, their independent fading is assumed in this treatise, which implies that the users

are sufficiently far apart. A more sophisticated technique was proposed in [51], which redesigned the transmitter using a pre-filter based on *a priori* knowledge of the inter-user channels. In practice, Interleaver Division Multiple Access (IDMA) [52] may be employed for differentiating SDMA UL and SDMA DL users with the aid of their unique, user-specific interleavers. The resultant IDMA system may also be viewed as a chip-interleaved CDMA arrangement.

Channel prediction and estimation In the coherent SDMA DL system considered, the transmitter employing the spatio-temporal DL pre-processing technique of Section 2.1.2 may adopt the knowledge of the individual users' CIRs to be encountered during the next transmission burst, which may also be needed by the receiver to assist in the signal's detection. In practice, the CSI adopted at the transmitter may be predicted into the future on the basis of the previous stored CSI, which was periodically fed back via the UL feedback channel from the MSs, by using realistic long-range channel prediction algorithms [53, 54]. The CSI adopted at the receiver may also be generated by using realistic channel estimation algorithms [23]. Unless stated otherwise, we will assume that perfect CSI is available at both the transmitter and receiver. Since the study of channel prediction and estimation is not within the main scope of this treatise, the CSI is assumed to be uncorrelated in the time domain. Therefore the effect of different Dopper frequencies is not investigated. However, the impact of imperfect CSI on the systems' performance will be investigated and further discussed in Section 2.2, Section 3.3, Section 4.3 and Section 5.3.

Chapter 2

Downlink SDMA Systems

2.1 Downlink Space Division Multiple Access System

Multiple Input and Multiple Output (MIMO) systems employing multiple antennas at both the transmitter and receiver exhibit a substantially higher spectral efficiency than conventional single-antenna systems. The flexible configuration of a MIMO system's antennas allows us to satisfy a number of potentially contradictory design objectives in terms of the achievable multiplexing and diversity gain, hence this topic has recently attracted substantial research attention [55,56]. Space Division Multiple Access (SDMA) constitutes an attractive MIMO subclass, which is capable of achieving a high user capacity by supporting a multiplicity of subscribers within the same frequency bandwidth [5,13] [1].

The efficient design of the down-link transmitter is of paramount importance for the sake of achieving a high throughput. The effects of Multi-User Interference (MUI) may be mitigated by employing Spatio-Temporal Pre-processing (STP) at the transmitter. Consequently, the down-link receiver's complexity may be reduced with the advent of transmit pre-processing at the base station, a technique, which is also often referred as Multi-User Transmission (MUT) [57].

The main contributions of this chapter are that first we introduce the general system model of DL-SDMA systems in Section 2.1.1, which is the main underlying system structure of this thesis. Moreover, the system model introduced in Section 2.1.1 will be characterized in terms of the impact of the MUI also in Section 2.1.1, which assists us in designing the linear STP schemes to be employed at the transmitter. Secondly, we will introduce a non-linear near-ML detector in order to support multiple-stream data transmission in the context of the system model introduced in Section 2.1.1.

[1] Other MIMO systems, such as beamformers [7] and space-time codes [22] are not considered in this treatise.

In Section 2.1.1, we will commence our discussions with the general system model of DL-SDMA systems. Different linear STP schemes designed for eliminating the MUI will be discussed in Section 2.1.2. In Section 2.1.3, we continue by quantifying the achievable information rate of DL-SDMA systems assisted by different linear STP arrangements. In Section 2.2, we will consider the design of a SVD-MUT assisted DL-SDMA system invoking a reduced-complexity ML detector in order to support a high throughput, complemented by our complexity analysis and performance results.

2.1.1 System Model

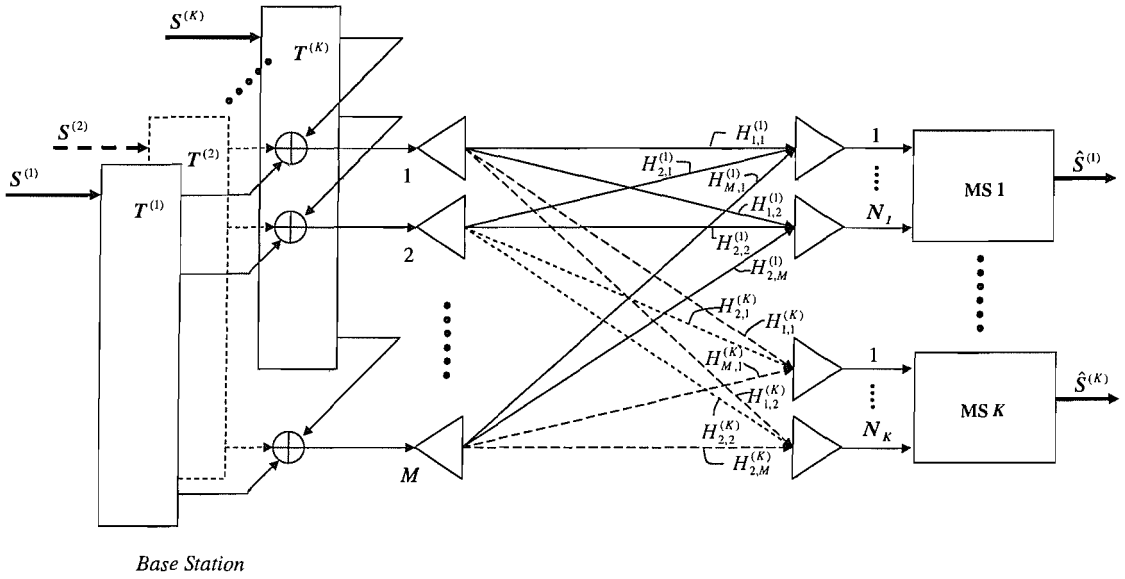

Figure 2.1: Multiuser transmission in the DL-SDMA system

The DL-SDMA system considered is depicted in Figure 2.1. More specifically, our system comprises a Base-Station (BS) employing M transmit antennas as well as K Mobile Stations (MS), each employing N_k receive antennas.

In this treatise we consider a flat fading MIMO channel. Consequently, each link between the i-th BS transmit antenna and the j-th MS receiver antenna of the k-th user may be characterized by a complex-valued scalar channel coefficient $H^{(k)}_{i,j}$, which we assume to be an i.i.d. Gaussian random variable having a variance of unity and a mean of zero. Moreover, the MIMO channel corresponding to the k-th user may be described as an $(N_k \times M)$-dimensional complex-valued time-domain channel

matrix $\boldsymbol{H}^{(k)}$, which may be defined as follows

$$\boldsymbol{H}^{(k)} = \begin{bmatrix} H_{1,1}^{(k)} & H_{1,2}^{(k)} & \cdots & H_{1,M}^{(k)} \\ H_{2,1}^{(k)} & H_{2,2}^{(k)} & \cdots & H_{2,M}^{(k)} \\ \vdots & \vdots & \cdots & \vdots \\ H_{N_k,1}^{(k)} & H_{N_k,2}^{(k)} & \cdots & H_{N_k,M}^{(k)} \end{bmatrix}. \tag{2.1}$$

Finally, the entire multi-user MIMO channel may be characterized by the supermatrix $\boldsymbol{H}$, which may be constructed by concatenating the corresponding channel matrices associated with each of the MSs. Thus we have

$$\mathbf{H} = \begin{bmatrix} \boldsymbol{H}^{(1)} & \boldsymbol{H}^{(2)} & \cdots & \boldsymbol{H}^{(K)} \end{bmatrix}^T. \tag{2.2}$$

Let $\boldsymbol{s}^{(k)} \in \mathbb{C}^{L_k \times 1}$ be a complex-valued column vector, which denotes the data symbol vector to be transmitted for the k-th MS. Furthermore, let $\boldsymbol{r}^{(k)}$ and $\boldsymbol{n}^{(k)}$ be the received signal vector and noise vector associated with the k-th MS, respectively. Additionally, we define a so-called *space-time preprocessor* matrix $\boldsymbol{T}^{(k)} \in \mathbb{C}^{M \times L_k}$, which was designed for the sake of eliminating the MUI [35]. The composite multiuser received signal, denoted by $\mathbf{r}$, encountered by all receivers may be formulated as a column-based supervector constituted by the received signal vectors associated with each of the user terminals. Thus we have

$$\mathbf{r} = \mathbf{HTs} + \mathbf{n}, \tag{2.3}$$

where we have

$$\mathbf{r} = \begin{bmatrix} \boldsymbol{r}^{(1)} & \boldsymbol{r}^{(2)} & \cdots & \boldsymbol{r}^{(K)} \end{bmatrix}^T, \tag{2.4}$$

and

$$\mathbf{T} = \begin{bmatrix} \boldsymbol{T}^{(1)} & \boldsymbol{T}^{(2)} & \cdots & \boldsymbol{T}^{(K)} \end{bmatrix} \tag{2.5}$$

is the space-time preprocessor's supermatrix. The multi-user data-stream is hosted by the supervector

$$\mathbf{s} = \begin{bmatrix} \boldsymbol{s}^{(1)} & \boldsymbol{s}^{(2)} & \cdots & \boldsymbol{s}^{(K)} \end{bmatrix}^T \tag{2.6}$$

and the complex-valued Additive White Gaussian Noise (AWGN) noise supervector is given by

$$\mathbf{n} = \begin{bmatrix} \boldsymbol{n}^{(1)} & \boldsymbol{n}^{(2)} & \cdots & \boldsymbol{n}^{(K)} \end{bmatrix}^T, \tag{2.7}$$

where each constituent element of $\boldsymbol{n}^{(k)}$, $k = 1, 2, \cdots K$, has a zero mean and a variance of $N_0 = 2\sigma_n^2$.

To elaborate a little further, we may express the *effective channel* supermatrix **HT** of Equation (2.3) as follows

$$\mathbf{HT} = \begin{bmatrix} H^{(1)}T^{(1)} & \cdots & H^{(1)}T^{(k)} & \cdots & H^{(1)}T^{(K)} \\ \vdots & \cdots & \vdots & \cdots & \vdots \\ H^{(k)}T^{(1)} & \cdots & H^{(k)}T^{(k)} & \cdots & H^{(k)}T^{(K)} \\ \vdots & \cdots & \vdots & \cdots & \vdots \\ H^{(K)}T^{(1)} & \cdots & H^{(K)}T^{(k)} & \cdots & H^{(K)}T^{(K)} \end{bmatrix}. \tag{2.8}$$

The received signal model of the k-th user is given by,

$$r^{(k)} = H^{(k)}T^{(k)}s^{(k)} + \sum_{i=1, i\neq k}^{K} H^{(k)}T^{(i)}s^{(i)} + n^{(k)}. \tag{2.9}$$

The second term of Equation 2.9 represents the MUI imposed on the received signal of the k-th user.

Moreover, we assume that the power constraint $P_T \geq \mathtt{tr}\left(T^{(k)}(T^{(k)})^H\right)$ of the STP matrix $T^{(k)}$ is satisfied for all values of k. Therefore we may define the Signal to Noise Ratio (SNR) for each receiver antenna as

$$SNR = \frac{P_T E_s}{N_0}, \tag{2.10}$$

where $E_s = \mathtt{E}\left\{\|s^{(k)}\|^2\right\}$ is the average power of the k-th user's modulated signal.

2.1.2 Linear Spatio-Temporal Preprocessing

In the context of MUT, a witty approach to spatio-temporal preproccessing was proposed by Vandenameele *et. al.* in [13], where the MUT transformation matrix was specifically designed so that its product with the channel matrix yielded an identity matrix. This MUT transformation matrix may be regarded as a perfect pre-equalizer, which effectively results in a MUI-free channel. A STP scheme based on the Minimum Mean Squared Error (MMSE) criterion was introduced in [58]. Furthermore, Choi and Murch [35] proposed an attractive precoder design, which allows for a specific user to receive his/her dedicated signal, entirely free from MUI inflicted by other users. A somewhat similar pre-processing method, which is referred to as the Block Diagonalization (BD) algorithm [34], which relied on employing the SVD. More specifically, the spatio-temporal pre-processing technique of [35] decomposes a MIMO channel into a set of parallel single-user MIMO channels, which facilitates the employment of well-known MIMO-processing techniques [5, 13].

In this forthcoming section, we will summarise the most prominent STP techniques, which were designed for eliminating the MUI in the context of the linear algorithms of Figure 1.2. Unless otherwise stated, these techniques assume that the CIR to be encountered by the transmitted signal is

perfectly known at the transmitter. This simplifying assumption will be relaxed by quantifying the effects of imperfect channel estimation/prediction in Section 2.2.5.

2.1.2.1 Zero Forcing Aided Multi-User Transmission

The most straight-forward method of designing the STP matrix $\mathbf{T}$ of Equation 2.3 is to mimick the inverse of the channel matrix $\mathbf{H}$. This technique is referred to as Zero-Forcing (ZF). When it is employed at the transmitter of the DL-SDMA system, we refer to it as Zero Forcing aided Multi-User Transmission (ZF-MUT), which is formulated as

$$\mathbf{T} = \mathbf{H}^{-1}. \tag{2.11}$$

However, this technique is only suitable for the full-rank scenario, when the number of transmit antennas is equal to the number of receive antennas.

2.1.2.2 Minimum Mean Squared Error Aided Multi-User Transmission

When designing the STP matrix $\mathbf{T}$ to minimize the Mean Squared Error (MSE) between the transmitted signal $\mathbf{s}$ and received signal $\mathbf{r}$ of Equation 2.3, which we refer to as Minimum Mean Squared Error aided Multi-User Transmission (MMSE-MUT) [2], we have

$$\mathbf{T} = \arg \min_{\mathrm{E}\{\|\mathbf{Ts}\|^2\}=P_T\mathrm{E}\{\|\mathbf{s}\|^2\}} \mathrm{E}\left\{\|\mathbf{r}-\mathbf{s}\|^2\right\}, \tag{2.12}$$

where $\mathrm{E}\{\cdot\}$ represents the expectation value, while P_T is the power constraint value imposed on the transmitted signals after preprocessing with the aid of $\mathbf{T}$. Again, the CIR to be encountered is assumed to be known at the transmitter.

We reformulate the cost function of Equation 2.12 as

$$\begin{aligned} C(\mathbf{T}) &= \mathrm{E}\left\{\|\mathbf{r}-\mathbf{s}\|^2\right\} && (2.13)\\ &= \mathrm{E}\left\{\|\mathbf{HTs}+\mathbf{n}-\mathbf{s}\|^2\right\} && (2.14)\\ &= \mathrm{E}\left\{\|\mathbf{HTs}-\mathbf{s}\|^2\right\} + \mathrm{E}\left\{\|\mathbf{n}\|^2\right\} && (2.15)\\ &= \mathrm{E}\left\{\|\mathbf{HTs}-\mathbf{s}\|^2\right\} + \mathrm{E}\left\{\|\mathbf{n}\|^2\right\} \frac{\mathrm{E}\left\{\|\mathbf{Ts}\|^2\right\}}{P_T\mathrm{E}\left\{\|\mathbf{s}\|^2\right\}} && (2.16)\\ &= \mathrm{E}\left\{\|\mathbf{HTs}-\mathbf{s}\|^2\right\} + \beta\mathrm{E}\left\{\|\mathbf{Ts}\|^2\right\}, && (2.17) \end{aligned}$$

[2]The STP scheme based on the MMSE criterion in [58], which was referred to as TOMIMO, was designed for a single-user MIMO system. However, it can be readily extended to multi-user MIMO systems. Hence, while giving the credit to [58], we referred to this solution as the MMSE-MUT. On the other hand, the Transmit-MMSE (T-MMSE) multi-user system discussed in [59] is joint or coordinated transmit-receive design. This arrangement is different from our MMSE-MUT arrangement, which is simply a transmitter-only pre-processing scheme.

where we have

$$\beta = \frac{\mathrm{E}\left\{\|\mathbf{n}\|^2\right\}}{P_T \mathrm{E}\left\{\|\mathbf{s}\|^2\right\}}. \tag{2.18}$$

Since the transmitted signal $\mathbf{s}$ is independent of the channel matrix $\mathbf{H}$ and STP matrix $\mathbf{T}$, we may rewrite Equation 2.17 as

$$\begin{aligned} C(\mathbf{T}) &= \mathrm{E}\left\{\|\mathbf{s}\|^2\right\}\left\{\mathrm{E}\left\{\|\mathbf{HT}-\mathbf{I}\|^2\right\}+\beta\mathrm{E}\left\{\|\mathbf{T}\|^2\right\}\right\} && (2.19)\\ &= \mathrm{E}\left\{\|\mathbf{s}\|^2\right\} R(\mathbf{T}), && (2.20)\end{aligned}$$

where the cost function to be optimized is given by $R(\mathbf{T}) = \mathrm{E}\left\{\|\mathbf{HT}-\mathbf{I}\|^2\right\}+\beta\mathrm{E}\left\{\|\mathbf{T}\|^2\right\}$.

Since $\mathrm{E}\left\{\|\mathbf{s}\|^2\right\}$ does not affect the design of the STP matrix $\mathbf{T}$, the $\mathbf{T}$ which minimizes the cost function $C(\mathbf{T})$ also minimizes the cost function $R(\mathbf{T})$. Therefore, we aim for finding the STP matrix $\mathbf{T}$, which minimizes $R(\mathbf{T})$ and derive $R(\mathbf{T})$ as follows

$$\begin{aligned} R(\mathbf{T}) &= \mathrm{E}\left\{\|\mathbf{HT}-\mathbf{I}\|^2\right\}+\beta\mathrm{E}\left\{\|\mathbf{T}\|^2\right\} && (2.21)\\ &= \mathtt{tr}\left(\mathrm{E}\left\{(\mathbf{HT}-\mathbf{I})(\mathbf{HT}-\mathbf{I})^H\right\}\right)+\beta\mathtt{tr}\left(\mathrm{E}\left\{\mathbf{TT}^H\right\}\right) && (2.22)\\ &= \mathtt{tr}\left(\mathbf{HTT}^H\mathbf{H}^H-\mathbf{HT}-\mathbf{T}^H\mathbf{H}^H+\mathbf{I}+\beta\mathbf{TT}^H\right) && (2.23)\\ &= \mathtt{tr}\left(\mathbf{HTT}^H\mathbf{H}^H\right)-\mathtt{tr}\left(\mathbf{HT}\right)-\mathtt{tr}\left(\mathbf{T}^H\mathbf{H}^H\right)+\mathtt{tr}\left(\mathbf{I}\right)+\beta\mathtt{tr}\left(\mathbf{TT}^H\right), && (2.24)\end{aligned}$$

where $\mathtt{tr}\left(A\right)$ is the sum of the diagonal elements in the matrix A.

In order to derive the STP matrix $\mathbf{T}$, which minimizes $R(\mathbf{T})$ of Equation 2.24, we derive the gradient of the cost function $R(\mathbf{T})$ and set it to zero [60], which is given by

$$\begin{aligned} \nabla_{\mathbf{T}} R(\mathbf{T}) &= 0 && (2.25)\\ \Rightarrow \mathbf{H}^H\mathbf{HT}-\mathbf{H}^H+\beta\mathbf{T} &= 0 && (2.26)\\ \Rightarrow \mathbf{T} &= (\mathbf{H}^H\mathbf{H}+\beta\mathbf{I})^{-1}\mathbf{H}^H && (2.27)\end{aligned}$$

Finally, Equation 2.27 reveals the MMSE-MUT solution for the STP matrix $\mathbf{T}$.

2.1.2.3 Singular Value Decomposition Based Multi-User Transmission

In this section we introduce the Singular Value Decomposition based Multi-User Transmission (SVD-MUT). As it was demonstrated in [35], the n-th column of the MUT preprocessor $\boldsymbol{T}^{(k)}$, which we denote as $t_n^{(k)}$, has to be in the null space of $\boldsymbol{H}^{(i)}, i \neq k$. More explicitly, we have [35]

$$t_n^{(k)} \in \bigcap_{i=1, i\neq k}^{K} ker\left(\boldsymbol{H}^{(i)}\right), \quad \text{for } k = 1, 2, \cdots, K, \tag{2.28}$$

where $ker(X)$ denotes the null space or kernel of the matrix X, while $\bigcap_{i=1,i\neq k}^{K} \mathcal{Y}_i$ is the intersection of the sets $\mathcal{Y}_i, i = 1,2,\cdots$.

Let $V^{(k)}$ denote an $(M \times n_k)$-dimensional matrix representing an orthogonal basis of the subspace $\bigcap_{i=1,i\neq k}^{K} ker\left(H^{(i)}\right)$, where n_k is the dimension of this subspace. As suggested by Choi and Murch in [35], we may formulate a solution of the MUT preprocessor design problem as $T^{(k)} = V^{(k)}A^{(k)}$, where $A^{(k)}$ is a nonzero $(n_k \times L_k)$-dimensional matrix. Subsequently, the design of the matrices $V^{(k)}$ and $A^{(k)}$ may be summarized in the following three steps.

Step 1 Let us define the quantity $\tilde{\mathbf{H}}^{(k)}$ by omitting the k-th matrix-element from the supermatrix $\mathbf{H}$ of Equation (2.2) describing the channels. Thus, we have

$$\tilde{\mathbf{H}}^{(k)} = \left[\begin{array}{cccccc} H^{(1)} & \cdots & H^{(k-1)} & H^{(k+1)} & \cdots & H^{(K)} \end{array} \right]^T. \tag{2.29}$$

The null space basis $V^{(k)}$ can be calculated using the SVD [61] of $\tilde{\mathbf{H}}^{(k)}$ expressed as:

$$\tilde{\mathbf{H}}^{(k)} = \left[\begin{array}{cc} \tilde{U}^{(k)} & U^{(k)} \end{array} \right] \cdot \left[\begin{array}{cc} \Sigma & 0 \\ 0 & 0 \end{array} \right] \cdot \left[\begin{array}{c} \tilde{V}^{(k)^H} \\ V^{(k)^H} \end{array} \right]. \tag{2.30}$$

Step 2 The specific choice of the $(n_k \times L_k)$-dimensional matrix $A^{(k)}$ in $T^{(k)} = V^{(k)}A^{(k)}$ may depend on a particular system design. For instance, in the simple scenario considered in this discourse, where we have $n_k = L_k$, we may choose $A^{(k)}$ to be a scaled identity matrix. As an example of an alternative solution, consider the somewhat more sophisticated system design described in [62]. More specifically, the system outlined in [62] employs pre-filters at the transmitter and post-filters at all the receivers, in order to achieve a near-capacity throughput. Correspondingly, the matrix $A^{(k)}$ was chosen as the right-hand-side SVD factor of the matrix $H^{(k)}V^{(k)}$ [62].

Step 3 Calculate $T^{(k)} = V^{(k)}A^{(k)}$ according to the results obtained in Steps 1 and 2.

Note that according to Equation 2.30 the nonzero matrices $T^{(k)}$ exist only in the scenario when $\tilde{\mathbf{H}}^{(k)}$ has more columns than rows. Consequently, we have to satisfy the following condition

$$M > max\left\{ \sum_{i=1,i\neq k}^{K} N_i, k = 1,2,\ldots,K \right\}. \tag{2.31}$$

Moreover, the rank n_k of the null space basis $V^{(k)}$ may be expressed as

$$n_k = M - \sum_{i=1,i\neq k}^{K} N_i. \tag{2.32}$$

2.1.3 Capacity of DL-SDMA

In this subsection, we will discuss the capacity of DL-SDMA systems. According to [63], the achievable information rate of a system can be quantified by evaluating the mutual information between with the transmitted signal s and received signal r, which is defined as [63]

$$\mathbb{I}(\mathbf{r}|\mathbf{s}) = \mathbb{H}(\mathbf{r}) - \mathbb{H}(\mathbf{r}|\mathbf{s}), \tag{2.33}$$

where $\mathbb{H}$ represents the entropy of a random variable defined as $\mathbb{H}(\cdot) = -log_2(\mathtt{P}(\cdot))$, and $\mathtt{P}(\cdot)$ is the Probability Density Function (PDF) of the signal considered.

Therefore, the capacity of a system is defined as the average of the maximum achievable information rate [4], formulated as

$$\mathfrak{C} = \mathrm{E}\left\{\mathbb{I}(\mathbf{r}|\mathbf{s})\right\}, \tag{2.34}$$

where $\mathrm{E}\{\cdot\}$ represents the expectation with respect to the complex-valued Gaussian noise.

2.1.3.1 Gaussian Input Signals

Although in practice the transmitted signal is quantized to a discrete-amplitude, discrete-phase modulated signal [64], the assumption of encountering a continuous Gaussian-distributed input signal assists us in quantifying the capacity of an idealized system. According to [4], the assumption of having a Gaussian transmitted signal achieves the maximum mutual information in Equation 2.34. Therefore, in the following paragraphs we will first discuss the capacity of systems based on idealized Gaussian input signals and illustrate the capacity upper bound of DL-SDMA systems in different scenarios.

MIMO capacity bound The capacity of the single-user MIMO system achieved for transmission over flat Rayleigh fading channels was quantified in [4]. According to [4], the MIMO capacity can be formulated as

$$\mathfrak{C} = \mathrm{E}\left\{\log_2 \det\left(I + \frac{E_s}{N_0} H^H H\right)\right\}, \tag{2.35}$$

where $\mathrm{E}\{\cdot\}$ represents the expectation operation with respect to the different realizations of the channel matrix H and the complex-valued Gaussian noise.

In contrast to a multi-user DL-SDMA system where the MSs are geographically dispersed, the receiver of a single-user MIMO system may jointly detect the signals received by all allocated antennas. More explicitly, in a DL-SDMA system, when the MSs are geographically dispersed, they have

to separately detect their own signals. Hence, the capacity of the single-user MIMO system represents the upper bound of the DL-SDMA system's capacity.

DL-SDMA capacity in the absence of MUI As long as the STP matrix $\mathbf{T}$ of Equation 2.3 is capable of perfectly eliminating the MUI, the DL-SDMA system may be considered as a number of parallel single-user MIMO systems. Provided that the CIRs to be encountered by the transmitted signals are perfectly known, the DL-SDMA system is MUI-free and hence the capacity of the DL-SDMA system may be considered to be equivalent to the sum of the capacities of the individual MIMO streams transmitted in parallel. As suggested in [65], the capacity of the MUI-free DL-SDMA can be quantified as

$$\mathfrak{C} = \mathrm{E}\left\{\sum_{k=1}^{K} \log_2 \det\left(I + \frac{E_s}{N_0} \boldsymbol{H}^{(k)} \boldsymbol{T}^{(k)} (\boldsymbol{T}^{(k)})^H (\boldsymbol{H}^{(k)})^H\right)\right\}. \tag{2.36}$$

In the previous discussions of Section 2.1.2, linear STP schemes, such as ZF-MUT and SVD-MUT assisted arrangements were proposed for diagonalizing the effective channel matrix $\mathbf{HT}$ of Equation 2.3. The resultant DL-SDMA system employing these linear STP schemes results in MUI-free received signals for each user. Therefore, we may use Equation 2.36 to quantify the capacity of the linear STP assisted DL-SDMA system.

DL-SDMA capacity in the presence of MUI In practical scenarios, the DL-SDMA system's received signal will be contaminated by residual MUI. For example, the MMSE-MUT assisted DL-SDMA system does not aim for decomposing the system into parallel single-user or single-stream MIMO systems, it rather generates a STP matrix $\mathbf{T}$, which minimizes the MSE between the transmitted and received signals. By contrast, for the ZF-MMSE and SVD-MUT assisted STP schemes we need perfect CSI to perfectly eliminate the MUI, which is unavailable in practice. Hence, the realistic imperfect CSI will impose residual MUI on the users' received signals for both the ZF-MUT and SVD-MUT assisted DL-SDMA systems. When the users' received signals are contaminated by residual MUI, this scenario becomes analogous to that of an uplink SDMA system, where the BS detects all receive antennas' signals separately, as discussed in [66]. More specifically, the capacity of the SDMA uplink was quantified in [66], when each receive BS antenna's receivers separately detects the received signals contaminated by residual MUI. Analogously, the capacity of the MUI-contaminated DL-SDMA system may be upper-bounded by [67]

$$\mathfrak{C} = \sum_{i=1}^{K} \mathrm{E}\left\{\log_2\left(\frac{\det\left(I + \frac{E_s}{N_0}\left(\boldsymbol{H}^{(k)}\boldsymbol{T}^{(k)}(\boldsymbol{T}^{(k)})^H(\boldsymbol{H}^{(k)})^H + \sum_{i=1,i\neq k}^{K} \boldsymbol{H}^{(k)}\boldsymbol{T}^{(i)}(\boldsymbol{T}^{(i)})^H(\boldsymbol{H}^{(k)})^H\right)\right)}{\det(I + \frac{E_s}{N_0}\sum_{i=1,i\neq k}^{K} \boldsymbol{H}^{(k)}\boldsymbol{T}^{(i)}(\boldsymbol{T}^{(i)})^H(\boldsymbol{H}^{(k)})^H)}\right)\right\}. \tag{2.37}$$

It also has to be noted in Section 1.5 that owing to the MSs' different geographic position, the UL CIRs are typically less correlated than the DL CIRs, which is expected to lead to a significantly lower practically achievable DL capacity and a more challenging system design. Equation 2.37 may be considered as a more general capacity formula of DL-SDMA systems, which encapsulates the MUI-free scenario of Equation 2.36.

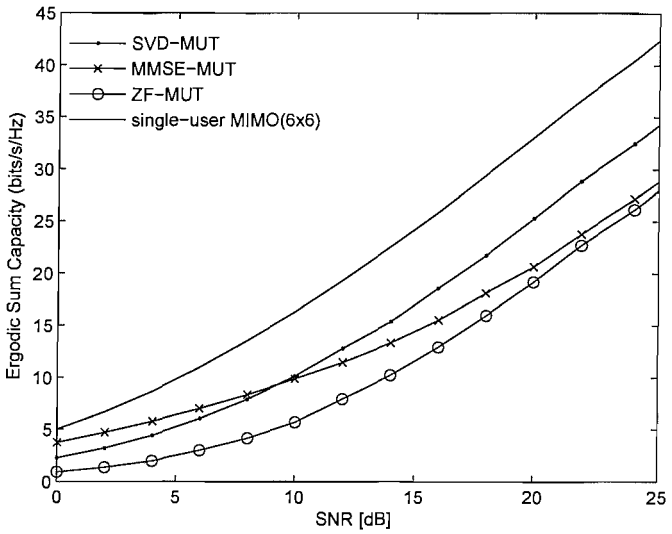

Figure 2.2: Capacity of the DL-SDMA systems of Figure 2.1 using different STP schemes for a (6×6)-element MIMO channel. The DL-SDMA systems using different linear STP arrangements are assumed to have the same system configuration. The system supports $K = 3$ users. Each MS has $N_k = 2$ receive antennas and is receiving $L_k = 2$ independent data streams from the BS's transmitter. The total number of transmit antennas at the BS is $M = 6$. The capacity of the single-user MIMO system employing $M = 6$ transmit antenna and $K \cdot N_k = 6$ receive antennas is provided as a benchmarker. The power constraint is assumed to be the same for the different linear STP schemes employed. Assuming perfect ST-CIRT knowledge at the transmitter, the capacity of the SVD-MUT and ZF-MUT aided DL-SDMA systems characterized in this figure with the aid of Equation 2.36 are MUI-free. On the other hand, the MMSE-MUT aided DL-SDMA system benefitting from perfect ST-CIRT at the transmitter still experienced some residual MUI. Its capacity was quantified in this figure using Equation 2.37.

Figure 2.2 portrays the ergodic sum capacity of DL-SDMA using different linear STP techniques in a (6×6)-element MIMO channel, having $M = 6$ transmit antennas and $K \cdot N_k = 6$ receive antennas, which was evaluated by Equation 2.37. More explicitly, based on the capacity formulas of Equation 2.37, we evaluate sum capacity of the systems by employing different STP matrix $\mathbf{T}$ of Equation 2.3, which were generated by ZF-MUT, MMSE-MUT and SVD-MUT scheme using Equation

2.11, Equation 2.27 and Equation 2.30 respectively. Also by averaging the results of Equation 2.37 for different channel realizations we evaluate the ergodic sum capacity for each linear STP scheme. In Figure 2.2, the DL-SDMA systems using different linear STP techniques have assumed the same system configuration supporting $K = 3$ users. Furthermore, each MS has $N_k = 2$ receive antennas and detects $L_k = 2$ independent data streams received from the BS. The total number of transmit antennas at the BS is $M = 6$. The capacity of the single-user SDMA DL system using $M = 6$ transmit antenna and $K \cdot N_k = 6$ receive antennas is also provided in Figure 2.2 as a benchmarker. For the sake of fair comparison, the power constraint of $\mathbf{T}$ was assumed to be the same for the different linear STP schemes. Observe that in the moderate to high SNR region, the SVD-decomposition assisted STP scheme has a higher information rate than the other two.

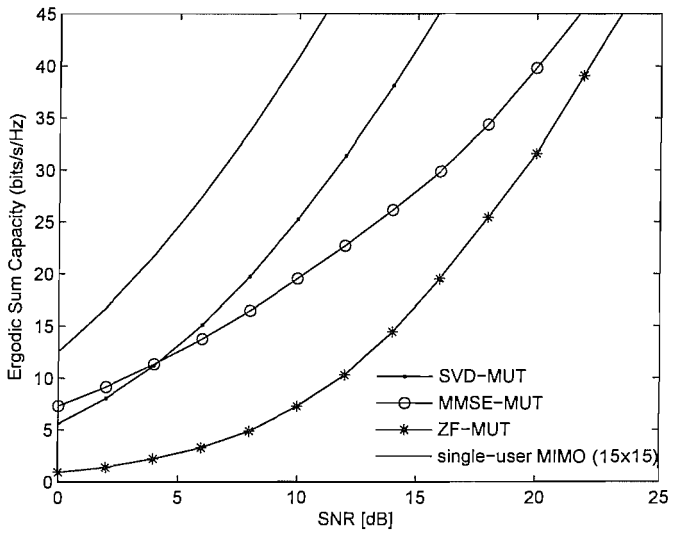

Figure 2.3: Capacity of the DL-SDMA systems of Figure 2.1 using different STP schemes for a (15×15)-element MIMO channel. The DL-SDMA systems using different linear STP arrangements are assumed to have the same system configuration. The system supports $K = 3$ users. Each MS has $N_k = 5$ receive antennas and is receiving $L_k = 5$ independent data streams from the BS's transmitter. The total number of transmit antennas at the BS is $M = 15$. The capacity of the single-user MIMO system employing $M = 15$ transmit antenna and $K \cdot N_k = 15$ receive antennas is provided as a benchmarker. The power constraint is assumed to be the same for the different linear STP schemes employed. Assuming perfect ST-CIRT knowledge at the transmitter, the capacity of the SVD-MUT and ZF-MUT aided DL-SDMA systems characterized in this figure with the aid of Equation 2.36 are MUI-free. On the other hand, the MMSE-MUT aided DL-SDMA system benefitting from perfect ST-CIRT at the transmitter still experienced some residual MUI. Its capacity was quantified in this figure using Equation 2.37.

As a further result, in Figure 2.3, we quantify the ergodic sum capacity of DL-SDMA using different linear STP schemes for a (15×15)-element MIMO channel. Again, for fair comparison, the DL-SDMA systems using different linear STP scheme are assumed to operate in the same system configurations. All systems support $K = 3$ users. Each MS has $N_k = 5$ receive antennas and is receiving $L_k = 5$ independent data streams from the BS. The total number of transmit antennas at the BS is $M = 15$. The capacity of the single-user MIMO system employing 15 transmit and 15 receive antennas is also provided as a benchmarker. The power constraint imposed on $\mathbf{T}$ of Equation 2.3 is assumed to be the same for the different linear STP schemes. As expected, compared to Figure 2.2, the information rate of the DL-SDMA systems becomes higher for the increased number of transmit and receive antennas. Specifically, observe that the SVD-decomposition assisted DL-SDMA system has a higher information rate than the other two linear STPs in the moderate to high SNR region.

2.1.3.2 Discrete Input Signals

In contrast to the previous section, in this section we assume that the modulated signal transmitted over the channel is a discrete-valued signal, such as that of an $\mathcal{M}$-ary QAM scheme, which has $log2(\mathcal{M})$ different modulation levels. Unfortunately at the time of writing, there is no closed-form formula for the capacity of MIMO systems communicating using discrete input signals.

An alternative was suggested in [16], for characterizing the transmission of non-Gaussian input signals, where we may quantify the achievable information rate by the amount of mutual information between the transmitted signal $\boldsymbol{s}$ and received signal $\boldsymbol{r}$ of a $(M \times N)$-element MIMO system:

$$\mathbb{I}(\boldsymbol{r}|\boldsymbol{s}) = \mathbb{H}(\boldsymbol{r}) - \mathbb{H}(\boldsymbol{r}|\boldsymbol{s}), \tag{2.38}$$

where we have [16]

$$\mathbb{H}(\boldsymbol{r}|\boldsymbol{s}) = N \log_2(2\pi e \sigma_n^2) \tag{2.39}$$

and [16]

$$\mathbb{H}(\boldsymbol{r}) = -\mathrm{E}\left\{\log_2\left(\frac{1}{\mathcal{M}^M(2\pi\sigma_n^2)^N}\sum_{\check{\boldsymbol{s}}\in\mathcal{S}}\exp\left(-\frac{1}{2\sigma_n^2}\|\boldsymbol{r}-\boldsymbol{H}\check{\boldsymbol{s}}\|^2\right)\right)\right\}, \tag{2.40}$$

where $\mathcal{S}$ is the set containing all $\mathcal{M}^M$ candidates of the transmitted signal $\boldsymbol{s}$.

Again, the capacity of the MUI-free DL-SDMA system may be upper-bounded by the sum capacity of the constituent parallel single-user MIMO systems. Therefore, we may quantify the achievable information rate of the MUI-free DL-SDMA system, which employs an $\mathcal{M}$-ary QAM scheme, by

using Equation 2.38 for evaluating the corresponding achievable rate of each equivalent single-user single-stream MIMO system and then sum them. Hence, the achievable rate of the linear STP assisted DL-SDMA scheme considered can be quantified by

$$\mathbb{I}(\mathbf{r}|\mathbf{s}) = \sum_{k=1}^{K} \mathbb{I}(\boldsymbol{r}^{(k)}|\boldsymbol{s}^{(k)}). \tag{2.41}$$

For the purpose of illustration, in Figure 2.4 we used Equation 2.41 to quantify the achievable information rate of the SVD-MUT assisted DL-SDMA system employing 4QAM, while the lines marked using black dots provided as benchmarkers were obtained by using Equation 2.36. The term $\mathbb{I}(\boldsymbol{r}^{(k)}|\boldsymbol{s}^{(k)})$ of the k-th user in Equation 2.41 was evaluated by Equation 2.38. Figure 2.4 characterizes the different antenna configurations, where the legend $[K, M, N_k, L_k]$ represents the corresponding parameters of the system configurations. The first digit specifies the number of users K, while the second digit the number of transmit antennas M. Furthermore, the third digit indicates the number of receive antennas N_k of each user, and finally the last parameter L_k specifies the number of independent data streams destined for each supported user. Interestingly, observing that when the number of streams received by each user is increased in the context of the same (6×6)-element scenario, the sum of the information rate of all users is also increased, although naturally, the system is capable of supporting a reduced number of users. This implies that when the users have more antennas for which they perform a joint detection, we will have a higher total achievable information rate. A single-user MIMO system then constitutes a special case, where the user has all the available antennas at his/her disposal to perform a joint detection and that results in attaining the highest achievable information rate. This observation also supports our argument that the capacity of a single-user MIMO scheme constitutes the upper bound of the DL-SDMA system's capacity.

On the other hand, the ZF-MUT and MMSE-MUT assisted DL-SDMA systems benefit from no receive diversity due to their specific design. The ZF-MUT scheme removes all the MUI and Inter-Channel Interference (ICI), which is imposed by multiple antennas. By contrast, the MMSE-MUT criterion minimizes the MSE between the transmitted and received signals, as seen in Equation 2.12. Hence, these two systems have the same achievable information rate in the context of different parameters. By contrast, the SVD-MUT assisted DL-SDMA system is capable of decomposing the DL-SDMA system into a number of parallel single-user/multi-stream schemes with the aid of the multiple transmit and multiple receive antennas and may simultaneously benefit from a spatial multiplexing gain and transmit-receive diversity gain. Our further discussions on SVD-MUT assisted DL-SDMA systems will be presented in the following section. In summary of this section, in Table 2.1 we outline the system configurations supported by the various linear STP schemes.

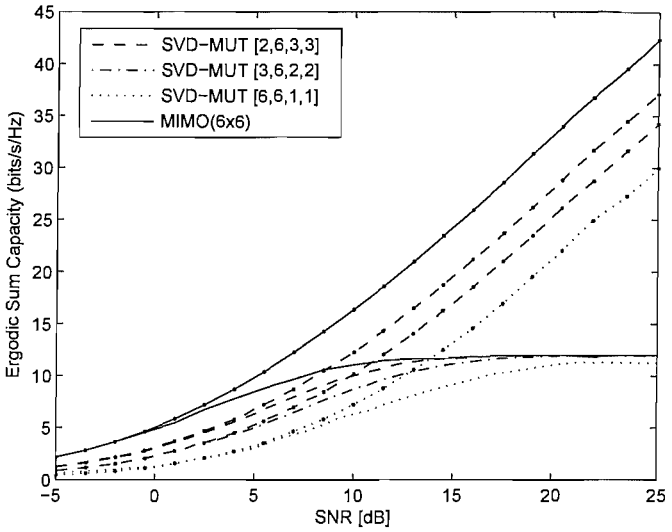

Figure 2.4: Capacity of the SVD-MUT assisted DL-SDMA scheme of Figure 2.1 for a (6×6)-element MIMO channel. The legend $[K, M, N_k, L_k]$ represents the corresponding parameters of the system configurations. The first digit specifies the number of users K, while the second digit the number of transmit antennas M. Furthermore, the third digit indicates the number of receive antennas N_k of each user, and finally the last parameter specifies the number of independent data streams for each supported user. Provided that perfect ST-CIRT is available at the transmitter, this figure characterizes a MUI-free case.

	SVD-MUT	MMSE-MUT	ZF-MUT
$M > N, L_k > N_k$	$\surd$	$\times$	$\times$
$M = N, L_k = N_k$	$\surd$	$\surd$	$\surd$
$M < N, L_k < N_k$	$\surd$	$\surd$	$\times$

Table 2.1: System configurations supported by the different Linear STP schemes

2.2 Reduced Complexity Maximum Likelihood Detection Aided DL-SDMA for High Data Throughput

As mentioned in the previous section, the SVD-MUT assisted DL-SDMA system is capable of decomposing the SDMA DL into a number of parallel single-user systems. As a benefit of using multiple transmit antennas and multiple receive antennas, the system may benefit from both spatial multiplexing and transmit-receive diversity gains at the same time. Hence, for the sake of increasing the effective system throughput, we consider a so-called rank-deficient scenario, where we have a higher number of antennas in the transmitter than that in the receiver. Furthermore, we advocate a MUT technique, which is capable of reliable detection in this rank-deficient system. However, a powerful detection algorithm is required at the receiver, in order to support the high-integrity operation of our rank-deficient system configuration. The performance of the family of classic linear detectors, such as the Minimum Mean Squared Error (MMSE) detector was shown to be unsatisfactory in the rank-deficient scenario [20]. Consequently, we invoke a nonlinear detector. However, the typically high complexity of nonlinear detectors is often prohibitive in practical systems. Thus, a Reduced Search Algorithm (RSA) may be employed for reducing the complexity of the nonlinear detector. In this contribution a novel Optimized Hierarchy (OH) RSA-aided ML detection method is advocated [20], which may be regarded as an advanced extension of the CSD techniques portrayed in [17]. As opposed to the CSD, the OHRSA considered exhibits a relatively low complexity even in heavily rank-deficient scenarios and thus its employment is meritorious. In the next subsection, we introduce an objective measure for quantifying the system's achievable throughput in support of our performance-related discussions.

2.2.1 The Normalized System Load

The SVD-MUT assisted DL-SDMA system considered in this application provides a flexible system design framework capable of supporting various spatial multiplexing and diversity requirements. More specifically, an equivalent single-user SDMA system may potentially provide a spatial multiplexing gain of factor $\min\{n_k, N_k\}$ [55]. Furthermore, in the scenario of having a K-user SDMA system, where the corresponding MIMO channel may be decomposed into K number of parallel single-user MIMO channels, the system may potentially achieve a spatial multiplexing gain, which increases linearly with the value of $\min\{Kn_k, KN_k\}$.

As stated above, in this contribution we considered a particular scenario of having $L_k = n_k$,

where the corresponding dimension of the effective transmit antenna array encountered by the k-th MS is L_k. Consequently, the achievable spatial multiplexing gain will increase linearly with the value of $\min\{KL_k, KN_k\}$. Furthermore, the achievable transmit diversity increases with the number of physical transmit antennas, M. Observe that the MUT's preprocessor matrix $\mathbf{T}^{(k)}$ of Equation 2.9 transforms the signal vector $\mathbf{s}^{(k)}$ into the column space of $\mathbf{T}^{(k)}$. Hence, each element of $\mathbf{s}^{(k)}$ contributes to each of the signals transmitted from the corresponding physical transmit antennas. For instance, let x_i denote the symbol transmitted from the i-th transmit antenna. Then x_i, $i = 1, \cdots, M$, comprises contributions from each element of the transmit symbol vector $\mathbf{s}^{(k)}$, which results in the transmit diversity gain achievable by the system.

In the scenario of having an $(M \times N)$-dimensional MIMO channel, where M and N refer to the number of transmit antennas as well as to the total number of antennas employed by all user terminals, different system configurations of M and N provide different spatial multiplexing and transmit diversity gains. In order to categorize the potential system design options relevant to the current discussion, let us introduce the measure of the normalized *system load* expressed as

$$L_s = \frac{M}{N}. \tag{2.42}$$

Consequently, we may distinguish three different scenarios as follows:

1. lightly-loaded scenario, for $L_s < 1$;
2. fully-loaded scenario, for $L_s = 1$;
3. rank-deficient or 'over-loaded' scenario, for $L_s > 1$.

In the lightly-loaded case, the number of the antennas in the receiver exceeds that in the transmitter. Hence, the extra receiver antennas may potentially provide the system with the corresponding receive diversity. On the other hand, in the fully-loaded case, the receiver antennas provide a degree of freedom, which is just sufficient for a linear detector to separate the M independent users' signals. Finally, in the rank-deficient scenario, the number of receiver antennas is insufficient for providing an adequate degree of freedom required by a linear detector. Thus, non-linear detection techniques have to be employed. The normalized system load L_s of Equation 2.42 may be utilized in order to characterize both up- and down-link SDMA systems.

2.2.2 Optimized Hierarchy Reduced Search Algorithm Aided Maximum likelihood Detection

In this subsection we outline the principles of the OHRSA [20], which we adapted for our DL-SDMA system in order to reduce the computational complexity imposed by the ML detector employed by each of the MSs. For the sake of convenience, in our forthcoming discussions we will focus on a single MS and omit the user index k. Assuming that the MUI of Equation 2.9 is entirely eliminated by using the SVD-MUT of Section 2.1.2.3, according to Equation 2.9, the received signal model of the each user, is given by,

$$r = HTs. \tag{2.43}$$

The optimum ML solution of Equation 2.43, is given by [20]

$$\hat{s} = \arg \min_{\check{s} \in \mathcal{M}_c^L} \|\mathbf{U}(\check{s} - \hat{x})\|^2, \tag{2.44}$$

where $\mathcal{M}_c$ denotes the set of $\mathcal{M}$ complex-valued constellation points of the modulation scheme employed and $\mathcal{M}_c^L$ is the total set of legitimate values hosted by the transmitted symbol vector $\check{s}$. Moreover, $\mathbf{U}$ is an upper-triangular matrix having real-valued elements on its main diagonal and satisfying

$$\mathbf{U}^H\mathbf{U} = ({H_e}^H H_e + 2\sigma_n^2 I), \tag{2.45}$$

while

$$\hat{x} = ({H_e}^H H_e + 2\sigma_n^2 I)^{-1} {H_e}^H r, \tag{2.46}$$

and the effective channel matrix is given by $H_e = H \cdot T$, where again, we omit the user index k for the sake of brevity. Consequently, let us define the following objective function [20]

$$\begin{aligned} \mathcal{J}(\check{s}) &= \|\mathbf{U}(\check{s} - \hat{x})\|^2 = (\check{s} - \hat{x})\mathbf{U}^H\mathbf{U}(\check{s} - \hat{x}), \\ &= \sum_{i=1}^{L} \left| \sum_{j=i}^{L} u_{ij}(\check{s}_j - \hat{x}_j) \right|^2 = \sum_{i=1}^{L} \phi_i(\check{s}_i), \end{aligned} \tag{2.47}$$

$$\mathcal{J}_i(\check{s}_i) = \mathcal{J}_{i+1}(\check{s}_{i+1}) + \phi_i(\check{s}_i), \quad i = 1, \cdots, L, \tag{2.48}$$

where we have $\check{s}_i = [\check{s}_i, \cdots, \check{s}_L]$ and

$$\mathcal{J}(\check{s}) = \mathcal{J}_1(\check{s}_1) > \mathcal{J}_2(\check{s}_2) > \cdots > \mathcal{J}_L(\check{s}_L) > 0. \tag{2.49}$$

Equation (2.48) and (2.49) enable us to employ a highly efficient reduced-complexity search algorithm, which decreases the number of objective function evaluations associated with solving the minimization problem of Equation (2.44) to a small fraction of the entire set $\mathcal{M}_c^L$.

2.2.3 Generation of Soft-Bit Information

It is widely recognized [5] that the BER associated with the process of communicating over a noisy fading MIMO channel can be dramatically reduced by means of employing channel coding. A particularly effective channel coding scheme is constituted by the *soft-input soft-output* turbo coding technique [22]. Turbo coding, however, requires *soft* information concerning the bit decisions at the output of the detector, in other words the *a posteriori* soft information regarding the confidence of the bit-decision is required.

The derivation of an expression for the low-complexity evaluation of the soft-bit information associated with the bit estimates of the detector's output characterized by Equation (2.44) is given in [20]. Specifically, it is demonstrated in [20] that the soft-bit value associated with the mth bit of the ith QAM symbol of the data symbol vector assigned to the kth user may be closely approximated as

$$L_{im}^{(k)} \approx \frac{1}{2\sigma_n^2}\left[\mathcal{J}(\check{\mathbf{s}}_{im;\min}^{0}) - \mathcal{J}(\check{\mathbf{s}}_{im;\min}^{1})\right], \tag{2.50}$$

where both $\check{\mathbf{s}}_{im;\min}^{b}$ and the corresponding cost function value $\mathcal{J}(\check{\mathbf{s}}_{im;\min}^{b})$ may be obtained by applying the extended OHRSA-aided search derived in [20] and briefly summarized above in Section 2.2.2. The resultant soft-output OHRSA method exhibits a near-Log-MAP performance, while requiring a dramatically reduced computational complexity, as we will demonstrate in Section 2.2.5.

2.2.4 Complexity Analysis

Although the non-linear Maximum-Likelihood (ML) detection method of Section 2.2.2 attains the best possible BER performance [5], the excessive complexity of the associated exhaustive search in the solution-space constituted by all the legitimate transmitted signal vector candidates makes its implementation difficult challenging. More explicitly, assuming that $\mathcal{M}$-ary QAM is employed, as quantified in [20] the computational complexity of the ML detection at each MS is on the order of

$$C_{ML} = \mathcal{O}\left\{\mathcal{M}^{L} \cdot (3N_k + 2N_k L)\right\}, \tag{2.51}$$

where $(3N_k + 2N_k L)$ represents the complexity associated with a single search step, i.e. the computational complexity of evaluating the ML's cost function of $\|\boldsymbol{H}\check{\boldsymbol{s}} - \boldsymbol{r}\|^2$ [20], where $\mathcal{M}^L$ is the number of legitimate transmitted signal vector candidates $\boldsymbol{s}$. Clearly, the complexity will increase, when we increase the number of the independent data streams L transmitted to each MS, and the number of receivers N_k. However, the computational complexity is dominated by L and the $\mathcal{M}$. For example,

while the system employing 4-QAM, i.e. $\mathcal{M} = 4$, in conjunction with $L = 4$ and $N_k = 2$, which represents a rank-deficient scenario, the computational complexity associated with the full-search based ML detection is of the order of 10^3. By contrast, the system employing 16-QAM, i.e. $\mathcal{M} = 16$, $L = 4$ and $N_k = 2$, has a computational complexity associated with ML detection, which is near the order of 10^7. Furthermore, the generation of soft-bit information will impose a substantial additional increase of the associated computational complexity. More explicitly, the soft-output Log-MAP detection advocated in [20] has a computational complexity on the order of

$$C_{LM} = \mathcal{O}\left\{L \log_2 \mathcal{M} \cdot 2^{L \log_2 \mathcal{M}-1} \cdot (3N_k + 2N_k L)\right\}. \tag{2.52}$$

The linear MMSE detector, on the other hand has a computational complexity on the order of [20]

$$C_{MMSE} = \mathcal{O}\left\{L^3 + LN_k^2 + L^2 N_k + LN_k\right\}. \tag{2.53}$$

Clearly, the computational complexity of MMSE detection is substantially lower than that associated with the full-search based ML detector. Naturally, the achievable performance of the linear detector is more limited, as demonstrated in [20]. Moreover, linear detectors, such as the MMSE detector, do not allow the system to operate in a rank-deficient scenario, where the number of transmit antennas exceeds that of the receive antennas.

In order to mitigate the excessive complexities of the ML detector, the reduced-complexity OHRSA detector advocated in [20] may be used, which imposes a substantially lower complexity and yet attains a nearly-optimum performance. The computational complexity of OHRSA depends on the SNR and Figure 2.5 quantifies this as a function of the E_b/N_0 value, which was evaluated with the aid of simulations. Clearly, upon increasing the normalized system load, a higher computational complexity will be imposed by the detection process. However, the computational complexity of the OHRSA detector will decrease in the high E_b/N_0 region.

To elaborate further, Figure 2.6 characterizes the computational complexity imposed by the different detectors considered. The corresponding system configuration and the normalized system load characteristics are detailed in Table 2.2. The associated complexity is quantified in Figure 2.6 in terms of the total number of additions and multiplications per detected QAM symbol as a function of the normalized system load L_s recorded at E_b/N_0=6 dB. The complexity figures associated with the exhaustive search-based ML and the log-MAP detector [5] are also provided for the sake of comparison. Observe that the OHRSA detector exhibits a complexity, which is two orders of magnitude lower than that imposed by the Log-MAP detector, while their performance is quite similar. Moreover, the superior efficiency of the OHRSA detector becomes more obvious upon increasing the system load.

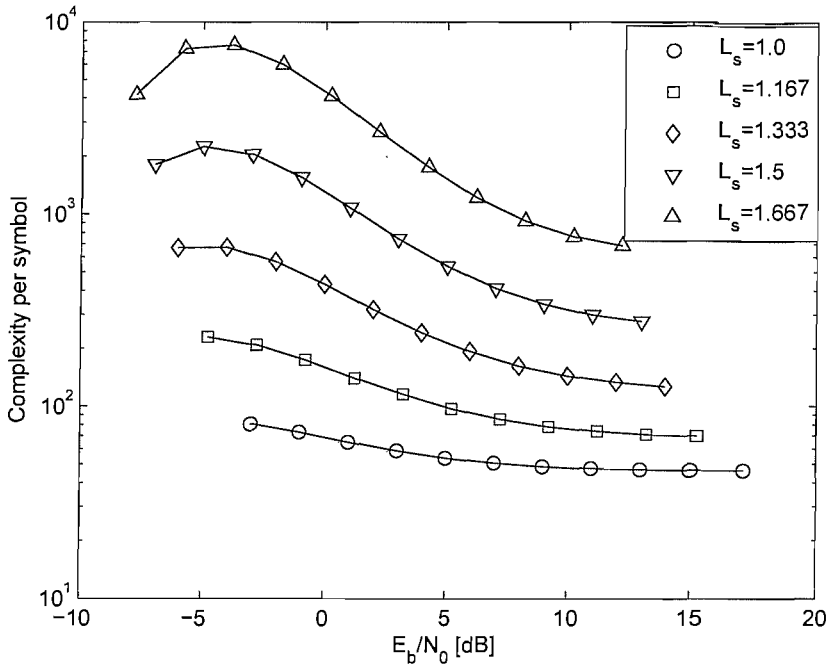

Figure 2.5: Complexity comparison of the OHRSA detector aided DL-SDMA scheme of Figure 2.1 having different normalized loads. The normalized system load L_s ranging from 1 to 1.667 corresponds to the system configuration (A) detailed in Table 2.2, supporting $K = 3$ users with the aid of $N_k = 2$ antennas at each receiver. The uncorrelated Rayleigh fading channel model was used.

2.2.5 Performance Analysis

In this section, we characterize the achievable performance of the DL-SDMA system employing the proposed OHRSA detector. Our simulations were performed in the discrete base-band domain. We employed 4-QAM modulation protected by rate-1/2 turbo coding using a 1000-bit interleaver.[3] The system configuration as well as the corresponding system load characteristics considered in our simulations are listed in Tables 2.2 and 2.3. All system configurations considered supported $K = 3$ users. Finally, for the sake of convenience, we assume $L_1 = L_2 = \cdots = L_K = L$.

Figure 2.7 portrays our performance results corresponding to two different system load scenarios, namely to $L_s = 1.0$ and 1.5. The system configuration and the corresponding normalized system loads are detailed in Table 2.2. For each system load scenario, we characterize the BER performance exhibited by the OHRSA detector along with the corresponding BER performances exhibited by both the MMSE and the log-MAP detectors as benchmarkers. In the scenario of $L_s = 1.0$ all three de-

[3]The component codes of the turbo coder employed are RSC [5,7] schemes, where the octal generator polynomials are 5 and 7. (The value 7 should be used for the feedback generator polynomial [22].)

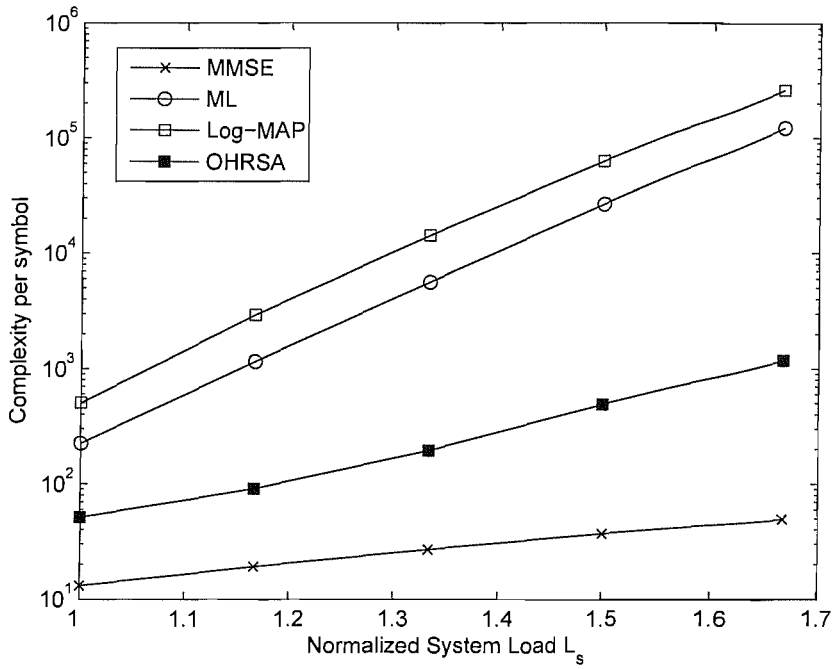

Figure 2.6: Complexity comparison of the 4QAM DL-SDMA scheme of Figure 2.1 having different normalized loads at an E_b/N_0 of 6 dB. The normalized system load L_s ranging from 1 to 1.667 corresponds to the system configuration (A) outlined in Table 2.2, supporting $K = 3$ users with the aid of $N_k = 2$ antennas at each receiver. The uncorrelated Rayleigh fading channel model was used.

Table 2.2: System configuration (A)

M	6	7	8	9	10
L	2	3	4	5	6
L_s	1	1.167	1.333	1.5	1.667

Table 2.3: System configuration (B)

M	9	10	11	12	13	14
L	3	4	5	6	7	8
L_s	1	1.111	1.222	1.333	1.444	1.556

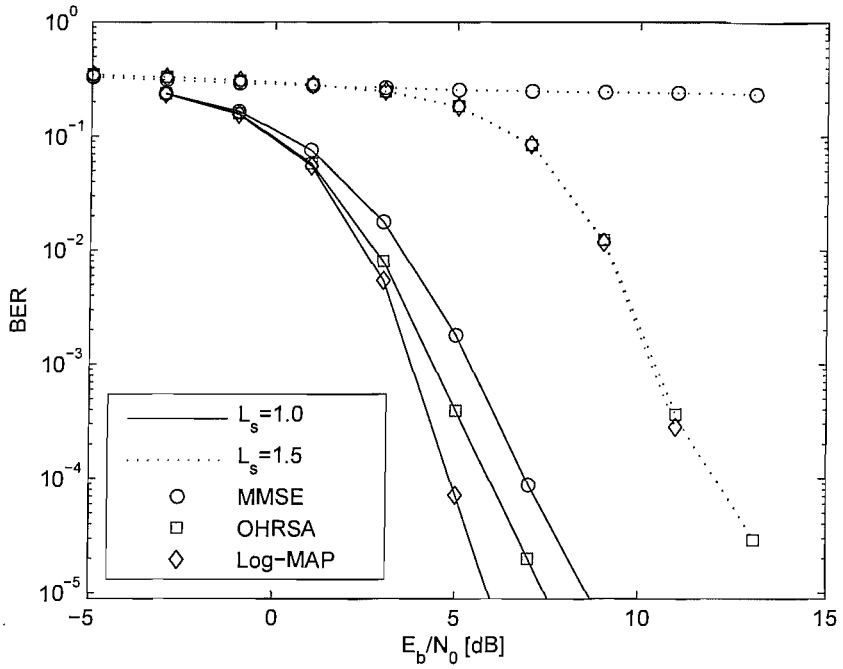

Figure 2.7: BER performance of the 4QAM DL-SDMA scheme of Figure 2.1 having a normalized system load of $L_s = 1.0$ and 1.5, which corresponds to the configuration of Table 2.2. Our system supports $K = 3$ users, where each user employs $N_k = 2$ receives antennas. A rate-1/2 turbo coding using a 1000-bit interleaver was employed. The uncorrelated Rayleigh fading MIMO channel model was used.

tectors exhibit an adequate performance. However, when the normalized system load L_s is increased to 1.5, which corresponds to a severely rank-deficient scenario, the MMSE detector fails to attain a satisfactory BER performance. The OHRSA detector, on the other hand, performs well and the corresponding BER performance is fairly close to that exhibited by the exhaustive search aided log-MAP detector. The E_b/N_0required by the different systems for the sake of achieving a target BER of 10^{-4} is quantified in Figure 2.8 as a function of the system load L_s. The associated system configuration and normalized system load are detailed in Table 2.3. As we can see in Figure 2.8, the E_b/N_0 required by the system employing the linear MMSE detector diverges rapidly escalates upon increasing L_s. On the other hand, the E_b/N_0 required by the OHRSA-aided system increases at a moderate rate upon increasing the system load. Finally, the E_b/N_0 requirements imposed by the OHRSA and Log-MAP detectors are nearly identical.

To elaborate a little further, Figure 2.9, reveals the ability of the OHRSA detector operating in the high-integrity detection mode, where the number of transmit antennas is higher than that of the receive antennas and hence it results in a rank-deficient scenario. By increasing the normalized sys-

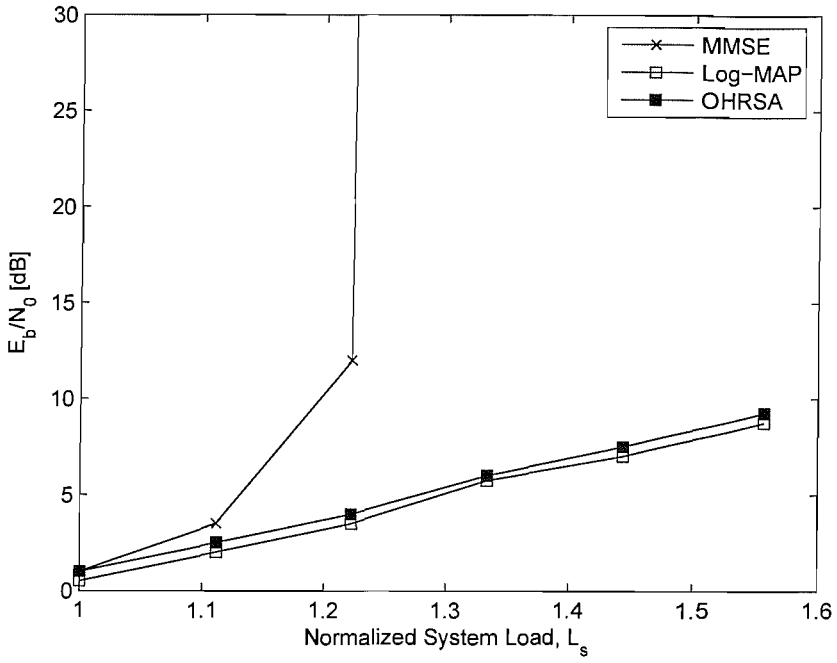

Figure 2.8: The E_b/N_0 required for maintaining a target BER=10^{-4} in different system load scenarios, where L_s is ranging from 1 to 1.556 in the system configuration (B) outlined in Table 2.3 when supporting $K = 3$ users and employing $N_k = 3$ antennas at each receiver. A rate-1/2 turbo coding using a 1000-bit interleaver was employed. An uncorrelated Rayleigh fading MIMO channel model and 4-QAM transmission was employed

tem load L_s ranging from $L_s = 1.0$ to 1.667, which corresponds to the configurations seen in Table 2.2, Figure 2.9 shows a slightly increased power is required by the DL-SDMA scheme employing the OHRSA detector. Figure 2.9 demonstrates that the OHRSA detector is capable of closely approaching the performance of the full-search-Log-MAP detector in rank-deficient scenario, despite its low complexity.

In order to increase the achievable data throughput, higher-order modulation schemes, such as 16QAM and 64QAM may be employed in the system. We portray the DL-SDMA system employing the OHRSA detector in conjunction with 4QAM, 16QAM and 64 QAM for different normalized system loads in Figure 2.10.

In Figure 2.11, we compare the BER performance of the OHRSA detector aided DL-SDMA system using half-rate turbo and half-rate Recursive Systematic Convolutional (RSC) coding [22] having a memory of three and an octal generator polynomial of G = [5 7]. In Figure 2.11(a), the systems support a normalized system load of $L_s = 1.0$ and explicitly demonstrates the benefit of employing a powerful turbo codec. Quantitatively, as a benefit of turbo coding, there is an approximately 3 dB

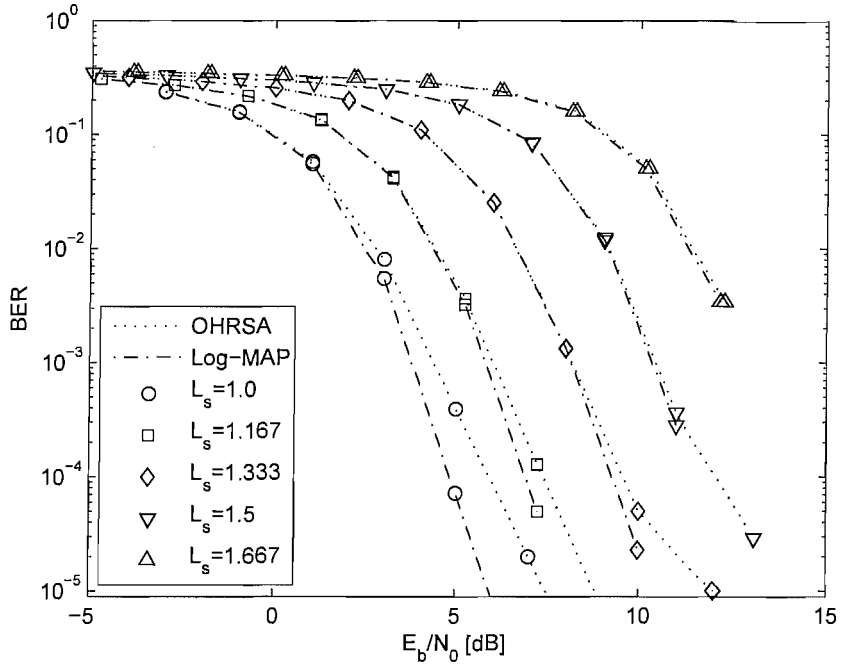

Figure 2.9: BER performance of the 4QAM DL-SDMA scheme of Figure 2.1 using OHRSA detector at a normalized system load ranging from $L_s = 1.0$ to 1.667, which corresponds to the configuration of Table 2.2. The performance results of DL-SDMA scheme employing the Log-MAP are provided as benchmarkers. Our system supports $K = 3$ users, where each user employs $N_k = 2$ receives antennas. A rate-1/2 turbo coding using a 1000-bit interleaver was employed. The uncorrelated Rayleigh fading MIMO channel model was used.

E_b/N_0 gain for all the systems maintaining a target BER=10^{-5}, regardless of the choice of the detectors. In Figure 2.11(b), the systems support a normalized system load of $L_s = 1.5$, also demonstrating the benefit of employing a powerful turbo codec, although the turbo-coding gains are less significant at this high system load.

The previous discussions were based on the assumption that perfect CSI is available at both the transmitters and the receivers. In the following discussion, we will demonstrate the impact of imperfect CSI on the attainable BER performance of the OHRSA detector aided DL-SDMA systems. In practice the CSI will be obtained by employing long-range prediction algorithm [54] and CSI estimation algorithm to assist the transmitters and receivers, respectively. We define $\hat{H}_{ST-CIRT}$ as the Spatio-Temporal Channel Impulse Response available at the Transmitters (ST-CIRT), which is used for designing the STP matrix T of Equation 2.9 according to Section 2.1.2.3. Furthermore, $\sigma^2_{ST-CIRT}$ is the variance of the estimation error between $\hat{H}_{ST-CIRT}$ and the perfect ST-CIRT $H_{ST-CIRT}$, which is defined as $\sigma^2_{ST-CIRT} = E\{\|\hat{H}_{ST-CIRT} - H_{ST-CIRT}\|^2\} / E\{\|H_{ST-CIRT}\|^2\}$. Similarly, we

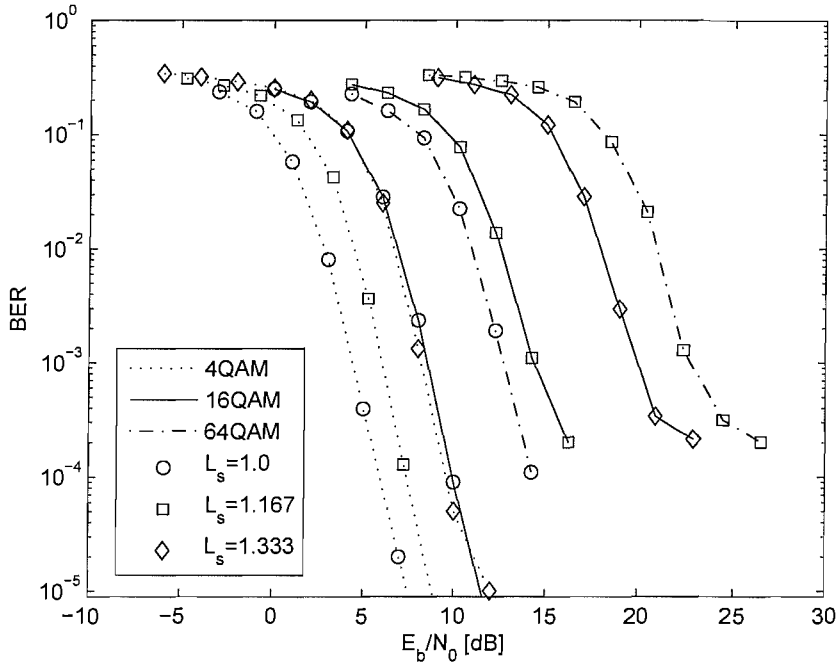

Figure 2.10: BER performance of the DL-SDMA scheme of Figure 2.1 employing the OHRSA detector for 4QAM, 16QAM and 64QAM. The systems have a normalized system load ranging from $L_s = 1.0$ to 1.333, which corresponds to the system configuration of Table 2.2. The performance results of the DL-SDMA scheme employing the OHRSA detector are provided as benchmarkers. Our system supports $K = 3$ users, where each user employs $N_k = 2$ receives antennas. A rate-1/2 turbo coding using a 1000-bit interleaver was employed. The uncorrelated Rayleigh fading MIMO channel model was used.

define $\hat{H}_{ST-CIRR}$ as the Spatio-Temporal Channel Impulse Response at the Receivers (ST-CIRR), which assists the receivers in detecting the signals. The variance $\sigma^2_{ST-CIRR}$ represents the variance of the estimation error between $\hat{H}_{ST-CIRR}$ and the perfect ST-CIRR $H_{ST-CIRR}$, which is defined as $\sigma^2_{ST-CIRR} = E\{\|\hat{H}_{ST-CIRR} - H_{ST-CIRR}\|^2\} / E\{\|H_{ST-CIRR}\|^2\}$. We investigate the impact of imperfect ST-CIRT and ST-CIRR quantified in terms of both the ST-CIRT prediction error variance $\sigma^2_{ST-CIRT}$ and the ST-CIRR estimation error variance $\sigma^2_{ST-CIRR}$, which adequately characterizes the quality of the ST-CIRT and ST-CIRR under the assumption of encountering a Gaussian estimation error model. [4] In Figure 2.12(a) and Figure 2.12(b), we illustrate the impact of imperfect ST-CIRT and ST-CIRR on the OHRSA detector aided DL-SDMA system, respectively. The imperfect ST-CIRT

[4] In order to illustrate the detrimental impact of imperfect ST-CIRT on the DL-SDMA system, the ST-CIRT error imposed by ST-CIRT prediction and estimation was modelled by using a Gaussian estimation error model. However the probability density function of the ST-CIRT prediction and estimation error depends on both the propation environment and on the prediction and estimation algorithms employed in reality.

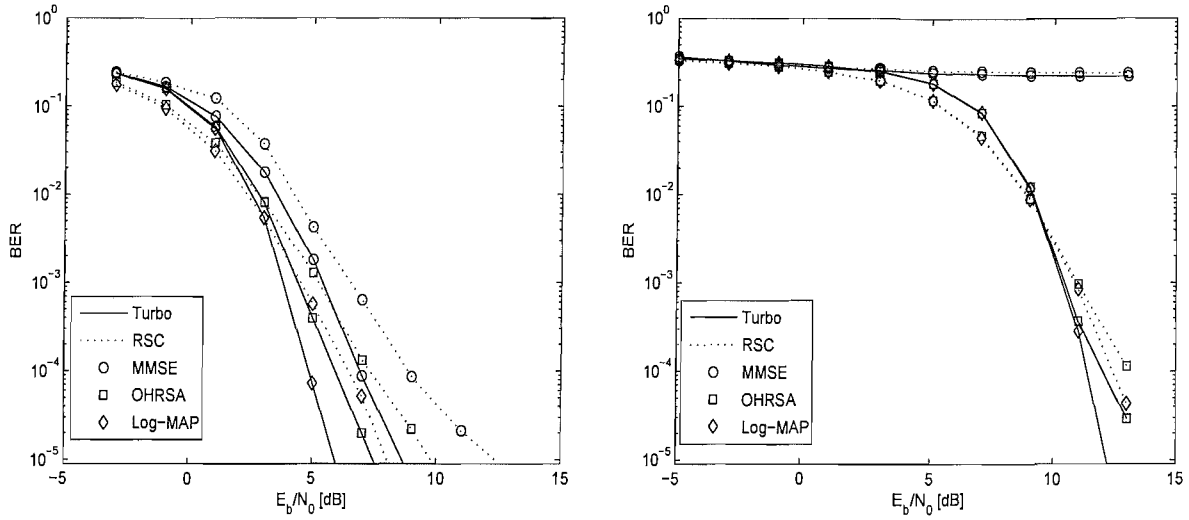

Figure 2.11: BER performance of the 4QAM-modulated DL-SDMA schemes of Figure 2.1 employing half-rate turbo and half-rate RSC[5,7] channel codecs. In (a), the systems have a normalized system load of $L_s = 1.0$, while in (b), the normalized system load is increased to $L_s = 1.5$, which corresponds to Table 2.2. Our system supports $K = 3$ users, where each user employs $N_k = 2$ receive antennas. The uncorrelated Rayleigh fading MIMO channel model was used.

inflicts an increased MUI upon each user's received signal and hence degrades the attainable performance of the system as illustrated in Figure 2.12(a). Similarly, the imperfect ST-CIRR induces an increased detection error and hence results in a limited system performance, as evidenced by Figure 2.12(b).

2.3 Summary and Conclusions

In this chapter, we introduced the concept of DL-SDMA systems assisted by different linear STP schemes, which render transmitted signals robust to MUI. The achievable capacity of different linear STP assisted DL-SDMA systems has been investigated. The SVD-MUT assisted DL-SDMA system invoking the reduced complexity ML detector of Section 2.2 was advocated as the most attractive design option.

In Section 2.1, we first introduced a general model for the DL-SDMA system. Spatio-temporal preprocessing was invoked at the transmitters, which eliminated the multi-user/multi-stream interfer-

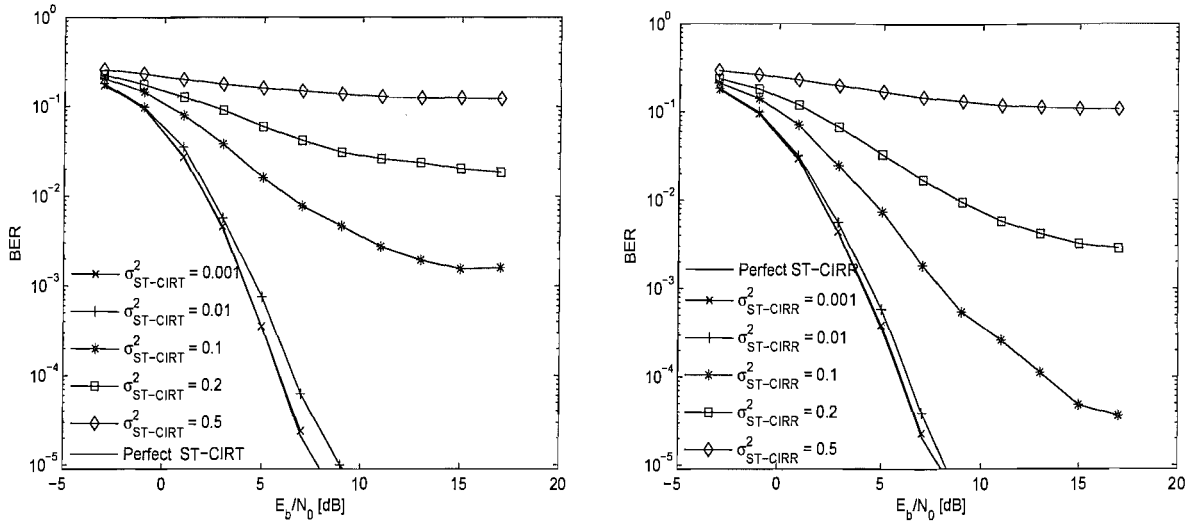

(a) (b)

Figure 2.12: BER performance of the OHRSA detector aided DL-SDMA scheme of Figure 2.1 employing imperfect CSI. (a) shows the BER performance of the system for different values of $\sigma^2_{ST-CIRT}$, while employing perfect ST-CIRR. (b) shows the BER performance of the system for different values of $\sigma^2_{ST-CIRR}$, while employing perfect ST-CIRT. The systems have a normalized system load of $L_s = 1.0$, which corresponds to Table 2.2. Our system supports $K = 3$ users, where each user employs $N_k = 2$ receives antennas. A rate-1/2 turbo coding using a 1000-bit interleaver was employed. The uncorrelated Rayleigh fading MIMO channel model was used. The 4-QAM modulation scheme was employed

ence. The ZF-MUT, MMSE-MUT and SVD-MUT schemes were introduced in Section 2.1.2. In Figure 2.2 of Section 2.1.3, we investigated the achievable capacities of the different linear STP assisted DL-SDMA systems. In Section 2.1.3, we found that the SVD-MUT assisted DL-SDMA system exhibits a higher information rate than the other two linear STP assisted systems in the moderate to high SNR region. By contrast in the low-SNR range of Figure 2.2, where the Gaussian noise dominates the attainable performance, the MMSE-MUT exploiting the perfect knowledge of the noise level has a slightly higher information rate than the SVD-MUT assisted DL-SDMA system. These observations were illustrated in Figure 2.2 and Figure 2.3. Additionally, due to their specific design limitations, we found that the ZF-MUT and MMSE-MUT algorithm did not achieve a receive diversity gain. By contrast, the SVD-MUT assisted DL-SDMA system was capable of decomposing the DL-SDMA into a number of parallel single-user/multi-stream schemes and benefited from both a spatial multiplexing gain and a transmit-receive diversity gain at the same time.

In Section 2.2, we introduced an objective measure of the system's achievable throughput, which we referred to as the normalized system load L_s, in support of our performance-related discussions. With the assistance of the normalized system load L_s, we investigated the SVD-MUT assisted DL-SDMA system in different system configurations. We have demonstrated that the SVD-MUT assisted DL-SDMA system employing the reduced-complexity ML detector is capable of achieving the near-optimum Log-MAP performance in the rank-deficient scenarios considered. Finally, in Section 2.2.4 we provided a brief complexity analysis. The selected results were published in [42].

Having introduced a non-iterative near ML detector, we will further improve the achievable BER performance of the DL-SDMA system discussed in this chapter by introducing an iterative DL-SDMA system in Chapter 3.

Chapter 3

Iterative Downlink SDMA Systems

3.1 Introduction

In the previous chapter, we introduced the philosophy of DL-SDMA multiuser systems, which employed the low-complexity near-ML OHRSA detector of Section 2.2. We showed that the low-complexity near ML OHRSA detector works efficiently in DL-SDMA multiuser systems, especially for the rank-deficient DL-SDMA multiuser systems capable of receiving from more transmitters than the number of receivers. Furthermore, the soft-bit information provided by the OHRSA detector improves the decoding process in the channel decoder.

In order to further improve the robustness of the DL-SDMA multiuser systems considered in Section 3.2, we first embed the iterative decoding into the receivers of the DL-SDMA multiuser systems, as an extension of the system introduced in the previous chapter. Based on the context of EXIT chart [68], we will demonstrate the OHRSA detector may not facilitate rapid convergence to an infinitesimally low BER. Therefore, we propose an iterative near ML receiver for rank-deficient DL-SDMA multiuser systems, which is aided by a unity-rate precoder. We will demonstrate using EXIT charts that the convergence of the iterative detector is improved with the aid of precoding by exchanging extrinsic information between the constituent decoders.

Since there are no indepth near-ML DL-SDMA rank-deficient system studies in the open literature, the novel contribution of Section 3.2 is that the low-complexity near ML uplink OHRSA detector of [20] is invoked for the challenging scenario of a rank-deficient DL-SDMA multiuser system, which is capable of receiving from more transmitters than the number of receivers. Furthermore, the convergence of the iterative receiver is improved with the aid of precoding by exchanging extrinsic

information between the constituent decoders, which is investigated using EXIT Charts.

In order to cast our study in a practical context, in Section 3.3, we will investigate the precoded and iteratively detected downlink multiuser system employing imperfect Spatio-Temporal Channel Impulse Response at the Transmitters (ST-CIRT). In practice, the ST-CIRT has to be estimated by using realistic channel prediction algorithms [53,54], which is particularly challenging for high throughput systems, where $(M \times N)$ number of ST-CIRs have to be estimated [5] for an M-element transmitter and N-element receiver. The resultant imperfect ST-CIRT will inflict an increased MUI upon each user's received signal and hence degrades the attainable performance of the system. Hence, we investigate the impact of imperfect ST-CIRTs quantified in terms of the ST-CIRT prediction error variance, which adequately characterizes the quality of the ST-CIRT for a Gaussian error model.[1] Again, we employ the EXIT charts to analysis the impact of imperfect ST-CIRTs. Furthermore, we employ sophisticated IrRegular Convolutional Codes (IRCC) [69] using several different-rate component codes for producing a closely-matching outer EXIT curve, which allows us to improve the attainable BER performance. By matching the outer decoder's EXIT curve to that of the inner decoder, we may still obtain an open EXIT-tunnel for a severe impact of imperfect ST-CIRT.

The novel contribution of Section 3.3 is that we propose an EXIT-chart based design technique for precoded and iteratively detected DL-SDMA using IRCCs, which allows us to take into account the expected level of ST-CIRT prediction/estimation error, hence resulting in an infinitesimally low BER, despite using imperfect channel prediction for the MUT-aided transmitter.

3.2 Iterative Near-Maximum-Likelihood Detection in Downlink SDMA Systems

In this section, an iteratively detected downlink multiuser system is proposed. In order to further improve our previous Near-Maximum-Likelihood (NML) Detection aided DownLink (DL) SDMA systems, we redesign the previous system by embedding it into a serial-concatenated iterative arrangement, which is capable of providing a better performance after a number of iterations.

In Chapter 2, the performance of the family of classic linear detectors, such as the Minimum Mean

[1] As we mentioned in Section 2.2, the probability density function of the ST-CIRT prediction and estimation error will be sensitive to the time-variant propagation environment and to the prediction as well as estimation algorithms employed. However, in this section the ST-CIRT error imposed by ST-CIRT prediction and estimation was modelled by using a Gaussian estimation error model in order to mimic the detrimental impact of imperfect ST-CIRT on the DL-SDMA. The proposed analysis technique and the resultant solution may be applicable in diverse communication environments.

Squared Error (MMSE) detector [5] was shown to be unsatisfactory in high-throughput rank-deficient scenarios [20]. As a solution, nonlinear (NL) detectors may be used [5]. However, the typically high complexity of NL detectors [5] is often prohibitive in practical systems. Thus, Reduced Search Algorithms (RSA) may be employed for mitigating the complexity of the NL detector. A novel Optimized Hierarchy (OH) RSA-aided Maximum-Likelihood (ML) detection method was advocated in [20], which may be regarded as an advanced extension of the Complex-valued Sphere Decoding (CSD) techniques portrayed in [17]. As opposed to the CSD, the OHRSA exhibits a relatively low complexity even in highly rank-deficient scenarios and thus its employment is meritorious.

In order to further improve the performance of the OHRSA aided DL-SDMA systems, especially in rank-deficient system configurations, where the number of transmit antennas is higher than the number of receive antennas, we first characterize an iterative NML detection aided DL-SDMA system. Additionally, we will propose a precoded iterative DL-SDMA system. Our EXIT chart analysis will demonstrate in Section 3.2.3 that the convergence of the iterative decoding is improved with the aid of precoding by exchanging extrinsic information between the constituent decoders. The precoder employed is a unity-rate convolutional encoder using a single shift register stage [70]. We will demonstrate in Section 3.2.4 that the proposed precoder aided iterative DL-SDMA scheme is capable of obtaining an infinitesimally low BER. For example, the proposed system having a normalized system load of $L_s = 1.333$ - i.e. 1.333-times higher effective throughput facilitated by having 1.333 times more DL-SDMA transmitter antennas than receiver antennas - exhibits a 'turbo-cliff' at an E_b/N_0 value of 5dB and hence results in an infinitesimally low BER. By contrast, at E_b/N_0 = 5dB the equivalent system dispensing with precoding exhibits a BER in excess of 10%.

The forthcoming discussions are structured as follows. In Section 3.2.1 we outline the system model used. The portrayal of the iterative decoding algorithm is in Section 3.2.2. Our EXIT chart analysis is provided in Section 3.2.3, leading to the performance results provided in Section 3.2.4. Finally, we conclude our discourse in Section 3.2.5.

3.2.1 System Model

Based on the DL-SDMA system depicted in Section 2.1.1, we briefly summarize the structure of the DL-SDMA system considered in this chapter.

We repeat the structure of the DL-SDMA system of Section 2.1.1 in Figure 3.1, where the system comprises a BS employing M transmit antennas while it supports K MSs and each of the MSs employs N_k receive antennas. Again, we consider a flat fading MIMO channel. Consequently, each

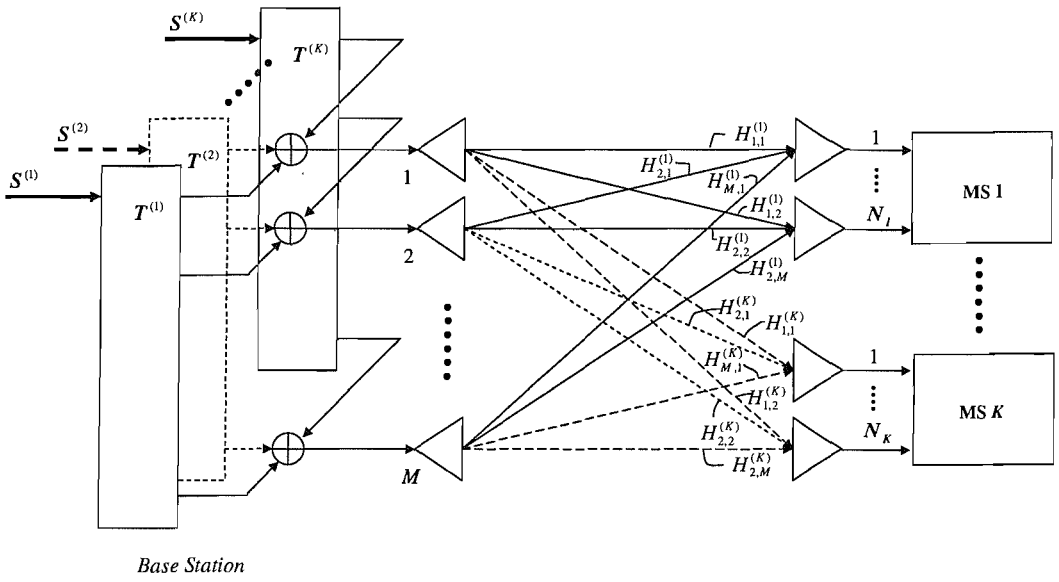

Figure 3.1: Multiuser transmission in the DL-SDMA system, repeated from Figure 2.1

link between the i-th BS transmit antenna and the j-th MS receiver antenna of the k-th user may be characterized by a complex-valued scalar channel coefficient $H^{(k)}_{i,j}$, which we assume to be an i.i.d. Gaussian random variable having a variance of unity and a mean of zero. Moreover, the MIMO channel corresponding to the k-th user may be described as an $(N_k \times M)$-dimensional complex-valued time-domain channel matrix $\boldsymbol{H}^{(k)}$, which may be defined as follows

$$\boldsymbol{H}^{(k)} = \begin{bmatrix} H^{(k)}_{1,1} & H^{(k)}_{1,2} & \cdots & H^{(k)}_{1,M} \\ H^{(k)}_{2,1} & H^{(k)}_{2,2} & \cdots & H^{(k)}_{2,M} \\ \vdots & \vdots & \cdots & \vdots \\ H^{(k)}_{N_k,1} & H^{(k)}_{N_k,2} & \cdots & H^{(k)}_{N_k,M} \end{bmatrix}. \tag{3.1}$$

Based on the system model of the DL-SDMA system portrayed in Figure 3.1, we detail the structures of the iterative detector aided DL-SDMA system and the precoder aided iterative DL-SDMA system in the following sections.

3.2.1.1 Iterative Detector Aided DL-SDMA system

As illustrated in Figure 3.2, the data bits are encoded by the channel encoder before modulation. Let $\boldsymbol{s}^{(k)} \in \mathbb{C}^{L_k \times 1}$ be a complex-valued column vector, which denotes the modulated data symbol vector to be transmitted to the k-th MS, while L_k represents the number of independent data symbols contained in $\boldsymbol{s}^{(k)}$.

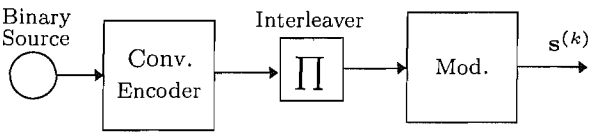

Figure 3.2: Generating the modulated data symbols $s^{(k)}$ of Figure 3.1 for the k-th user

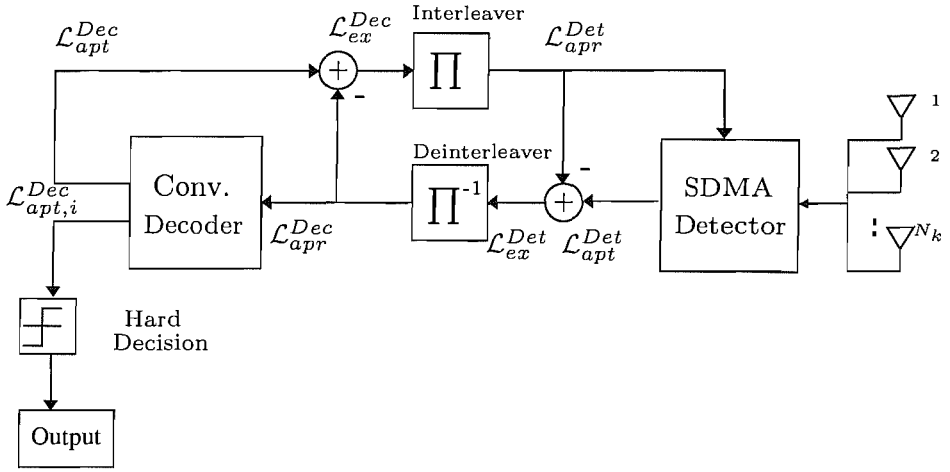

Figure 3.3: Iterative detector aided receiver design of the MS of Figure 3.1

Additionally, we define the so-called *space-time preprocessor* matrix $T^{(k)} \in \mathbb{C}^{M \times L_k}$, which was designed for the sake of eliminating the MUI [35] as detailed in Section 2.1.2. In this chapter we employ the SVD-MUT of Section 2.1.2.3, which is summarized as follows. As suggested by Choi and Murch [35], we may formulate a solution of the MUT design problem as $T^{(k)} = V^{(k)} A^{(k)}$, where $A^{(k)}$ is a nonzero $(n_k \times L_k)$-dimensional matrix and $V^{(k)}$ can be calculated using the SVD [61] of $\tilde{H}^{(k)}$ expressed as:

$$\tilde{\mathbf{H}}^{(k)} = \begin{bmatrix} \tilde{U}^{(k)} & U^{(k)} \end{bmatrix} \cdot \begin{bmatrix} \Sigma & \mathbf{0} \\ \mathbf{0} & \mathbf{0} \end{bmatrix} \cdot \begin{bmatrix} \tilde{V}^{(k)H} \\ V^{(k)H} \end{bmatrix}, \tag{3.2}$$

while

$$\tilde{\mathbf{H}}^{(k)} = \begin{bmatrix} H^{(1)} & \dots & H^{(k-1)} & H^{(k+1)} & \dots & H^{(K)} \end{bmatrix}^T. \tag{3.3}$$

Furthermore, let $r^{(k)}$ and $n^{(k)}$ be the received signal vector and noise vector associated with the k-th MS, respectively. As it was demonstrated in [35] and Section 2.1.1, once the MUI was eliminated by the MUT, the received signal vector associated with the k-th MS can be expressed in the following form

$$r^{(k)} = H^{(k)} T^{(k)} s^{(k)} + n^{(k)}, \tag{3.4}$$

where the $(N_k \times L_k)$-dimensional matrix $\boldsymbol{H}^{(k)}\boldsymbol{T}^{(k)}$ characterizes the *effective channel* corresponding to the k-th MS.

As detailed in Section 2.1.2.3, according to Equation 3.2 the non-zero matrices $\boldsymbol{T}^{(k)}$ exist only in the scenario, when $\tilde{\mathbf{H}}^{(k)}$ has more columns than rows. Consequently, we have to satisfy the following condition

$$M > max\left\{\sum_{i=1,i\neq k}^{K} N_i, k = 1,2,\ldots,K\right\}. \tag{3.5}$$

Moreover, the rank n_k of the null space basis $\mathbf{V}^{(k)}$ may be expressed as

$$n_k = M - \sum_{i=1,i\neq k}^{K} N_i. \tag{3.6}$$

Observe that the particular value of n_k will directly affect the spatial multiplexing gain achievable by the system as detailed in Section 2.2.1. In the following discussions, we assume $L_k = n_k$ in order to obtain the maximum spatial multiplexing gain.

As seen in Figure 3.3, the OHRSA aided SDMA detector, which has been discussed in the previous chapter, constitutes the first stage of the receiver. Iterative decoding is carried out by exchanging extrinsic information between the OHRSA aided SDMA detector and the channel decoders. Figure 3.3 illustrates the iterative receiver's structure. The further discussion of iterative decoding will be presented in Section 3.2.2.

3.2.1.2 Precoder Aided Iterative DL-SDMA system

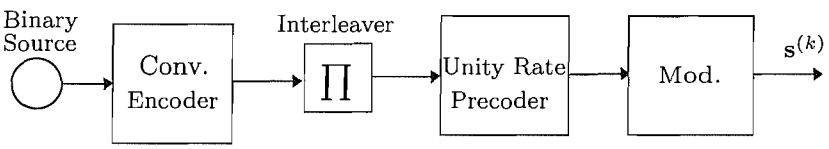

Figure 3.4: Generating the precoded data symbols $s^{(k)}$ of Figure 3.1 for the k-th user

In the structure of the precoder aided iterative DL-SDMA system, the data bits are encoded by both the channel encoder and the unity-rate precoder before modulation as illustrated in Figure 3.4. More explicitly, the unity-rate precoder is a convolutional encoder using a single shift register stage [70].

Again, let $s^{(k)} \in \mathbb{C}^{L_k \times 1}$ be a complex-valued column vector, which denotes the precoded data symbol vector to be transmitted to the k-th MS, while L_k represents the the number of independent data symbols contained in $s^{(k)}$. Similarly, the *space-time preprocessor* matrix $\boldsymbol{T}^{(k)} \in \mathbb{C}^{M \times L_k}$ will be

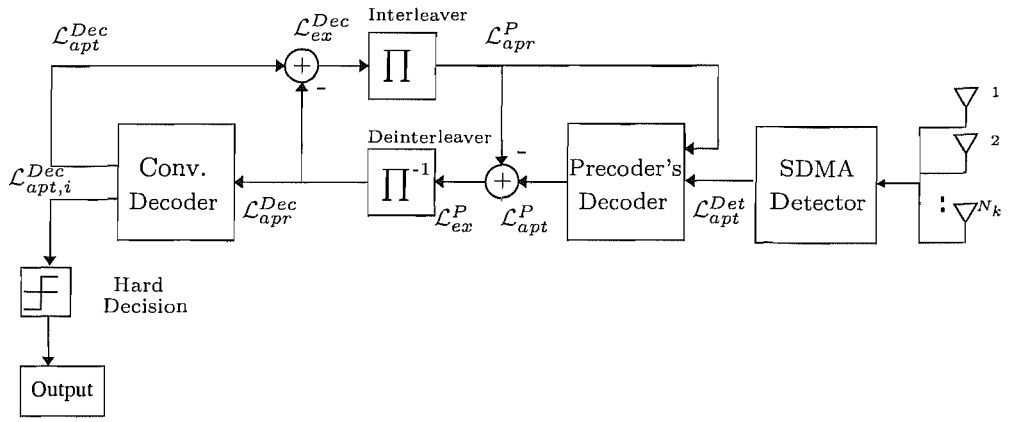

Figure 3.5: Iteratively decoded receiver design of the MS of Figure 3.1

employed to eliminate the MUI [35] as summarized in Section 3.2.1.1. Each column-vector $s^{(k)}$ is multiplied by the STP matrix $T^{(k)}$ and combined with the other users' signals before being transmitted via M transmitter's antennas as illustrated in Figure 3.1.

As seen in Figure 3.5, the OHRSA aided SDMA detector, which has been discussed in Section 2.2.2, constitutes the first stage of the receiver. Iterative decoding of the precoder aided iterative DL-SDMA system is carried out by exchanging extrinsic information between the unity-rate precoder's decoder and the channel decoders. Figure 3.5 illustrates the iterative receiver's structure. The further discussion of iterative decoding will be presented in Section 3.2.2.

3.2.2 Iterative Decoding

3.2.2.1 Iterative Detector Aided DL-SDMA

In the iterative detector aided DL-SDMA system of Section 3.2.1.1, the iterative decoding is carried out by exchanging extrinsic information between the OHRSA aided SDMA detector and the channel decoder. Figure 3.3 illustrates the iterative receiver structure, where $\mathcal{L}$ represents the Log Likelihood Ratios (LLRs). The super-script *Det* indicates the detector, while *Dec* represents the channel decoder. The subscripts *apr*, *ex* and *apt* indicate *a priori*, extrinsic and *a posteriori* LLRs, respectively. First, the OHRSA aided SDMA detector generates the soft-bit output $\mathcal{L}_{apt}^{Det}$ as detailed in [20] and Section 2.2.3. Then the extrinsic information $\mathcal{L}_{ex}^{Det}$ to be used by the channel decoder is obtained from $\mathcal{L}_{apt}^{Det}$ by subtracting the *a priori* LLR values $\mathcal{L}_{apr}^{Det}$. Then, the channel decoder processes $\mathcal{L}_{apr}^{Dec}$, which was generated by the deinterleaver Π^{-1} from $\mathcal{L}_{ex}^{Det}$, and outputs the *a posteriori* LLRs $\mathcal{L}_{apt}^{Dec}$ to be used as a feedback for the next decoding iteration. When the iterations are curtailed, the channel decoder

outputs $\mathcal{L}_{apt,i}^{Dec}$, which represents the hard decision based data bits.

3.2.2.2 Precoder Aided Iterative DL-SDMA

In the precoder aided iterative DL-SDMA system of Section 3.2.1.2, the iterative decoding is carried out by exchanging extrinsic information between the unity-rate precoder and the channel decoder. Figure 3.5 illustrates the iterative receiver structure, where $\mathcal{L}$ represents the Log Likelihood Ratios (LLRs). Simiarly, the super-script *Det* indicates the detector, *P* denotes the precoder, while *Dec* represents the channel decoder. The subscripts *apr*, *ex* and *apt* indicate *a priori*, extrinsic and *a posteriori* LLRs, respectively. First, the unity-rate precoder's decoder processes the soft-bit output $\mathcal{L}_{apt}^{Det}$ of the detector generated in the previous stage and the *a priori* LLR values $\mathcal{L}_{apr}^{P}$, which are appropriately arranged by the interleaver Π are produced from the extrinsic information $\mathcal{L}_{ex}^{Dec}$ of the channel decoder. Then the extrinsic information $\mathcal{L}_{ex}^{P}$ to be used by the unity-rate precoder is obtained from $\mathcal{L}_{apt}^{P}$ by subtracting the *a priori* LLR values $\mathcal{L}_{apr}^{P}$. Then, the channel decoder processes $\mathcal{L}_{apr}^{Dec}$, which was generated by the deinterleaver Π^{-1} from $\mathcal{L}_{ex}^{P}$, and outputs the *a posteriori* LLRs $\mathcal{L}_{apt}^{Dec}$ to be used as a feedback for the next decoding iteration. When the iterations are curtailed, the channel decoder outputs $\mathcal{L}_{apt,i}^{Dec}$, which represents the hard decision based data bits. In the following section, we will use EXIT charts [68] in our detailed investigations of the iterative receiver.

3.2.3 EXIT Chart Analysis

The system used the low-complexity OHRSA detector employed 4-QAM and half-rate Recursive Systematic Convolutional (RSC) coding [22] having a memory of three and an octal generator polynomial of G = [5 7]. The system configuration and the corresponding normalized system loads are detailed in Table 3.1.

M	6	7	8	9	10
L	2	3	4	5	6
L_s	1	1.167	1.333	1.5	1.667

Table 3.1: System configurations investigated in Figure 3.7

According to [68], if the extrinsic transfer curves intersect at the $(I_{apr}^{det}, I_{ex}^{det}) = (1.0, 1.0)$ point in Figure 3.6 and an open EXIT tunnel exists at a certain value of E_b/N_0, then the system will exhibit an infinitesimally low Bit Error Ratio (BER). In Figure 3.6, the system operates at an E_b/N_0 of 7dB. Observe that the non-precoded DL-SDMA system of Section 3.2.1.1 does not exhibit an

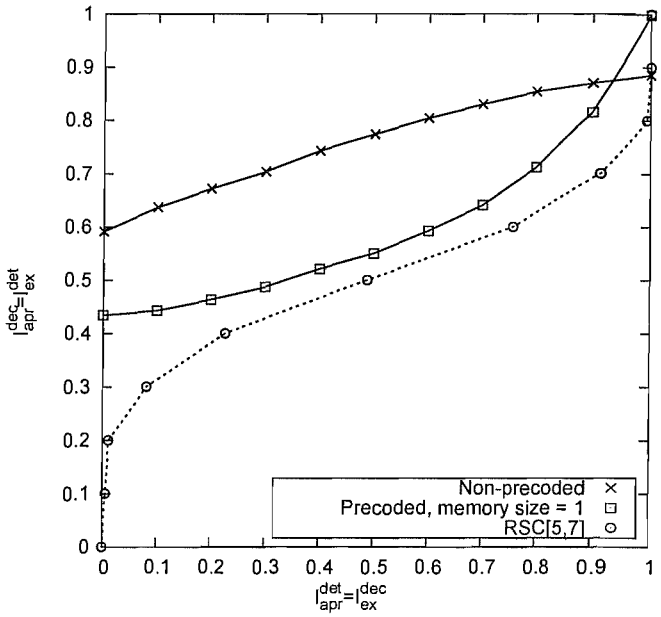

Figure 3.6: EXIT chart comparison of the non-precoded and precoded DL-SDMA systems of Figure 3.1 having a normalized system load of $L_s = 1.333$ at $E_b/N_0 = 7$ dB and the system configuration of $(M, L_k) = (8, 4)$ as seen in Table 3.1. This system supports $K = 3$ users, where each user employs $N_k = 2$ receive antennas. The channel model was a uncorrelated flat fading MIMO channel. The other system parameters employed are listed in Table 3.2.

open EXIT tunnel, despite emerging from a higher I_{apr}^{dec} point than its precoded counterpart. More explicitly, its EXIT curve intersects with that of the rate-0.5 RSC[5,7] code at a point lower than $(I_{apr}^{det}, I_{ex}^{det}) = (1.0, 1.0)$. Therefore, the non-precoded DL-SDMA system operating at an E_b/N_0 of 7dB is expected to exhibit a rather high BER. On the other hand, at the same E_b/N_0 of 7 dB the precoded system of Section 3.2.1.2 exhibits an open EXIT tunnel, despite emerging from a lower I_{apr}^{dec} point, since it intersects the EXIT curve of the rate-0.5 RSC[5,7] code at the $(I_{apr}^{det}, I_{ex}^{det}) = (1.0, 1.0)$ point. Hence the precoded DL-SDMA system has a better iterative decoding convergence than the non-precoded system, hence consequently exhibiting a better BER performance.

Table 3.2: System Parameters

Channel Encoder	rate-0.5 RSC [5,7]
Interleaver length	10^5 bits
Modulation	4QAM
Number of users	$K = 3$
Number of transmit antennas	$M = 6$
Number of data symbols in the transmit signal vector for the k-th user	$L_k = 2$, for $k = 1, 2, 3$.
Number of receive antennas of each MS	$N_k = 2$, for k=1,2,3.

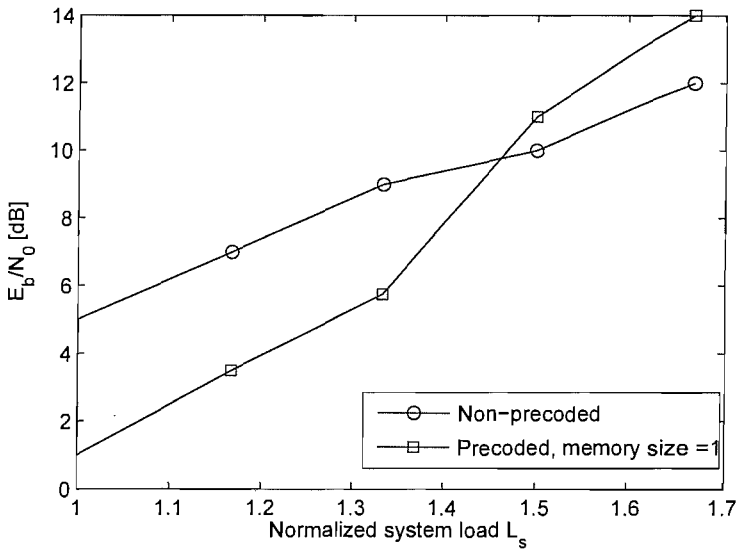

Figure 3.7: The E_b/N_0 required by both the non-precoded and precoded DL-SDMA systems of Figure 3.1 to exhibit an open EXIT tunnel at different system loads. The five points recorded correspond to the system configurations of $(M, L_k) = [(6,2)(7,3)(8,4)(9,5)(10,6)]$ seen in Table 3.1. The channel model was a uncorrelated flat fading MIMO channel. The other system parameters employed are listed in Table 3.2.

Figure 3.7 shows the minimum E_b/N_0 required by both the non-precoded and the precoded DL-SDMA systems in order to exhibit open EXIT tunnels at different normalized system loads. When the systems operate at those E_b/N_0s, we expect to see the emergence of turbo cliffs in the corresponding BER curves. As observed in Figure 3.7, a lower E_b/N_0 value is required for the precoded DL-SDMA system of Section 3.2.1.2 to exhibit a turbo cliff than by the non-precoded DL-SDMA system of Section 3.2.1.1, when the normalized system load is lower than $L_s = 1.333$. Beyond the corresponding

E_b/N_0 values the systems are capable of operating at an infinitesimally low BER. By contrast, when the normalized system load is increased beyond 1.333, the precoded system requires a high E_b/N_0 value for maintaining an open EXIT tunnel associated with an infinitesimally low BER.

Figure 3.8 illustrates the actual decoding trajectory of the proposed precoded and OHRSA decoded DL-SDMA system of Section 3.2.1.2 using interleaver lengths of 10^4 and 10^5 bits. Again, the system operates at an E_b/N_0 of 7 dB and $L_s = 1.333$. As expected, the interleaver length substantially affects the number of iterations required for maintaining an open EXIT tunnel. While the precoded DL-SDMA OHRSA detector using an interleaver length of 10^4 bits needs $I = 13$ iterations for maintaining an open EXIT tunnel, at an interleaver length of 10^5 bits only $I = 8$ iterations are required.

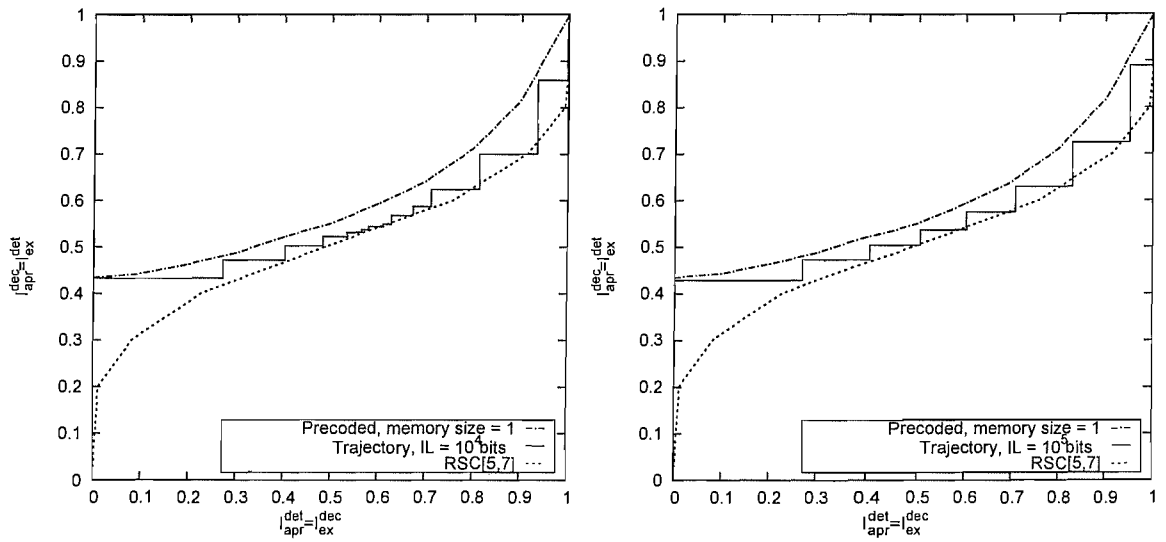

(a) (b)

Figure 3.8: EXIT chart comparison of the precoded DL-SDMA systems of Figure 3.1 using different lengths of interleavers with a normalized system load of $L_s = 1.333$ at $E_b/N_0 = 7$ dB and the system configuration of $(M, L_k) = (8, 4)$ as seen in Table 3.1. These systems support $K = 3$ users, where each user employs $N_k = 2$ receive antennas. The interleaver lengths (IL) used are 10^4 for (a) and 10^5 for (b). The channel model was a uncorrelated flat fading MIMO channel. The other system parameters employed are listed in Table 3.2.

In general, the narrower the EXIT tunnel, the closer the system operates to the Shannon limit [71] and hence a high number of iterations is required for reaching the point of decoding convergence. As shown in Figure 3.9, the system operating at an E_b/N_0 of 7 dB needs $I = 8$ iterations to reach decoding convergence. At the same time, upon simply increasing the E_b/N_0 by 1 dB, the number of

iterations required is down to $I = 4$.

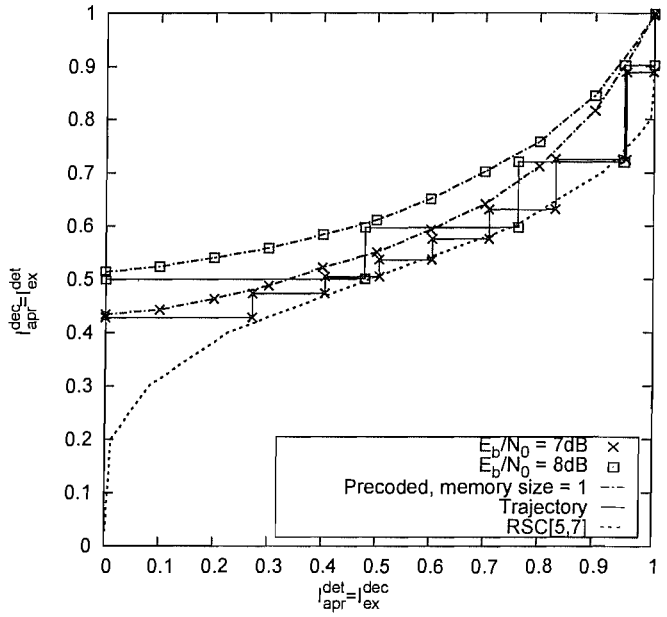

Figure 3.9: EXIT chart comparison of the precoded DL-SDMA systems of Figure 3.1 with a normalized system load of $L_s = 1.333$ at a E_b/N_0 of 7dB and 8dB and the system configuration of $(M, L_k) = (8, 4)$ as seen in Table 3.1. These systems support $K = 3$ users, where each user employs $N_k = 2$ receive antennas. The length of the interleaver used is 10^5. The channel model was a uncorrelated flat fading MIMO channel. The other system parameters employed are listed in Table 3.2.

3.2.4 Performance Results

Finally, in Figure 3.10 we characterize the achievable BER performance of the precoded DL-SDMA system of Section 3.2.1.2 employing the OHRSA detector. Again, we employed 4-QAM protected by the half-rate RSC[5,7] code having a memory of three and using a 10^5-bit interleaver. The channel model was a flat-fading MIMO channel. All system configurations considered supported $K = 3$ users. Finally, for the sake of convenience, we assume $L_1 = L_2 = \cdots = L_K = L$.

Figure 3.10 portrays our BER performance results corresponding to two different system load scenarios, namely to $L_s = 1.0$ and 1.333. The system configuration and the corresponding normalized system loads are detailed in Table 3.1. For each system load scenario, we characterize the BER performance of the precoded DL-SDMA system invoking the OHRSA detector along with that of the precoded DL-SDMA system employing the MMSE detector. The non-precoded DL-SDMA system employing the OHRSA detector is also characterized in Figure 3.10 as a benchmarker. In the full-

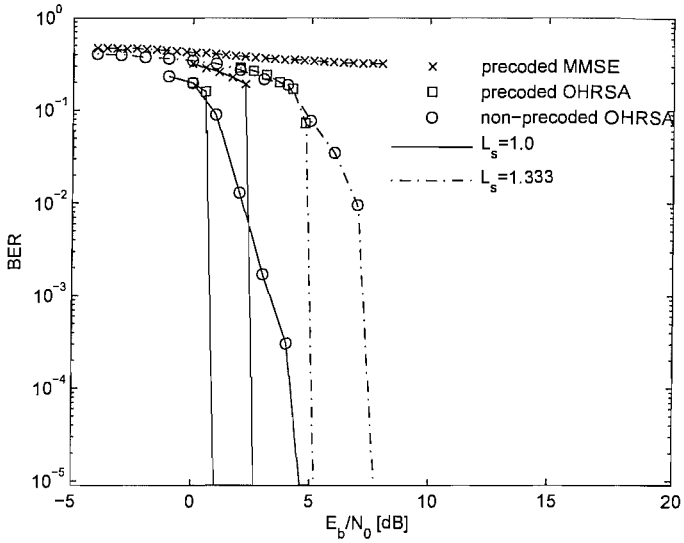

Figure 3.10: BER performance of the precoded DL-SDMA scheme of Figure 3.1 having a normalized system load of $L_s = 1.0$ and 1.333 as seen in Table 3.1. Our system supports $K = 3$ users, where each user employs $N_k = 2$ receive antennas. The length of the interleaver used is 10^5 and $I = 10$ iterations are employed by the iterative decoder. The channel model was a uncorrelated flat fading MIMO channel. The other system parameters employed are listed in Table 3.2.

loaded scenario of $L_s = 1.0$ all three detectors exhibit an adequate performance. However, the precoded DL-SDMA system using both the MMSE and the OHRSA detectors outperforms the non-precoded OHRSA aided system. The precoded DL-SDMA system using the MMSE detector has a 2 dB E_b/N_0 gain over the non-precoded DL-SDMA OHRSA aided system at a target BER of 10^{-5}. At the same time, the E_b/N_0 required by the precoded DL-SDMA OHRSA aided system for maintaining a target BER of 10^{-5} is 2 dB less than that of the MMSE detector.

Furthermore, when the normalized system load is increased to $L_s = 1.333$, which corresponds to a highly rank-deficient scenario, the MMSE detector fails to attain a satisfactory BER performance. On the other hand, both the non-precoded and precoded DL-SDMA OHRSA aided systems perform well. However, the E_b/N_0 needed by the OHRSA aided precoded system for achieving a target BER of 10^{-5} is about 2 dB lower than that necessitated by the OHRSA aided non-precoded system for attaining the same target BER. At an E_b/N_0 of 5dB the precoded OHRSA-aided DL-SDMA system exhibits a turbo cliff and results in an infinitesimally low BER, while the non-precoded system supporting the same system load exhibits a BER in excess of 10%.

3.2.5 Conclusion

Although the uplink performance of SDMA systems is well documented, there is a paucity of DL-SDMA studies and no indepth studies can be found in the open literature for high-throughput rank-deficient systems. In this scenario low-complexity linear detectors, such as the MMSE detector exhibit a high residual error floor, while most NL detectors exhibit an excessive complexity. Hence the near-ML OHRSA detector was adopted for employment in the DL and it was amalgamated with an iteratively detected unity-rate precoder. This amalgamated and iteratively detected rank-deficient system was capable of achieving an infinitesimally low BER at a normalized system load of $L_s = 1.333$ and $E_b/N_0 = 5dB$, when supporting $K = 3$ users, each employing $N_k = 2$ receiver antennas over a flat fading MIMO channel.

3.3 Iterative Downlink SDMA Systems Using Imperfect Channel State Information

In this section, we analyze the precoder aided iterative downlink SDMA system of Section 3.2.1.2 employing imperfect ST-CIRT with the aid of EXIT charts. We will show that the Precoder aided Iterative DL-SDMA (PI-DL-SDMA) system remains capable of maintaining an infinitesimally low BER, despite using an imperfect ST-CIRT. A further novel feature of the PI-DL-SDMA system is that we design an IrRegular Convolutional Code (IRCC) with the aid of EXIT chart analysis for creating an open EXIT tunnel between the inner decoder's and outer decoder's EXIT curve at a reduced E_b/N_0 value and hence maintain an infinitesimally low BER.

In the considered PI-DL-SDMA systems, the transmitter of the system adopted the spatio-temporal DL pre-processing technique of [35] for eliminating the effects of MUI, which may also be termed as a MUT technique. The philosophy of this MUT is that in the presence of perfect knowledge of the individual users' ST-CIR to be encountered, the MUT scheme exploits the unique, user-specific ST-CIRs accurately differentiating the user's transmitted signals.

Given that the MUT essentially eliminated the MUI, the low-complexity soft-out MMSE detector of [5] may be invoked by the PI-DL-SDMA multiuser system for the full-loaded system configuration considered in this section. As mentioned, a unity-rate convolutional encoder using a single shift register stage [70] is employed for precoding. As it was demonstrated in previous section and [43], the performance of iterative decoding is substantially improved, when carried out by exchanging extrinsic information between the unity-rate precoder's decoder and the channel decoder.

Again, when the idealized scenario of having perfect knowledge of the ST-CIRT is assumed, our system employing the spatio-temporal pre-processing technique of [35] becomes capable of separating the signals destined for the different users at the base station's DL transmitter and hence results in MUI-free performance. However, as we mentioned in Section 3.1, the accuracy of the ST-CIRT may be expected to depend on the specific channel prediction algorithms [53, 54] and channel estimation techniques [5] employed. Although the statistics of the ST-CIRT prediction and estimation error will be sensitive both to the time-variant propagation environment and to the prediction as well as estimation algorithms employed, for the sake of convenience the ST-CIRT error imposed by ST-CIRT prediction and estimation was modelled by using a Gaussian estimation error mode in this section. Again, the proposed analysis method and the resultant solution may apply to diverse communication environments.

We will demonstrate using EXIT chart analysis that as expected, the area under the inner decoder's EXIT curve – where we refer to the MMSE detector concatenated with the precoder's decoder as the inner decoder – is reduced upon increasing the ST-CIRT prediction error variance, which may result in the closure of the decoder's open EXIT tunnel. More explicitly, once the inner decoder's EXIT curve crosses the outer decoder's owing to ST-CIRT errors, the system exhibits a high residual error rate. In order to improve the achievable performance of our system proposed in [43] we design sophisticated IrRegular Convolutional Codes (IRCC) [69] using several different-rate component codes for producing a better-matching outer EXIT curve, which allows us to improve the attainable BER performance.

The rest of this treatise is structured as follows. In Section 3.3.1 we outline the system model used, while in Section 3.3.2 we summarize the design of IRCCs. Our EXIT chart analysis is provided in Section 3.3.3, leading to the performance results of Section 3.3.4. Finally, we conclude our discourse in Section 3.3.5.

3.3.1 System Model

The structure of the PI-DL-SDMA system considered was described in Section 3.2.1.2 and in [43]. As detailed in Section 3.2.1, let $s^{(k)} \in \mathbb{C}^{L_k \times 1}$ be a complex-valued column vector, which denotes the precoded data symbol vector to be transmitted to the k-th MS, while L_k represents the number of independent data symbols contained in $s^{(k)}$. Additionally, we defined the so-called *space-time preprocessor* matrix $T^{(k)} \in \mathbb{C}^{M \times L_k}$, which was designed for the sake of eliminating the MUI [35]. As it was demonstrated in Section 3.2.1, once the MUI was eliminated by the MUT, the received signal vector $r^{(k)}$ associated with the k-th MS can be expressed as Equation 3.4, which we rewrite here,

$$r^{(k)} = H^{(k)} T^{(k)} s^{(k)} + n^{(k)}, \tag{3.7}$$

where the $(N_k \times L_k)$-dimensional matrix $H^{(k)} T^{(k)}$ characterizes the *effective channel* corresponding to the k-th MS.

Furthermore, in this section the MMSE aided SDMA detector constitutes the first stage of the receiver of Figure 3.5. Iterative decoding is carried out by exchanging extrinsic information between the unity-rate precoder's decoder and the channel decoder, which is the IRCC decoder in this section.

Let us now consider the impact of imperfect ST-CIRT. More specifically, let $H^{(k)}_{pred}$ denote the predicted channel of the k-th MS, which is modeled as $H^{(k)}_{pred} = H^{(k)} + \varepsilon_k$, where ε_k is assumed to be the Gaussian channel prediction error of the k-th MS. When the BS uses the predicted channel

$H_{pred}^{(i)}, i = 1,2,\cdots,k-1,k+1,\cdots,K$ to generate the space-time preprocessor matrix $\tilde{T}^{(k)}$ for transmission to the k-th MS, the system becomes unable to entirely eliminate the MUI and hence the resultant residual MUI contaminates the received signal of the k-th MS according to

$$r^{(k)} = H^{(k)}\tilde{T}^{(k)}s^{(k)} + I_{MUI}(\varepsilon_i, i = 1,2,\cdots,k-1,k+1,\cdots,K) + n^{(k)}, \tag{3.8}$$

where the MUI term $I_{MUI}(\varepsilon_i, i = 1,2,\cdots,k-1,k+1,\cdots,K)$ is a function of ε_i.

When using the space-time preprocessor matrix $\tilde{T}^{(k)}$, the closed-form analytical formula is not available at the moment of writing for deriving the MUI in terms of the channel prediction error ε_i. Hence we used Monte Carlo simulations combined with semi-analytical EXIT charts to characterize the impact of channel prediction errors ε_i, which is assumed to be a Gaussian distributed random variable having a variance with $\sigma^2_{ST-CIRT}$ and a zero mean. Nonetheless, in order to establish a benchmarker, initially we assume that the receiver has perfect ST-CIRT.

3.3.2 Design of Irregular Convolutional Codes

In order to design a near-capacity system, the outer decoder's EXIT chart has to match the inner decoder 's EXIT curve as accurately as possible, which results in an infinitesimally low EXIT-chart-tunnel area [71]. We employ IRCCs for solving this curve-fitting problem. Tüchler and Hagenauer [69,72] proposed the employment of IRCCs, which are constituted by a family of convolutional codes having different code rates. They were specifically designed with the aid of EXIT charts, for the sake of improving the convergence behaviour of iteratively decoding systems. To be specific, an IRCC is constructed from a family of P subcodes. First a rate-r convolutional mother code C_1 is selected and the $(P-1)$ other subcodes C_j of rate $r_j > r$ are obtained by puncturing. Let l denote the total number of encoded bits generated from the κ uncoded information bits. Each subcode encodes a certain fraction $\alpha_j r_j l$ of the original uncoded information bits and generates $\alpha_j l$ encoded bits. Given the target overall average code rate of $R \in [0,1]$, the weighting coefficient α_j has to satisfy:

$$1 = \sum_{j=1}^{P} \alpha_j, R = \sum_{j-1}^{P} \alpha_j r_j, \text{and } \alpha_j \in [0,1], \forall j. \tag{3.9}$$

For example, the EXIT functions of the 17 subcodes used in [69] are shown in Figure 3.11. In order to solve this curve-fitting problem, our optimized weighting coefficients are generated with the aid of the algorithm proposed by Tüchler and Hagenauer [69].

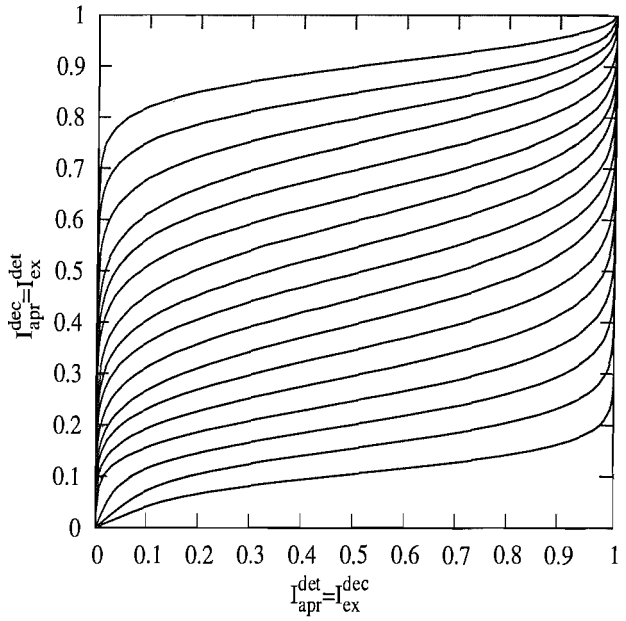

Figure 3.11: EXIT functions of the 17 subcodes in [69]

3.3.3 EXIT Chart Analysis for Imperfect ST-CIRT

In this section, we provide the EXIT chart analysis of the PI-DL-SDMA system in the presence of imperfect ST-CIRT. We adapt the IRCCs to match the inner decoder's EXIT curve in order to maintain a marginally open tunnel, which implies having both an infinitesimally low open-tunnel area as well as a low BER at the target E_b/N_0 value.

Figure 3.12 characterizes the impact of different ST-CIRT prediction error variances $\sigma^2_{ST-CIRT}$ on the system invoking the rate-0.5 RSC [5,7] channel decoder of [43] and operating at an E_b/N_0 of 7dB. The value of $\sigma^2_{ST-CIRT}$ characterized in Figure 3.12 is ranging from 0 to 0.2, where $\sigma^2_{ST-CIRT} = 0$ represents a perfect ST-CIRT. Observe that when $\sigma^2_{ST-CIRT}$ increases, the corresponding EXIT curves of the inner decoder move closer to the curve of the RSC [5,7] outer channel decoder, potentially crossing the EXIT curve of the outer decoder. When the value of $\sigma^2_{ST-CIRT}$ is less than 0.1, an open tunnel appears between the inner and outer EXIT curves. By contrast, the system fails to exhibit an open tunnel, when the value of $\sigma^2_{ST-CIRT}$ increases to 0.15.

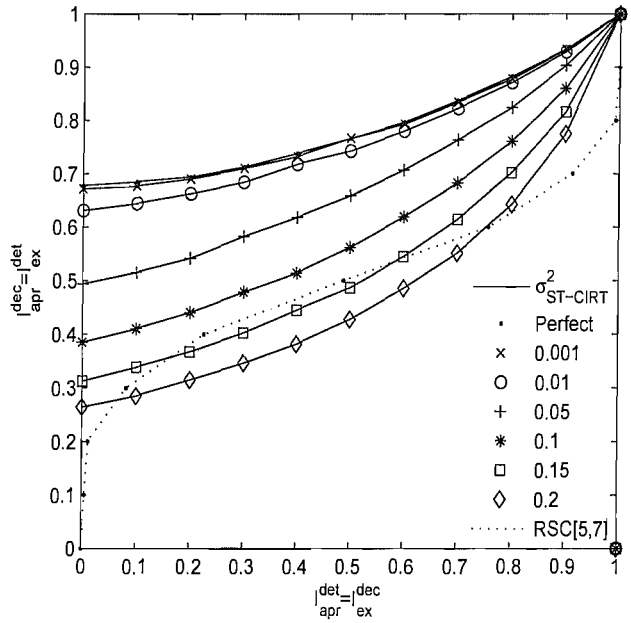

Figure 3.12: EXIT chart analysis of the PI-DL-SDMA system of Figure 3.5 employing rate-0.5 RSC [5,7]. The system operates at an E_b/N_0 of 7dB and uses the parameters of Table 3.3. The value of $\sigma^2_{ST-CIRT}$ assumes $0, 0.001, 0.01, 0.05, 0.1, 0.15$ to 0.2.

Table 3.3: System Parameters

Channel Encoder	rate-0.5 RSC or rate-0.5 IRCC
Interleaver length	10^5 bits
Modulation	4QAM
Number of users	$K = 3$
Number of transmit antennas	$M = 6$
Dimension of transmitted signal vector of the k-th user	$L_k = 2$, for $k = 1, 2, 3$.
Number of receive antennas of the k-th user	$N_k = 2$, for k=1,2,3.

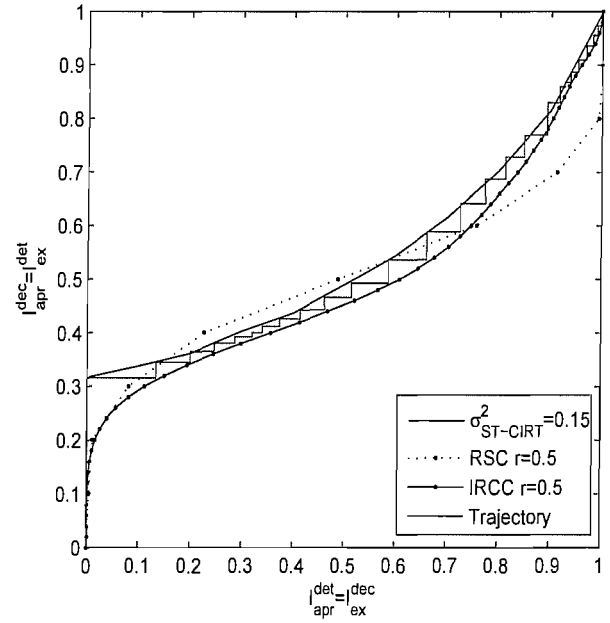

Figure 3.13: EXIT chart analysis of the PI-DL-SDMA system of Figure 3.5 employing rate-0.5 IRCC for $\sigma^2_{ST-CIRT} = 0.15$. The system operates at an E_b/N_0 of 7dB and uses the parameters of Table 3.3.

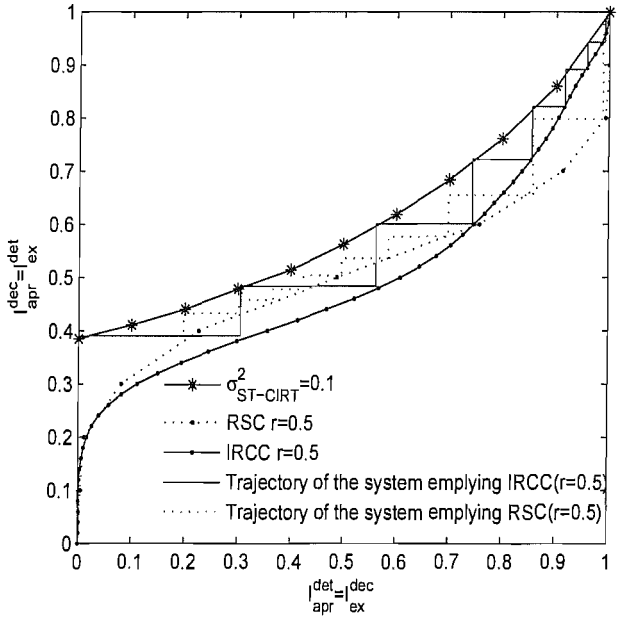

Figure 3.14: The EXIT chart convergence behavior of the PI-DL-SDMA system of Figure 3.5 employing rate-0.5 RSC [5,7] and rate-0.5 IRCC for $\sigma^2_{ST-CIRT} = 0.1$. The system using the parameters of Table 3.3 operates at an E_b/N_0 of 7dB.

Clearly, if the value of $\sigma^2_{ST-CIRT}$ reaches 0.15, it becomes necessary to design a better-fitting outer curve. Hence, we employ the IRCCs briefly introduced in Section 3.3.2 in order to obtain a better fitting outer curve. Using the iterative algorithm of [69], we designed a rate-0.5 IRCC employing the weighting coefficients $\alpha = [0, 0, 0, 0, 0, 0, 0.574825, 0.167428, 0, 0, 0, 0.0291502, 0.149874, 0, 0, 0, 0.0787566]$. The resultant EXIT chart is shown in Figure 3.13, which is seen to exhibit an open tunnel. The recorded iterative decoding trajectory seen in Figure 3.13 more accurately characterizes the convergence behavior of the system. When using $I = 25$ iterations, the system employing a rate-0.5 IRCC exhibits an open tunnel, which implies that an infinitesimally low BER is expected at the $E_b/N_0 = 7dB$. We will provide the corresponding BER performance results in the next section.

Figure 3.14 characterizes the convergence behavior of the system at $\sigma^2_{ST-CIRT} = 0.1$, where the system employing the rate-0.5 RSC exhibits a marginally open tunnel. The iterative decoding trajectory of the system employing the rate-0.5 RSC was recorded using dotted lines in Figure 3.14 and requires $I = 13$ iterations for approaching an infinitesimally low BER, because the EXIT-tunnel exhibits a constriction. By contrast, the recoded decoding trajectory of the system employing a rate-0.5 IRCC requires only $I = 7$ iterations for maintaining an open tunnel, as shown using solid lines, since the tunnel is more widely open.

3.3.4 Performance Results

In this section, we provide the corresponding BER performance results, showing their reasonable consistency with our EXIT chart analysis. The system parameters used are listed in Table 3.3.

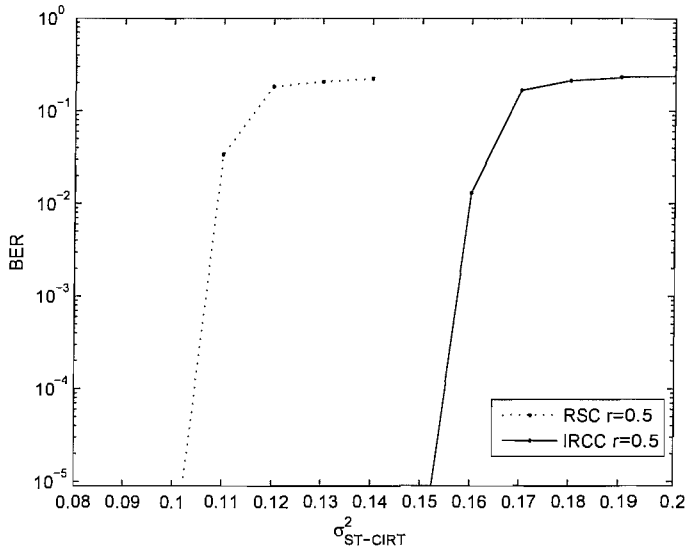

Figure 3.15: BER performance of the PI-DL-SDMA system of Figure 3.5 operating at an E_b/N_0 of 7dB with different values of $\sigma^2_{ST-CIRT}$, ranging from 0.08 to 0.2. The rate-0.5 IRCC and rate-0.5 RSC are tested with the system, using 8 decoding iterations. The channel model was a flat fading MIMO channel and the parameters of Table 3.3 were used.

In Figure 3.13, we already showed that the rate-0.5 IRCC exhibits an open tunnel for the system having $\sigma^2_{ST-CIRT} = 0.15$. However, it is beneficial to explore the tolerable range of the ST-CIRT prediction variance of $\sigma^2_{ST-CIRT}$ for the system employing the rate-0.5 IRCC. In Figure 3.15, we portray the BER performance of the system operating at an E_b/N_0 of 7dB for different ST-CIRT variances $\sigma^2_{ST-CIRT}$, ranging from 0.08 to 0.20. As illustrated in Figure 3.15, the system employing the rate-0.5 IRCC and $I = 25$ decoding iterations is capable of providing an infinitesimally low BER for $\sigma^2_{ST-CIRT} = 0.15$. The BER performance of the system employing rate-0.5 RSC is also provided as a benchmarker. It appears that the system employing the rate-0.5 RSC using $I = 25$ decoding iterations exhibits an infinitesimally low BER for $\sigma^2_{ST-CIRT} = 0.1$.

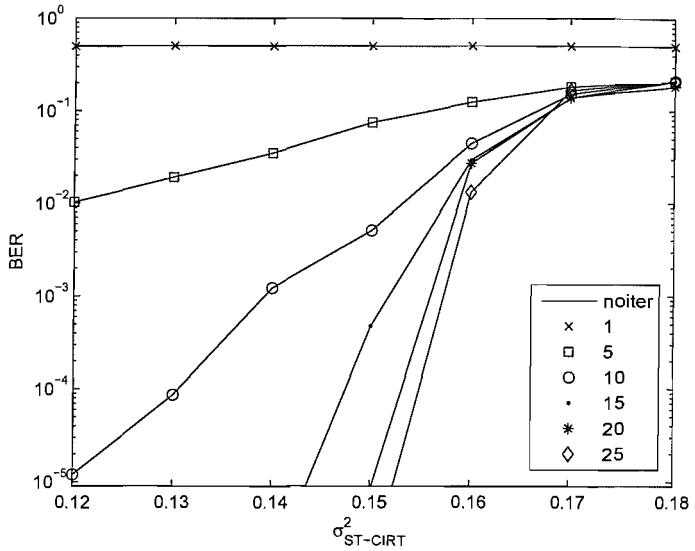

Figure 3.16: BER performance of the PI-DL-SDMA system of Figure 3.5 invoking rate-0.5 IRCC operating at an E_b/N_0 of 7dB for different values of $\sigma^2_{ST-CIRT}$, ranging from 0.12 to 0.18. The BER performance results of the system with different numbers of decoding iterations are compared. The channel model was a flat fading MIMO channel and the parameters of Table 3.3 were used.

Figure 3.16 portrays the BER performance of the system employing the rate-0.5 IRCC at different numbers of decoding iterations. We observed that when the number of decoding iterations increases, the system reaches an infinitesimally low BER for $\sigma^2_{ST-CIRT} = 0.15$. This shows the consistency with Figure 3.13, which also exhibits an open tunnel for $I = 25$.

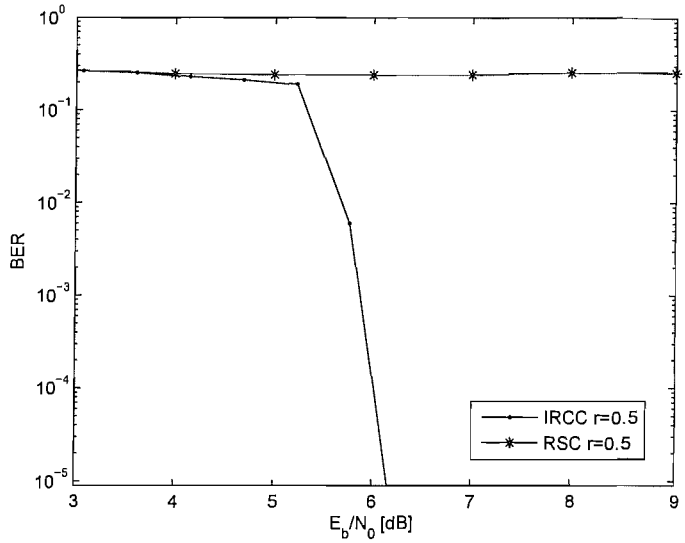

Figure 3.17: BER performance of the PI-DL-SDMA system of Figure 3.5 invoking the rate-0.5 IRCC using I=25 decoding iterations for $\sigma^2_{ST-CIRT} = 0.15$. The BER performance of the system invoking a rate=0.5 RSC using I=25 decoding iterations is provided as a benchmarker. The channel model was a flat fading MIMO channel and the parameters of Table 3.3 were used.

Figure 3.17 portrays the attainable BER performance of the system employing the rate-0.5 IRCC in conjunction with I=25 decoding iterations for $\sigma^2_{ST-CIRT} = 0.15$. While Figure 3.13 exhibits an open tunnel for $I = 25$ and $\sigma^2_{ST-CIRT} = 0.15$ at the target of $E_b/N_0 = 7dB$, which implies an infinitesimally low BER for our system operating at an E_b/N_0 of at least $7dB$, the results shown in Figure 3.17 demonstrate that an even lower E_b/N_0 is sufficient. We observed that the system employing the rate-0.5 IRCC reaches an infinitesimally low BER at the E_b/N_0 value about 6.3 dB. By contrast, the system employing a rate-0.5 RSC exhibits a high BER in the excess of 10% at the same E_b/N_0.

3.3.5 Conclusion

In this section, we investigated the impact of imperfect ST-CIRT on our PI-DL-SDMA system with the aid of EXIT charts. In this study, the impact of imperfect ST-CIRT was quantified in terms of the ST-CIRT prediction error variance, which adequately characterizes the quality of the ST-CIRT for a Gaussian error model. We found that increasing variance of the ST-CIRT estimation error, namely $\sigma^2_{ST-CIRT}$, results in a narrower EXIT-tunnel for system, which would either require an increased number of iterations to open the EXIT-tunel or an increased E_b/N_0 value. As an alternative solution, a novel IRCC scheme was designed for matching the outer decoder's EXIT curve to that of the inner

decoder for obtaining an open EXIT-tunnel. Matching the outer decoder's EXIT curve to that of the inner decoder for the sake of minimizing the EXIT tunnel's area allowed us to operate at a reduced E_b/N_0 value.

3.4 Summary and Conclusions

In Section 3.2, we introduced an iterative DL-SDMA system, which was then further improved with the aid of a unity-rate convolutional encoder using a single shift register stage [70]. We have shown in Figure 3.6 that using EXIT chart analysis the convergence of the iterative decoder was improved with the aid of precoding by exchanging extrinsic information between the constituent decoders. We also demonstrated that the OHRSA aided iterative DL-SDMA system was particularly suitable for the rank-deficient scenario, as shown in Figure 3.10. Quantitatively, the proposed system having a normalized system load of $L_s = 1.333$ - i.e. 1.333-times higher effective throughput facilitated by having 1.333 times more DL-SDMA transmitters than receivers - exhibits a 'turbo-cliff' at an E_b/N_0 value of 5dB and hence results in an infinitesimally low BER. By contrast, at E_b/N_0 = 5dB the equivalent system dispensing with precoding exhibits a BER in excess of 10%. In Table 3.4, we summarized the E_b/N_0 values required by the system to reach a target BER of 10^{-5} based on Figure 3.10. As seen in Table 3.4, the precoded OHRSA DL-SDMA system outperformed the otherwise identical non-precoded OHRSA DL-SDMA system by about $2.5 - 3.0$ dB, when the normalized system loads were $L_s = 1.0$ and $L_s = 1.333$.

Normalized System Load L_s	1.0	1.333
Precoded OHRSA DL-SDMA	2 dB	5 dB
Non-precoded OHRSA DL-SDMA	5 dB	7.5 dB

Table 3.4: The E_b/N_0 values required by the iterative DL-SDMA system to reach a target BER of 10^{-5} based on Figure 3.10.

In Section 3.3, we investigated the impact of imperfect ST-CIRT quantified in terms of the channel estimation error variance, assuming that it obeys a Gaussian error model. We demonstrated that the resultant imperfect ST-CIRT inflicted an increased MUI upon each user's received signal and hence degraded the attainable performance of the system. In Figure 3.12, we observed the degradation imposed by the MUI introduced by the imperfect ST-CIRT. The higher the error variance of $\sigma^2_{ST-CIRT}$, the narrower the EXIT-tunnel of the iterative processing aided the system. As a solution, the system

may be operated either at an increased E_b/N_0 level or at an increased number of decoding iterations. We demonstrated that the IRCC aided DL-SDMA system in Section 3.3 was capable of creating an open EXIT tunnel between the inner decoder's and outer decoder's EXIT curve at a reduced E_b/N_0 value and hence achieved an infinitesimally low BER, as illustrated in Figure 3.13 and Figure 3.17.

Having introduced a two-stage iterative detection aided DL-SDMA system in this chapter, in Chapter 4 we will design three-stage iterative detection aided DL-SDMA scheme, which attains an improved BER performance, while striking a balance between the computational complexity imposed and the system performance attained.

Chapter 4

Irregular Iterative Downlink SDMA Systems

4.1 Introduction

In 1993, Berrou introduced the iterative decoding of parallel concatenated codes, referred to as"turbo codes" [6]. These iterative decoding principles were also extended to turbo equalization [22], multiuser detection [73], iterative joint detection and channel estimation [20], and numerous other detection problems [24]. In order to further improve the achievable iterative decoding performance and hence approach the theoretical capacity limit, a class of forward error correction codes (FEC), referred to as irregular codes was proposed in [74–76]. In [69, 72], Tüchler and Hagenauer employed EXIT charts to facilitate the design and analyze the irregular codes. Their witty solution may be highlighted as follows. It was shown in [71] for the Binary Symmetric Channel (BSC) that the open EXIT chart tunnel area between the inner and outer decider's EXIT curves is proportional to the excess SNR above the channel's capacity. There is experimental evidence that this also holds for other channels [77]. Hence the design of near-capacity systems may exploit this observation by encoding different fractions of the input bit-stream using different rate codes for example in order to fit the inner and outer code's EXIT curves to each other hence reducing the area of the EXIT tunnel and approaching capacity. This design principle will be further detailed in Section 4.2.

In Chapter 3, we extended the iterative decoding principle of Berrou [6] to a serially concatenated iterative decoding process adopted for the detector of a DL-SDMA system. *In this chapter, our novel contribution is that we invoke the novel design concept of irregular codes and apply it in our iterative*

DL-SDMA system. In contrast to [69], where the authors design an irregular outer code to fit the EXIT curve of the inner code and hence approach the attainable capacity, here we intend to use this design concept in our iterative DL-SDMA system for reducing the complexity required for achieving a specific target BER in Section 4.2 and for mitigating the performance degradation imposed by having a limited CSI feedback in Section 4.3.

4.2 Irregular Generic Detection Aided Iterative DL-SDMA Systems

Iterative detection aided systems may dramatically improve the attainable system performance and often result in a near-capacity performance [16]. However, this may impose an increased complexity. As an extension of Chapter 3 [43], we introduce the "complexity-conscious" frame work of a generic hybrid detection algorithm, which is optimized using EXIT charts [68].

In order to reduce the overall iterative decoding complexity, we take into account both the complexity per iterative detection stage and the number of iterations required. We observed with the aid of ten Brink's EXIT charts [68] that the different detectors require different numbers of iterations for reaching the $(I_A, I_E) = (1,1)$ point of the EXIT chart, provided that the E_b/N_0 value experienced is sufficiently high for maintaining an open EXIT tunnel. Specifically, more powerful detectors, such as the Maximum *A Posteriori* probability (MAP) and the Optimized Hierarchy Reduced Search Algorithm (OHRSA) aided detector of [18, 20] require a lower number of iterations. At the same time, the family of less powerful detectors, such as the Minimum Mean Squared Error (MMSE) based [5], necessitate a higher number of iterations. At higher E_b/N_0 values the resultant EXIT-tunnel tends to be more widely open and hence the system tends to require a lower number of iterations to reach the point of perfect convergence at $(I_A, I_E) = (1,1)$, where typically an infinitesimally low BER is achieved. By contrast, at lower E_b/N_0 values the system tends to require a higher number of iterations to attain an infinitesimally low BER. Therefore, the complexity of iterative decoding depends on the complexity of the detector as well as on the E_b/N_0 level encountered. In order to reduce the complexity imposed by the iterative receiver of [43], we will propose a novel detection algorithm, which we refer to as the Irregular Generic Detection (IrGD) algorithm, where the terminology 'irregular' will be justified later in this section.

The philosophy of the IrGD is that of utilizing multiple detectors in the iterative decoding process, instead of a single detector. When invoking multiple detectors applied to different appropriately selected fractions of the input bit-stream, the complexity of the IrGD may be quantified by weighting the complexity of each constituent detector according to their 'duty cycle', which is defined here the

aforementioned relative fraction of the input bit-stream. Designing a IrGD requires searching for the lowest-complexity 'optimum' duty cycle of the candidate detectors, namely that which has the lowest total complexity for the entire iterative decoding process and hence we refer to this as the optimization of the IrGD scheme. The details of the IrGD scheme's optimization will be discussed in Section 4.2.4.

The proposed IrGD algorithm has the following attractive properties:

1. By invoking appropriately amalgamated multiple detectors, the complexity of the IrGD becomes tunable, since it is obtained by weighting the complexity of the individual detectors invoked according to their duty cycle.

2. The design of the IrGD scheme may be readily accomplished with the aid of EXIT charts. The EXIT function of the IrGD aided system and its convergence behaviour can also be readily predicted and analyzed. In other words, the design of the IrGD arrangement can be simplified to an inner-EXIT curve fitting or matching problem, adopting a philosophy originally suggested for the design of near-capacity IrRegular Convolutional Codes (IRCC) [69]. This conceptual similarity between the IRCCs [69] and the IrGDs justified our choice of terminology.

3. Similarly to IRCCs, the design of the IrGD requires finding the specific weighting coefficients for the various IrGD receiver components, which results in the lowest total complexity. This requires an 'off-line' optimization. Hence its complexity does not contribute to the complexity of the real-time iterative decoding process.

The rest of this section is structured as follows. First, we introduce the IrGD algorithm in more depth in Section 4.2.1. In Section 4.2.2, we illustrate the structure of the IrGD aided iterative DL-SDMA system considered and the constituent detectors of the IrGD in Section 4.2.3, followed by the details of the weighting factor optimization process applied to our iterative DL-SDMA system in Section 4.2.4. In Section 4.2.5, we analyze the convergence of our iterative DL-SDMA scheme with the aid of EXIT charts. The corresponding performance results are detailed in Section 4.2.6, followed by our conclusions in Section 4.2.7.

4.2.1 Irregular Generic Detection Algorithm

The philosophy of the IrGD technique is that of utilizing different candidate detectors for detecting predetermined segments of the transmitted signals, instead of using a single detector, as justified later in this section. Based on the appropriately optimized fractions of the received signal, each detector

generates its soft-bit estimates of the appropriate fractions of the transmitted signals. More specifically, for a transmission block containing L encoded bits and assuming that N_{bps} bits per symbol are transmitted by the modulator, we have L/N_{bps} symbols per transmission block, where each transmission block is mapped to a separate time-slot. At the receiver, we invoke the proposed IrGD scheme, which is constituted by N_{det} component detectors. Let C_j be the complexity of the j-th component detector of the IrGD scheme. Then the weighting coefficient α_j has to satisfy:

$$1 = \sum_{j=1}^{N_{det}} \alpha_j, \; C_{gd} = \sum_{j=1}^{N_{det}} \alpha_j C_j, \text{ and } \alpha_j \in [0,1], \forall j, \tag{4.1}$$

where C_{gd} is the average complexity of the IrGD scheme.

Furthermore, each constituent detector generates $\alpha_j L$ soft-bits for a transmission block containing L bits. The IrGD's design philosophy is that it allows us to superimpose the EXIT curves of the individual component detectors appropriately weighted by the optimum α_j value, which facilitates the matching of the detector's EXIT curve to that of the outer channel decoder. It was shown in [69] that this EXIT-curve matching has the potential of minimizing the open EXIT-tunnel's area and hence it is capable of a near-capacity operation, while maintaining an infinitesimally low BER. To elaborate a little further, according to [69], the EXIT function $T_{gd}(I_{in})$, which characterizes the detector referred to synonymously as the inner 'decoder' of the IrGD aided system, is given by

$$T_{gd}(I_{in}) = \sum_{j=1}^{N_{det}} \alpha_j T_j(I_{in}), \tag{4.2}$$

where $T_j(I_{in})$ is the EXIT function of the j-th component detector invoked by the IrGD scheme.

In summary, using the weighting-coefficient vector $\boldsymbol{\alpha}$ formed by the weighting coefficients α_j for $j = 1, 2, \cdots, N_{det}$ satisfying Equation 4.1 creates a IrGD having a given average computational complexity of C_{gd}. Given the weighting-coefficient vector $\boldsymbol{\alpha}$, the EXIT function of $T_{gd}(I_{in})$, characterizing the inner decoder's EXIT curve can be generated based on Equation 4.2. Therefore, we can design the superimposed EXIT function $T_{gd}(I_{in})$ of the IrGD aided system by optimizing the weighting-coefficient vector $\boldsymbol{\alpha}$, for the sake of minimizing the open EXIT-tunnel area and hence to facilitate near-capacity operation, while maintaining an infinitesimally low BER.

In the next section, we will apply the IrGD in the context of an iterative DL-SDMA system in [43].

4.2.2 System Model

Based on the iterative DL-SDMA system of Chapter 3 [43], the iterative DL-SDMA system considered in this chapter combines the two-stage iterative decoding schemes of Section 3.2.1.1 [1] and 3.2.1.2 [2] into a three-stage iterative decoding scheme [3]. The structure of the DL-SDMA system's MUT scheme considered in this chapter is depicted in Figure 4.1, which is repeated from Figure 3.1. The Base-Station (BS) employs M transmit antennas for supporting K Mobile Stations (MSs), where each of the MSs employs N_k receive antennas. We assume a flat-fading Multi-Input and Multi-Output (MIMO) channel. Let $s^{(k)} \in \mathbb{C}^{L_k \times 1}$ be a complex-valued column vector, which denotes the

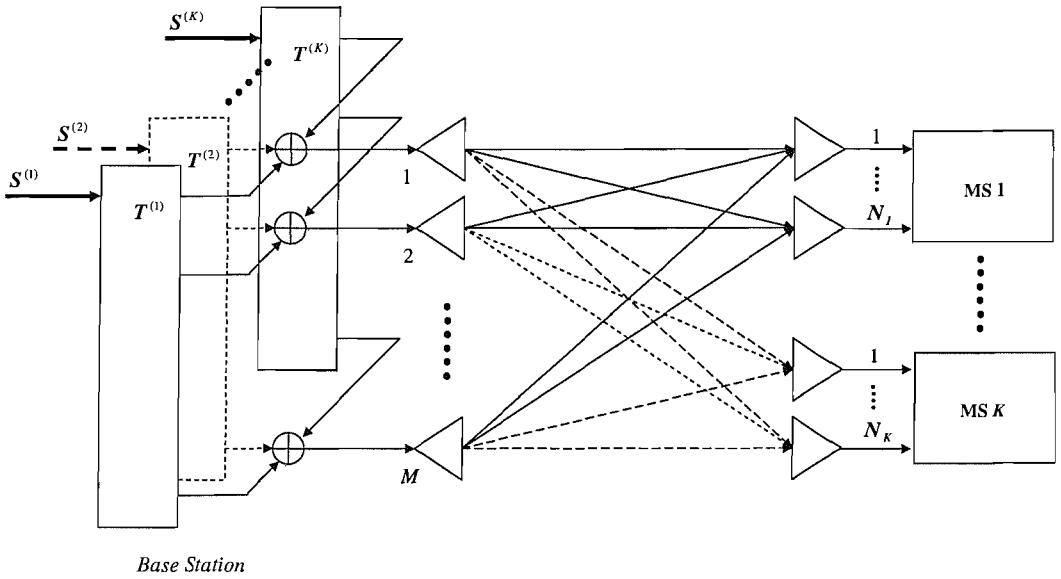

Figure 4.1: Multiuser transmission in the DL-SDMA system, repeated from Figure 3.1

data symbol vector to be transmitted to the k-th MS, while L_k represents the number of independent data symbols contained in $s^{(k)}$ and is defined as $L_k = \sum_{j=1, j\neq k}^{K} N_j$ as detailed in Section 3.2.1. Additionally, we define the so-called *Space-Time Preprocessor* (STP) matrix $T^{(k)} \in \mathbb{C}^{M \times L_k}$, which was designed for the sake of eliminating the MUI [35] as detailed in [43] and Section 3.2.1.

As illustrated in Figure 4.2, the data bits are encoded by both the channel encoder and the Unity-Rate Coder (URC), which is constituted by a convolutional encoder using a single shift register

[1]The iterative decoding process of Section 3.2.1.1 is carried out by exchanging the extrinsic information between the detector and the channel decoder employed.

[2]The iterative decoding process of Section 3.2.1.2 is carried out by exchanging the extrinsic information between the unity-rate precoder and the channel decoder employed.

[3]The iterative decoding process of Section 4.2.2 is carried out by exchanging the extrinsic information between the detector, the unity-rate precoder and the channel decoder employed.

stage [70]. The interleaver placed between the channel encoder and the URCs is denoted by Π_1, as seen in Figure 4.2. The three parallel paths in Figure 4.2 indicate that not only the IrGD, but also the transmitter has to process the fraction of $\alpha_1 L, \alpha_2 L$ and $\alpha_3 L$ bits separately, although the same URC and modulation schemes are employed. The weighting-coefficient vector $\boldsymbol{\alpha}$ is used for partitioning the coded bits into the appropriate-length segments for the URC encoders. For example, for a transmission block containing L encoded bits, the j-th URC encoder encodes $\alpha_j L$ bits. Assuming that N_{bps} bits per symbol are used for transmission, $\alpha_j L / N_{bps}$ modulated symbols are generated by the j-th modulator. Furthermore, the length of the interleaver between the j-th URC and the j-th modulators, denoted as $\Pi_{2,j}$ in Figure 4.2, is equal to $\alpha_j L / N_{bps}$. Both the number N_{det} and the weight of the constituent detectors used for creating the IrGD may be chosen to minimize the complexity of the IrGD while maintaining the target BER. As an illustration, in this study, we utilize three detectors ($N_{det} = 3$) to create the IrGD, as detailed in Section 4.2.3.

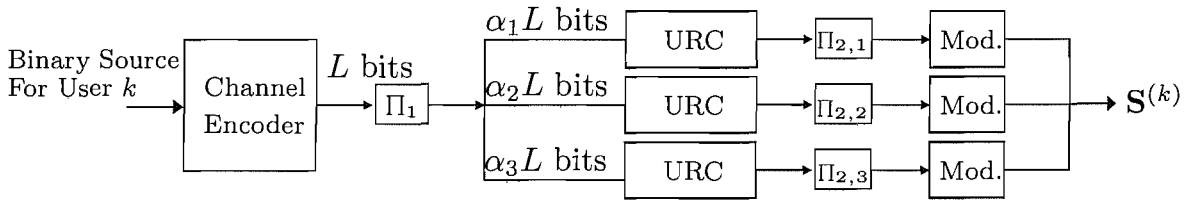

Figure 4.2: Generating the precoded data symbols for the k-th user of Figure 4.1.

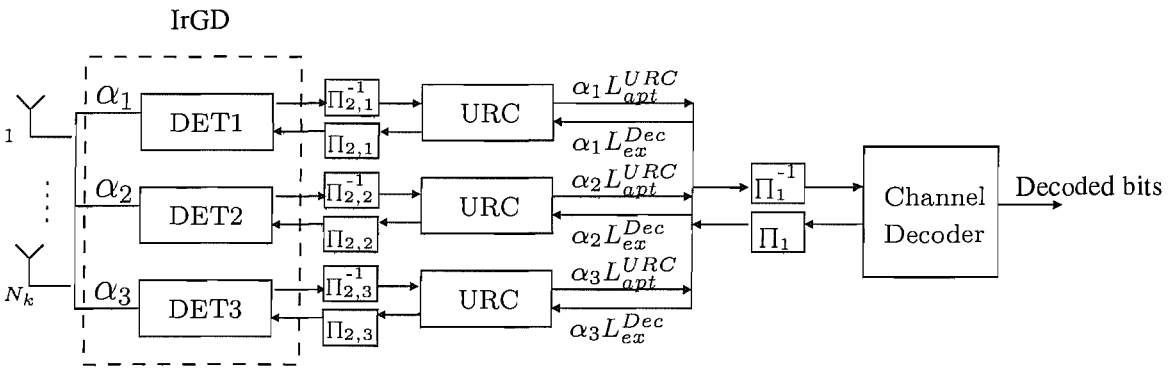

Figure 4.3: The structure of the receiver of the IrGD aided iterative DL-SDMA system. This is a three-stage iterative decoding scheme, which combines two-stage iterative decoding schemes depicted Figure 3.3 and 3.5.

Furthermore, Figure 4.3 illustrates the structure of the MS's receivers. As shown in Figure 4.3, the IrGD is assembled from three different detectors. The received signals are partitioned into appropriate-length segments according to the weighting-coefficient vector $\boldsymbol{\alpha}$. Each detector then pro-

cesses the corresponding fraction of the received signal. The j-th URC decoder generates $\alpha_j L_{apt}^{URC}$ number of soft-bits for the channel decoder. [4] Then iterative detection is invoked for exchanging extrinsic information between the constituent detectors, URC decoders and the channel decoder. The extrinsic information bits generated by the channel decoder are also partitioned into appropriate-length segments according to the weighting-coefficient vector $\boldsymbol{\alpha}$ and then they are fed back to the URC decoders.

As a simplifying assumption, the perfect channel knowledge is assumed to be available at both the transmitter and receiver side in this study. Therefore the MUI may be entirely eliminated [43]. In this case, the system can be considered as a number of parallel single-user MIMO systems.

4.2.3 The Constituent Detectors

We use the following linear and nonlinear detectors for constructing the IrGD:

1. Log Maximum *A Posteriori* Probability (Log-MAP) detector [5];
2. Optimized Hierarchy Reduced Search Algorithm (OHRSA) aided detector [18], which is a reduced-complexity near-ML sphere detector;
3. Minimum Mean Squared Error (MMSE) detector [5], which has the lowest complexity;

Any of these detectors can be considered as a stand-alone SDMA detector, which were detailed in [5, 20]. All of these detectors are capable of generating soft-bit LLR information for supporting iterative detection.

While amalgamating these detectors into a IrGD, the resultant computational complexity of the IrGD arrangement may also be controlled by appropriately designing the weighting-coefficient vector $\boldsymbol{\alpha}$. In Table 4.1, we summarize the average computational complexity of each component detector, which was quantified in term of the number of multiplications and additions required for generating the LLR of each soft-bit. Given Equation 4.1, the associated computational complexity of the IrGD may be characterized by taking the computational complexity of the individual component detectors of Table 4.1 into account. As stated in [18], the direct calculation of the OHRSA detector's computational complexity is infeasible, since it is SNR-dependent. Hence the complexity of the OHRSA detector was compared to that of the other detectors using the computer simulations illustrated in [18].

[4] L_{apt}^{URC} is the number of the soft-bits, which are represented by the Log Likelihood Ratio (LLR) [5] values generated by the URC as the *a posteriori* information. L_{ex}^{Dec} is the number of the extrinsic soft-bits generated by the channel decoder.

Table 4.1: The average computational complexity of component detectors on the basis of generating the LLR of each soft-bit

$C_{\text{Log-MAP}}$	$2 \cdot [2^{L_k \log_2 \mathcal{M}-1} \cdot (3N_k + 2N_k L_k)]$, where $\mathcal{M}$ is the constellation size of the modulation scheme used.
C_{OHRSA}	calculated using computer simulations as illustrated in [18]
C_{MMSE}	$[{L_k}^3 + 2(L_k {N_k}^2 + L_k^2 N_k + L_k N_k + L_k)]/(L_k \log_2 \mathcal{M}) + (2N_k + 3)$

4.2.4 Optimization of the Irregular Generic Detector

The weighting-coefficient vector $\boldsymbol{\alpha} \in \mathbb{R}^{N_{det}}$ has to satisfy Equation 4.1 and Equation 4.2. Let $\mathcal{F}$ be a set containing all the candidate solutions $\boldsymbol{\alpha}$. We may find the weighting-coefficient vector $\boldsymbol{\alpha} \in \mathcal{F}$ by conducting a search similar to that suggested in [69]. By defining a $(N_p \times N_{det})$-element matrix $\mathbf{A}$, which is constituted by N_{det} number of EXIT functions $T_j(I_{in}), j = 1, \cdots, N_{det}$, and a vector $\mathbf{b} = T_{cc}^{-1}(I_{in})$, for $I_{in} \in \{i_1, i_2, \cdots, i_{N_p}\}$, we have

$$\mathbf{A} = \begin{bmatrix} T_1(i_1) & T_2(i_1) & \cdots & T_{N_{det}}(i_1) \\ T_1(i_2) & T_2(i_2) & \cdots & T_{N_{det}}(i_2) \\ \vdots & \vdots & \cdots & \vdots \\ T_1(i_{N_p}) & T_2(i_{N_p}) & \cdots & T_{N_{det}}(i_{N_p}) \end{bmatrix}, \tag{4.3}$$

and

$$b = \begin{bmatrix} T_{cc,1}^{-1}(i_1) \\ T_{cc,1}^{-1}(i_2) \\ \vdots \\ T_{cc,1}^{-1}(i_{N_p}) \end{bmatrix}. \tag{4.4}$$

Our Objective Function (OF) $\Omega(\boldsymbol{\alpha})$ may be defined as

$$\Omega(\boldsymbol{\alpha}) = ||\mathbf{A}\boldsymbol{\alpha} - \mathbf{b}||^2, \tag{4.5}$$

which represents the area between the outer channel decoder's EXIT curve and the inner decoder's EXIT curve, where the latter is constituted by the combined IrGD and URC decoder. Naturally, all elements of e, where we have $e = (\mathbf{A}\boldsymbol{\alpha} - \mathbf{b})$, have to be larger than zero, since they physically represent the area between the outer and inner decoder's EXIT curve. We define a subset $\mathcal{A} \subset \mathcal{F}$ containing all weighting coefficient vectors $\boldsymbol{\alpha}$ meeting this constraint. Secondly, for a specific fixed computational complexity C_{gd}, we opt for that particular $\boldsymbol{\alpha}$ value, which is associated with a higher

Algorithm 4.1: Optimization of the IrGD weighting-coefficient vector α

Set the value of the affordable computational complexity C_{gd} of the IrGD.

Let

$$\mathbf{C} = \begin{bmatrix} 1 & 1 & \cdots & 1 \\ C_1 & C_2 & \cdots & C_{N_{det}} \end{bmatrix}, \mathbf{d} = \begin{bmatrix} 1 \\ C_{gd} \end{bmatrix},$$

$$\mathbf{A} = \begin{bmatrix} T_1(i_1) & T_2(i_1) & \cdots & T_{N_{det}}(i_1) \\ T_1(i_2) & T_2(i_2) & \cdots & T_{N_{det}}(i_2) \\ \vdots & \vdots & \cdots & \vdots \\ T_1(i_{N_p}) & T_2(i_{N_p}) & \cdots & T_{N_{det}}(i_{N_p}) \end{bmatrix}, \mathbf{b} = \begin{bmatrix} T_{cc,1}^{-1}(i_1) \\ T_{cc,1}^{-1}(i_2) \\ \vdots \\ T_{cc,1}^{-1}(i_{N_p}) \end{bmatrix}.$$

Find α_{opt} using the following steps:

Step 1) Find $\alpha \in \mathcal{F}$ which satisfies $\mathbf{C}\alpha = \mathbf{d}$ of Equation 4.1 using the algorithm summarized in Appendix A.

Step 2) Find $\alpha_{opt} = \max_{\alpha} \Omega(\alpha) = ||\mathbf{A}\alpha - \mathbf{b}||^2$.

area $\Omega(\alpha)$ between the outer EXIT curve $T_{cc}^{-1}(I_{in})$ and the inner EXIT curve $T_{gd}(I_{in})$, which implies requiring a low number of decoding iterations. Therefore, we assume that the optimal weighting-coefficient vector α_{opt} can be obtained by finding the α value satisfying:

$$\alpha_{opt} = \max_{\alpha \in \mathcal{A}} \Omega(\alpha). \tag{4.6}$$

We summarize the IrGD technique in Algorithm 4.1, which was generalized for an arbitrary number of constituent detectors N_{det}.

4.2.5 IrGD Design and Analysis Using EXIT Charts

In this section, we will demonstrate how EXIT charts may be used to assist us in the design of the IrGD and in the analysis of the systems' iterative decoding performance.

Let us first define the IrGD's per-iteration target complexity ratio r_{gd} with respect to the Log-MAP detector's complexity $C_{Log-MAP}$ as follows:

$$r_{gd} = C_{gd}/C_{Log-MAP}, \tag{4.7}$$

where again C_{gd} is the computational complexity of the IrGD.

Furthermore, the total complexity $C_{gd,iter}$ [5] of the IrGD embedded into the iterative decoding

[5]The total complexity is defined here as the product of the per-iteration complexity and the number of iterations required for approaching an infinitesimally low BER.

Table 4.2: System Parameters of Figure 4.1

Channel Coder	rate-0.5 RSC [5,7]
Interleaver length	10^5 bits
Modulation	4QAM
Number of users	$K = 3$
Number of transmit antennas	$M = 6$
Number of independent data streams transmitted for the k-th user	$L_k = 2$, for $k = 1, 2, 3$.
Number of receive antennas	$N_k = 2$, for $k = 1, 2, 3$.

process, is given by

$$C_{gd,iter} = C_{gd} \times I_{gd}, \tag{4.8}$$

where $I_{iter,gd}$ is the number of IrGD iterations required for achieving convergence to the $(I_A, I_E) = (1, 1)$ point in the EXIT chart. Therefore, the total complexity ratio of the IrGD is given by

$$r_{gd,iter} = C_{gd,iter} / C_{Log-MAP,iter}, \tag{4.9}$$

where $C_{Log-MAP,iter}$ is the total complexity imposed by the iterative Log-MAP detector, when attaining perfect convergence to the $(I_A, I_E) = (1, 1)$ point in the EXIT chart.

The system parameters employed for the EXIT analysis in this section are listed in Table 4.2.

In Figure 4.4, we illustrate a IrGD design example for $r_{gd} = 0.4$, configured for operation at $E_b/N_0 = 1.7dB$. The inner EXIT curve $T_{gd}(I_{in})$ of the IrGD aided iterative DL-SDMA system using $\alpha = [0.27; 0.73; 0]$ is shown as the solid line in Figure 4.4. According to Equation 4.2, the inner EXIT curve of the IrGD aided iterative DL-SDMA system is constituted by a linear combination of the inner EXIT curves of the iterative DL-SDMA system employing the MMSE, OHRSA and Log-MAP detectors. Recall that α determines the percentage of soft-bits decoded by each constituted detector and in this case only the MMSE and OHRSA detectors were employed, where the MMSE detector had a duty cycle of 27%, while the OHRSA detector a duty cycle of 73%. The elements in $\alpha = [0.27; 0.73; 0]$ represent the duty cycles of the MMSE, OHRSA and Log-MAP detectors in this order.

For further characterizing the complexity of the IrGD, in Figure 4.5 we illustrate the inner decoder's EXIT-curves for the IrGD aided iterative DL-SDMA system designed for different complexity ratios r_{gd}, ranging from 0.4,0.3,0.2 to 0.19. The weighting-coefficient vectors α designed for

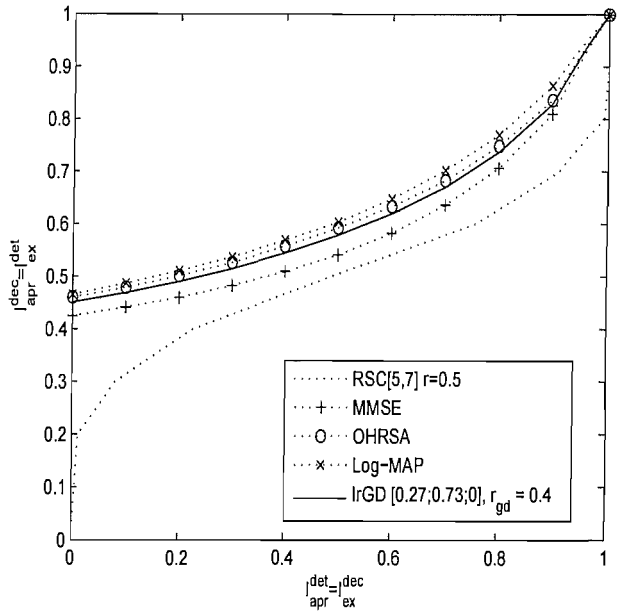

Figure 4.4: EXIT chart analysis of the iterative DL-SDMA system of Figure 4.1 invoking IrGD of Figure 4.2 and 4.3 having a complexity ratio of $r_{gd} = 0.4$ and a weighting-coefficient vector of $\alpha = [0.27; 0.73; 0]$. The system operated at $E_b/N_0 = 1.7dB$. A rate-0.5 Recursive Systematic Convolutional (RSC) channel coder, having the octal generator polynomials of G=[5,7], was employed for the system. The channel model was a flat-fading MIMO channel and the system parameters of Table 4.2 were used.

each of the corresponding complexity ratios r_{gd} are listed in Table 4.3. As expected, by reducing the complexity ratio r_{gd}, the duty-cycles of the lower-complexity detectors, such as the MMSE detector, becomes higher than those of the higher-complexity detectors, such as the OHRSA and Log-MAP schemes. On the other hand, as a consequence of reducing the complexity ratio r_{gd}, the EXIT-tunnel becomes narrower. The number of iterative decoding iterations required for attaining perfect convergence increases due to having a narrower EXIT-tunnel. Therefore, there is a tradeoff between the complexity ratio r_{gd} corresponding to the single-iteration-complexity and the number of the decoding iterations I_{gd}. In order to reduce the overall complexity of the iterative DL-SDMA receiver, we have to take both effects into account. In Table 4.3, we illustrated this trade-off. The required number of iterations I_{gd} is increased, when reducing the complexity ratio r_{gd}. When r_{gd} is lower than 0.18, the EXIT-tunnel becomes narrow and the number of iterations required for navigating through the EXIT-tunnel becomes excessive.

Furthermore, in Table 4.3, we record the overall complexity of the IrGD aided iterative decoding process, i.e. $C_{gd,iter}$ and its complexity ratio, $r_{gd,iter}$, for different values of r_{gd}. We have found that the IrGD aided DL-SDMA system has the lowest iterative decoding complexity, when we have $r_{gd} = 0.2$

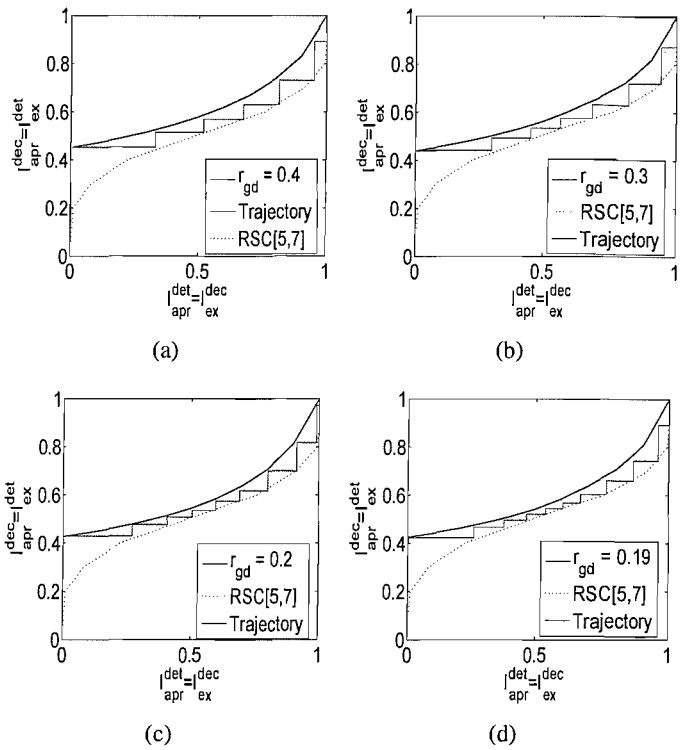

Figure 4.5: EXIT chart analysis of the iterative DL-SDMA system of Figure 4.1 invoking IrGD of Figure 4.2 and 4.3 associated with different values of r_{gd}, ranging from $0.4, 0.3, 0.2, 0.19$ in (a)(b)(c)(d), respectively. The systems operated at $E_b/N_0 = 1.7dB$. A rate-0.5 RSC[5,7] channel coder was employed for the system. The channel model was a flat-fading MIMO channel and the parameters of Table 4.2 were used.

and the corresponding weighting-coefficient vector is $\alpha = [0.957; 0.043; 0]$ at $E_b/N_0 = 1.7$dB. The overall complexity ratio $r_{gd,iter}$ of the IrGD in the case of $r_{gd} = 0.2$ is equal to 0.36. In other words, it reduces the complexity by about 64% (1-0.36), compared to the Log-MAP detector aided iterative decoder.

Table 4.3: Parameters of the IrGD of Figure 4.2 and 4.3 at E_b/N_0 = 1.7dB

r_{gd}	α	I_{gd}	$C_{gd,iter}$	$r_{gd,iter}$
1	[0;0;1]	5	2240.00	1.0
0.4	[0.27;0.73;0]	7	1254.40	0.56
0.3	[0.61;0.39;0]	8	1075.20	0.48
0.21	[0.922;0.078;0]	9	846.72	0.37
0.2	[0.957;0.043;0]	9	806.40	0.36
0.19	[0.992;0.008;0]	10	851.20	0.38
0.18	N/A	N/A	N/A	N/A

4.2.6 Performance Results

In this section, we characterize the attainable performance of the IrGD aided iterative DL-SDMA system. The system parameters used are listed in Table 4.2.

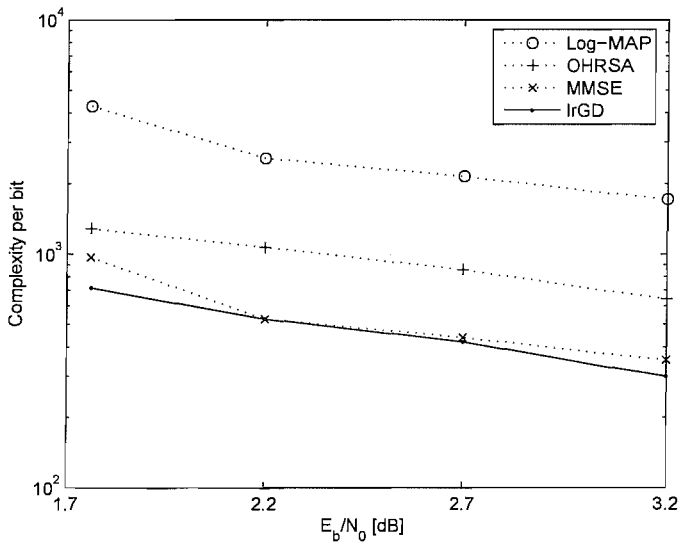

Figure 4.6: Comparison of the computational complexity per detect bit for iterative decoding in the iterative DL-SDMA systems of Figure 4.1, 4.2 and 4.3 employing different detectors. 4-ary QAM was used by the systems. The channel model was a flat-fading MIMO channel and the parameters of Table 4.2 were used. The weighting-coefficient vector α of the IrGD employed at the recorded E_b/N_0 from 1.7,2.2,2.7 to 3.2 dB are [0.957;0.043;0], [1;0;0], [0.9;0.1;0] and [0.88;0.12;0], respectively.

In Figure 4.6, we recorded the computational complexity of the iterative DL-SDMA system designed for reaching a target BER of 10^{-5}. The 4-ary QAM modulator was employed by the systems discussed in Figure 4.6. Observe in Figure 4.6 that the IrGD aided iterative DL-SDMA systems have

a lower computational complexity than the benchmark systems.

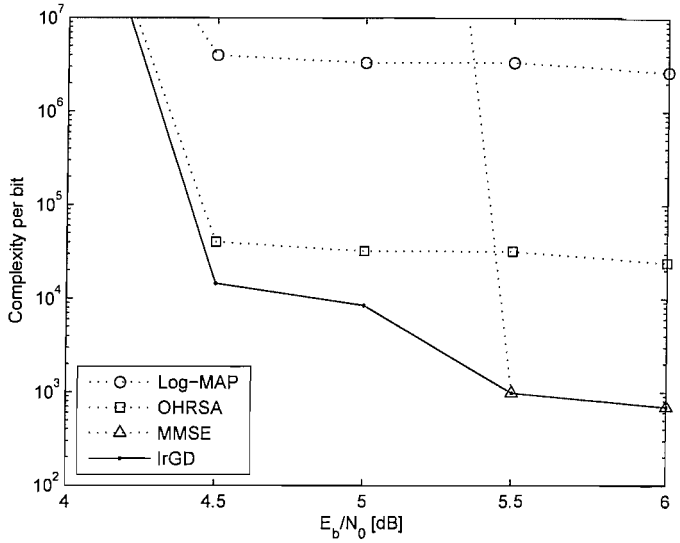

Figure 4.7: Comparison of the computational complexity per detect bit for iterative decoding in the iterative DL-SDMA systems of Figure 4.1, 4.2 and 4.3 employing different detectors. 16-ary QAM was used by the systems. The channel model was a flat-fading MIMO channel and the parameters of Table 4.2 were used. The weighting-coefficient vector α of the IrGD employed at the E_b/N_0 values of 4, 4.5, 5, 5.5 and 6 dB are [0.8;0.2;0], [0.9;0.1;0], [1;0;0] and [1;0;0], respectively.

Similarly, in Figure 4.7, we recorded the computational complexity of the iterative DL-SDMA system designed for reaching a target BER of 10^{-5}, but the 16-ary QAM modulator was employed by the systems discussed in Figure 4.7. Observe in Figure 4.7 that the IrGD aided iterative DL-SDMA systems have a lower computational complexity than the benchmark systems. Additionally, observe in Figure 4.7 that the inner component's EXIT-curve in the MMSE aided iterative DL-SDMA system was intersected by the outer RSC channel decoder's EXIT curve at $E_b/N_0 = 5.5$ dB and hence the MMSE aided iterative DL-SDMA system fails to reach the target BER of 10^{-5}, regardless of the number of iterations. The other detectors used by the iterative DL-SDMA system also failed to have an open EXIT tunnel at $E_b/N_0 = 4$ dB. Observe furthermore in Figure 4.7 that when the E_b/N_0 value is sufficiently high, such as $E_b/N_0 = 5.5$dB, the IrGD aided system employed the MMSE detector during the entire iterative decoding process. Therefore, the proposed IrGD provides a flexible detection framework. By switching amongst multiple detectors according to the appropriately designed weighting-coefficient vector α, the system may be expected to operate at the lowest possible iterative decoding complexity.

4.2.7 Conclusions

We proposed the IrGD design philosophy for reducing the complexity of the iterative decoding aided DL-SDMA system. By appropriately designing the weighting-coefficient vector α, the IrGD aided system may potentially provide the lowest possible iterative decoding complexity. Quantitatively, the IrGD aided iterative DL-SDMA system associated with $\alpha = [0.957; 0.043; 0]$ reduces the complexity by about 64%, compared to the log-MAP aided benchmark systems.

Table 4.4: Comparison of the complexity ratio of iterative DL-SDMA systems using different detectors (extracted from Figure 4.6)

E_b/N_0 [dB]	1.7	2.2	2.7	3.2
Log-MAP	1	1	1	1
OHRSA	0.64	0.4167	0.4000	0.3750
MMSE	0.41	0.2056	0.2056	0.2056
IrGD	0.36	0.2056	0.1967	0.1752

Table 4.5: Comparison of the complexity ratio of iterative DL-SDMA systems using different detectors (extracted from Figure 4.7)

E_b/N_0 [dB]	4	4.5	5	5.5	6
Log-MAP	1	1	1	1	1
OHRSA	N/A	0.0101	0.0097	0.0095	0.0091
MMSE	N/A	N/A	N/A	0.0003	0.0003
IrGD	N/A	0.0037	0.0028	0.0003	0.0003

The complexity imposed by the iterative DL-SDMA systems using different detectors has been extracted from Figure 4.6 and summarized in Table 4.4. By using the complexity ratio, which is obtained by normalizing the complexity of each detector to the complexity imposed by the Log-MAP detector, Table 4.4 indicates that IrGD has the lowest complexity compared to the other detectors. Additionally, Table 4.5 summarizes the complexity of the iterative DL-SDMA system characterized in Figure 4.7.

4.3 Iterative DL-SDMA Systems Using Limited Feedback

In this section, we analyze the achievable performance of iterative DL-SDMA systems employing imperfect ST-CIRT due to finite-accuracy CSI feedback, which is both outdated and prone to channel errors. Its impact on the convergence behavior of the system will be demonstrated by using EXIT charts. The fundamental question is namely, how high this normalized overhead has to be? In response to this question, we propose an algorithm, which assists us in exploring the overhead required for maintaining an open EXIT-tunnel. Therefore we refer to the CSI quantization employing this algorithm as the EXIT-Chart Optimized CSI Quantizer (ECO-CQ), where the terminology will be further justified when the algorithm is detailed in Section 4.3.3.

In our forthcoming discussions *CSI Quantization* (CQ) will be referred to as ST-CIRT quantization. When the idealized scenario of having perfect knowledge of ST-CIRT is assumed, our system employing the spatio-temporal pre-processing technique of [35] becomes capable of separating the signals destined for the different users at the base station's DL transmitter and hence results in a MUI-free single-user performance. In practice, the ST-CIRT required by the BS's DL transmitter may be obtained via a feedback channel from the DL receiver. The DL receiver is typically designed to feed back the quantized ST-CIRT to the BS by striking a balance between reducing the amount of the feedback information and maintaining a near-perfect MUI rejection. However, limited amount of feedback bits to BS results in having partial ST-CIRT only. Even if no errors are imposed on the feedback channel, the imperfect ST-CIRT converged by the limited feedback will result in a residual MUI and hence will further degrade the performance of the system. The overhead required by the transmission of the sampled ST-CIRT is determined by striking a trade-off between maintaining a low BER and a low feedback overhead.

In our forthcoming study, we will first illustrate the scenario of ST-CIRT feedback in Section 4.3.1 and provide a brief overview of CSI quantization in Section 4.3.2, while in Section 4.3.3 we summarize the proposed ECO-CQ algorithm. In Section 4.3.4 we outline the system model used. Our EXIT chart analysis is provided in Section 4.3.5, leading to the performance results of Section 4.3.6. Finally, we conclude our related discourse in Section 4.3.7.

4.3.1 The Scenario of ST-CIRT Feedback

Consider the scenario when the BS periodically sends pilots to the DL receivers, so that the MSs may estimate the ST-CIRTs and use the allocated feedback channels to periodically feed back the

ST-CIRTs, as illustrated in Figure 4.8. The DL channel and the UL feedback channels of the MSs are typically allocated in different bandwidths and the UL feedback information is assumed to be transmitted over the strongly protected UL control channel. Additionally, the BS may avoid the latency involved in awaiting the current ST-CIRTs by employing their predicted value generated by the ST-CIRT prediction [78] based on the previously received quantized ST-CIRTs.

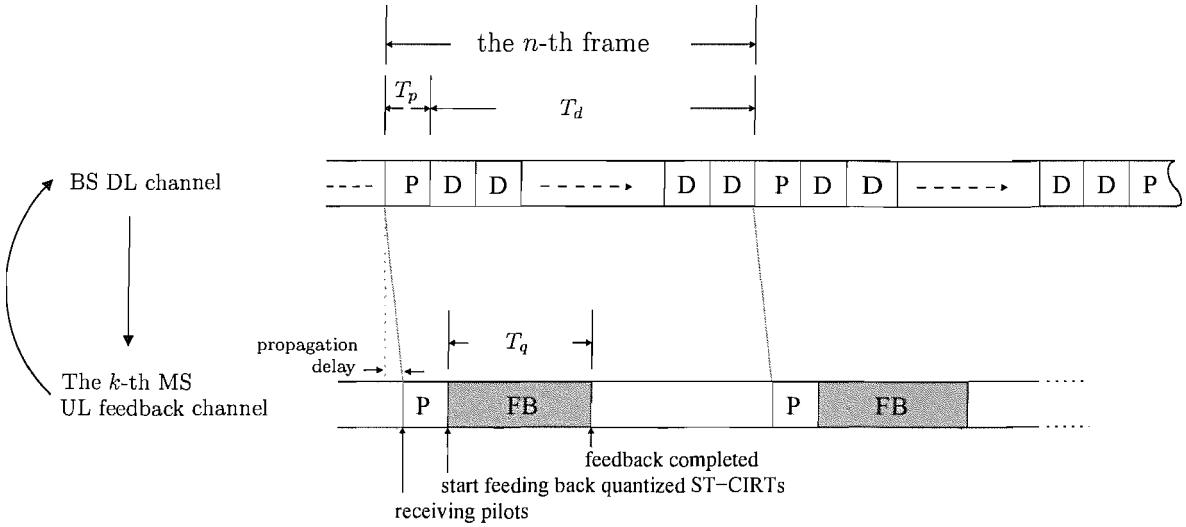

Figure 4.8: The pilot-aided ST-CIRT estimation

Let T_p denote the duration of a pilot symbol interval which typically identical to the data symbol interval and T_d denote the total duration of data-transmission symbol intervals between two pilots, as seen in Figure 4.8. The pilot symbols are used for sampling the fading channel's envelope according to the Nyquist theorem [64], which requires a sampling rate f_s in excess of $2f_D$, where f_D denotes the normalized Doppler frequency. According to Figure 4.8, we have $f_s = \frac{1}{T_p+T_d}$ and the condition of

$$f_s = \frac{1}{T_p + T_d} \geq 2 \cdot f_D \tag{4.10}$$

should be satisfied.

On the other hand, each MS estimates its ST-CIRTs using the received pilots as indicated in Figure 4.8. Assuming that there are $(M \times N)$ ST-CIRT coefficients for each frame – which tacitly implies having a single complex-valued CIR tap – and the DL receivers quantize each ST-CIRT coefficient using q bits for the magnitude and q bits for the phase, the symbol interval T_q required for feeding back all the ST-CIRT coefficients of each transmission frame is given by

$$T_q = \frac{(M \cdot N) \cdot 2 \cdot q}{N_{bps}}, \tag{4.11}$$

where N_{bps} is the feedback transmission rate of the MS's UL transmitter. The propagation delay of the channel may be negligible compared to T_q, due to the high number of ST-CIRT coefficients representing the MIMO channels.

Assuming that 10% DL pilot overhead is employed, we have $T_p/T_d = 0.1$. According to Equation 4.10 and letting $\frac{1}{T_p+T_d} = 2 \cdot f_D$, we may define the *normalized feedback overhead* Λ when the DL-receivers use q-bit quantization as

$$\Lambda_q = \frac{T_q}{T_d} \approx T_q \cdot 1.1 \cdot 2 \cdot f_D \approx T_q \cdot f_D. \tag{4.12}$$

Let us now consider two schemes. First, the MSs employ a-bit quantization to convey the ST-CIRT coefficients to the BS, which are subject to a feedback duration of T_a. In the second scheme, the MSs employing b-bit quantization to signal the ST-CIRT coefficients to the BS and have the corresponding feedback duration of T_b. Then we define *the normalized overhead reduction ratio* R_Λ associated with using b instead of a bits as

$$R_\Lambda = \frac{\Lambda_a - \Lambda_b}{\Lambda_a} = \frac{\frac{T_a - T_b}{T_d}}{\frac{T_a}{T_d}} = \frac{T_a - T_b}{T_a} = \frac{a-b}{a}. \tag{4.13}$$

Example 4.1: The UL ST-CIRT overhead calculation

Consider a scenario that the BS equipped $M = 6$ DL transmit antennas and supports $K = 3$ MSs. Each MS has $N = 2$ receive antennas.

Scheme A: When the MS employs a $q = 3$-bit quantization scheme, we have $T_q = (6 \cdot 2) \cdot 2 \cdot 3/4 = 18$ symbols, where we assumed that the MS had a feedback transmission rate of $N_{bps} = 2 \cdot 2$ bits per transmit symbol interval by using 4QAM and two transmit antennas. Let us furthermore assume that $f_D = 0.001$. Then the normalized overhead of the $q = 3$-bit quantization scheme is $\Lambda_q = 0.018$, i.e. 1.8%.

Scheme B: When the MS employs $q = 2$-bit quantization scheme, we have $T_q = (6 \cdot 2) \cdot 2 \cdot 2/4 = 12$ symbols, where we assumed that the MS had a feedback transmission rate of $N_{bps} = 2 \cdot 2$ bits per transmit symbol interval by using 4QAM and two transmit antennas. Let us furthermore assume that $f_D = 0.001$. Then the normalized overhead of $q = 2$-bit quantization scheme is $\Lambda_q = 0.012$, i.e. 1.2%.

The resultant normalized overhead reduction ratio becomes $R_\Lambda = (3-2)/3 = 0.33(33\%)$,

when we use the q = 2-bit ST-CIRT quantization of Scheme B instead of using the q = 3-bit ST-CIRT quantization of Scheme A.

In this study, we did not take the channel prediction error into account in order to focus our attention on the investigation of the limited ST-CIRT feedback. Assuming that the channel prediction is perfect, the ST-CIRT coefficients are contaminated by the quantization error only. Hence, at every symbol interval we assume that the MUT exploits the current ST-CIRT coefficients quantized by using the CQs. Consequently, in our forthcoming discourse the inaccuracy of the ST-CIRT employed by the BS will be dominated by the limited ST-CIRT feedback.

4.3.2 Introduction to Channel Quantization

In general, the quantization of ST-CIRT may utilize two different types of quantization schemes, namely Scalar Quantization (SQ) and Vector Quantization (VQ) [79]. Vector quantization may be viewed as a generalization of SQ, where several ST-CIRT coefficients are quantized jointly. The attainable performance of VQ may be superior to that of SQ, because VQs exploit the correlation between the components of the input-vector [79], which in our case is either the spatial-domain or time-domain correlation of ST-CIRT coefficients. However, since in our study uncorrelated ST-CIRT coefficients are assumed, we employ a SQ scheme.

The accuracy of quantization is typically measured by the *distortion* D, defined as the mean squared error of the quantized signal h_q, namely as

$$D = \mathrm{E}\left\{(h_q - h)^2\right\}, \tag{4.14}$$

where h is the signal to be quantized. In order to reduce the distortion D, we may use a high-resolution quantizer, which increases the number of quantization levels. Let us denote the number of quantization levels of the SQ by N_q. Then, $q = log_2(N_q)$ bits are required to represent N_q quantization levels. Furthermore, we may design the spacing between quantization levels to be uniform or nonuniform [80]. The benefit of using nonuniform quantization [79] is that the dynamic range that can be accommodated for a given number of bits may be significantly increased without increasing the average distortion of the quantizer. This is achieved by exploiting the knowledge of the Probability Distribution Function (PDF), of the input signal. A NonUniform Quantizer (NUQ) is typically designed by placing the quantization intervals more densely, where the PDF indicates a high relative frequency of the input samples. The most widely used codebook design algorithm is the Generalized Lloyd Algorithm (GLA) [79].

In our study, the magnitude of the input signal's PDF is assumed to be Rayleigh distributed, while the phase of it is assumed to be uniformly distributed. Therefore we employ a scalar ST-CIRT quantizer using NUQ to separately quantize the magnitude and phase of each CIR coefficient using q bits. We used the GLA [79] to obtain the N quantization intervals for both the magnitude and phase of the ST-CIRT coefficients. In Figure 4.9, we illustrate the magnitude and phase quantization characteristic of the scalar NUQ scheme employed for $q = 4$. The solid lines indicate the quantization levels and the dashed lines portray the input signals' PDF. Figure 4.9(a) shows that the quantization intervals of the ST-CIRT's magnitude has more densely spaced quantization intervals in high-probability region. In contrast, in Figure 4.9(a) the quantization intervals are equi-spaced, since the PDF of the ST-CIRT's phase is uniform.

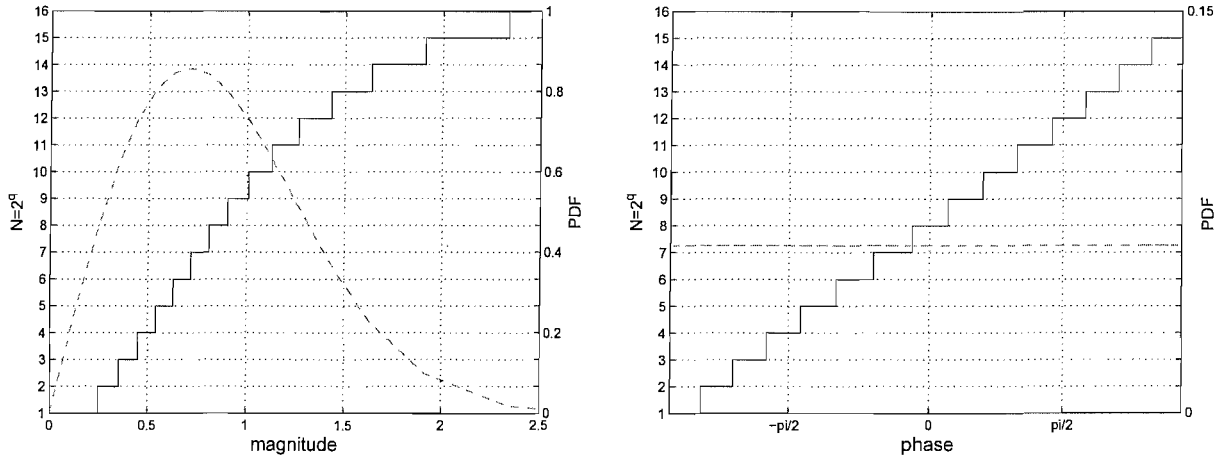

Figure 4.9: Non-uniform SQ characteristic for $q = 4$, which was constructed using the GLA.

In our forthcoming discussions we focus our attention on the investigation of our iterative DL-SDMA system using limited-feedback, while perfect CSI is assumed to be available at the DL receivers. Furthermore, for the sake of simplicity, an free-error feedback channel is assumed. Hence, the mean square error of the ST-CIRT quantizer, which is denoted by $\sigma^2_{ST-CIRT}$, is given by

$$\sigma^2_{ST-CIRT} = D = \mathrm{E}\left\{(h_q - h)^2\right\}. \tag{4.15}$$

By recording $\sigma^2_{ST-CIRT}$ for different number of ST-CIRT quantization bits under the assumption of having a narrow-band Rayleigh-faded ST-CIRT, we illustrate their relationship in Figure 4.10. Naturally, the higher the number of quantization bits, the lower the quantization error of the ST-CIRT. On the other hand, in order to reduce the feedback overhead, we have to strike a good compromise by employing the minimum number of quantization bits, while maintaining a high system performance.

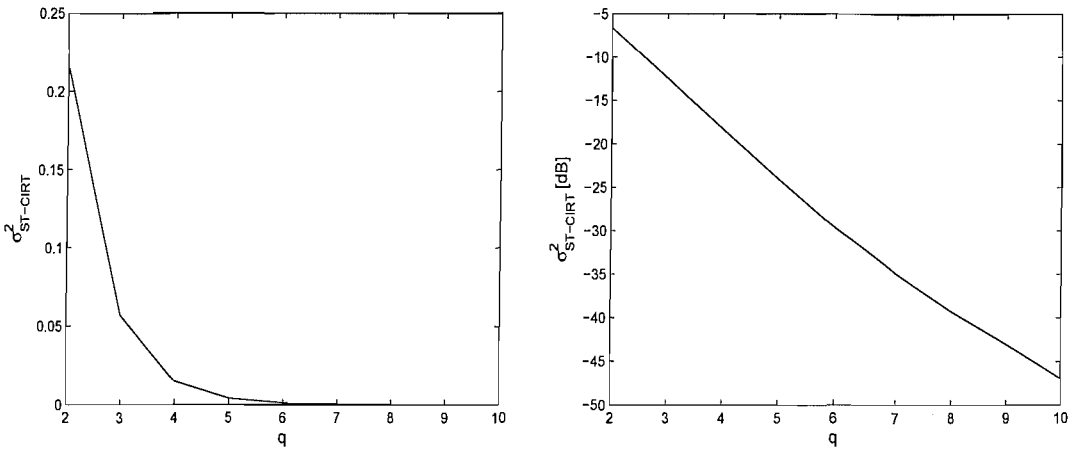

(a) (b)

Figure 4.10: Quantization error $\sigma^2_{ST-CIRT}$ of the ST-CIRT for different number of quantization bits

4.3.3 EXIT-Chart Optimized Channel Quantization

In this section we continue our discourse by proposing an algorithm, which allows the system to use a different number of quantization bits q in different symbol intervals. The goal is to minimize the average of q over a number of symbol intervals, while maintaining a certain target performance. Let us assume for example that there are 100 symbol intervals. The receiver quantizes the ST-CIRTs of 40 symbol intervals using q = 2-bit quantization and the rest of the ST-CIRTs of 60 symbol intervals using 3-bit quantization. Therefore during the observed 100 symbol intervals, the average number of feedback bits for each sampled ST-CIRT conveying both the magnitude and phase is $q = 2 \cdot 0.4 + 3 \cdot 0.6 = 2.6$. The question is now, how to determine the required number of quantization bits q for the sampled ST-CIRTs.

In order to resolve this design dilemma, we adopt the design concept of irregular convolution codes [69] and aim to minimize the average value of q, while assuming that an open EXIT-tunnel is still attainable for the iterative system at a given E_b/N_0 values. More explicitly, we exploit the fact that similarly to having different channel SNRs, the different amount of ST-CIRT quantization noise imposed by varying q allows us to shape the EXIT-curve of the inner component of our DL-SDMA system. Assume that there are N_{ts} symbol intervals in an observed transmission block and we employ N_Q different number of quantization bits to quantize the ST-CIRT. For example, we have $q = \{2,3,4,5\}$ for $N_Q = 4$. The ST-CIRTs in the segment of $\alpha_j N_{ts}$ symbol intervals will be quantized by using a specific number of quantization bits q, where α_j is a weight, controlling the size

of each segment. Then the weighting coefficient α_j has to satisfy:

$$1 = \sum_{j=1}^{N_Q} \alpha_j, \ \bar{q} = \sum_{j=1}^{N_Q} \alpha_j q, \text{ and } \alpha_j \in [0,1], \forall j. \tag{4.16}$$

where $\bar{q}$ is an averaged value over the observed transmission block.

According to [69], the corresponding EXIT function $T_I(I_{in})$, which characterizes the inner decoder's EXIT-curve in the system, is given by

$$T_I(I_{in}) = \sum_{j=1}^{N_Q} \alpha_j T_q(I_{in}), \tag{4.17}$$

where $T_q(I_{in})$ denotes the EXIT function, when the ST-CIRTs are quantized by using q-bit channel quantization.

Observe that this algorithm provides a framework for managing the ST-CIRT quantization at the DL receivers and their UL transmitter counterparts by using different number of quantization bits q for feeding the ST-CIRTs back to the BS. This design principle may also be applied for different types of channel quantizers, namely to uniform, nonuniform, scalar or vector channel quantization. Again, we refer to the proposed algorithm as the EXIT-Chart Optimized Channel Quantizer (ECO-CQ). For the sake of simplicity, we demonstrate this EXIT-chart based optimization procedure in the context of the scalar NUQ, which has been introduced in Section 4.3.2.

4.3.4 System Model

In this section, we illustrate the system models of the iterative DL-SDMA using conventional CQ and the proposed ECO-CQ. Assume that our system equips M transmit antennas at BS for supporting K MSs while each MS employs N_k receive antennas. We denote the $(M \times N_k)$-element channel matrix by $\boldsymbol{H}^{(k)}$, which is constituted by the sampled flat-fading channel impulse responses of each AE experienced by the k-th user. The elements $[\boldsymbol{H}^{(k)}]_{i,j}$, where we have $1 \leq i \leq N_k$ and $1 \leq j \leq M$, are i.i.d complex Gaussian random variables with distribution $\mathcal{CN}(0,1)$.

4.3.4.1 Iterative DL-SDMA Systems Using Conventional CQ

The structure of the iterative DL-SDMA system using a conventional CQ is depicted in Figure 4.11. The source bits are encoded by the channel encoder as well as the URC precoder and are mapped to the modulated symbols. Let $\mathbf{s}^{(k)} \in \mathbb{C}^{L_k \times 1}$ be a complex-valued column vector, which denotes the data symbol vector to be transmitted to the k-th MS, while L_k represents the number of independent data

symbols contained in $\mathbf{s}^{(k)}$, which is defined as $L_k = M - \sum_{j=1,j\neq k}^{K} N_j$ as detailed in Section 3.2.1. Furthermore, we utilize the MUT-STP matrix $\boldsymbol{T}^{(k)} \in \mathbb{C}^{M\times L_k}$ of Section 2.1.2.3, which was designed for the sake of eliminating the MUI [35] by exploiting the knowledge of channel state information at transmitter, as detailed in Chapter 2. In this section, we assume that $\boldsymbol{T}^{(k)}$ is generated based on the quantized ST-CIRT fed back from the DL receivers, which is indicated by the notation $\boldsymbol{T}^{(k)}(\boldsymbol{H}_q)$, as shown in Figure 4.11. After the processing of the MUT-STP, the K DL signals transmitted to K the MSs will be superimposed and transmitted by the M transmit antennas.

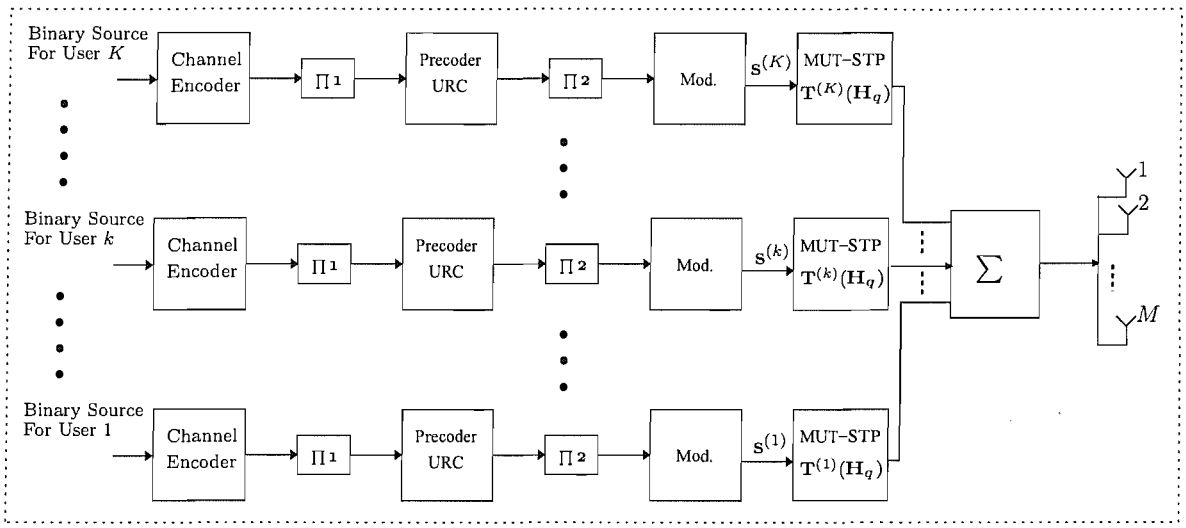

Figure 4.11: The structure of the BS transmitter in the iterative DL-SDMA system using conventional CQ

Figure 4.12 depicts the structure of the MS receiver in the iterative DL-SDMA system using conventional CQ. As seen in Figure 4.12, the MMSE aided SDMA detector constitutes the first stage of the receiver. The iterative decoding process is carried out between MMSE detector, URC decoder and channel decoder.

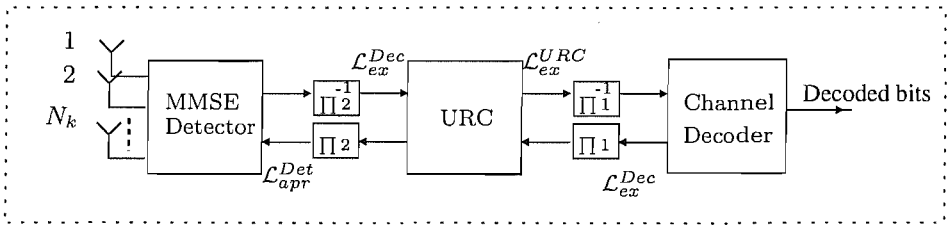

Figure 4.12: The structure of the MS receiver in the iterative DL-SDMA system using conventional CQ

Let $\boldsymbol{r}^{(k)}$ and $\boldsymbol{n}^{(k)}$ be the received signal vector and noise vector associated with the k-th MS, respectively. If the MUT-STP matrix $\boldsymbol{T}^{(k)}$ is generated based on perfect ST-CIRTs, the MUI can be

perfectly eliminated. The received signal vector associated with the k-th MS can be expressed in the following form

$$\boldsymbol{r}^{(k)} = \boldsymbol{H}^{(k)}\boldsymbol{T}^{(k)}\boldsymbol{s}^{(k)} + \boldsymbol{n}^{(k)}, \tag{4.18}$$

where the $(N_k \times L_k)$-dimensional matrix $\boldsymbol{H}^{(k)}\boldsymbol{T}^{(k)}$ characterizes the *effective channel* corresponding to the k-th MS.

Naturally, when the MUT-STP matrix $\boldsymbol{T}^{(k)}$ is generated based on imperfect ST-CIRT, the system becomes unable to entirely eliminate the MUI and hence the resultant residual MUI contaminates the received signal of the k-th MS according to

$$\boldsymbol{r}^{(k)} = \boldsymbol{H}^{(k)}\boldsymbol{T}^{(k)}\boldsymbol{s}^{(k)} + \sum_{i=1, i\neq k}^{K} \boldsymbol{H}^{(k)}\boldsymbol{T}^{(i)}\boldsymbol{s}^{(i)} + \boldsymbol{n}^{(k)}, \tag{4.19}$$

where the second term of Equation 4.19 represents the experienced MUI. We define $I_{MUI}^{(k)} = \sum_{i=1, i\neq k}^{K} \boldsymbol{H}^{(k)}\boldsymbol{T}^{(i)}\boldsymbol{s}^{(i)}$ and use the denotation σ_{MUI}^2 to represent the recorded variance of $I_{MUI}^{(k)}$ in the later discussions.

4.3.4.2 Iterative DL-SDMA Systems Using ECO-CQ

Certain structural modifications are required by the iterative DL-SDMA system, when it employs an ECO-CQ. Let us utilize four conventional CQs having different number of quantization bits, namely $q = 2, 3, 4$ and 5, to construct an ECO-CQ. As illustrated in Figure 4.13, the data bits encoded by the channel encoder will be partitioned into four segments corresponding to the weighting coefficient vector of $\boldsymbol{\alpha} = [\alpha_1, \alpha_2, \alpha_3, \alpha_4]$. Each of the four segments of the channel-encoded bits will also be encoded by the URC encoder of Figure 4.13 before the modulation stage. For example, for a coding block containing L encoded bits, the j-th URC encoder encodes $\alpha_j L$ bits. Assuming that N_{bps} bits per modulated symbol are used for transmission, we have a total of $\alpha_j L / N_{bps}$ transmitted symbols generated by the j-th modulator of 4.13. Accordingly, as illustrated in Figure 4.13, the MUT-STP matrix $\boldsymbol{T}^{(k)}$ will be generated by using the ST-CIRTs, which were quantized using four different number of quantization bits per ST-CIRT coefficient for the four segments of transmitted symbols. The MUT-STP matrix $\boldsymbol{T}^{(k)}$ generated by the q-bit quantized ST-CIRTs is denoted by $\boldsymbol{T}^{(k)}(\mathbf{H}_q^{q-bit})$, as shown in Figure 4.13.

Figure 4.14 shows the structure of the iterative DL-SDMA using ECO-CQ. First, the received signal will be partitioned into four segments. Accordingly, for each segment of the received signals, the MMSE detector will generate the soft-bits as the input of the URC decoder. The four segments

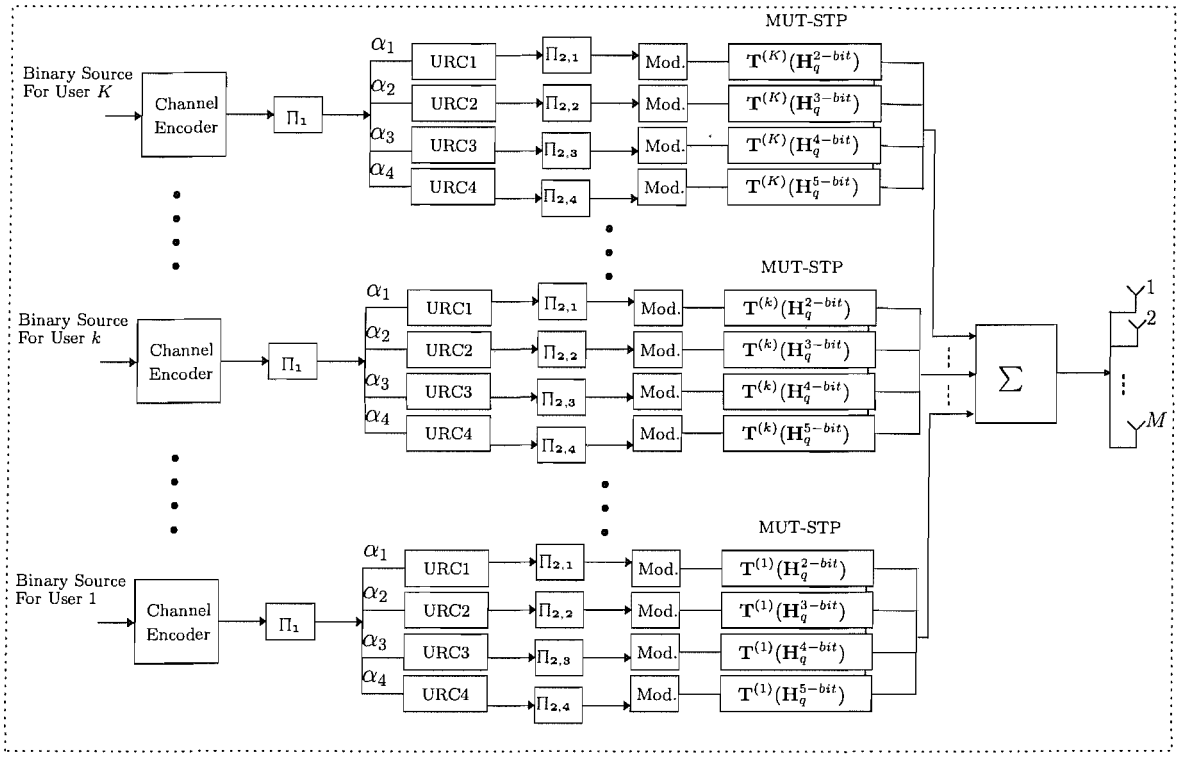

Figure 4.13: The structure of the BS's transmitter in the iterative DL-SDMA system using ECO-CQ

of the extrinsic information bits generated by the URC decoder will become the *a priori* information bits of the channel decoder of Figure 4.14. As the iterative decoding process is carried out, the extrinsic information bits of the channel decoder will be partitioned into four segments again in order to construct four segments of *a priori* bits of the URC decoder. The four-segment output of the URC decoder will then be forwarded to the MMSE detector for the next iteration of the decoding process.

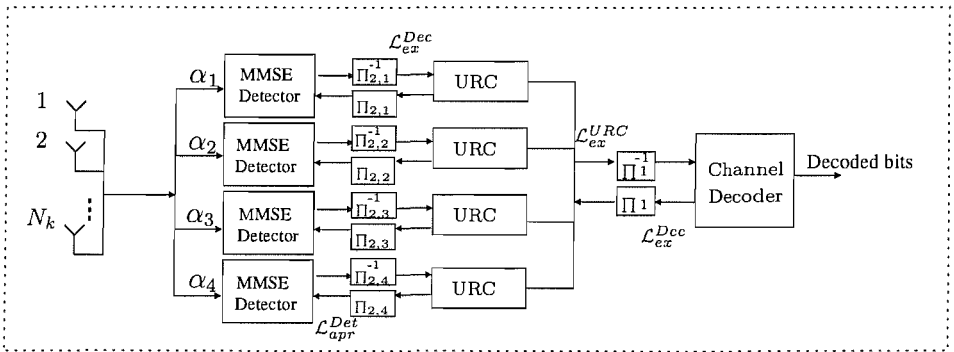

Figure 4.14: The structure of the MS receiver in the iterative DL-SDMA system using ECO-CQ

Again, the specific partitioning of the bits or symbols into segments is carried out according to Equation 4.17, where the transfer functions represent the four segments of soft-bits, i.e. LLRs.

4.3.5 EXIT Chart Analysis

In the following discussions, we provide the EXIT chart analysis of our iterative DL-SDMA systems using conventional CQs and the proposed ECO-CQs.

4.3.5.1 Iterative DL-SDMA Systems Using Conventional CQ

Figure 4.15 illustrates the EXIT chart of the iterative DL-SDMA systems using the conventional CQs in conjunction with different number of quantization bits, q, which is ranging from $q = 2,3,4$ to 5. Observe that by reducing the number of quantization bits, the inner EXIT-curves, which characterizes the MMSE detector and URC-decoder represented inner systems, are getting closer to the outer EXIT-curve, which characterizes the employed RSC channel decoder, until the open tunnel disappears between them. Based on this EXIT chart, we expect that the system will suffer from a high BER, when using 2-bit CQ at $E_b/N_0 = 6$ dB. On the other hand, the system using a 5-bit CQ performs close to the one benefiting from perfect ST-CIRT.

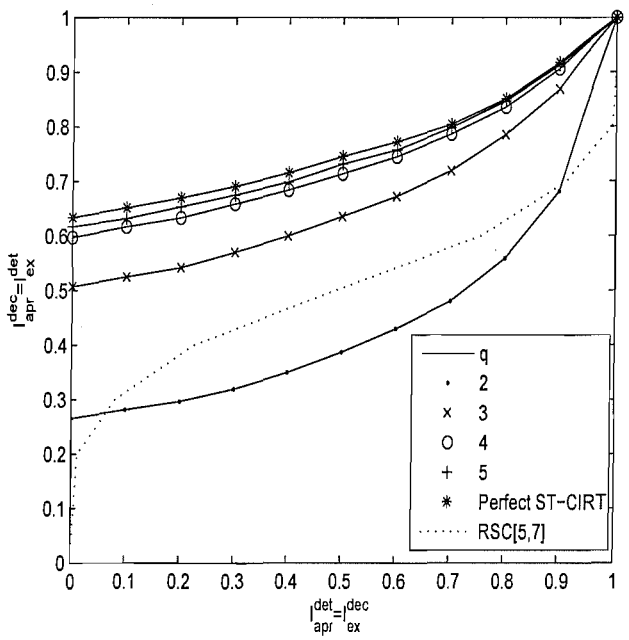

Figure 4.15: EXIT chart analysis of the iterative DL-SDMA system of Figure 4.11 and 4.12 using a q-bit conventional CQ, where q is ranging from 2,3,4 to 5. The systems are operated at $E_b/N_0 = 6$ dB. A rate-0.5 RSC[5,7] channel coder is employed by the system. The channel model was a flat-fading MIMO channel and the parameters of Table 4.6 were used.

Table 4.6: System Parameters

Channel Encoder	rate-0.5 RSC code
Interleaver length	10^5 bits
Modulation	4QAM
Number of users	$K = 3$
Number of transmit antennas	$M = 6$
Dimension of transmitted signal vector	$L_k = 2$, for $k = 1, 2, 3$.
Number of receive antennas	$N_k = 2$, for $k = 1, 2, 3$.

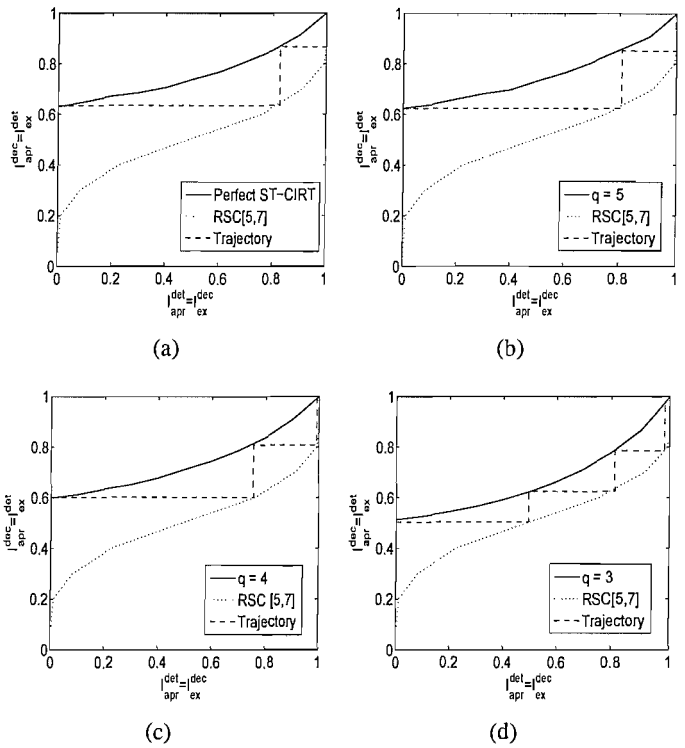

Figure 4.16: EXIT chart analysis of iterative DL-SDMA system of Figure 4.11 and 4.12 using conventional CQ having different values of quantization bit, ranging from 3, 4 to 5 in (b)(c)(d), respectively, when (a) indicates the system employs the perfect ST-CIRT. The systems are operated at $E_b/N_0 = 6$dB. A rate-0.5 RSC[5,7] channel coder is employed for the system. The channel model was a flat-fading MIMO channel and the parameters of Table 4.6 were used.

Furthermore, Figure 4.16 shows the recorded iterative decoding trajectory of the DL-SDMA systems using a q-bit conventional CQ for $E_b/N_0 = 6$dB. Observe that after iterative decoding, the systems using 3-bit, 4-bit, and 5-bit CQs will be able to maintain an open EXIT-tunnel. This implies that the system may reach an infinitesimally low BER for $E_b/N_0 = 6$ dB.

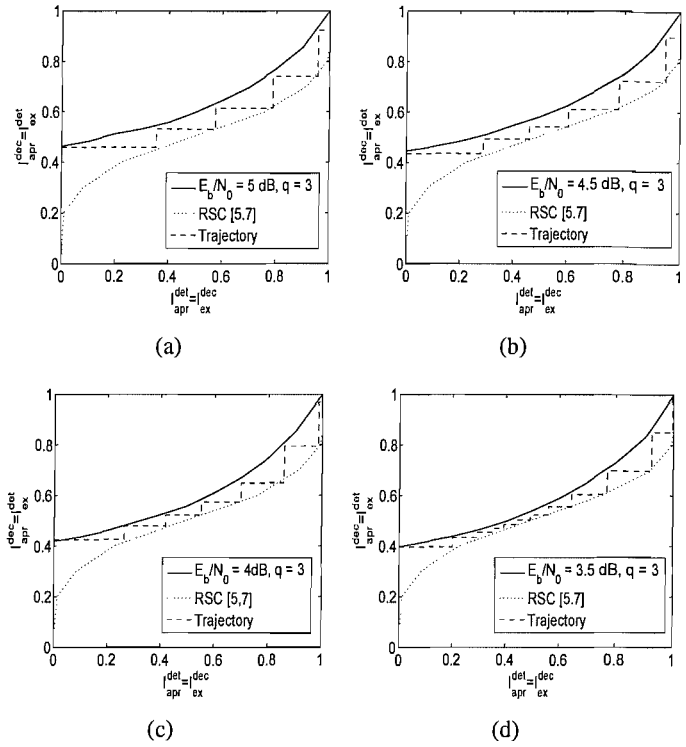

Figure 4.17: EXIT chart analysis of the iterative DL-SDMA system of Figure 4.11 and 4.12 using a 3-bit CQ for different values of E_b/N_0, ranging from 5, 4.5, 4 to 3.5dB in (a)(b)(c)(d), respectively. A rate-0.5 RSC[5,7] channel coder is employed for the system. The channel model was a flat-fading MIMO channel and the parameters of Table 4.6 were used.

Figure 4.17 shows the EXIT chart analysis of iterative DL-SDMA systems using a 3-bit CQ for different values of E_b/N_0. Observe that an EXIT-tunnel is maintained for the tested E_b/N_0 range. With the aid of Figure 4.16 and Figure 4.17, we are able to demonstrate it is feasible to analyze the impact of quantized ST-CIRT on the iterative DL-SDMA systems.

4.3.5.2 Iterative DL-SDMA Systems Using ECO-CQ

In Figure 4.15, we found that the systems using 2-bit CQ are unable to maintain an open EXIT-tunnel for $E_b/N_0 = 6$dB. Therefore, in order to assist the system in maintaining an open EXIT-tunnel at $E_b/N_0 = 6$dB, we have to increase the number of quantization bits to $q = 3$. However, the EXIT-tunnel of the systems using 3-bit CQ is rather wide. With the aid of the proposed algorithm of Section 4.3.3, and given a certain level of E_b/N_0, we will be able to design the system for maintaining a narrow but still open EXIT-tunnel using an average of less than $q = 3$-bit accuracy quantization. According to Equation 4.16, we can design ECO-CQ having a low value of q corresponding to the weighting vector $\boldsymbol{\alpha}$. Figure 4.18(a) shows the EXIT-curves of the iterative DL-SDMA system using

ECO-CQ and $q = 2.6$ as well as $\alpha = [0.4, 0.6, 0, 0]$, namely that 40% ST-CIRTs in a transmission block were quantized by 2-bit CQ, while 60% ST-CIRTs were quantized with 3-bit CQ. In this way, we reduce the number of bits to be fed back to the transmitters. In this example, we reduced 0.4 bits feedback of each sampled ST-CIRT for both the magnitude and phase parts, which means we reduce 0.13%(0.4/3) overall feedback-rate.

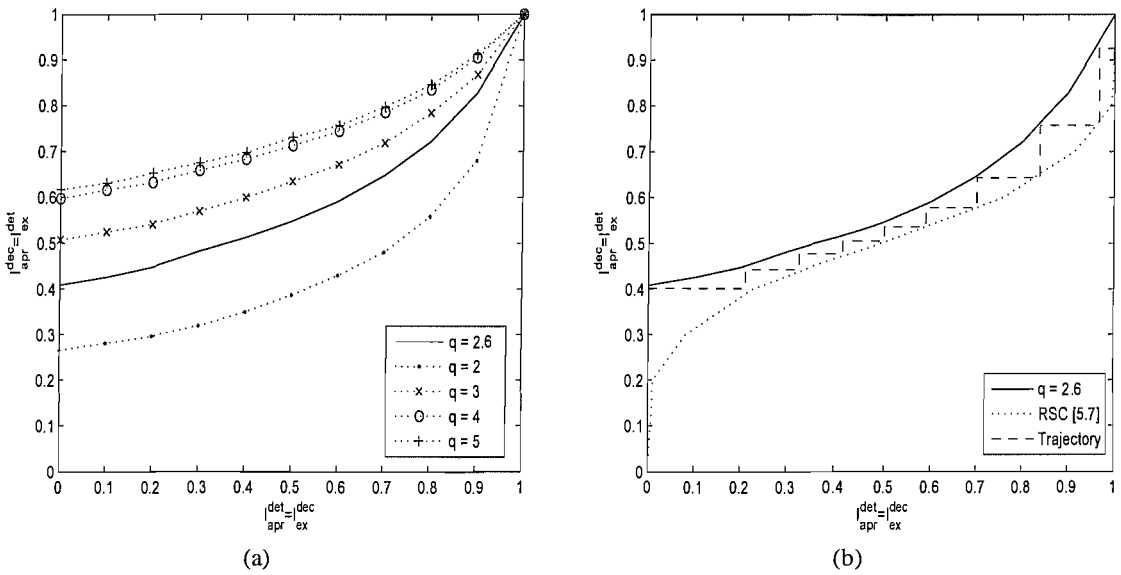

(a) (b)

Figure 4.18: EXIT chart analysis of the iterative DL-SDMA system of Figure 4.13 and 4.14 using ECO-CQ in conjunction with $q = 2.6$ for $E_b/N_0 = 6$dB. (a) shows the inner EXIT-curve of the iterative DL-SDMA system using ECO-CQ. (b) shows the recorded iterative decoding trajectory of the iterative DL-SDMA system using ECO-CQ. A rate-0.5 RSC[5,7] channel coder is employed for the system. The channel model was a flat-fading MIMO channel and the parameters of Table 4.6 were used.

Furthermore, Figure 4.19 characterizes the iterative DL-SDMA system using ECO-CQ in conjunction with different values of q along with the corresponding weighting vector α listed in Table 4.7.

Table 4.7: q and corresponded weighting vector α

q	2.6	2.7	2.8	2.9	3.5
α	[0.4,0.6,0,0]	[0.3,0.7,0,0]	[0.2,0.8,0,0]	[0.1,0.9,0,0]	[0,0.5,0.5,0]

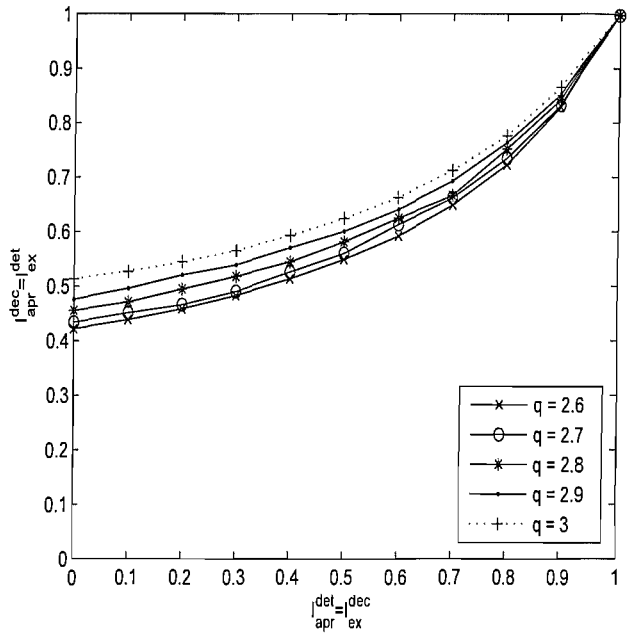

Figure 4.19: EXIT chart analysis of the iterative DL-SDMA system of Figure 4.13 and 4.14 using ECO-CQ in conjunction with different values of q for $E_b/N_0 = 6$dB. A rate-0.5 RSC[5,7] channel coder is employed for the system. The channel model was a flat-fading MIMO channel and the parameters of Table 4.6 were used.

4.3.6 Performance Results

In the following discussions we provide the corresponding BER performance results and also show their consistency with our EXIT chart analysis. The system parameters used are listed in Table 4.6.

4.3.6.1 BER performance of the iterative DL-SDMA system using CQ and ECO-CQ

Figure 4.20 characterizes the BER performance of the iterative DL-SDMA system using a conventional CQ and am ECO-CQ. As illustrated in Figure 4.20, the iterative DL-SDMA systems using ECO-CQ in conjunction with $q = 2.6$ bits are capable of obtaining an infinitesimally low BER lower at $E_b/N_0 = 6$ dB. This confirms the prediction of the EXIT chart analysis seen in Figure 4.18. Upon increasing q, we are able to achieve an infinitesimally low BER at lower E_b/N_0. The BER performance of system using perfect ST-CIRT is also provided in Figure 4.20 as a benchmark. Figure 4.20 shows the performance of the system using 5-bits CQ is close to the one benefiting from perfect ST-CIRT. Compared to $q = 5$, we are able to reduce 1.5 quantization bits per ST-CIRT sample for both magnitude and phase quantization by using ECO-CQ in conjunction with $q = 3.5$ at an E_b/N_0 loss

of less than 0.5 dB.

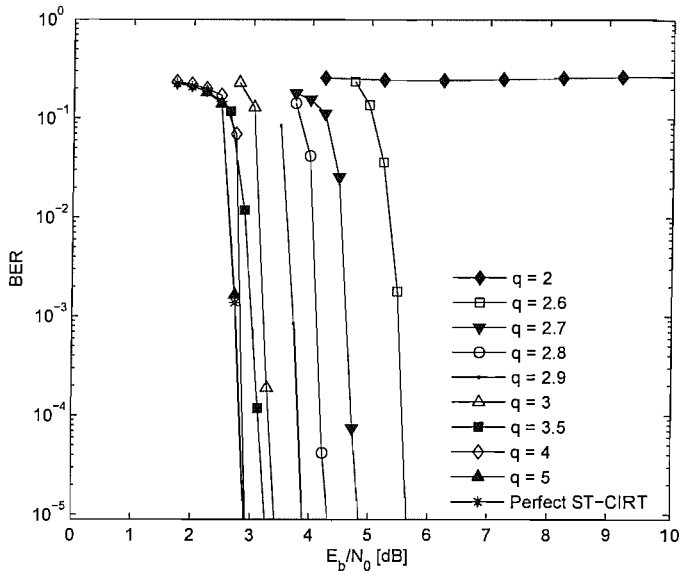

Figure 4.20: BER performance of the iterative DL-SDMA systems of Figure 4.13 and 4.14 using ECO-CQ in conjunction with different values of q. The number of decoding iteration is $I = 12$. A rate-0.5 RSC[5,7] channel coder is employed for the system. The channel model was a flat-fading MIMO channel and the parameters of Table 4.6 were used.

Figure 4.21 portrays the BER performance of the ECO-CQ aided iterative DL-SDMA system for different values of q at $E_b/N_0 = 5dB$, which was recorded for different numbers of decoding iterations. As expected, the achievable system performance will improve upon increasing the number of decoding iterations I. As illustrated in Figure 4.21, the BER of the system employing $q = 3$ is improved from 10^{-1} to a value below 10^{-5} upon increasing I from 2 to 5. Secondly, when using the ECO-CQ, we are able to employ lower value of q. For example, for $I = 10$, the ECO-CQ aided system is capable of achieving a target BER of 10^{-5} using $q = 2.7$, while the system uses conventional CQ requires $q = 3$ for the same. In other words, the flexibility of ECO-CQ assists the system in employing lower number of quantization bits, which reduces the feedback bitrate at a given BER performance.

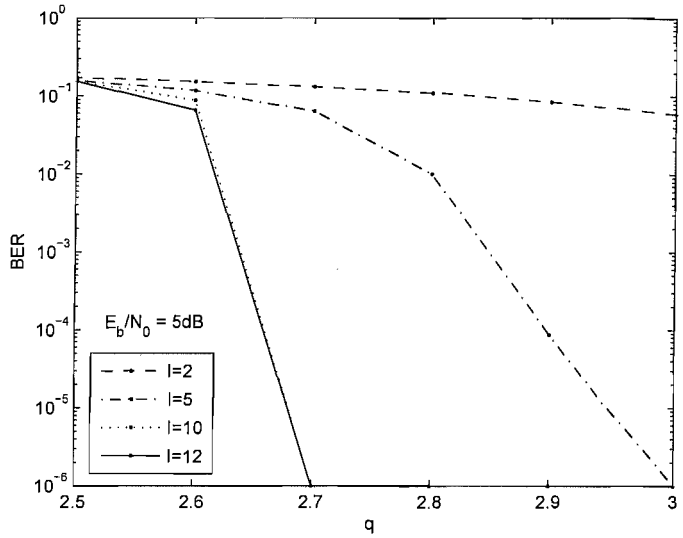

Figure 4.21: BER performance of the ECO-CQ aided iterative DL-SDMA systems of Figure 4.13 and 4.14 for different values of q at $E_b/N_0 = 5dB$. The performance of the system at different numbers of decoding iterations are investigated. A rate-0.5 RSC[5,7] channel coder is employed for the system. The channel model was a flat-fading MIMO channel and the parameters of Table 4.6 were used.

4.3.6.2 BER performance of the iterative DL-SDMA system subjected to MUI

As mentioned, the imperfect ST-CIRT will introduce MUI. In Figure 4.22(a), we illustrate the BER performance of the system subject to MUI, which is characterized by recording the variance σ^2_{MUI} of the MUI. Also, the σ^2_{MUI} induced by different values of q is illustrated in Figure 4.22(b). In the low E_b/N_0 range, such as 2 dB, the systems become less sensitive to σ^2_{MUI}, because the ST-CIRT quantization error effects are masked by the noise. However, for higher E_b/N_0 values, such as 5, 10 dB, the BER performance of the systems improves upon reducing the effects of σ^2_{MUI}, which is achieved by using a higher q. Observe in Figure 4.22(a) that when σ^2_{MUI} is less than -4 dB, the BER performance can be further improved by using a higher number of decoding iterations. If σ^2_{MUI} is higher than this -4dB, the system tends to exhibit a high BER.

4.3.6.3 Further improvement of the ECO-CQ-aided iterative DL-SDMA system using IRCCs

In the above discussions, the systems employed a rate-0.5 RSC[5,7] channel coder. However, we can further improve the achievable performance by employing IRCC [69]. With the aid of EXIT charts, we may redesign the outer EXIT-curve, which characterizes the channel decoder, by employing IR-CCs for reducing the value of q of ECO-CQ. In Figure 4.23 we characterize the iterative DL-SDMA

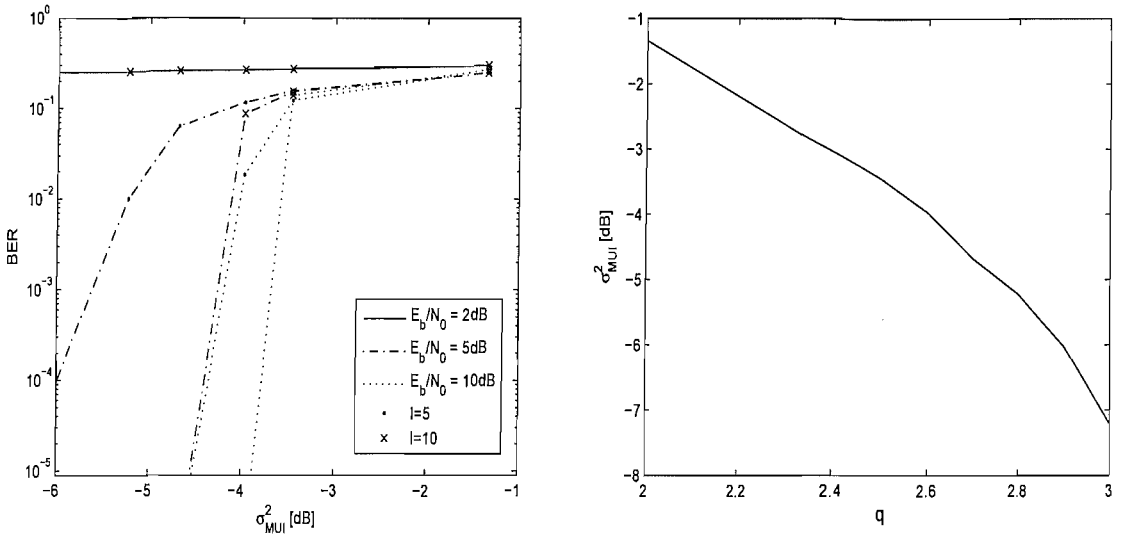

(a) (b)

Figure 4.22: (a) shows the BER performance of the iterative DL-SDMA systems of Figure 4.13 and 4.14 subject to the variance σ^2_{MUI} of the MUI. The performance at different numbers of decoding iterations and different E_b/N_0s are investigated. (b) shows the variance σ^2_{MUI} of the MUI subject to different values of q. A rate-0.5 RSC[5,7] channel coder is employed for the system. The channel model was a flat-fading MIMO channel and the parameters of Table 4.6 were used.

system of Table 4.6 employing an IRCC having a rate-0.5, while using an ECO-CQ having $q = 2.5$ and operating at $E_b/N_0 = 5$ dB. First, we show the EXIT chart of the rate-0.5 IRCC in Figure 4.23(a) with its weight vector set to $\boldsymbol{\alpha}_{ircc} = [0, 0, 0, 0, 0, 0, 0.574825, 0.167428, 0, 0, 0, 0.0291502, 0.149874, 0, 0, 0, 0.0787566]$. In the EXIT chart analysis of the system we employ a rate-0.5 RSC[5,7], provided as a benchmarker, Figure 4.23(a) illustrates the absence of an open EXIT-tunnel for the system employing a rate-0.5 RSC[5,7] for the ECO-CQ having $q = 2.5$. On the other hand, by employing a rate-0.5 IRCC using the appropriate weighting vector $\boldsymbol{\alpha}_{ircc}$, we had an open EXIT-tunnel. We also illustrate the recorded decoding trajectory in Figure 4.23(a) showing the Monte Carlo simulation based convergence behaviour. Additionally, we characterize the attainable BER performance of the systems employing rate-0.5 IRCC and RSC channel coders in Figure 4.23(b) in conjunction with different numbers of decoding iterations at $E_b/N_0 = 5$ dB. The associated BER performance further indicated that the rate-0.5 IRCC employed enables the system using ECO-CQ having $q = 2.5$ to achieve a good BER performance upon increasing the number of decoding iterations. For example, the system employing the rate-0.5 IRCC is capable of achieving a BER less than 10^{-5}, when the number of iteration is higher than $I = 35$. On the other hand, the system employing the rate-0.5 RSC experiences a high BER, around 10^{-1} even at a high numbers of decoding iterations.

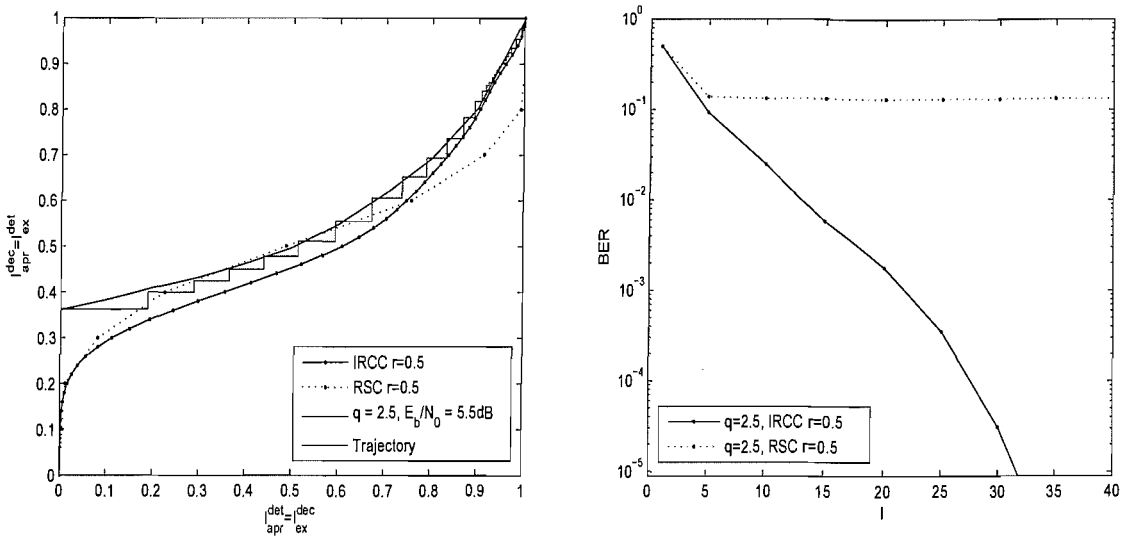

(a) (b)

Figure 4.23: (a) shows the EXIT chart analysis of the iterative DL-SDMA systems of Figure 4.13 and 4.14 employing the rate-0.5 IRCC and the ECO-CQ having $q = 2.5$ at $E_b/N_0 = 5$ dB. (b) shows the corresponding BER performance subject to the number of decoding iterations, I. The EXIT chart analysis and BER performance of the iterative DL-SDMA systems employing a rate-0.5 RSC[5,7] channel coder are provided as benchmarkers. The results show that the rate-0.5 IRCC employed further assist the iterative DL-SDMA system utilizing $q = 2.5$ in maintaining a low BER, while the system employing a half-rate RSC[5,7] results in a high BER. The channel model was a flat-fading MIMO channel and the parameters of Table 4.6 were used.

4.3.7 Conclusions

In this section, we characterized the iterative DL-SDMA systems using ST-CIRT quantization. The quantization error of ST-CIRTs introduce MUI and degrade the attainable performance of the system. We quantified the ST-CIRT imperfection by measuring the variance of ST-CIRT quantization error, i.e. $\sigma^2_{ST-CIRT}$ and investigated its relationship with the number of channel quantization bits employed in Figure 4.10. In addition, in Figure 4.22(a) we quantified MUI by measuring the variance of MUI, i.e. σ^2_{MUI} and related it to the degradation of the BER performance in the iterative DL-SDMA systems. The relationship between σ^2_{MUI} and the number of channel quantization bit employed presented in Figure 4.22(b).

Furthermore, we demonstrated in Figure 4.15 and Figure 4.16 that the impact of imperfect ST-CIRT on the systems can be analyzed with the aid of EXIT chart. We found that when the number of quantization bits q employed in the conventional CQ is increased to $q = 5$, the EXIT chart anal-

ysis predicts a performance close to that using perfect ST-CIRT. This implies that the impact of the imperfect ST-CIRT becomes negligible, when the number of quantization bits employed increases to $q = 5$ bits. Moreover, we proposed an ECO-CQ aided iterative DL-SDMA system designed with the aid of EXIT charts. The merit of ECO-CQ is that it allows to more flexibly utilize the ST-CIRT quantization and hence further assists us in reducing the number of quantization bits and hence to reduce the feedback bit-rate. Quantitatively, at $E_b/N_0 = 5$ dB, by using ECO-CQ having $q = 2.7$ quantization bits, the iterative DL-SDMA becomes capable of achieving a BER less than 10^{-5}. By contrast, the conventional CQ needs $q = 3$ quantization bits. In addition, we further improved the achievable performance by reshaping the outer EXIT-curve by employing a rate-0.5 IRCC. Observe in Figure 4.23(b) that the system employing the rate-0.5 IRCC resulted in a BER less than 10^{-5}, while the system using the rate-0.5 RSC experienced a high BER, around 10^{-1}.

4.4 Summary and Conclusions

In this chapter, we used the design concept of [69] to assist us in configuring the iterative DL-SDMA system for different operating conditions, namely reducing the complexity of iterative detection in Section 4.2 and when using a limited-rate ST-CIRT feedback channel in Section 4.3.

In Section 4.2, we proposed a generic detection framework, which was referred to as the IrGD scheme. By taking into account both the complexity per iterative detection stage and the number of iterations required, the proposed IrGD arrangement may reduce the overall iterative decoding complexity. We showed in Figure 4.6 and Figure 4.7 that the IrGD aided iterative DL-SDMA system has the lowest complexity compared to the benchmark systems. Tables 4.8 and 4.9 summarize the complexity ratio of the IrGD aided iterative systems and the benchmarker systems in comparison to the Log-MAP detector. Again, the IrGD aided system had the lowest complexity.

Table 4.8: Comparison of the complexity ratio achieved by the iterative DL-SDMA systems using different detectors (extracted from Figure 4.6)

E_b/N_0 [dB]	1.7	2.2	2.7	3.2
Log-MAP	1	1	1	1
OHRSA	0.64	0.4167	0.4000	0.3750
MMSE	0.41	0.2056	0.2056	0.2056
IrGD	0.36	0.2056	0.1967	0.1752

Table 4.9: Comparison of the complexity ratio achieved by the iterative DL-SDMA systems using different detectors (extracted from Figure 4.7)

E_b/N_0 [dB]	4	4.5	5	5.5	6
Log-MAP	1	1	1	1	1
OHRSA	N/A	0.0101	0.0097	0.0095	0.0091
MMSE	N/A	N/A	N/A	0.0003	0.0003
IrGD	N/A	0.0037	0.0028	0.0003	0.0003

In Section 4.3, we proposed an algorithm referred to as ECO-CQ, which assists the system in maintaining the minimum feedback overhead, while ensuring that an open EXIT-tunnel is still attainable. In Table 4.10, we characterized the ECO-CQ aided iterative DL-SDMA system using the minimum required number of quantization bits q for both magnitude and phase of each ST-CIRT coefficient, while maintaining a target BER of 10^{-5}. In order to attain the target BER, the system employing conventional CQ may be required to use a 3-bit CQ to quantize the ST-CIRT, when we have $E_b/N_0 \geq 4$dB, as illustrated in Figure 4.20. On the other hand, the ECO-CQ aided system may use a reduced value of q to quantize the ST-CIRT, such as 2.9, 2.8, 2.7, and 2.6, while maintaining the same target BER. The corresponding reduced feedback overheads are listed in Table 4.10. For example, the ECO-CQ aided iterative DL-SDMA system associated with $q = 2.7$ has 10% normalized overhead reduction at $E_b/N_0 = 5$dB.

Table 4.10: Reduced feedback rate of the ECO-CQ aided iterative DL-SDMA systems (extracted from Figure 4.20)

	E_b/N_0 [dB]	3	3.5	4	4.5	5	6
Conventional CQ	Minimum required q-bit	4	3	3	3	3	3
	Normalized overhead Λ	0.024	0.018	0.018	0.018	0.018	0.018
ECO-CQ	Minimum required q-bit	4	3	2.9	2.8	2.7	2.6
	Normalized overhead Λ	0.024	0.018	0.0174	0.0168	0.0162	0.0156
Normalized overhead reduction ratio R_Λ		0	0	0.033	0.067	0.1	0.13

Chapter 5

Irregular Sphere Detection Aided Iterative Downlink SDMA Systems Using Linear Dispersion Codes

5.1 MUT Aided DL-SDMA Using Linear Dispersion Codes

An attractive space-time signaling technique, referred to as Linear Dispersion Coding (LDC), was proposed by the Hassibi and Hochwald [81]. The merits of the LDC are two-fold: 1) They have high capacity. 2) They have a high grade of flexibility, when designing space-time coded signaling schemes operating at different coding rates. In contrast, the family of orthogonal space-time block codes [9] guarantees achieving the maximum diversity gain, but not the maximum channel capacity of MIMOs. Furthermore, orthogonal space-time block codes have a limited choice in terms of their code rate. Therefore, the family of LDCs constitutes a more advanced space-time signaling scheme than that of the orthogonal space-time block codes. According to the design concept of LDCs [81], the transmitted symbols are dispersed in the spatial domain to several transmit antennas by multiplying them with the basis matrices, or the so-called dispersion matrices, and then combined into a new codeword, which we refer to as an LDC symbol. Generating the LDC symbols with the aid of the basis matrices may be viewed as a type of linear matrix modulation [47], where the linear modulation matrix is constructed based on optimized basis matrices. The design of LDCs is based on finding basis matrices, which maximize the ergodic MIMO capacity, defined in [4]. Hence, the LDC scheme proposed in [81] may be considered as a capacity-approaching space-time signaling technique. This

motivates us to redesign the MUT scheme of Chapter 2 invoking LDC-aided space-time signaling for ensuring that the LDC-aided MUT DL-SDMA scheme approaches the MIMO channel's capacity.

Moreover, in Chapter 2 we considered a scenario, which is similar to a V-BLAST-type downlink (DL) transmission scheme and may be classified as an SDM-SDMA MUT scheme. In Chapter 3 and 4 we studied the design of iterative joint detection and decoding based on this MUT scheme. However, this MUT scheme exploited the independent fading of the Array Elements (AE) in the spatial domain only. This spatial diversity scheme may, however, have a limited diversity gain owing to the correlated nature of shadow-fading. In order to counteract this limitation, *our contribution in this chapter is that we introduce an MUT aided DL-SDMA using an LDC based space-time signaling scheme in Section 5.1.2, which jointly exploits the independent nature of fading in both the spatial- and time- domain in order to increase the achievable degree of freedom and hence to further increase the attainable diversity gain. Furthermore, we proposed the concept of irregular sphere detection, which was designed to reduce the complexity imposed by the joint iterative detection and decoding of the LDC aided iterative DL-SDMA system.*

In order to differentiate the MUT scheme of Chapter 2 and the MUT invoking the LDC based space-time signaling scheme proposed in this chapter, we refer to the former as the basic MUT scheme and to the latter as the LDC-aided MUT scheme. The exploitable degree of freedom provided by the basic MUT scheme is proportional to the number of transmit antennas, which is limited due to the physical size of the BS's transmitters. This limits the achievable data throughput and the diversity gain attained by the system. As a countermeasure, the proposed LDC-aided MUT DL-SDMA system has an increased diversity gain, which results in an improved BER performance, as we will demonstrate in Section 5.1.4. Furthermore, the increased flexibility of the proposed LDC aided MUT assisted DL-SDMA system allows us to accommodate time-variant channel conditions, as we will discuss in Section 5.1.4.

The rest of this section is structured as follows. First, we highlight the general structure of LDCs in Section 5.1.1. Then we introduce the LDC-aided MUT DL-SDMA system model in Section 5.1.2. In Section 5.1.3, we detail the design of the LDC-aided MUT scheme, followed by our discussions of the system's capacity. The normalized system load is defined in Section 5.1.4, complemented by the corresponding performance results. Finally, we conclude in Section 5.1.5.

5.1.1 Linear Dispersion Code

In this section we briefly summarize the general structure of LDCs [47, 81]. The basic philosophy of LDCs is to encode the Q data symbols which are about to be transmitted in an interval of T symbol Time Slots (TS) into a new codeword with the aid of a set of dispersion matrices, which we refer to as an LDC symbol. Then the code rate of the LDC is given by $N_{bps} \cdot Q/T$, where N_{bps} is the number of bits contained in each data symbol. Let us consider a single-user MIMO system having M transmit antennas and N receive antennas. Let $d_n|_{n=1}^{Q}$ be the complex data symbol, which may be generated by a QPSK or QAM modulator. Let $\mathbf{M}_n|_{n=1}^{Q}$ be the set of $(M \times T)$-element dispersion matrices. Therefore, the LDC symbol, denoted by $\mathbf{Z}$, obeys

$$\mathbf{Z} = \sum_{n=1}^{Q} \mathbf{M}_n d_n. \tag{5.1}$$

Example 5.1: Use LDC in a (2×2)-MIMO system

Let us consider a (2×2)-MIMO system as an example, where the MIMO system has $M = 2$ transmit antennas and $N = 2$ receiver antennas. As illustrated in Figure 5.1, there are $(Q = 2)$ data symbols d_1 and d_2 to be encoded into an LDC symbol $\mathbf{Z}$. First, the data symbols d_1 and d_2 will be multiplied by the dispersion matrices $\mathbf{M}_1$ and $\mathbf{M}_2$, respectively and then they will be added to construct the LDC symbol $\mathbf{Z}$. Also, let $T = 2$, which means that the LDC symbol $\mathbf{Z}$ will be transmitted in $T = 2$ consecutive symbol-slots.

As seen in Figure 5.1, the coefficients of $\mathbf{Z}$, z_1 and z_3 are transmitted via AE 1 in the TS $t = 0$ and $t = 1$, respectively. Similarly, z_2 and z_4 are transmitted via AE 2 in TS $t = 0$ and $t = 1$, respectively. Observe that due to the LDC coding, the both data symbols d_1 and d_2 contribute all the coefficients of the LDC symbol $\mathbf{Z}$, namely the z_1, z_2, z_3 and z_4, which indicates that the data symbols d_1 and d_2 are both dispersed to the two AEs and to the two time slots. Hence they benefit from both spatial- and time-diversity.

The coefficient $[\mathbf{Z}]_{m,t}$ represents the symbol to be transmitted from the m-th transmit antenna in the t-th QPSK/QAM-symbol slot of the LDC-symbol interval T. Let $\mathbf{H}_t$ be the $(N \times M)$-element matrix which represents the Rayleigh fading MIMO channel realization experienced during the t-th QPSK/QAM-symbol slot. Let us now define the diagonal channel matrix $\mathcal{H} = \text{diag}\left([\mathbf{H}_1, \mathbf{H}_2, \cdots, \mathbf{H}_T]^T\right)$ and the *linear dispersion matrix* $\mathcal{X}$ as $\mathcal{X} = [vec(\mathbf{M}_1), vec(\mathbf{M}_2), \cdots, vec(\mathbf{M}_Q)]$ [1] as well as $\boldsymbol{d} =$

[1] $vec(\cdot)$ is the operator that forms a column vector from successive columns of a matrix, where $vec^{-1}(\cdot)$ is the reverse operation, reconstructing the original matrix from the column vector.

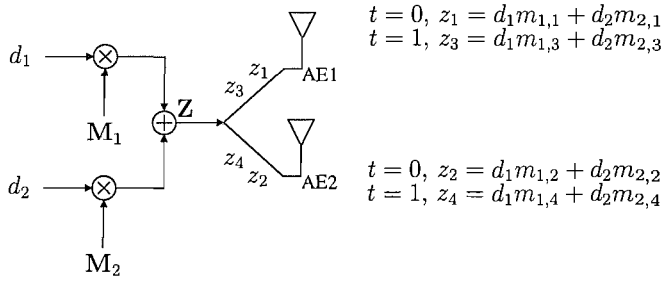

$$\mathbf{Z} = d_1\mathbf{M}_1 + d_2\mathbf{M}_2$$

$$\mathbf{Z} = \begin{bmatrix} z_1 & z_3 \\ z_2 & z_4 \end{bmatrix} \quad \mathbf{M}_1 = \begin{bmatrix} m_{1,1} & m_{1,3} \\ m_{1,2} & m_{1,4} \end{bmatrix} \quad \mathbf{M}_2 = \begin{bmatrix} m_{2,1} & m_{2,3} \\ m_{2,2} & m_{2,4} \end{bmatrix}$$

Figure 5.1: LDC in a (2×2)-MIMO system

$[d_1, d_2, \cdots, d_Q]^T$. The received signal vector observed over the duration of T, denoted by $\boldsymbol{Y}$, is then given by

$$\boldsymbol{Y} = \mathcal{H}\mathcal{X}\boldsymbol{d} + \boldsymbol{N}, \tag{5.2}$$

where $\boldsymbol{N}$ represents the AWGN vector observed over the duration of T QPSK/QAM-symbol slots. Each constituent element of $\boldsymbol{N}$ obeys the distribution $\mathcal{CN}(0, N_o)$. We may express the LDC symbol in vectorical form as $\mathbf{S} = \mathcal{X}\boldsymbol{d}$, where $\mathbf{S} = vec(\mathbf{Z})$.

According to [47, 81], the ergodic capacity of the system described by Equation 5.2 when using the optimum LDC is given by

$$\mathfrak{C} = \max_{\mathrm{tr}(\mathcal{X}\mathcal{X}^H) \le T} \frac{1}{T} \mathrm{E}\left\{ \log_2 \det\left(\boldsymbol{I} + \frac{E_d}{N_o} \mathcal{H}\mathcal{X}\mathcal{X}^H\mathcal{H}^H \right) \right\}, \tag{5.3}$$

where we have $E_d = \mathrm{E}\left\{ ||\boldsymbol{d}||^2 \right\}$.

The algorithms designed for finding $\mathcal{X}$, which optimizes Equation 5.3 were detailed in [47, 81–83]. LDCs may be optimized using different criteria. For example, Hassibi and Hochwald [81] proposed the design of LDCs maximizing the ergodic capacity of a single-user MIMO system. On the other hand, Heath and Paulraj [47] designed LDCs for minimizing the Bit Error Ratio (BER). By contrast, the design objective of Wang *et. al.* [82] was to design LDCs for achieving a low BLock Error Ratio (BLER). In contrast to the pervious randomly-search LDC design, [84] proposed a structured LDC. Against this background, we aim for designing LDCs for achieving the maximum attainable sum capacity of the DL-SDMA system, which will be detailed in Section 5.1.3. Let us now continue by introducing the system model of our LDC-aided DL-SDMA scheme in the following section. We will further discuss the highest- capacity LDC in Section 5.1.3 in the context of the LDC-aided MUT DL-SDMA system. Let us continue by introducing the system model of the LDC-aided DL-SDMA scheme in the following section.

5.1.2 System Model

In this section, we first brief by outline the structure of the iterative DL-SDMA using the basic MUT scheme and later extend it to the system using the LDC-aided MUT scheme.

5.1.2.1 Iterative DL-SDMA Using Basic Multi-User Transmission

The structure of the iterative DL-SDMA schemes of Chapter 3 [43] using the basic MUT scheme is repeated here for the reader's convenience in Figure 5.2. The BS employs M transmit antennas for supporting K MSs, while the k-th MS invokes N_k receive antennas for receiving L_k independent transmitted data streams, where L_k has been defined in Section 3.2.1 as $L_k = M - \sum_{j=1,j\neq k}^{K} N_j$. We assume a flat-fading MIMO channel. We denote the $(M \times N_k)$-element channel matrix by $\boldsymbol{H}_t^{(k)}$, which is constituted by the sampled flat-fading channel impulse responses of each AE experienced by the k-th user at the t-th symbol instant. The elements $[\boldsymbol{H}_t^{(k)}]_{i,j}$, where we have $1 \leq i \leq N_k$ and $1 \leq j \leq M$, are i.i.d complex Gaussian random variables obeying the distribution $\mathcal{CN}(0,1)$.[2]

As illustrated in Figure 5.2, the source bits $b_i^{(k)}|_{i=1}^{L_k N_{bps}}$ transmitting to the k-th user are encoded both by the channel encoder and URC precoder encoder before being modulated using the $2^{N_{bps}}$-ary QAM modulator. Let $\boldsymbol{s}_t^{(k)} \in \mathbb{C}^{L_k \times 1}$ be a complex-valued column vector, which is constituted by the QPSK/QAM modulated data symbols $d_n^{(k)}|_{n=1}^{L_k}$ and denotes the modulated signal vector to be transmitted to the k-th MS in the t-th DL-SDMA symbol time slot, while $L_k = M - \sum_{j=1,j\neq k}^{K} N_j$ represents the number of independent signal streams contained in the DL-SDMA symbol stream $\boldsymbol{s}_t^{(k)}$. Additionally, we define the so-called *Space-Time Preprocessor* (STP) matrix $\boldsymbol{T}_t^{(k)} \in \mathbb{C}^{M \times L_k}$, which was designed for the sake of eliminating the MUI [35] as detailed in [43] and Section 3.2.1. Briefly, $\boldsymbol{T}_t^{(k)}$ may be constructed based on the nullspace of the matrix $\tilde{\boldsymbol{H}}_t^{(k)}$, where the elements of $\tilde{\boldsymbol{H}}_t^{(k)}$ are constituted by $\boldsymbol{H}_t^{(i)}|_{i=1,i\neq k}^{K}$, in order to prevent the users' signals from being transmitted to other users. Hence, the general received signal model of the k-th user is given by,

$$\boldsymbol{r}_t^{(k)} = \boldsymbol{H}_t^{(k)} \boldsymbol{T}_t^{(k)} \boldsymbol{s}_t^{(k)} + \sum_{i=1,i\neq k}^{K} \boldsymbol{H}_t^{(k)} \boldsymbol{T}_t^{(i)} \boldsymbol{s}_t^{(i)} + \boldsymbol{n}_t^{(k)}, \tag{5.4}$$

where the second term of Equation 5.4 represents the MUI, which will be entirely eliminated, when $\boldsymbol{T}_t^{(i)}$ is designed based on the perfect knowledge of $\boldsymbol{H}_t^{(i)}|_{i=1}^{K}$. Furthermore, $\boldsymbol{n}_t^{(k)}$ represents the AWGN noise vectors obeying the distribution $\mathcal{CN}(0, N_0)$ for each constituent element and we have $N_0 = 2\sigma_n^2$.

[2] $[\boldsymbol{A}]_{i,j}$ indicates the i-th row and j-th column element of matrix $\boldsymbol{A}$.

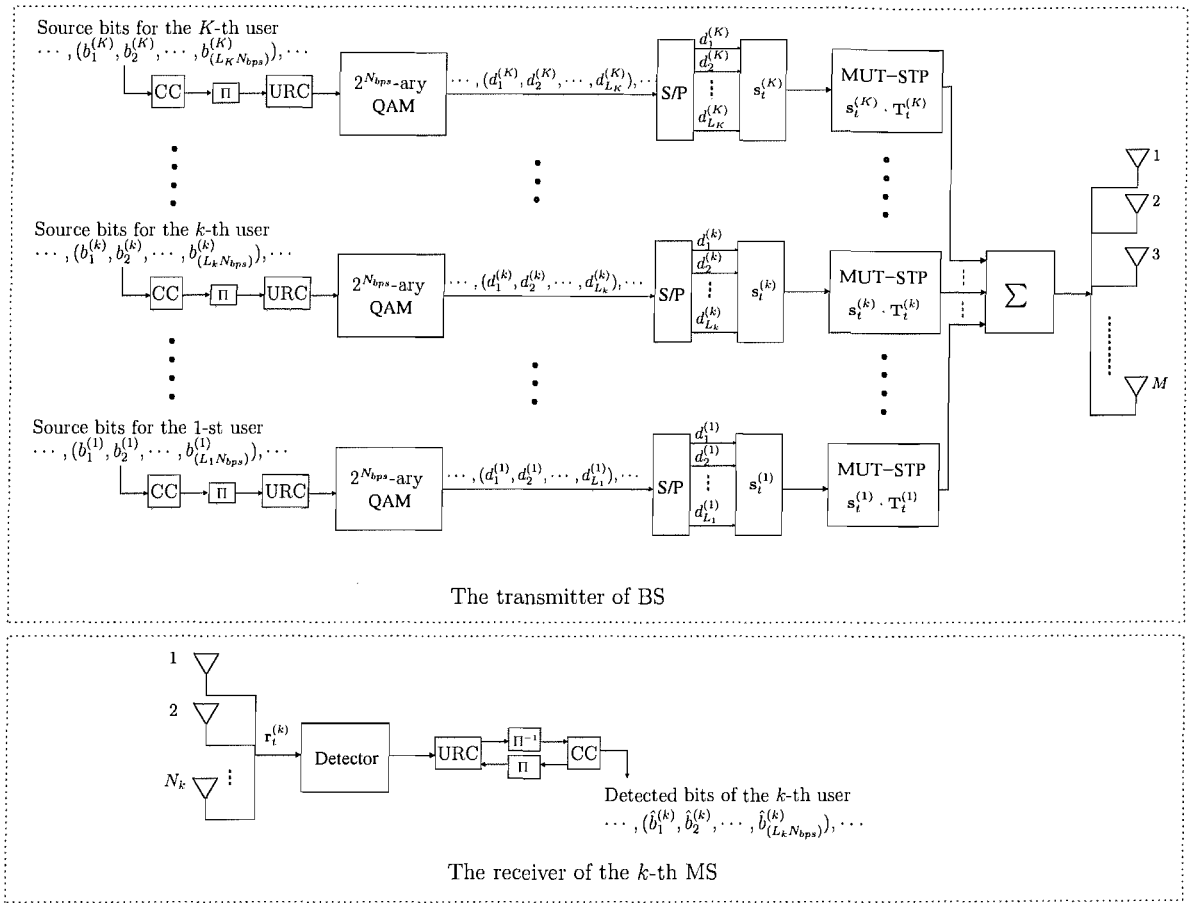

Figure 5.2: Multiuser transmission in the DL-SDMA system

Moreover, we assume that the power constraint $P_T \geq \mathtt{tr}\left(\boldsymbol{T}_t^{(k)}(\boldsymbol{T}_t^{(k)})^H\right)$ of the STP matrix $\boldsymbol{T}_t^{(k)}$ is satisfied for all values of k and t. Therefore we may define the Signal to Noise Ratio (SNR) for each receiver antenna as

$$SNR = \frac{P_T E_s}{N_0}, \tag{5.5}$$

where $E_s = \mathtt{E}\left\{\|s_t^{(k)}\|^2\right\}$ is the average power of the k-th user's modulated signal.

Figure 5.2 also illustrates the structure of each MS's receiver. The detector constitutes the first stage of the receiver and provides soft-bits for the URC decoder. The extrinsic information exchange is carried out between the URC decoder and the channel decoder employed. More detailed discussions of the benefits of this iterative design and its operation have been detailed in Chapter3.

5.1.2.2 Iterative DL-SDMA Using LDC-aided Multi-User Transmission

In this section, we extend the iterative DL-SDMA system of Figure 5.2 using the basic MUT scheme of Section 5.1.2.1 to the system of Figure 5.3 using the LDC aided MUT scheme. As mentioned in

Section 5.1.1, the LDC scheme's space-time symbol is transmitted over an interval of T conventional time slots. Therefore, in order to formulate the system model of the LDC aided MUT in an equivalent input-output format, similarly to Section 5.1.1, we rewrite the related parameters of the basic MUT scheme of Section 5.1.2.1.

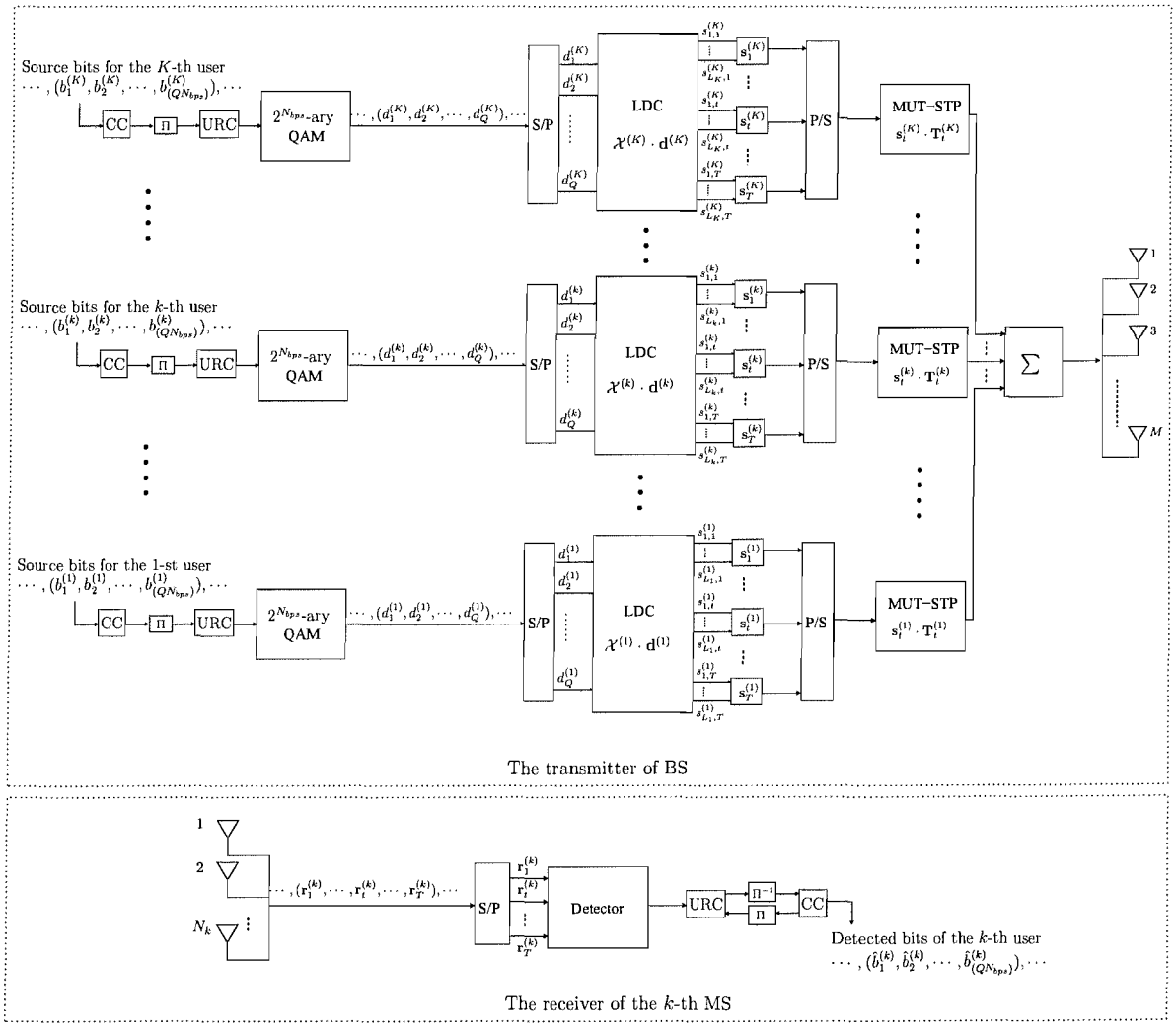

Figure 5.3: LDC-aided Multiuser transmission in the DL-SDMA system

We portray the structure of the iterative DL-SDMA system using the more sophisticated LDC-aided MUT schemes in Figure 5.3. As illustrated in Figure 5.3, the source bits $b_i^{(k)}|_{i=1}^{QN_{bps}}$ transmitted to the k-th user are encoded both by the channel encoder and the URC encoder, before being modulated using the $\mathcal{M}$-ary QAM modulator, where we have $\mathcal{M} = 2^{N_{bps}}$ and N_{bps} denotes the number of bits per modulated symbol. The QAM modulated data symbols $d_n^{(k)}|_{n=1}^{Q}$, which constitute the data vector $\mathbf{d}^{(k)}$, are encoded into the LDC symbol $\mathbf{S}^{(k)}$ by multiplying the data vector $\mathbf{d}^{(k)}$ with the optimum *linear dispersion matrix* $\mathcal{X}^{(k)}$, where the LDC symbol $\mathbf{S}^{(k)}$ is a hyper-vector constituted by T column-vectors, i.e. we have $s_t^{(k)}|_{t=1}^{T}$. Each column-vector $s_t^{(k)}$, constituted by the elements

$s_{j,t}^{(k)}|_{j=1}^{L_k}$, is multiplied by the MUT-STP matrix $T_t^{(k)}$ and combined with the other users' signals before being transmitted via M AEs.

Figure 5.3 also illustrates the structure of each MS's receiver. First, the detector will detect the received signals of the T slots. Then, similar to the basic MUT scheme of Figure 5.2, the extrinsic information exchange is carried out between the URC decoder and the channel decoder employed.

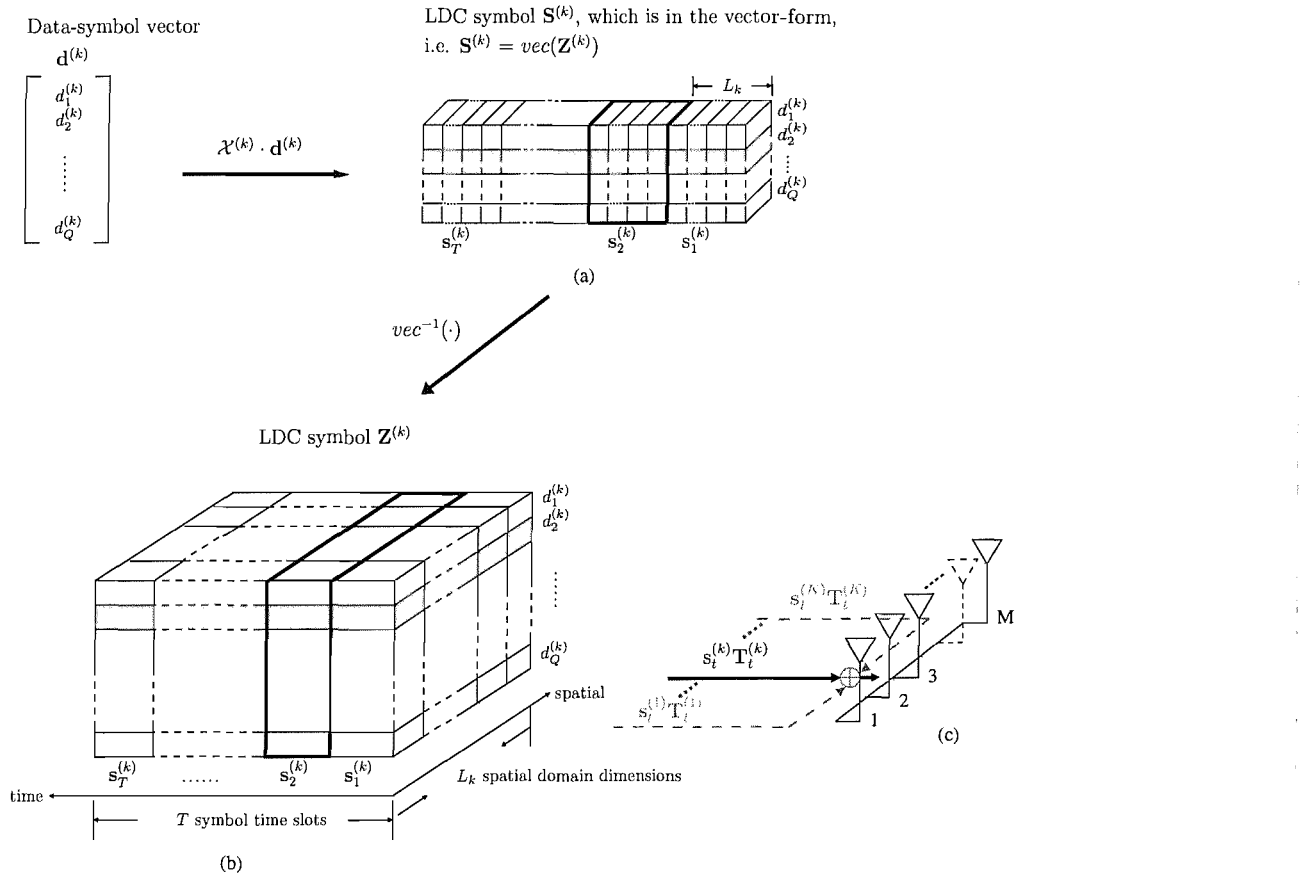

Figure 5.4: The illustration of the LDC symbol encoded from the data symbol

Figure 5.4 illustrates how the Q data symbols $d_n^{(k)}|_{n=1}^{Q}$ benefit from having joint space-time domain diversity gains by virtue of being mapped to the LDC symbols. Again, in the LDC aided MUT DL-SDMA scheme, the LDC symbol is represented by the T-element hyper-vector $\mathbf{S}^{(k)}$, which is constructed by multiplying the $(L_kT \times Q_k)$-element linear dispersion matrix $\mathcal{X}^{(k)}$ with the $2^{N_{bps}}$-ary QAM modulated signal vector $\mathbf{d}^{(k)}$, i.e. we have $\mathbf{S}^{(k)} = \mathcal{X}^{(k)} \cdot \mathbf{d}^{(k)}$. As illustrated in Figure 5.4(a), the t-th column-vector $s_t^{(k)}$ in the LDC symbol $\mathbf{S}^{(k)}$ is constituted by the Q data symbols $d_n^{(k)}|_{n=1}^{Q}$. Therefore, the total transmit power of each data symbol $d_n^{(k)}|_{n=1}^{Q}$ is dispersed into $L_k \cdot T$ transmit symbols over the interval of T slots, as illustrated in Figure 5.4(a). The vectorically segmented LDC symbol $\mathbf{S}^{(k)}$ will be transformed to the LDC symbol $\mathbf{Z}^{(k)}$ of Figure 5.4(b) by using the operator $vec^{-1}(\cdot)$ or

equivalently the parallel-to-serial operation shown in Figure 5.3, namely $\mathbf{Z}^{(k)} = vec^{-1}(\mathbf{S}^{(k)})$. As illustrated in 5.4(b), for each LDC symbol $\mathbf{Z}^{(k)}$, the constituent column-vectors $s_t^{(k)}$ are transmitted during the T consecutive slots. The t-th constituent column-vectors $s_t^{(k)}$ are also distributed to the L_k spatial-domain dimensions, namely the L_k effective transmit antennas allocated to the k-th user. Due to the MUT-STP, shown in Figure 5.4(c), the number of effective transmit antennas allocated to the k-th user L_k obeys $L_k = M - \sum_{j=1,j\neq k}^{K} N_j$. As illustrated in Figure 5.4(b), the power of each data symbol $d_n^{(k)}|_{n=1}^{Q}$ is distributed over T time slots and L_k spatial-domain dimension. This provides joint space-time domain diversity gains for each data symbol.

Let $\mathbf{H}^{(k)}$ represents the observed MIMO CIR of the k-th user, which is assumed to be time-variant over an interval of T slots, i.e. we have $\mathbf{H}^{(k)} = [\boldsymbol{H}_1^{(k)}, \boldsymbol{H}_2^{(k)}, \cdots, \boldsymbol{H}_t^{(k)}, \cdots, \boldsymbol{H}_T^{(k)}]^T$. Furthermore, let $\mathbf{T}^{(k)} = [\boldsymbol{T}_1^{(k)}, \boldsymbol{T}_2^{(k)}, \cdots, \boldsymbol{T}_t^{(k)}, \cdots, \boldsymbol{T}_T^{(k)}]^T$. Therefore, we may express the effective channel matrix $\mathcal{H}^{(k)}$ experienced by the k-th user over the interval of T slots, i.e. over the duration of an LDC symbol, as

$$\mathcal{H}^{(k)} = \text{diag}\left(\mathbf{H}^{(k)}\right) \text{diag}\left(\mathbf{T}^{(k)}\right), \tag{5.6}$$

where $\text{diag}(\mathbf{h})$ represents a diagonal matrix having the elements of $\mathbf{h}$.

Hence, we denote $\mathbf{Y}^{(k)}$ as the k-th user received signal observed successively over an interval of T slots, which is given by

$$\mathbf{Y}^{(k)} = \mathcal{H}^{(k)}\mathbf{S}^{(k)} + \sum_{i=1,i\neq k}^{K} \mathcal{H}^{(k)}\mathbf{S}^{(i)} + \mathbf{N}^{(k)}, \tag{5.7}$$

where again $\mathbf{S}^{(k)}$ represents a T-element hyper-vector, i.e. the generated LDC symbol given in vectorical form. The hyper-vector $\mathbf{S}^{(k)}$ is constituted by the column-vectors $s_t^{(k)}|_{t=1}^{T}$, which are defined in the basic MUT scheme illustrated in Figure 5.3. Similarly, $\mathbf{N}^{(k)}$ is a T-element vector, which is constituted by $n_t^{(k)}|_{t=1}^{T}$, while the second term represents the MUI.

5.1.3 Design of the Linear Dispersion Matrix

There are two main benefits of exploiting the linear dispersion matrix $\mathcal{X}^{(k)}$. Firstly, it increases the achievable transmit diversity of the system by exploiting the extra degree of freedom provided by the time domain, where the maximum joint transmit diversity order of the time and spatial domain is L_kT for the k-th user, as illustrated in Figure 5.4(b). In contrast, only spatial diversity is provided by the basic MUT scheme of Figure 5.2, described by the system model of Equation 5.4, where the maximum transmit diversity order is only L_k for the k-th user [43]. Secondly, the LDC matrix allows

us to increase the variety of the transmission data rates available by increasing the degrees of freedom, which is achieved by exploiting the different combinations of Q_k and L_kT.

In order to design the linear dispersion matrix $\mathcal{X}^{(k)}$ for achieving the maximum attainable degree of freedom, we may design the columns of $\mathcal{X}^{(k)}$ to be orthogonal vectors. This may be achieved, for example, by using the QR-decomposition [85] of a $(D \times D)$-element random matrix $\mathbf{A}$, according to $\mathbf{A} = \mathbf{QR}$, where we have $D = \max\{L_kT, Q\}$. Then we assign the column or row vectors of $\mathbf{Q}$ to the columns of $\mathcal{X}^{(k)}$ [47]. There are several alternative techniques of generating the orthogonal vectors used for constructing the linear modulation matrix $\mathcal{X}^{(k)}$, which have been further detailed in [47]. Suffice to say here that for a given set of parameters Q, L_k and T, the choice of $\mathcal{X}^{(k)}$ is not unique.

Example 5.2: Design of the orthogonal columns of the linear dispersion matrix by using the QR-decomposition

Assuming that we have $Q = 4, T = 2$ and $L_k = 2$, we demonstrate how to generate a linear dispersion matrix $\mathcal{X}^{(k)}$ for the k-th MS by using the QR-decomposition. First we randomly generate a (4×4)-matrix $\mathbf{A}$ and let $\mathbf{A} = \mathbf{QR}$ using using the QR-decomposition, where

$$\mathbf{A} = \begin{bmatrix} -0.4326 + 1.0668i & -1.1465 + 0.2944i & 0.3273 - 0.6918i & -0.5883 - 1.4410i \\ -1.6656 + 0.0593i & 1.1909 - 1.3362i & 0.1746 + 0.8580i & 2.1832 + 0.5711i \\ 0.1253 - 0.0956i & 1.1892 + 0.7143i & -0.1867 + 1.2540i & -0.1364 - 0.3999i \\ 0.2877 - 0.8323i & -0.0376 + 1.6236i & 0.7258 - 1.5937i & 0.1139 + 0.6900i \end{bmatrix}, \tag{5.8}$$

$$\mathbf{Q} = \begin{bmatrix} -0.1953 + 0.4818i & 0.2398 - 0.5443i & -0.1783 + 0.0227i & 0.5856 + 0.0271i \\ -0.7522 + 0.0268i & -0.1726 - 0.0072i & -0.2331 - 0.1521i & -0.2502 - 0.5134i \\ 0.0566 - 0.0432i & -0.5393 - 0.2589i & -0.3429 - 0.5556i & -0.0692 + 0.4538i \\ 0.1299 - 0.3759i & 0.2514 - 0.4419i & -0.5524 + 0.3985i & -0.3453 + 0.0126i \end{bmatrix}, \tag{5.9}$$

and

$$\mathbf{R} = \begin{bmatrix} 2.2143 & -1.1445 + 1.7566i & 0.1230 - 0.5439i & -2.4412 + 0.1808i \\ 0 & -2.1843 & 1.0815 - 0.9393i & 0.1631 - 0.3445i \\ 0 & 0 & -1.9141 & -0.0425 + 0.1040i \\ 0 & 0 & 0 & -1.4258 \end{bmatrix}. \tag{5.10}$$

Then, we use the column vectors of $\mathbf{Q}$ to construct the columns of $\mathcal{X}^{(k)}$. Due to the fact that $\mathbf{Q}$ and $\mathcal{X}^{(k)}$ are both a (4×4)-element square matrix and due to the orthogonality of $\mathbf{Q}$, we have $\mathcal{X}^{(k)} = \mathbf{Q}/\sqrt{2}$, where $1/\sqrt{2}$ is a normalizing factor. However, another randomly generated $\bar{\mathbf{A}}$ may result in another matrix $\bar{\mathbf{Q}}$ when using QR-decomposition and we may also use $\bar{\mathbf{Q}}$ to construct the orthogonal columns of the linear dispersion matrix $\mathcal{X}^{(k)}$. Therefore the choice of $\mathcal{X}^{(k)}$ is not unique.

Let us detail now how the LDC scheme of [47] may be invoked to assist in the design of $\mathcal{X}^{(k)}$. More specifically, we may design $\mathcal{X}^{(k)}$ to approach the attainable capacity as closely as possible, as advocated in [47]. When we have $L_k T = Q$, i.e. $\mathcal{X}^{(k)}$ is a square matrix, the system described by $\mathcal{X}^{(k)}$ becomes capable of approaching the attainable capacity, as long as it satisfies $\mathcal{X}^{(k)}(\mathcal{X}^{(k)})^H = \boldsymbol{I}/L_k$ [47]. This condition may be met by constructing $\mathcal{X}^{(k)}$ with the aid of orthogonal vectors. However, in the case of $L_k T = Q$, the choice of $\mathcal{X}^{(k)}$ is not unique, as demonstrated in Example 5.2. In the case of $L_k T > Q$ or $L_k T < Q$ and assuming that the data symbol $d_n^{(k)}|_{n=1}^{Q}$ is a continuous-valued Gaussian signal, we may conduct a numerical search to find that particular matrix $\mathcal{X}^{(k)}$ which maximizes the equivalent ergodic capacity for the k-th user, as expressed in [47],

$$\mathfrak{C}^{(k)} = \max_{\mathrm{tr}\left(\mathcal{X}^{(k)}(\mathcal{X}^{(k)})^H\right) \leq T} \frac{1}{T} \mathrm{E}\left\{ \log_2 \det\left(\boldsymbol{I}_{N_k T} + \frac{E_s}{N_o} \mathcal{H}^{(k)} \mathcal{X}^{(k)} (\mathcal{X}^{(k)})^H (\mathcal{H}^{(k)})^H \right) \right\}, \tag{5.11}$$

where the equivalent ergodic capacity $C^{(k)}$ is constituted by the mutual information between the transmitted and received signal, when the MUI in the second term of Equation 5.7 is entirely eliminated. The expectation $\mathrm{E}\{\cdot\}$ in Equation 5.11 is taken with respect to different channel realizations $\mathcal{H}^{(k)}$.

In contrast to the continuous-input continuous-output memoryless channel, in the case of $L_k T > Q$ or $L_k T < Q$ the discrete-input continuous-output QPSK or $\mathcal{M}$-ary QAM signals $\mathbf{d}^{(k)}$, we may conduct a numerical search to find that particular matrix $\mathcal{X}^{(k)}$, which maximizes the equivalent ergodic capacity expressed for the k-th user as [16],

$$\begin{aligned} \mathfrak{C}^{(k)} = \max_{\mathrm{tr}\left(\mathcal{X}^{(k)}(\mathcal{X}^{(k)})^H\right) \leq T} & -\frac{1}{T} \mathrm{E}\left\{ \log_2 \left(\frac{1}{\mathcal{M}^Q (\pi N_o)^{N_k}} \sum_{\check{\mathbf{d}}^{(k)} \in \mathcal{M}_c^Q} \exp\left(-\frac{1}{N_o} \| \mathbf{Y}^{(k)} - \mathcal{H}^{(k)} \mathcal{X}^{(k)} \check{\mathbf{d}}^{(k)} \|^2 \right) \right) \right\} \\ & - \frac{1}{T} N_k \log_2(\pi e N_0), \end{aligned} \tag{5.12}$$

where the equivalent ergodic capacity $C^{(k)}$ is quantified by assuming that the MUI in Equation 5.7 is entirely eliminated. Still referring to Equation 5.12, $\mathcal{M}_c$ denotes the set of $\mathcal{M}$ complex-valued constellation points of the modulation scheme employed and $\mathcal{M}_c^Q$ is the total set of legitimate values hosted by the transmitted data symbol vector $\mathbf{d}^{(k)}$. Again, $\mathrm{E}\{\cdot\}$ here is taken with respect to different effective channel realizations $\mathcal{H}^{(k)}$, QPSK or $\mathcal{M}$-ary QAM signals $\mathbf{d}^{(k)}$ and $\mathbf{N}^{(k)}$, respectively.

5.1.4 Spatial and Time Domain Loading Schemes

In this section, we further discuss the benefits of our LDC aided MUT scheme by introducing both the normalized Spatial-Domain (SD) load Γ_s and the normalized Time-Domain (TD) load Γ_t, as well as the overall normalized system load Γ_o, where all the normalized loads may be configured of each other in order independently to accommodate the near-instantaneous channel conditions experienced by each user as well as the data-rate requirement of each user. More specifically, we define the normalized SD load $\Gamma_s^{(k)}$ of the k-th user as

$$\Gamma_s^{(k)} = \frac{L_k}{N_k}, \tag{5.13}$$

which indicates the normalized SD load in a conventional symbol-time-slot. The most wide-spread scenarios is the fully loaded case, when the number of transmit and receive antennas dedicated to a user is the same.

Similarly, we define the normalized TD load $\Gamma_t^{(k)}$ of the k-th user as

$$\Gamma_t^{(k)} = \frac{Q_k}{L_k T}, \tag{5.14}$$

which quantified the normalized TD load for each spatial dimension.

Finally, the overall normalized system load $\Gamma_o^{(k)}$ of the k-th user is defined as

$$\Gamma_o^{(k)} = \frac{Q_k}{N_k T}, \tag{5.15}$$

which determines the effective system load of the k-th user.

Example 5.3: Normalized load scenarios

Let us assume that the LDC aided MUT DL-SDMA system has $M = 6$ transmit antennas, $N = 2$ receive antennas per MS and supports $K = 3$ users. The schematic of this system configuration is illustrated in Figure 5.5. The number of spatial domain dimension obtained of each user is hence $L = 6 - 2 \cdot 2 = 2$. The number of the LDC symbol slots is $T = 2$ and $Q = 2$ data symbols are encoded into a single LDC symbol. Then the resultant normalized SD load becomes $\Gamma_s^{(k)} = 2/2 = 1$, the normalized TD load $\Gamma_t^{(k)} = 2/(2 \cdot 2) = 1/2$ and the overall normalized system load $\Gamma_o^{(k)} = 2/(2 \cdot 2) = 1/2$.

The normalized load may be adaptively configured in response to different channel conditions. For example, if the fading envelopes of the spatial domain channels are nearly uncorrelated, we may opt for a high SD load $\Gamma_s^{(k)}$ for the k-th user in order to achieve a high throughput. On the other hand,

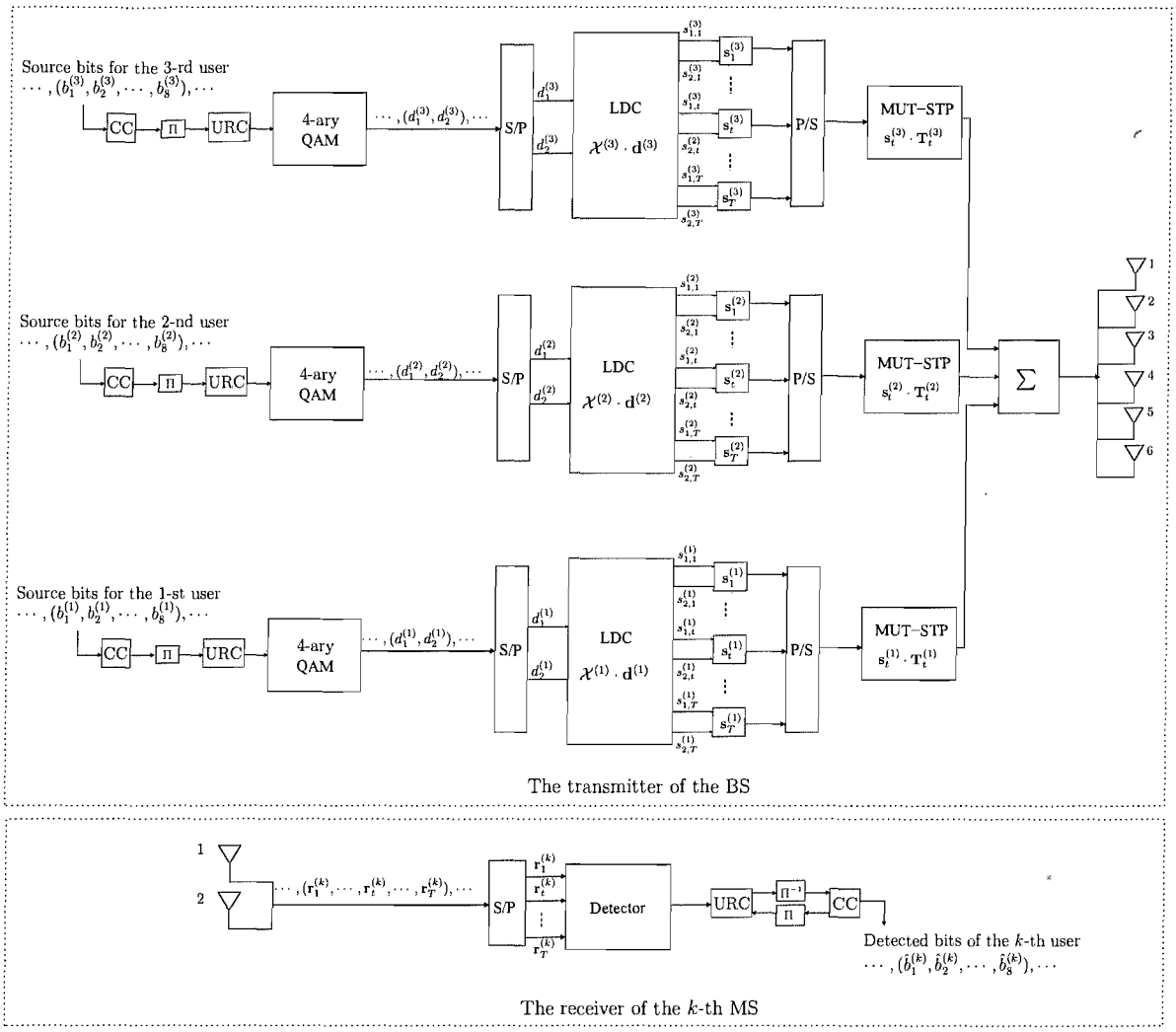

Figure 5.5: LDC-aided MUT in the iterative DL-SDMA system associated with the system configuration of $[M, N, L] = [6, 2, 2]$

if the k-th user encounters spatially correlated channels, we may reduce the normalized SD load $\Gamma_s^{(k)}$ in order to increase the achievable diversity gain. Similarly, we may adaptively configure the TD load $\Gamma_t^{(k)}$ in response to the correlation experienced in the time domain. For example, in fast-fading scenarios, the fading envelopes tend to be uncorrelated and hence we may increase the value of the TD load $\Gamma_t^{(k)}$, although maintaining accurate channel estimation will become more challenging in fast-fading channels. In contrast, we may achieve an increased diversity gain by reducing the level of normalized TD load $\Gamma_t^{(k)}$.

In short, when jointly exploiting the spatial and time domains in order to achieve a certain diversity order and diversity gain, multiplexing gain as well as multi-user interference cancellation capability, we may argue that the resultant scheme constitutes a *multi-functional* multi-user MIMO transmission scheme.

In our following discussions, we will quantify the system's capacity and performance as a function of the previously defined normalized load. For convenience, we will omit the user index k by assuming that each user has the same parameters, namely that we have $Q = Q_1 = Q_2 = \cdots = Q_K$, $L = L_1 = L_2 = \cdots = L_K$ and $N = N_1 = N_2 = \cdots = N_K$.

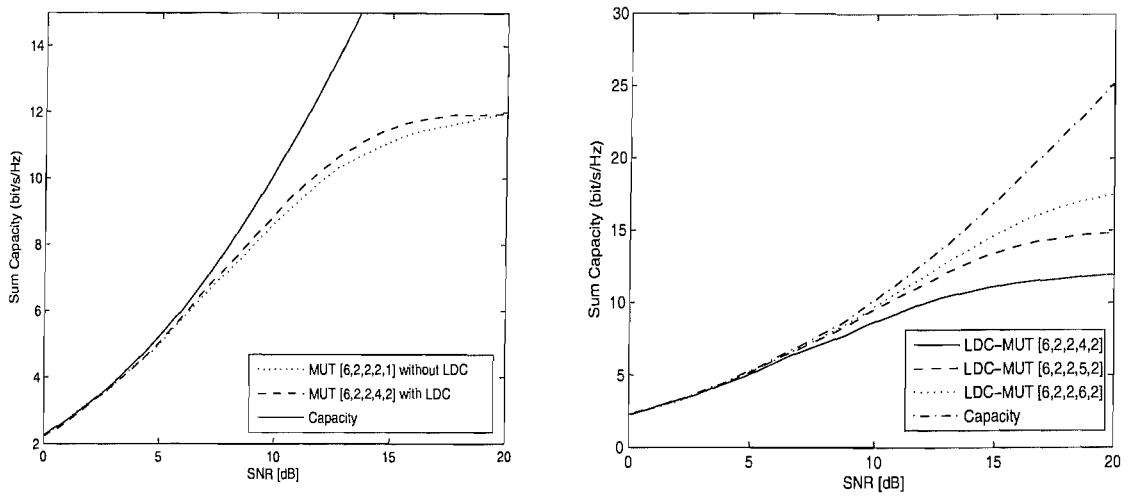

Figure 5.6: Sum capacity analysis of the LDC aided MUT assisted DL-SDMA system of Figure 5.3. (a) Sum capacity of the MUT DL-SDMA system with/without using LDC. (b) Sum capacity of the LDC aided MUT DL-SDMA system at different numbers of independent data stream $Q = 4, 5$ and 6. The system configurations expressed as $[M, N, L, Q, T]$ represents the number of transmit antennas M, the degree of freedom L in the spatial domain, the number of receive antennas N at each MS, the number of independent data streams Q transmitted to each user in a given LDC symbol and the number of slots T in the LDC symbol. The LDC matrices employed are listed in Appendix B

In Figure 5.6, we characterize the sum capacity of the LDC aided MUT DL-SDMA system using Equation 5.12. More explicitly, Figure 5.6(a) illustrates the achievable capacity improvement of the LDC aided MUT DL-SDMA system of Figure 5.3, compared to the basic MUT DL-SDMA arrangement of Figure 5.2 using no LDC. The system characterized in Figure 5.6(a) has the same normalized load of $\Gamma_o^{(k)} = 1$ and same data rate of $(Q/T = 2)$. The capacity of a (6x6)-element MIMO system assuming a Gaussian rather than discrete signal input is also included as our benchmarker. On the other hand, in Figure 5.6(b), we show that the capacity may be potentially increased upon increasing the number of independent data stream Q from 4 to 5 or 6 while having the same value of T, which in this case $T = 2$.

In Figure 5.7, we quantify the diversity gain of the LDC aided MUT DL-SDMA system for

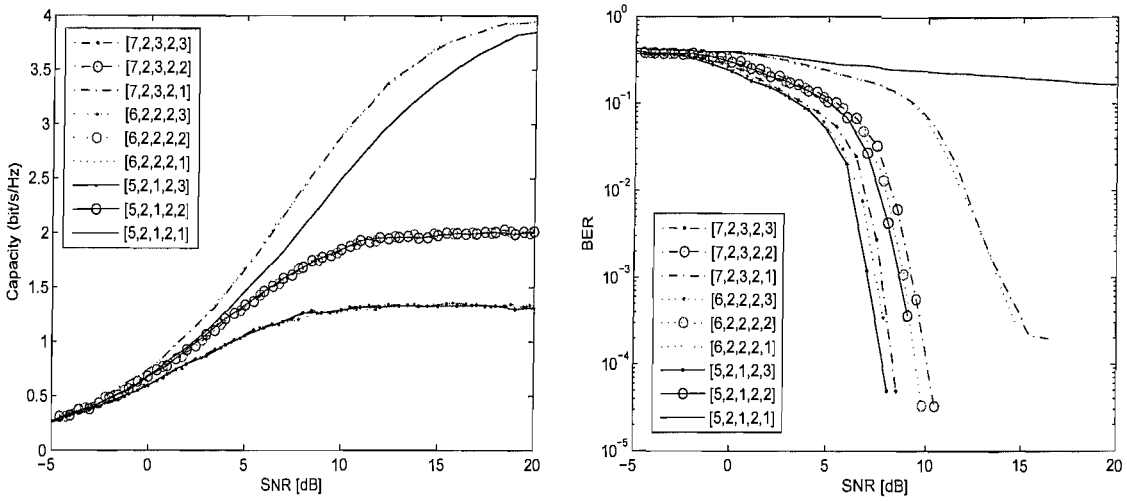

(a) (b)

Figure 5.7: (a) The capacity of the LDC-MUT aided DL-SDMA system for different normalized loads. (b) The BER performance of the LDC aided MUT DL-SDMA system for different loads using the system parameters listed in Table 5.2. The system configurations associated with different loading ratios in (a) and (b) are listed in Table 5.1.

$Q = 2$. More explicitly, we compare three different groups of system configurations. The first group has the system configuration of $[M, N, L] = [7, 2, 3]$ and obeys the schematic shown in Figure 5.8. This system has a normalized SD load of $\Gamma_s > 1$, which implies having a rank-deficient configuration in the spatial domain. The second group follows the schematic shown in Figure 5.5 and is associated with the system configuration of $[M, N, L] = [6, 2, 2]$ having a normalized SD load of $\Gamma_s = 1$, which implies supporting a fully-loaded configuration in the spatial domain. The third group employs the system configuration of $[M, N, L] = [5, 2, 1]$, obeys the schematic shown in Figure 5.9 and has a normalized load of $\Gamma_s < 1$, which implies having a lightly-loaded configuration in the spatial domain. When increasing the value of T, each group experienced an increasing diversity gain. In Figure 5.7(b), each group associated with the curves using the same line-type illustrates the achievable BER performance improvement, where the diversity gain is seen to be increased, upon increasing T. The achievable spatial domain diversity may be improved upon increasing the number of transmit antennas, while fixing the number of independent data streams transmitted. However, upon increasing the number of transmit antennas implies increasing the size and complexity of the BS. Therefore, we may jointly exploit the diversity gain gleaned in both the spatial and time domain in order to increase the attainable transmission integrity, which has been demonstrated in terms of the achievable BER performance in Figure 5.7(b). Additionally, the systems associated with the same value of Γ_o, which

were indicated in Figure 5.7(a) with the aid of the same markers have the same capacity, but a different BER performance. For example, in the group marked by the hollow circles, the curve associated with $\Gamma_s < 1$ exhibits a higher diversity gain and hence outperforms the systems having $\Gamma_s = 1$ and $\Gamma_s > 1$, which were marked by the dots and dash-dots lines, respectively. The BER performance seen in Figure 5.7(b) was obtained using the system parameters listed in Table 5.2.

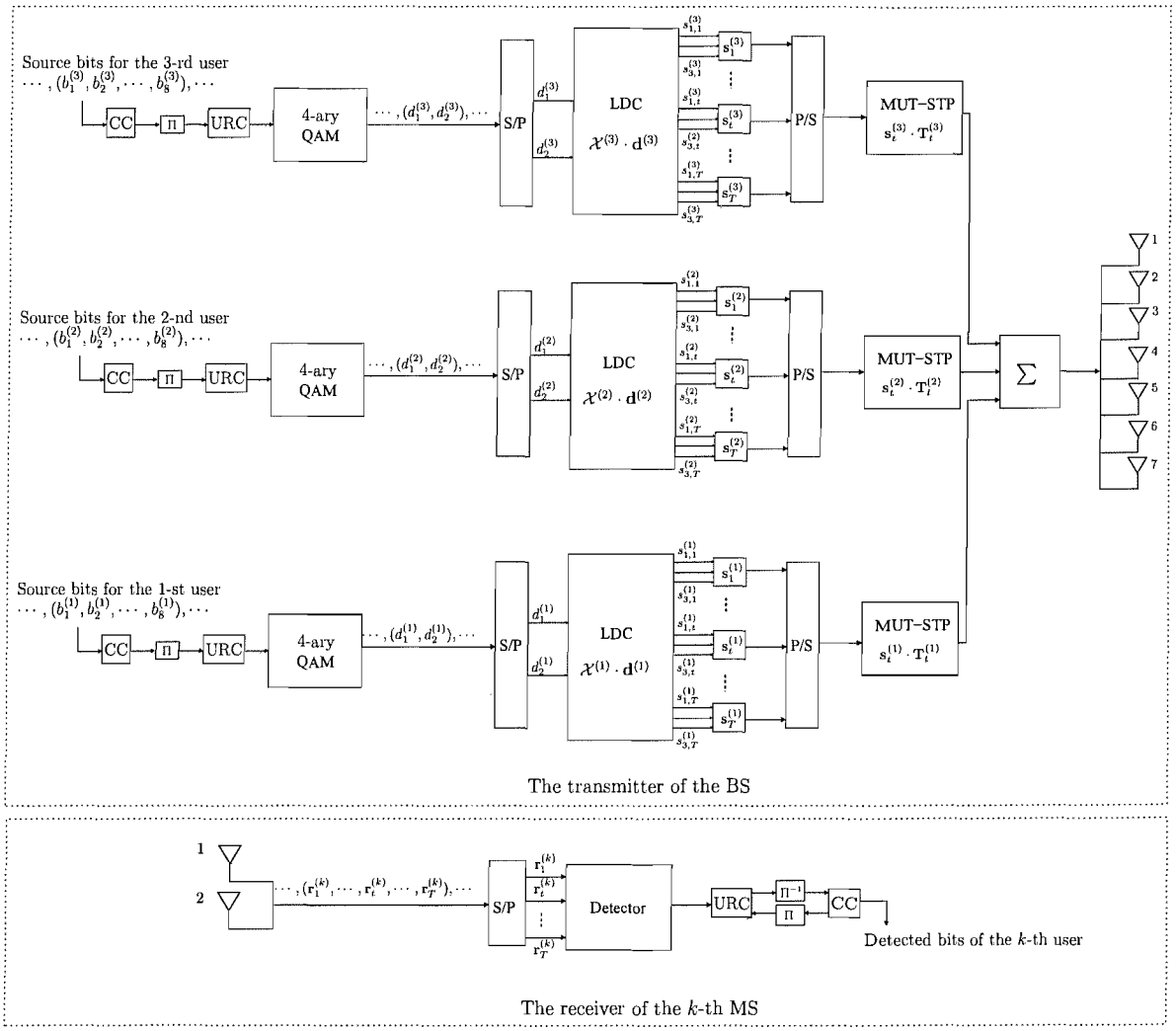

Figure 5.8: LDC-aided MUT in the iterative DL-SDMA system associated with the system configuration of $[M, N, L] = [7, 2, 3]$

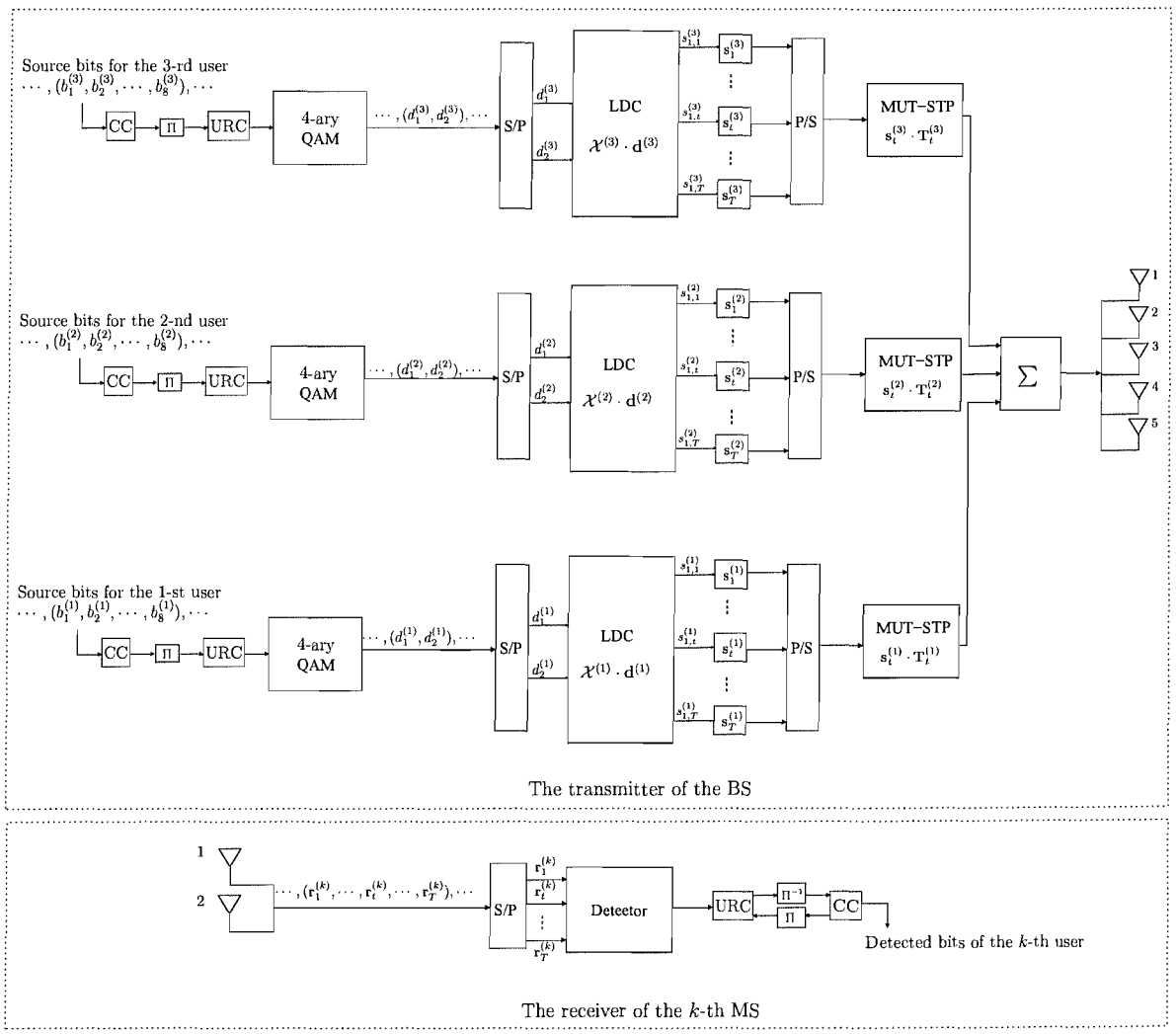

Figure 5.9: LDC-aided MUT in the iterative DL-SDMA system associated with the system configuration of $[M, N, L] = [5, 2, 1]$

Table 5.1: System configurations for different normalized loads in Figure 5.7, where we have $Q = 2$ and $N = 2$.

Schematic	M	L	T	Γ_t	Γ_s	Γ_o	Symbol rate (Q/T)
Figure 5.8	7	3	3	2/9	3/2	1/3	2/3
	7	3	2	1/3	3/2	1/2	1
	7	3	1	2/3	3/2	1	2
Figure 5.5	6	2	3	1/3	1	1/3	2/3
	6	2	2	1/2	1	1/2	1
	6	2	1	1	1	1	2
Figure 5.9	5	1	3	2/3	1/2	1/3	2/3
	5	1	2	1	1/2	1/2	1
	5	1	1	2	1/2	1	2

Table 5.2: System Parameters in Figure 5.7(b)

Channel model	uncorrelated flat-fading channel model
Channel Coder	rate-0.5 RSC [5,7] [22]
Interleaver length	10^5 bits
URC Coder	rate-1 Conv. Coder [22]
Detector	Log-MAP
Number of iterations	5
Modulation	4QAM
Number of users	$K = 3$
Number of receive antennas of each MS	$N_k = 2$, for $k = 1, 2, 3$.
LDC matrix χ	listed in Appendix B

5.1.5 Conclusions

In this section we proposed an iterative DL-SDMA system using LDC. The achievable SNR gain at a given sum capacity of the systems characterized in Figure 5.6(a) has been further summarized in Table 5.3. The maximum SNR gain recorded was 1 dB, when the sum capacity of the systems was 11 bits. Furthermore, the improved BER performance of the LDC aided MUT DL-SDMA systems was a benefit of the diversity gains shown in Figure 5.7(b), which were summarized in Table 5.4. It also indicated that a decreasing SNR was required by the systems in order to reach the target BER of 10^{-3}, when the value of T was increased. The maximum SNR gain recorded was about 6 dB in each group of systems, when the number of LDC-symbol intervals was is increased from $T = 1$ to $T = 3$. In the case of $T = 1$ the system is equivalent to the basic MUT scheme of Figure 5.2, which employed no LDCs.

Table 5.3: Required SNR of the LDC aided MUT DL-SDMA system at the specific target sum capacity (extracted from Figure 5.6(a))

Sum capacity (bits/s/Hz)	Basic MUT of Figure 5.2 (SNR [dB])	LDC aided MUT of Figure 5.3 using LDC (SNR [dB])	single-user MIMO (SNR [dB])
5	4.9	4.9	4.6
6	6.2	6.1	5.9
7	7.6	7.4	7.0
8	9.0	8.8	8.0
9	10.5	10.1	8.9
10	12.1	11.5	9.8
11	14.6	13.5	10.6

Table 5.4: Required SNR of the DL-SDMA system using the LDC aided MUT scheme at the target BER performance of 10^{-3} (extracted from Figure 5.7(b))

Schematic	LDC-MUT $[M, N, L, Q]$	The interval of the LDC symbol T	Γ_o	SNR [dB]
Figure 5.8	[7,2,3,2]	3	1/3	7.7
	[7,2,3,2]	2	1/2	9.2
	[7,2,3,2]	1	1	13.9
Figure 5.5	[6,2,2,2]	3	1/3	7.4
	[6,2,2,2]	2	1/2	8.8
	[6,2,2,2]	1	1	13.7
Figure 5.9	[5,2,1,2]	3	1/3	7.0
	[5,2,1,2]	2	1/2	8.5
	[5,2,1,2]	1	1	∞

5.2 Irregular Sphere Detection in the LDC-MUT Aided DL-SDMA System

In this section, we introduce the concept of irregular sphere detection, which is invoked for reducing the complexity imposed by the iterative joint detection and decoding process. As advocated in [18,43] and also investigated in Section 2.2, the sphere detection process is capable of providing a near-ML performance at a low complexity. The nature of this non-linear detection algorithm makes it eminently suitable for operation in rank-deficient scenarios[3], where the family of linear detection algorithms, such as MMSE detection, performs poorly. In the recent literature [16, 18, 86], most research efforts focus on the complexity reduction of each sphere detection iteration. By contrast, our aim is to introduce the concept of irregular sphere detection, which is designed to reduce the overall iterative decoding complexity by taking into account both the complexity per iterative detection stage and the number of iterations required.

Let us first assume that the ST-CIRT is perfectly known at the transmitter, so that the MUI may be perfectly eliminated. Then we can rewrite the received signal model of the k-th user provided in Equation 5.7 as

$$\mathbf{Y}^{(k)} = \mathcal{H}^{(k)}\mathbf{S}^{(k)} + \mathbf{N}^{(k)}, \tag{5.16}$$

where we have $\mathbf{S}^{(k)} = \mathcal{X}^{(k)} \cdot \mathbf{d}^{(k)}$.

For the sake of simplicity, we will remove the user index k, where this does not cause any confusion. Furthermore, by defining the *effective channel matrix* as $\mathcal{H}_e = \mathcal{H}\mathcal{X}$, we may write Equation 5.16 as

$$\mathbf{Y} = \mathcal{H}\mathcal{X}\mathbf{d} + \mathbf{N}, \tag{5.17}$$

$$= \mathcal{H}_e\mathbf{d} + \mathbf{N}. \tag{5.18}$$

In our forthcoming discussions, we will continue with a brief summary of sphere detection and further detail the proposed irregular sphere detection scheme in order to detect the transmitted signals of each MS.

[3]The rank-deficient scenario is defined as the case when the number of transmitter antennas is higher than the number of receive antennas, which has been detailed in Section 2.2.1

5.2.1 K-best Sphere Detection

The ML solution of Equation 5.16 may be equivalently expressed as [18]:

$$\hat{\mathbf{d}} = \arg \min_{\check{\mathbf{d}} \in \mathcal{M}_c^Q} \|\mathbf{U}(\check{\mathbf{d}} - \hat{\mathbf{x}}_c)\|^2, \tag{5.19}$$

where $\mathbf{U}$ is a $(Q \times Q)$-element upper-triangular matrix and $\mathbf{U}^H\mathbf{U} = ({\mathcal{H}_e}^H\mathcal{H}_e + 2\sigma_n^2\mathbf{I})$. Again, $\mathcal{M}_c^Q$ is the set of **all possible** candidates of the Q-element transmitted data vector $\mathbf{d}$. Furthermore, $\hat{\mathbf{x}}_c$ is the transmitted data vector candidate considered as the search centre of the SD, which is usually the MMSE solution. Consequently, the objective function $\mathcal{J}$ associated with the candidate $\check{\mathbf{d}}$ of the transmitted data vector, which will be evaluated during the SD's near-ML search, is defined as [18]

$$\begin{aligned} \mathcal{J}(\check{\mathbf{d}}) &= \|\mathbf{U}(\check{\mathbf{d}} - \hat{\mathbf{x}_c})\|^2 = (\check{\mathbf{d}} - \hat{\mathbf{x}}_c)\mathbf{U}^H\mathbf{U}(\check{\mathbf{d}} - \hat{\mathbf{x}}_c), \\ &= \sum_{i=1}^{Q} \left| \sum_{j=i}^{Q} u_{ij}(\check{d}_j - \hat{x}_{c,j}) \right|^2 = \sum_{i=1}^{Q} \phi_i(\check{\mathbf{d}}_i), \end{aligned} \tag{5.20}$$

where we have $\check{\mathbf{d}}_i = \left(\check{d}_i, \cdots, \check{d}_Q\right)$. Furthermore, we define the Partial Euclidean Distance (PED) as

$$\mathcal{J}_i(\check{\mathbf{d}}_i) = \mathcal{J}_{i+1}(\check{\mathbf{d}}_{i+1}) + \phi_i(\check{\mathbf{d}}_i), \quad i = 1, \cdots, Q, \tag{5.21}$$

and we have $\mathcal{J}(\check{\mathbf{d}}) = \mathcal{J}_1(\check{\mathbf{d}}_1) > \mathcal{J}_2(\check{\mathbf{d}}_2) > \cdots > \mathcal{J}_Q(\check{\mathbf{d}}_Q) > 0$ [18].

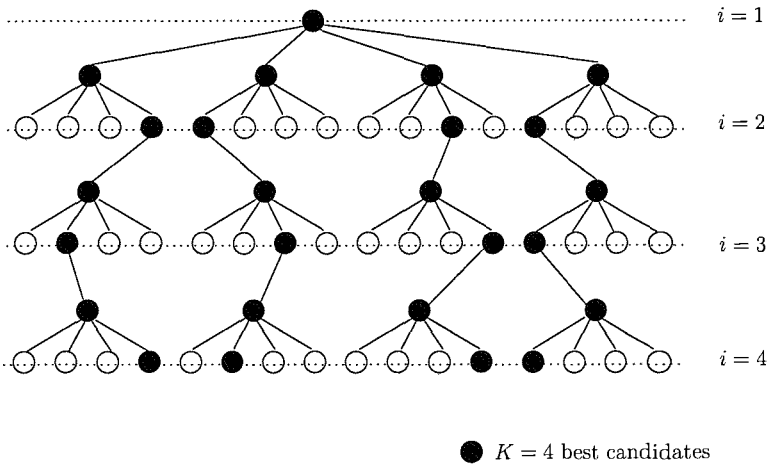

Figure 5.10: The illustration of the tree-search of the K best candidates of KSD

In general, the SD's near-ML search may be depicted as a tree search process [18]. In the class of K-best SDs [86], at each layer of search, i.e. from the layer $i = 1$ to the layer $i = Q$, the K-Best SD retains a fixed number of candidates N_{cand}, which have the smallest PEDs. Assuming that we have $Q = 4$ and there are four hypothesises for each data symbol d_i, Figure 5.10 illustrates an example of the tree search of KSD in conjunction with $N_{cand} = 4$. As illustrated in Figure 5.10, we only retain

a fixed number of four survivors associated with the smallest PED, marked with black circles at each tree-layer, instead of exponentially expanding the search tree. At the bottom of the tree search, there will be only $N_{cand} = 4$ candidates left, compared to $256(4^4)$ candidates of the full search of the ML detector.

The KSD is attractive, since it is capable of directly controlling the detection complexity by adjusting the number of SD candidates, N_{cand}. This is particularly useful and important to us in designing the proposed irregular SD, which will be shown in Section 5.2.3.

By defining $\mathcal{D}_{\mathcal{R}} \subset \mathcal{M}_c^Q$ as the **reduced** hypothesis set containing $N_{cand} = \mathcal{R}$ candidates only, the desired *a posteriori* Log Likelihood Ratio (LLR) of the i-th bit of the the n-th symbol element of the transmitted data vector $\mathbf{d}$ formulated in Equation 5.17 can be expressed as [20]

$$\mathcal{L}_{apt}^{det}(\mathbf{d}_{i,n}) = \min_{\check{\mathbf{d}} \in \mathcal{D}^0_{\mathcal{R},(i,n)}} \left\{ -\log p\left(\check{\mathbf{d}}\right) + \frac{\|\mathbf{Y} - \mathcal{H}_e \check{\mathbf{d}}\|^2}{2\sigma_n^2} \right\} - \min_{\check{\mathbf{d}} \in \mathcal{D}^1_{\mathcal{R},(i,n)}} \left\{ -\log p\left(\check{\mathbf{d}}\right) + \frac{\|\mathbf{Y} - \mathcal{H}_e \check{\mathbf{d}}\|^2}{2\sigma_n^2} \right\}, \tag{5.22}$$

where the hypothesis set $\mathcal{D}^b_{\mathcal{R},(i,n)}$ contains the candidates which have their i-th bit of the n-th symbol element equal to the binary bit $b = \{0, 1\}$. In addition, $p\left(\check{\mathbf{d}}\right)$ is the *a priori* soft information of the given hypothetical data vector being considered.

5.2.2 K-best Sphere Detection Using Center-Shifting

The initial value of the search center $\hat{\mathbf{x}}_c$ in Equation 5.19 may be chosen to be the MMSE solution. In the context of the iterative joint detection and decoding schemes, this search center can be updated at each iteration based on the *a priori* information input, which is expected to become more reliable upon using more iterations. Hence, by referring to this process as center-shifting, we introduce the center-shifting aided K-best SD concept. In Figure 5.11, we illustrate the structure of the Centre-Shifting (CS) aided KSD, where $\mathcal{L}_{apt}$ is denoted as the *a posteriori* information generated by the *soft* detection aided KSD. Additionally, the *a priori* information aided MMSE [33] based center calculation will generate a new center $\hat{\mathbf{x}}_c$ at each iteration according to the updated input *a priori* information $\mathcal{L}_{apr}$. Based on the updated center $\hat{\mathbf{x}}_c$, the K-best SD updates the set $\mathcal{D}_{\mathcal{R}}$ constituted by the N_{cand} number of SD candidates having the smallest PED.

Our EXIT analysis demonstrated that the KSD operating without CS may not have any iterative gain upon increasing the extrinsic information provided for the SD, as illustrated in Figure 5.12. On the other hand, the KSD-CS scheme exhibits a substantial iterative gain for both $N_{cand} = 64$ and

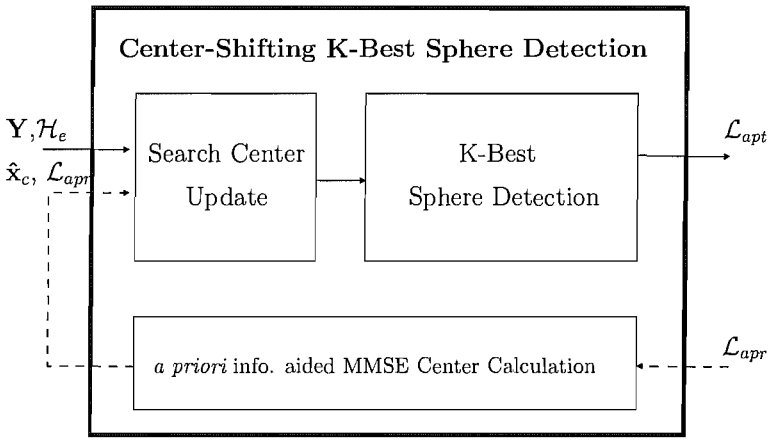

Figure 5.11: The structure of K-best SD using the center-shifting scheme

$N_{cand} = 256$ K-best SD candidates.

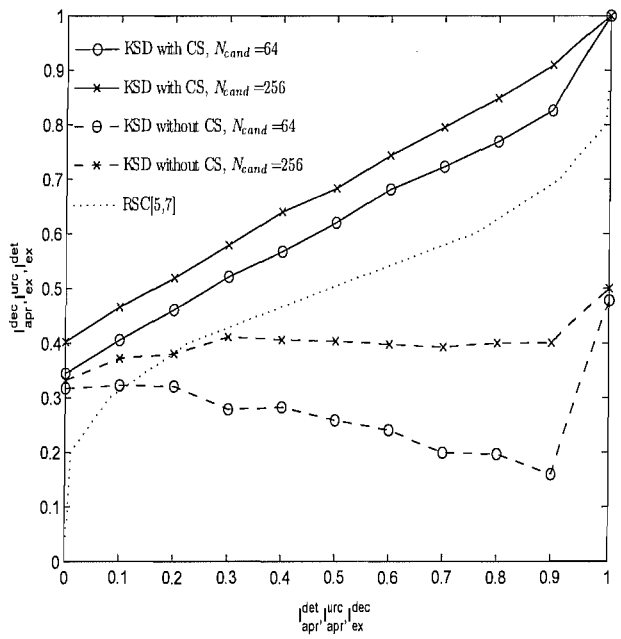

Figure 5.12: EXIT chart analysis of the iterative K-best SD using the center-shifting scheme. A rate-0.5 Recursive Systematic Convolutional (RSC) channel codec, having the octal generator polynomials of G=[5,7], was employed by the system. The system parameters of Table 5.5 were used.

5.2.3 Irregular Sphere Detection

In this section we introduce the framework of IrSD by appropriately amalgamating a number of CS aided K-best SD, each using a different value of N_{cand}, although this may be simply interpreted as using a single KSD-CS and a variable value of N_{cand}. The CS aided K-best SD using different values of N_{cand} have a different decoding performance and a different detection complexity. Hence,

by invoking appropriately amalgamated KSD-CS associated with different values of N_{cand}, the IrSD scheme is designed to reduce the overall complexity, which takes into account both the complexity per iterative detection stage and the number of iterations required, with each constituent KSD-CS processing the required fraction of the received bits.

More specifically, the philosophy of the Irregular SD technique is that of utilizing V KSDs employing different values of N_{cand} for detecting predetermined segments of the transmitted signals, instead of using a fixed value of N_{cand}, as justified later in this section. Based on the appropriately optimized fractions of the received signal, each KSD-CS generates its soft-bit estimates of the appropriate fractions of the transmitted signals. More specifically, for a transmission block containing L encoded bits and assuming that N_{bps} bits per symbol are transmitted by the modulator, we have L/N_{bps} symbols per transmission block, where each transmission block is mapped to a separate time-slot. At the receiver, we invoke the proposed IrSD scheme, which is constituted by V component KSD-CS employing different values of N_{cand}. Let C_v be the complexity of the v-th component detector of the IrSD scheme. Then the weighting coefficient α_v, $v = 1, \cdots V$, of the KSD-CS has to satisfy:

$$1 = \sum_{v=1}^{V} \alpha_v, \; C_{gd} = \sum_{v=1}^{V} \alpha_v C_v, \text{ and } \alpha_v \in [0,1], \forall v, \tag{5.23}$$

where C_{gd} is the average complexity of the IrSD scheme [4].

For each iterative stage, the computational complexity of the v-th KSD-CS associated with the given $N_{cand} = \mathcal{K}$ can be quantified as

$$C_v = Q \cdot N_{bps} \cdot \mathbf{\Phi}(\mathcal{K}), \tag{5.24}$$

where as before, Q is the number of elements in the transmitted signal vector $\mathbf{d}$ and $\mathbf{\Phi}(\mathcal{K})$ is the computational complexity of evaluating each bit's LLR in $\mathbf{d}$ formulated in Equation 5.22 and associated with the reduced hypothesis set $\mathcal{D}_{\mathcal{K}}$.

Furthermore, each constituent detector generates $\alpha_v L$ soft-bits for a transmission block containing L bits. Similarly to the irregular scheme [69], the IrSD design philosophy is that it allows us to superimpose the EXIT curves of the individual component detectors after appropriately weighting them by the optimum value of α_v, which facilitates the matching of the detector's EXIT curve to that of the outer channel decoder. It was shown in [69] that this EXIT-curve matching has the potential of minimizing the open EXIT-tunnel's area and hence it is capable of a near-capacity operation, while

[4]The subscript gd indicates generic detection, potentially using arbitrary detectors. However, in this paper we use KSD-CS in conjunction with different values of N_{cand} employed as the component detectors.

maintaining an infinitesimally low BER. To elaborate a little further, according to [69], the EXIT function $T_{gd}(I_{in})$, which characterizes the detector referred to synonymously as the inner 'decoder' of the IrSD aided system, is given by

$$T_{gd}(I_{in}) = \sum_{v=1}^{V} \alpha_v T_v(I_{in}), \tag{5.25}$$

where $T_v(I_{in})$ is the EXIT function of the v-th component KSD-CS invoked by the IrSD scheme.

In summary, using the weighting-coefficient vector $\boldsymbol{\alpha}$ formed by the weighting coefficients α_v for $v = 1, 2, \cdots, V$ satisfying Equation 5.23 creates a IrSD having a given average computational complexity of C_{gd}. Given the weighting-coefficient vector $\boldsymbol{\alpha}$, the EXIT function of $T_{gd}(I_{in})$, characterizing the inner decoder's EXIT curve can be generated based on Equation 5.25. Therefore, we can design the superimposed EXIT function $T_{gd}(I_{in})$ of the IrSD aided system by optimizing the weighting-coefficient vector $\boldsymbol{\alpha}$, for the sake of minimizing the open EXIT-tunnel area and hence to facilitate near-capacity operation, while maintaining an infinitesimally low BER.

5.2.4 Irregular Sphere Detection Aided Multi-User Transmission

As a practical design example, we utilize a V number of CS aided KSDs to create the IrSD shown in Figures 5.13 and 5.14. As shown in Figure 5.13, the data bits are encoded by both the channel encoder and the Unity-Rate Coder (URC), which is constituted by a convolutional encoder using a single shift register stage [70]. The interleaver placed between the channel encoder and the URCs is denoted by Π_1, as seen in Figure 5.13. The four parallel paths in Figure 5.13 indicate that not only the IrSD, but also the transmitter has to process the fraction of $\alpha_1 L, \cdots, \alpha_V L$ bits separately, although the same URC and modulation schemes are employed. The weighting-coefficient vector $\boldsymbol{\alpha}$ is used for partitioning the coded bits into the appropriate-length segments for the URC encoders. For example, for a transmission block containing L encoded bits, the v-th URC encoder encodes $\alpha_v L$ bits. Assuming that N_{bps} bits per symbol are used for transmission, $\alpha_v L / N_{bps}$ number of modulated symbols are generated by the v-th modulator. Furthermore, the length of the interleaver between the v-th URC and the v-th modulators, denoted as $\Pi_{2,v}$ in Figure 5.14, is equal to $\alpha_v L / N_{bps}$. Both the number V and the weight of the constituent detectors used for creating the IrSD may be chosen to minimize the complexity of the IrSD while maintaining the target BER. The output signal vector $\mathbf{d}^{(k)}$ seen in Figure 5.13 will be multiplied with the linear dispersion matrix $\mathcal{X}^{(k)}$ of Figure 5.3, as detailed in Section 5.1.2.2 and transmitted with the aid of the LDC-MUT scheme shown in Figure 5.3.

Furthermore, based on the MS receiver of LDC-MUT DL-SDMA system seen in Figure 5.3 of Section 5.1.2.2, Figure 5.14 illustrates the structure of the MS's receivers using IrSD. As shown in

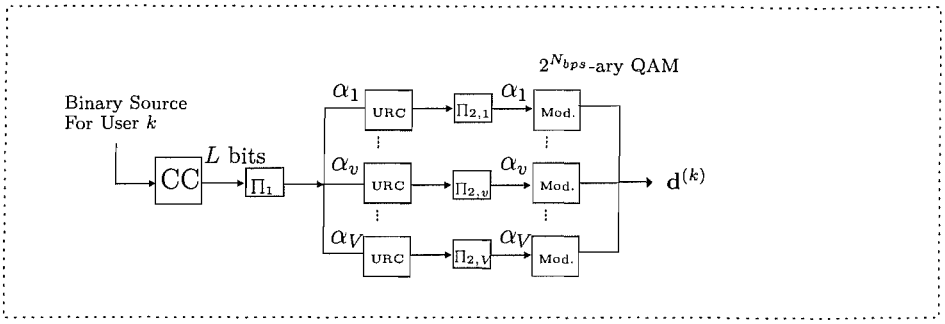

Figure 5.13: Generating the precoded data symbol vector $\mathbf{d}^{(k)}$ for the k-th user of Figure 5.3

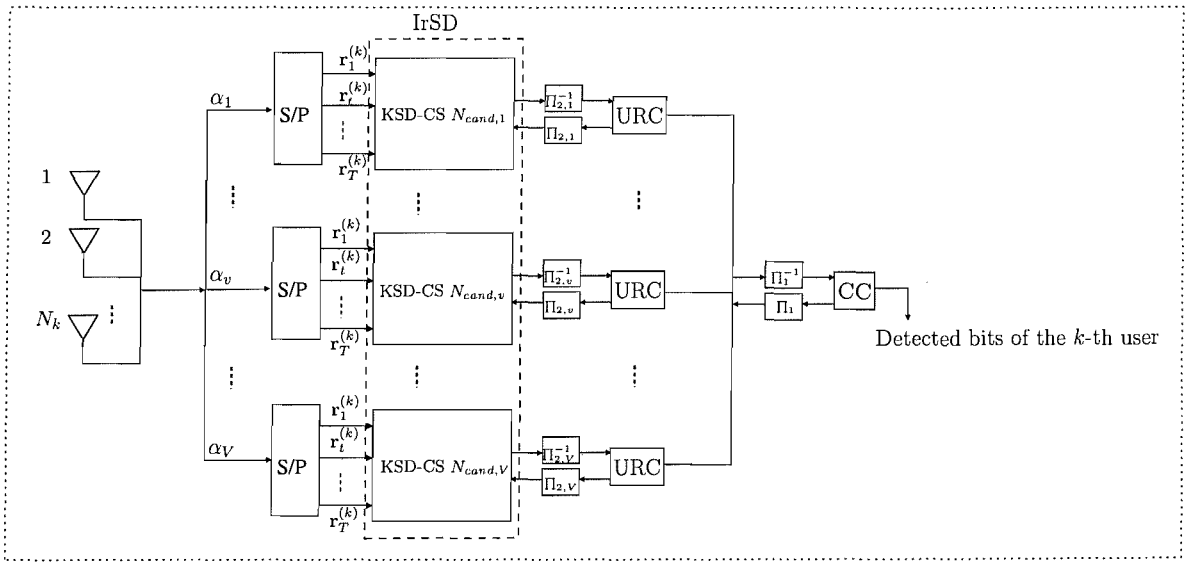

Figure 5.14: The structure of the IrSD aided iterative DL-SDMA receiver using LDC of Figure 5.3

Figure 5.14, the IrSD is assembled from V CS aided KSDs. The received signals are partitioned into appropriate-length segments according to the weighting-coefficient vector $\boldsymbol{\alpha}$. Each KSD-CS then processes the corresponding fraction of the received signal, and the same is true for the URC decoders.

Then iterative detection is invoked for exchanging extrinsic information among the IrSD detector, URC decoders and the channel decoder. The extrinsic information bits generated by the channel decoder are also partitioned into appropriate-length segments according to the weighting-coefficient vector $\boldsymbol{\alpha}$, which are then fed back to the URC decoders and the IrSD detector, as seen in Figure 5.14.

As a simplifying assumption, perfect channel knowledge is assumed to be available at both the transmitter and receiver in this study. Therefore the MUI may be entirely eliminated [43]. In this case, the system can be viewed as a number of parallel single-user MIMO systems. In this section, we focus our attention on introducing the IrSD algorithm itself. The impact of imperfect channel knowledge will be considered in Section 5.3.

In the next section, we will summarize the optimization of the IrSD, which requires finding the optimized weighting vector $\boldsymbol{\alpha}$.

5.2.5 Optimization of the Irregular Sphere Detection

We invoke KSD-CSs having V different values of N_{cand} in the irregular generic detector. The weighting-coefficient vector $\boldsymbol{\alpha} \in \mathbb{R}^V$ has to satisfy Equations 5.23 and 5.25. Let $\mathcal{F}$ be a set containing all the candidate solutions $\boldsymbol{\alpha}$. We may find the weighting-coefficient vector $\boldsymbol{\alpha} \in \mathcal{F}$ by conducting a search similar to that suggested in [69]. By defining an $(N_p \times V)$-element matrix A, which is constituted by V number of EXIT functions $T_v(I_{in}), v = 1, \cdots, V$, and a vector $\mathbf{b} = T_{cc}^{-1}(I_{in})$, for $I_{in} \in \{i_1, i_2, \cdots, i_{N_p}\}$, we have

$$\mathbf{A} = \begin{bmatrix} T_1(i_1) & T_2(i_1) & \cdots & T_V(i_1) \\ T_1(i_2) & T_2(i_2) & \cdots & T_V(i_2) \\ \vdots & \vdots & \cdots & \vdots \\ T_1(i_{N_p}) & T_2(i_{N_p}) & \cdots & T_V(i_{N_p}) \end{bmatrix}, \tag{5.26}$$

and

$$\mathbf{b} = \begin{bmatrix} T_{cc,1}^{-1}(i_1) \\ T_{cc,1}^{-1}(i_2) \\ \vdots \\ T_{cc,1}^{-1}(i_{N_p}) \end{bmatrix}. \tag{5.27}$$

Our Objective Function (OF) $\Omega(\boldsymbol{\alpha})$ may be defined as

$$\Omega(\boldsymbol{\alpha}) = ||\mathbf{A}\boldsymbol{\alpha} - \mathbf{b}||^2, \tag{5.28}$$

which represents the area between the inner and outer channel decoder's EXIT curve, where the former is constituted by the combined IrSD and URC decoder. Naturally, all elements of e, where we have $e = (\mathbf{A}\boldsymbol{\alpha} - b)$, have to be larger than zero, since they physically represent the area between the outer and inner decoder's EXIT curve. We define a subset $\mathcal{A} \subset \mathcal{F}$ containing all weighting coefficient vectors $\boldsymbol{\alpha}$ meeting this constraint. Secondly, for a specific fixed computational complexity C_{gd}, we opt for that particular $\boldsymbol{\alpha}$ value, which is associated with a higher area $\Omega(\boldsymbol{\alpha})$ between the outer EXIT curve $T_{cc}^{-1}(I_{in})$ and the inner EXIT curve $T_{gd}(I_{in})$, which implies requiring a low number of decoding iterations. Therefore, we assume that the optimal weighting-coefficient vector $\boldsymbol{\alpha}_{opt}$ can be obtained by finding the $\boldsymbol{\alpha}$ value satisfying:

$$\boldsymbol{\alpha}_{opt} = \max_{\boldsymbol{\alpha} \in \mathcal{A}} \Omega(\boldsymbol{\alpha}). \tag{5.29}$$

Algorithm 5.1: Optimization of the IrSD weighting-coefficient vector α

Set the value of the affordable computational complexity C_{gd} of the IrSD.

Let

$$\mathbf{C} = \begin{bmatrix} 1 & 1 & \cdots & 1 \\ C_1 & C_2 & \cdots & C_{N_{det}} \end{bmatrix}, \mathbf{d} = \begin{bmatrix} 1 \\ C_{gd} \end{bmatrix},$$

$$\mathbf{A} = \begin{bmatrix} T_1(i_1) & T_2(i_1) & \cdots & T_{N_{det}}(i_1) \\ T_1(i_2) & T_2(i_2) & \cdots & T_{N_{det}}(i_2) \\ \vdots & \vdots & \cdots & \vdots \\ T_1(i_{N_p}) & T_2(i_{N_p}) & \cdots & T_{N_{det}}(i_{N_p}) \end{bmatrix}, \mathbf{b} = \begin{bmatrix} T_{cc,1}^{-1}(i_1) \\ T_{cc,1}^{-1}(i_2) \\ \vdots \\ T_{cc,1}^{-1}(i_{N_p}) \end{bmatrix}.$$

Find α_{opt} using the following steps:

Step 1) Find $\alpha \in \mathcal{F}$ which satisfies $\mathbf{C}\alpha = \mathbf{d}$ of Equation 5.23 using the algorithm summarized in Appendix A.

Step 2) Find $\alpha_{opt} = \max_{\alpha} \Omega(\alpha) = ||\mathbf{A}\alpha - \mathbf{b}||^2$.

We summarize the IrSD technique in Algorithm 5.1, which was generalized for an arbitrary number of constituent detectors N_{det}.

5.2.6 IrSD Design and Analysis Using EXIT Charts

In this section, we will demonstrate how EXIT charts may be used to assist us in the design of the IrSD and in the analysis of the systems' iterative decoding performance.

Let us first define the IrSD's target complexity ratio r_{gd} with respect to the full candidate list searched by the KSD, i.e. by the ML, which is expressed as:

$$r_{gd} = C_{gd}/C_{ml}, \tag{5.30}$$

where again C_{gd} is the per-iteration computational complexity of the IrSD.

Furthermore, the total complexity $C_{gd,iter}$ of the IrSD embedded into the iterative decoding process, which is defined as the product of the per-iteration complexity and the number of iterations required for approaching an infinitesimally low BER., is given by

$$C_{gd,iter} = C_{gd} \times I_{gd}, \tag{5.31}$$

where $I_{iter,gd}$ is the number of IrKSD iterations required for achieving convergence to the $(I_A, I_E) =$

$(1,1)$ point in the EXIT chart. Therefore, the total complexity ratio of the IrSD is given by

$$r_{gd,iter} = C_{gd,iter}/C_{ml,iter}, \tag{5.32}$$

where $C_{Log-MAP,iter}$ is the total complexity imposed by the iterative Log-MAP detector, when attaining perfect convergence to the $(I_A, I_E) = (1,1)$ point in the EXIT chart.

In Figure 5.15, we illustrate the EXIT curves of the LDC-MUT aided DL-SDMA system employing the KSD-CS in conjunction with different values of N_{cand}. Observe that the systems employing the KSD-CS in conjunction with different values of N_{cand} have different inner EXIT-curves. According to Equation 5.24, the higher the value of N_{cand}, the higher the complexity at each detection stage. On the other hand, the wider EXIT-tunnel of the system using higher values of N_{cand} implies necessitating less iterative steps, which may be required for the iterative process to converge. Hence striking an attractive compromise between the value of N_{cand} and the number of iterations has the potential of reducing the overall complexity.

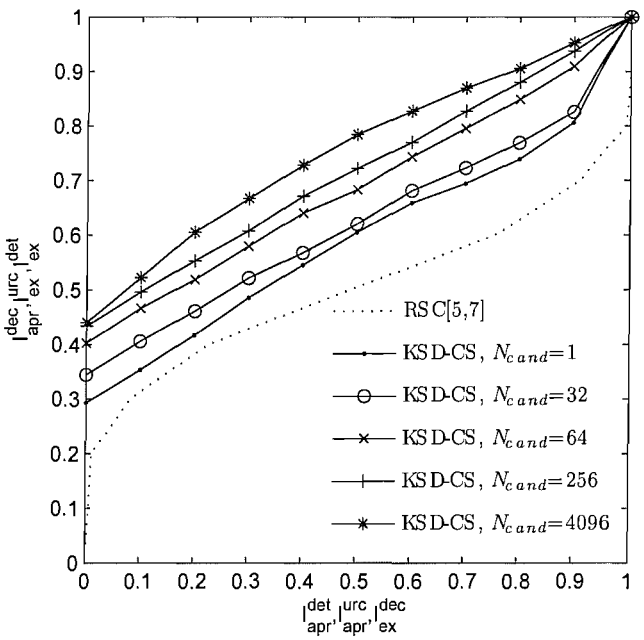

Figure 5.15: EXIT curves of LDC-MUT aided DL-SDMA system of Figure 5.3 employing the KSD-CS with different settings of N_{cand}. The systems operated at $E_b/N_0 = 5dB$. The channel model was a flat-fading MIMO channel and the system parameters of Table 5.5 were used.

By using the design detailed in Section 5.2.3, we construct the Irregular SD using CS aided KSDs. For further characterizing the complexity of the IrSD scheme, in Figure 5.16 we illustrate the inner decoder's EXIT-curves recorded for the IrSD aided iterative DL-SDMA system designed for different complexity ratios r_{gd}, ranging from 0,001,0.005,0.01 to 1, where $r_{gd} = 1$ corresponds to using the ML detector. The weighting-coefficient vectors α designed for each of the corresponding complexity

Table 5.5: System Parameters

Channel model	uncorrelated flat-fading channel model
Channel Coder	rate-0.5 RSC [5,7]
Interleaver length	10^5 bits
URC Coder	rate-1 Conv. Coder [22]
Modulation	4QAM
Number of users	$K = 3$
Total number of transmit antennas	$M = 7$
Number of receive antennas of the k-th user	$N_k = 2$, for $k = 1, 2, 3$.
Total number of receive antennas	6
Dimension in the spatial domain	$L_k = 3$, for $k = 1, 2, 3$.
Number of independent data streams transmitted for the k-th user in one LDC symbol	$Q_k = 6$, for $k = 1, 2, 3$.
The interval of one LDC symbol	$T = 2$
The LDC matrix χ	refer to Equation B.10 of Appendix B

ratios r_{gd} are listed in Table 5.6, where the elements of α, from the first element to the last element, represent the KSD-CS using $N_{cand} = 1, 32, 64, 256$ and 4096 in this order. For example, for the IrSD associated with $r_{gd} = 0.005$ and $\alpha = [0.62, 0.18, 0.2, 0, 0]$, the constituent KSD-CS using $N_{cand} = 1$ has a 62% duty cycle, the KSD-CS using $N_{cand} = 32$ has an 18% duty cycle, while the KSD-CS using $N_{cand} = 64$ has a 20% duty cycle. As expected, by reducing the complexity ratio r_{gd}, the duty-cycles of the lower-complexity detectors, which are the KSD-CS detectors associated with smaller values of N_{cand}, becomes higher than those of the higher-complexity detectors, which are the KSD-CS detectors associated with higher values of N_{cand}. On the other hand, as a consequence of reducing the complexity ratio r_{gd}, the EXIT-tunnel becomes narrower. The number of iterative decoding iterations required for attaining perfect convergence increases due to having a narrower EXIT-tunnel. Therefore, again, there is a tradeoff between the complexity ratio r_{gd} corresponding to the single-iteration-complexity and the number of the decoding iterations I_{gd}. In order to reduce the overall complexity of the iterative DL-SDMA receiver, we have to take both effects into account. In Figure 5.17(a), we quantitatively illustrated this trade-off. The required number of iterations I_{gd} is increased, when reducing the complexity ratio r_{gd}. When r_{gd} is lower than 0.001, the EXIT-tunnel becomes narrow and the number of iterations required for navigating through the EXIT-tunnel may become excessive.

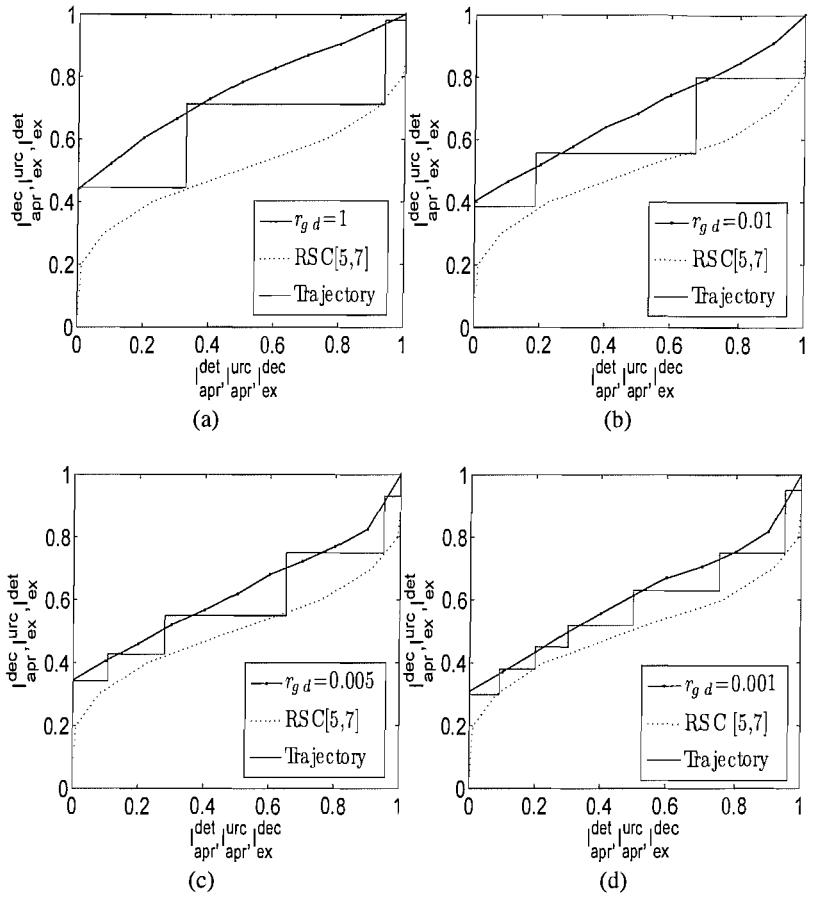

Figure 5.16: EXIT chart analysis of the iterative DL-SDMA system of Figure 5.3 invoking IrSD of Figure 5.13 and 5.14 associated with different values of r_{gd}, ranging from $1, 0.01, 0.005, 0.001$ in (a)(b)(c)(d), respectively. The systems operated at $E_b/N_0 = 5dB$. A rate-0.5 RSC[5,7] channel coder was employed for the system. The channel model was a flat-fading MIMO channel and the parameters of Table 5.5 were used.

When aiming for different values of r_{gd}, we arrive at Table 5.6. In Table 5.6, the computational complexity of $C_{gd,iter}$ is further quantified in terms of the number of Add-Compare-Selection (ACS) operations, when considering the joint complexity of the IrSD detector, URC decoder and the RSC[5,7] channel codec employed. Furthermore, based on Table 5.6, we have generated Figure 5.17(b), which illustrates the overall complexity of the IrSD aided iterative decoding process, i.e. $C_{gd,iter}$ and its complexity ratio, $r_{gd,iter}$, for different values of r_{gd}. We have found that the IrSD aided DL-SDMA system has the lowest iterative decoding complexity, when we have $r_{gd} = 0.001$ and the corresponding weighting-coefficient vector is $\alpha = [0.93, 0.07, 0, 0, 0]$ at E_b/N_0 = 5dB. The overall complexity ratio $r_{gd,iter}$ of the IrSD in the case of $r_{gd} = 0.001$ is equal to 0.00233. In other words, the proposed solution reduces the complexity by about three orders of magnitude, compared to the ML detector aided iterative receiver.

Table 5.6: Parameters of the IrSD at E_b/N_0 = 5dB

r_{gd}	α	I_{gd}	$C_{gd,iter}(ACS)$	$r_{gd,iter}$
1	[0,0,0,0,1]	3	50741964.00	1
0.5	[0,0,0,0.57,0.43]	3	25370982.00	0.5
0.1	[0,0,0.35,0.65,0]	3	5074196.40	0.1
0.09	[0,0,0.4,0.6,0]	3	4566776.76	0.09
0.08	[0,0,0.5,0.5,0]	3	4059357.12	0.08
0.07	[0,0,0.6,0.4,0]	3	3551937.48	0.07
0.06	[0,0,0.55,0.45,0]	3	3044517.84	0.06
0.05	[0,0,0.7,0.3,0]	3	2537098.20	0.05
0.04	[0.53,0.07,0.1,0.3,0]	3	2029678.56	0.04
0.03	[0.043,0.157,0.7,0.1,0]	4	1691398.80	0.0333
0.02	[0.39,0.01,0.5,0.1,0]	4	1217807.14	0.0267
0.01	[0.37,0.03,0.6,0,0]	5	879527.38	0.0167
0.008	[0.425,0.175,0.4,0,0]	5	676559.52	0.0137
0.005	0.62,0.18,0.2,0,0]	5	422849.70	0.0083
0.003	[0.77,0.13,0.1,0,0]	6	304451.78	0.00633
0.001	[0.93,0.07,0,0,0]	7	118397.92	0.00233
0.0005	N/A	N/A	N/A	N/A

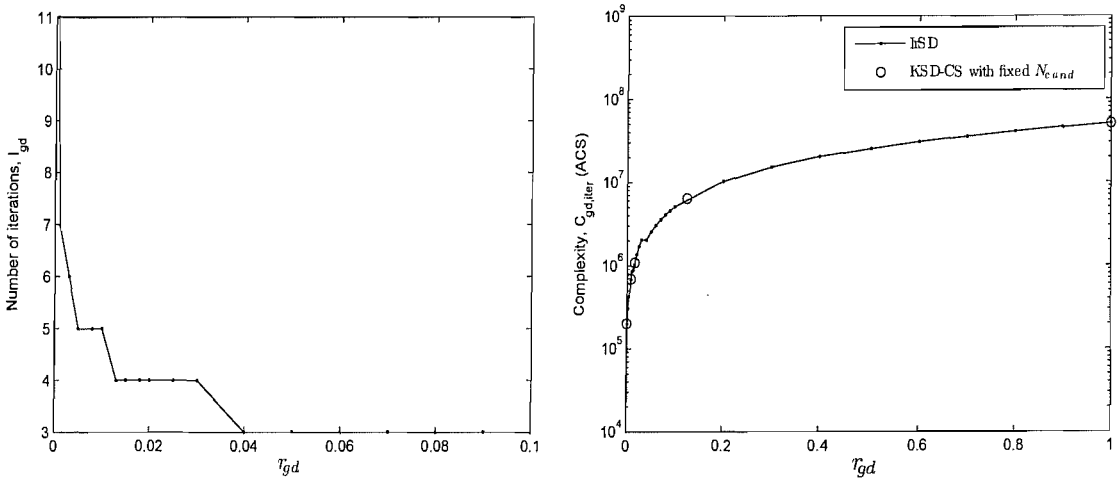

(a) (b)

Figure 5.17: (a) The required number of iterations I_{gd} of the IrSD associated with different values of r_{gd} (b) Total complexity of the iterative IrSD decoding process. The systems operated at $E_b/N_0 = 5dB$.

5.2.7 Performance Results

In this section, we characterize the attainable performance of the IrSD aided iterative DL-SDMA system. The system parameters used are listed in Table 5.5.

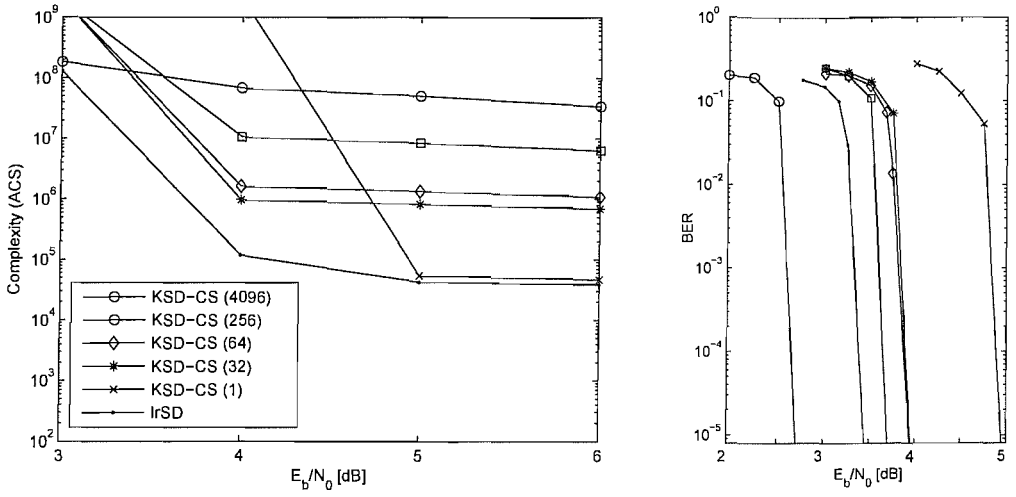

(a) (b)

Figure 5.18: Comparison of the **computational complexity** (a) per detect bit and **BER** (b) of the iterative decoding aided DL-SDMA system of Figure 5.3 employing different detectors. The channel model was a flat fading MIMO channel and the parameters of Table 5.5 were used. The weighting-coefficient vector α of the IrSD employed at the E_b/N_0 values ranging from 3, 4, 5 to 6 dB were [0,0,0,0.34,0.66], [0.37,0.03,0.6,0,0], [0.93,0.07,0,0,0] and [0.995,0.005,0,0,0], respectively.

In Figure 5.18(a), we recorded the computational complexity imposed, which is quantified by using the number of add-compare-selection (ACS) operations in the iterative DL-SDMA system designed for reaching a target BER of 10^{-5}. Observe in Figure 5.18(a) that the IrSD aided iterative DL-SDMA systems have a lower computational complexity than the other KSD-CS detection aided systems employing a fixed value of N_{cand}, where the IrSD employs $N_{cand} = 1, 32, 64, 256$ and 4096.

Moreover, when the system operated at $E_b/N_0 = 3$ dB, the KSD-CS(4096) detector may still maintain an open EXIT-tunnel between its EXIT-curve and the outer channel coder's EXIT-curve. However, the EXIT-curves of the other inner benchmarker detectors, such as the KSD-CS(1), KSD-CS(32), KSD-CS(64) and KSD-CS(256) scheme, may intersect the EXIT-curve of the outer channel encoder at $E_b/N_0 = 3$ dB. This resulted in an 'infinite computational complexity' of the iterative decoding imposed by the benchmarker detectors, because they would require an infinite number of iterations, in order to achieve a target BER of 10^{-5}. In Figure 5.18(a), the cross-over between the

curve portraying the computational complexity imposed by the KSD-CS(4096) detector and those of the other benchmarker detectors indicated this phenomenon.

Figure 5.18(b) shows that the IrSD detector has only a modest E_b/N_0 degradation of about 1 dB compared to the KSD-CS benchmarker associated with $N_{cand} = 4096$. The KSD-CS detector using $N_{cand} = 4096$ conducted a full search over the set of $\mathcal{M}^Q = 4^6$ candidates, i.e. by taking into account all the possible candidates. By contrast, the KSD-CS detector using $N_{cand} = 1$ represents the MMSE detector. Therefore, the proposed IrSD provides a flexible detection framework. By switching the value of N_{cand} of KSD-CS detector according to the appropriately designed weighting-coefficient vector α, the system may be expected to operate at the lowest possible iterative decoding complexity. Therefore, the proposed IrSD provides a flexible detection framework. By switching the value of N_{cand} of KSD-CS detector according to the appropriately designed weighting-coefficient vector α, the system may be expected to operate at the lowest possible iterative decoding complexity.

5.2.8 Conclusions

In this section, we proposed the IrSD algorithm designed for reducing the complexity of the iterative decoding aided system. By appropriately designing the weighting-coefficient vector α, the IrSD aided system may potentially provide the lowest possible iterative decoding complexity. Quantitatively, Figure 5.18 suggests that the IrSD aided iterative DL-SDMA system associated with $\alpha = [0.93, 0.07, 0, 0, 0]$ may reduce the complexity by three orders of magnitude at $E_b/N_0 = 5dB$, when compared to the KSD-CS benchmark detector associated with $N_{cand} = 4096$.

Table 5.7: Comparison of the complexity ratio of the DL-SDMA system using IrSD and KSD-CS for different values of N_{cand} (extracted from Figure 5.18)

SNR [dB]	3	4	5	6
KSD-CS(4096)	1	1	1	1
KSD-CS(256)	N/A	0.1567	0.1671	0.1879
KSD-CS(64)	N/A	0.0239	0.0266	0.0319
KSD-CS(32)	N/A	0.0143	0.0163	0.0204
KSD-CS(1)	N/ A	N/A	0.0098	0.0054
IrSD	0.6989	0.0057	0.00233	0.0011

The complexity of the DL-SDMA system using IrSD and KSD-CS at different values of N_{cand},

was extracted from Figure 5.18 and was summarized in Table 5.7. By normalizing the complexity of each detector to the complexity of the ML detector, which was represented by the curve KSD-CS(4096) in Figure 5.18, Table 5.7 indicated that IrSD has the lowest complexity against the detectors considered.

5.3 Pilot Assisted Channel Prediction Aided LDC-MUT DL-SDMA System

In this section, we study the impact of imperfect ST-CIRT on the LDC-MUT DL-SDMA system. In practice, the ST-CIRT may be estimated with the aid of pilot symbols fed into long range channel prediction algorithms [54]. Hence the scenario we considered in this section is based on the pilot-assisted channel prediction of MIMO channels [78]. By transmitting the DL pilots periodically to the MSs for the sake of sampling the channel's complex-valued envelope, the receivers estimate the ST-CIRTs and then feed their quantized estimates back to the BS via feedback channels. In order to reduce the required rate of the feedback channel and efficiently feed back the ST-CIRTs of the MIMO channels, well-designed channel quantizers have to be employed at the MS's receiver. Due to the imperfect ST-CIRTs, the residual MUI will detrimentally impact the achievable system performance. Hence, in our following discussions, we will focus our attention on the performance analysis of the LDC-MUT aided DL-SDMA system using pilot assisted channel prediction.

5.3.1 Pilot and Data Frame Structure

As illustrated in Figure 5.19(a), we consider the scenario that the BS has M transmit antennas Then there are $(M \cdot N)$ links between the BS and each of the MSs using N receiver antennas. Additionally, as illustrated in Figure 5.19(b), the pilots have been periodically inserted in the symbol intervals of each transmitted frame, where T_d is the data transmission symbol intervals and T_p is the pilot symbol intervals. The N-antenna aided receiver of each MS may estimate the ST-CIRTs of each link based on the received pilots and feeds the estimated and quantized ST-CIRTs back to the BS via the feedback channels. We denote the sampled ST-CIRTs of the (i,j)-th link of the n-th frame of Figure 5.19(a), which is experienced by the k-th MS, by $(\cdots, h_{i,j}^{(k)}[n], h_{i,j}^{(k)}[n+1], \cdots)$ as seen in Figure 5.19(b). The DL channel and the UL feedback channels of the MSs are typically allocated in different bandwidths and the UL feedback information is assumed to be transmitted over the strongly protected UL control channel. The BS may update current ST-CIRTs by employing the ST-CIRT prediction based on the previously received quantized ST-CIRTs . We denote the quantized ST-CIRTs by $(\cdots, \bar{h}_{i,j}^{(k)}[n-1], \bar{h}_{i,j}^{(k)}[n], \cdots)$ and the predicted ST-CIRTs by $(\cdots, \hat{h}_{i,j}^{(k)}[n], \hat{h}_{i,j}^{(k)}[n+1], \cdots)$ in Figure 5.19(b). Assuming the feedback channels are error-free, the performance of MUT is limited by employing imperfect ST-CIRT, which is composite of the pilot interval's ST-CIRT estimation error, quantization error, feedback latency and the BS's ST-CIRT prediction error.

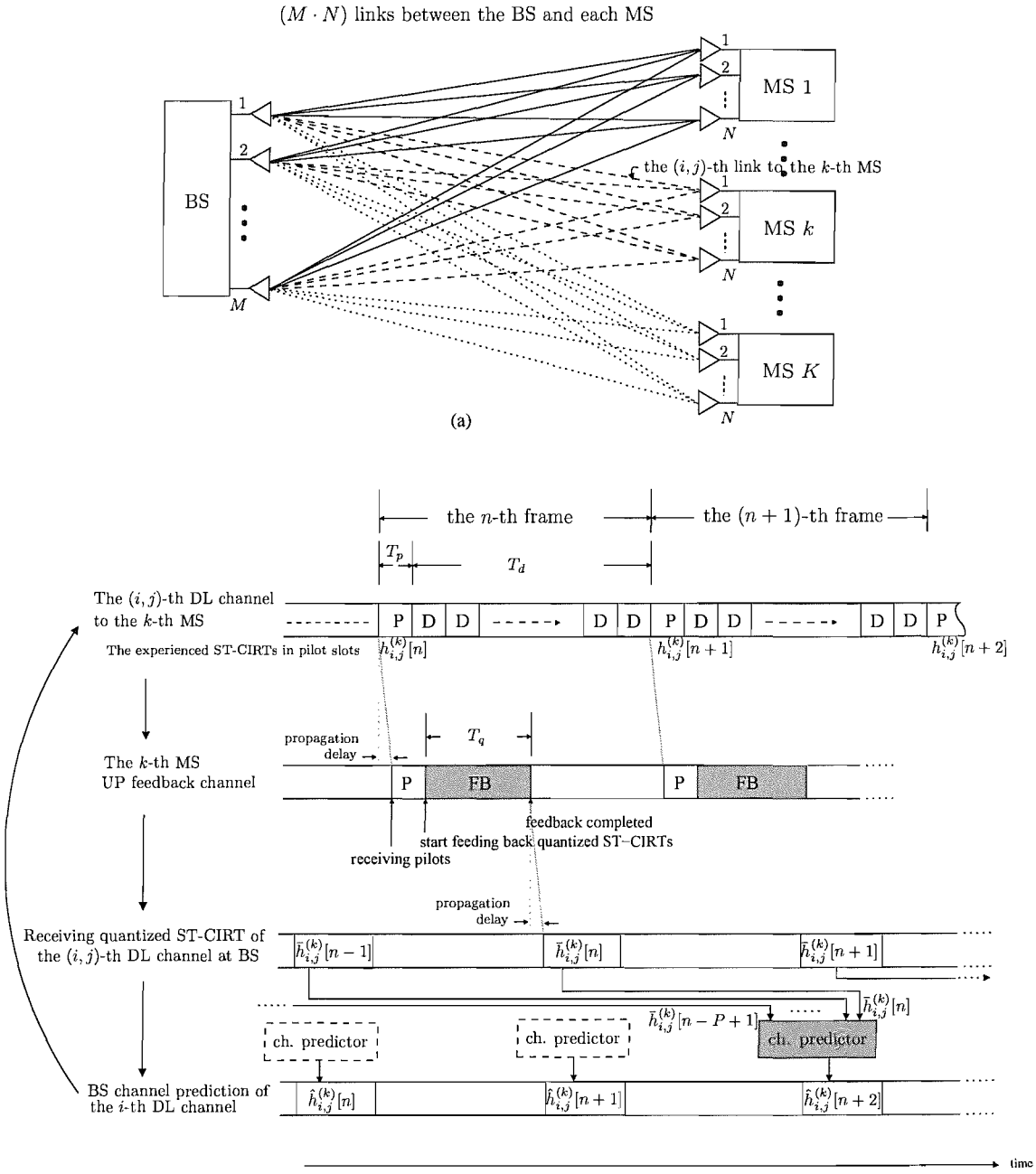

Figure 5.19: (a) $(M \cdot N) \cdot K$ links of the DL-SDMA system (b) Pilot assisted channel prediction in associated with the ST-CIRT feedback

Again, there are $(M \cdot N)$ links between the BS and the N receiver antennas of each MS. Hence each MS has to estimate $(M \cdot N)$ ST-CIRT coefficients based on the received pilots for each frame. Assuming that each MS employs a q-bit channel quantizer [5] and has a feedback transmission rate of N_{bps} bits per transmit symbol interval, the number of symbol intervals T_q required for feeding back all the ST-CIRT coefficients of each transmission frame to the BS is given by

$$T_q = \frac{(M \cdot N) \cdot 2 \cdot q}{N_{bps}}. \tag{5.33}$$

The propagation delay of the channel may be negligible compared to T_q, due to the high number of ST-CIRT coefficients representing the MIMO channels. Hence, the ST-CIRT signaling latency is determined by the amount of time required for signaling the T_q symbols.

Example 5.4:

Consider that the DL-SDMA system shown in Figure 5.3 has $M = 6$ transmit antennas and supports $K = 3$ MSs, where each MS has $N = 2$ receive antennas. When the MS employs a $q = 2$-bit quantization scheme, we have $T_q = (6 \cdot 2) \cdot 2 \cdot 3/4 = 18$ symbols, where we assume that the MS had a feedback transmission rate of $N_{bps} = 2 \cdot 2$ bits per transmit symbol interval by using 4QAM and two transmit antennas.

In order to reduce the impact of the ST-CIRT signaling latency, we assume $T_q < T_d$ in this study. Hence the BS will receive the quantized ST-CIRTs of the n-th transmission frame before the $(n+1)$st transmission frame.

Furthermore, the BS may update the current ST-CIRTs by employing the ST-CIRT prediction based on the P previously received quantized ST-CIRTs. Hence, as illustrated in Figure 5.19(b), the predicted ST-CIRT $\hat{h}_{i,j}^{(k)}[n+2]$ may be generated based on P quantized ST-CIRTs, i.e. $(\bar{h}_{i,j}^{(k)}[n-P+1], \cdots, \bar{h}_{i,j}^{(k)}[n])$, by assuming a prediction distance of two, which is guaranteed by letting $T_q < T_d$.

5.3.2 Pilot Assisted Channel Prediction Using MMSE Criterion

As advocated in [78], we may transmit the pilot symbols from each of the M DL transmit antennas to each of the $(N \cdot K)$ MS receive antennas in the pilot symbol intervals. Therefore, each of the K MS receivers may estimate the ST-CIRT of each of the $(M \cdot N)$ links. In this scenario, the number of symbol intervals required for pilot transmission will be at least $(M \cdot N \cdot K)$ for the $(M \cdot N \cdot K)$ links of Figure 5.19(a), i.e. we have $T_p \geq M \cdot N \cdot K$. Due to the high pilot overhead and latency imposed

[5] The q-bit channel quantizer quantizes both the amplitude and phase of the fading envelope using q bits hence requiring a total of $2q$ bits.

in this scenario, the authors of [78] suggested the employment of orthogonal pilot sequences for each link, where the orthogonal pilot sequences are transmitted simultaneously in parallel and the composite multi-stream pilot signal is then correlated with the individual pilot sequences at the receiver [78]. Naturally, owing to using orthogonal pilot sequences instead of individual user and stream-specific pilot symbols, the sequences transmitted in parallel have an extended bandwidth requirement. However, the total side-information requirement, i.e. the required number of symbol intervals T_q, remains the same, regardless of how the pilots are transmitted. Let us denote the orthogonal pilot sequence transmitted from the j-th transmit antenna by $c_{p,j}$, which is a N_c-element column-vector and may be constructed by using Walsh-Hadamard codes [87]. Additionally, we denote the pilot symbol transmitted from the j-th antenna by $s_{p,j}[n]$ and the signal received in the pilot symbol interval of the n-th frame of Figure 5.19(b) at the i-th receive antenna of the k-th MS's receiver by $y_{p,i}^{(k)}[n]$. Then we have

$$y_{p,i}^{(k)}[n] = \sum_{j=1}^{M} c_{p,j} s_{p,j}[n] h_{i,j}^{(k)}[n] + w_i^{(k)}[n], \tag{5.34}$$

where w_i is the receive's white noise having a variance of N_o.

Due to the orthogonality of the pilot sequences $c_{p,j}$, the estimated ST-CIRT coefficient $h_{i,j}^{(k)}$, denoted by $\tilde{h}_{i,j}^{(k)}$, may be expressed as

$$\tilde{h}_{i,j}^{(k)}[n] = h_{i,j}^{(k)}[n] + \tilde{w}_i^{(k)}[n], \tag{5.35}$$

where we have $\tilde{w}_i^{(k)}[n] = c_{p,j}^H w_i^{(k)}[n] / s_{p,j}[n]$.

The following discussions are applicable to each MS. For the sake of the concise notation, we will remove the user index k.

The estimated ST-CIRT $\tilde{h}_{i,j}$ may then be quantized and fed back to the transmitter via the feedback channel. Let us denote the quantized value of $\tilde{h}_{i,j}$ by $\bar{h}_{i,j}$. We now briefly summarize the channel prediction algorithm using the MMSE criterion, where the predictor is fed with the quantized ST-CIRTs. When denoting the predicted ST-CIRT coefficient of the $(n + n_q)$ frame by $\check{h}_{i,j}[n + n_q]$, where n_q is the number of frames over which prediction is carried out, we obtain the predicted ST-CIRT coefficient $\check{h}_{i,j}[n + n_q]$ based on the P previously received quantized ST-CIRT fading factors $\bar{h}_{i,j}[n - n_p]$, where we have $0 \leq n_p \leq (P - 1)$, in the form of

$$\check{h}_{i,j}[n + n_q] = \mathbf{w}_{i,j}^H \bar{\mathbf{h}}_{i,j}, \tag{5.36}$$

where $\mathbf{w}_{i,j}$ is a P-element linear predictive weighting vector and $\bar{\mathbf{h}}_{i,j} = [\bar{h}_{i,j}[n], \bar{h}_{i,j}[n-1], \cdots, \bar{h}_{i,j}[n - P + 1]$.

According to [88], we may obtain the optimal linear predictive coefficients $\mathbf{w}_{i,j}$ by minimizing the prediction error, which may be expressed as

$$\mathbf{w}_{op,i,j} = \arg_{\mathbf{w}_{i,j}} \min \mathrm{E}\left\{ \|h_{i,j}[n+n_q] - \mathbf{w}_{i,j}^H \bar{\boldsymbol{h}}_{i,j}\|^2 \right\}. \tag{5.37}$$

The optimal solution for the linear predictive coefficients $\mathbf{w}_{op,i,j}$ may be expressed as [88]

$$\mathbf{w}_{op,i,j} = \left(\mathrm{E}\left\{\bar{\boldsymbol{h}}_{i,j}\bar{\boldsymbol{h}}_{i,j}^H\right\}\right)^{-1} \mathrm{E}\left\{h_{i,j}^* \bar{\boldsymbol{h}}_{i,j}\right\}. \tag{5.38}$$

Furthermore, according to [88], assuming that the ST-CIRT fading factors $h_{i,j}[n]$ are Rayleigh distributed, the channel's correlation $\boldsymbol{R}$ may be modeled by using the zero-order Bessel function, J_o of the first kind according to [88]

$$\mathbf{w}_{op,i,j} = \boldsymbol{R}^{-1}\boldsymbol{r}, \tag{5.39}$$

where

$$[\boldsymbol{R}]_{a,b} = J_o(2\pi f_D |a-b| T_s) + \frac{N_0}{E_p}\delta(a-b), \tag{5.40}$$

$$[\boldsymbol{r}]_a = J_o(2\pi f_D |n_p + a| T_s), \tag{5.41}$$

where we have $a, b \in [0, P-1]$, and T_s is the symbol duration. Furthermore, $E_p = \|s_{p,j}(n)\|^2$ is the power of the pilot symbol.

Finally, the MMSE channel prediction error variance formulated in Equation 5.37 may be expressed as [88]

$$\sigma_\varepsilon^2 = 1 - \boldsymbol{r}^H \boldsymbol{R}^{-1}\boldsymbol{r}. \tag{5.42}$$

In closing, we define the Normalized Mean Squared Error (NMSE) $\sigma_{ST-CIRT}^2$ of the ST-CIRT as

$$\sigma_{ST-CIRT}^2 = E\left\{ \|\check{h}[n] - h[n]\|^2 \right\} / E\left\{ \|h[n]\|^2 \right\}, \tag{5.43}$$

where the expectation $\mathrm{E}\{\cdot\}$ is taken with respect to the time-variant fading coefficient $h[n]$.

Again, the NMSE $\sigma_{ST-CIRT}^2$ of the ST-CIRT is determined by the composite of the pilot interval's ST-CIRT estimation error, quantization error, feedback latency and the BS's ST-CIRT prediction error.

5.3.3 Performance Results

In this section we characterize the performance of the LD-MUT aided DL-SDMA system using pilot assisted channel prediction. The channel prediction used at the transmitter is based on the 2-bit

Table 5.8: System Parameters

Channel Coder	rate-0.5 RSC [5,7]
Interleaver length	10^5 bits
URC Coder	rate-1 Conv. Coder [22]
Modulation	4QAM
Number of MSs	$K = 3$
Number of transmit antennas	$M = 6$
Number of dimension in spatial domain of each MS	$L = 2$
Number of independent data streams transmitted for each MS in one LDC symbol	$Q = 3$.
The interval of one LDC symbol	$T = 2$
Number of receive antennas of each MS	$N = 2$.
Loading ratio	$\Gamma_o = 1/2$
Number of input samples of channel predictor	$P = 5$
The prediction distance of channel predictor	$n_p = 2$

quantized ST-CIRTs, which are fed back from the receivers. Using channel prediction based on the perfectly quantized ST-CIRT provided a benchmark, which we will denote using $q = \infty$, i.e. an infinite number of bit for channel quantizer. The system parameters used are listed in Table 5.8. In order to further emphasize the effects of the channel prediction and channel quantization, the detectors employed at the DL receivers are also characterized for the scenario of perfect DL channel knowledge.

In Figure 5.20, we characterize the performance of channel prediction at the normalized Doppler frequency $f_D = 0.001$. We plot the ST-CIRT error variance $\sigma^2_{ST-CIRT}$ as a function of the channel SNR, when using a pilot spacing determined by the data transmission symbol intervals T_d of each pilot-frame as seen in Figure 5.19(b), where we have $T_d = 50, 75$ and 100. The larger the pilot spacing T_d, the less accurate the predicted channel. Therefore, in Figure 5.20, $T_d = 50$ has the lowest $\sigma^2_{ST-CIRT}$. Naturally, the specific value of T_d in Figure 5.19 has an influence on the ST-CIRT feedback signaling rate. By considering the required ST-CIRT feedback latency, it is required for $T_q < T_d$. As exemplified in Example 5.4, we have $T_q = 18$ according to the system configuration of Table 5.8. In the following discussions, we assume the pilot spacing $T_d = 50$, which results in $0.02\%(1/50)$ pilot overhead and $0.36\%(18/50)$ feedback overhead.

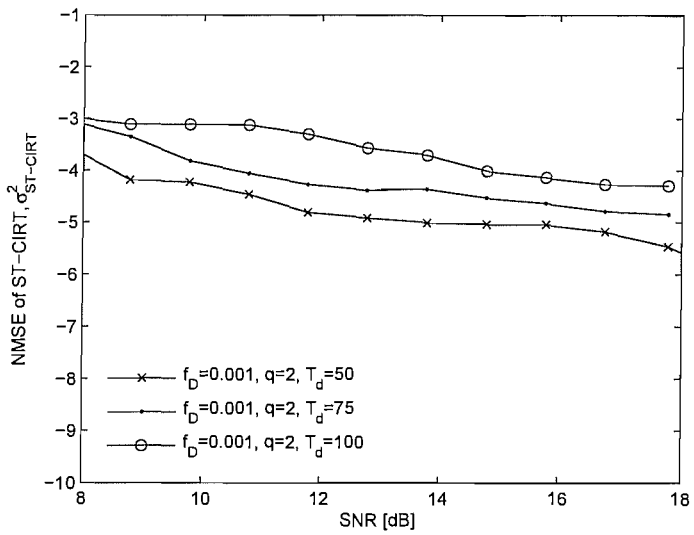

Figure 5.20: The NMSE $\sigma^2_{ST-CIRT}$ of ST-CIRT for pilot assisted channel prediction based on 2-bit ST-CIRT feedback. The systems used $T_d = 50, 75$ and 100 are investigated. The normalized Doppler frequency is $f_D = 0.001$. The other system parameters are listed in Table 5.8.

In Figure 5.21 we recorded the number of iterative decoding steps required for the LDC-MUT aided DL-SDMA systems to reach the target BER of 10^{-5}, when using different detectors. The KSD-CS detector using $N_{cand} = 16$ reduced the number of detection candidates required from 64 to 16. The performance of the LDC-MUT aided DL-SDMA systems using pilot assisted channel prediction based on the perfect ST-CIRT was also provided in Figure 5.21 as a benchmarker. Observe that the systems having imperfect ST-CIRT generated by using pilot assisted channel prediction based on $q = 2$-bit ST-CIRT feedback required an SNR of about 2.5 dB higher than the ones using imperfect ST-CIRT generated by using pilot assisted channel prediction based on perfectly quantized ST-CIRTs.

In Figure 5.22, we quantify the BER performance of the LDC-MUT aided DL-SDMA system using pilot assisted channel prediction. The number of iterative decoding steps was set to $I = 10$. By comparing the BER performance of the systems employing the MMSE and ML detectors, the system employing the Log-MAP detector outperformed the MMSE detector by about 1.5 dB. This indicates that a more powerful detector provides only a limited SNR gain when imperfect ST-CIRTs are employed in the systems. However, when using the KSD-CS in conjunction with $N_{cand} = 16$, it approaches the Log-MAP performance, despite its four-fold reduced complexity. More explicitly, observe that in Figure 5.22 when a 2-bit channel quantizer is used, the system employing the KSD-CS with $N_{cand} = 16$ becomes capable of reaching the BER of 10^{-5} at the same SNR as the systems

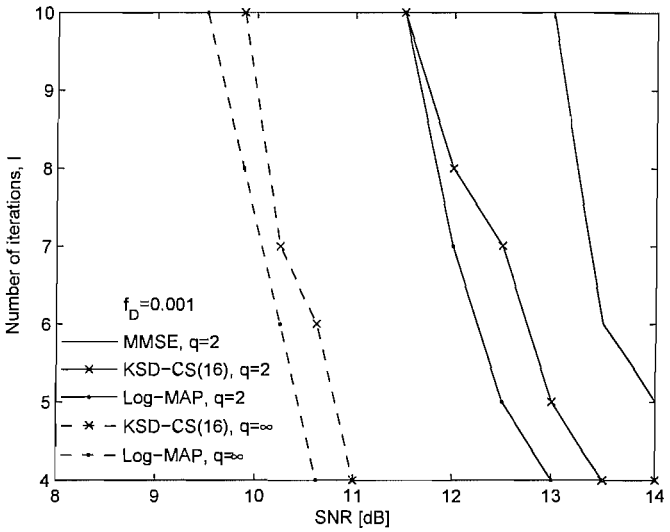

Figure 5.21: The number of iterative decoding steps required by the LDC-MUT aided DL-SDMA system of Figure 5.3 using pilot assisted channel prediction to reach the target BER of 10^{-5}, when invoking different detectors. The normalized Doppler frequency was $f_D = 0.001$. The other system parameters are listed in Table 5.8.

employing the Log-MAP detector. Even when a perfectly quantized ST-CIRT is assumed ($q = \infty$), the system employing the KSD-CS using $N_{cand} = 16$ performs similarly to the system employing the KSD-CS detector using $N_{cand} = 64$, which in this case is an ML detector conducting a full-candidate search, where the total number of detection candidates is $\mathcal{M}^Q = 4^3$.

In Figure 5.23, the performance of pilot assisted channel prediction is investigated at the normalized Doppler frequencies of $f_D = 0.001$ and $f_D = 0.0005$. As expected, the lower the normalized Doppler frequency, the smaller the NMSE $\sigma^2_{ST-CIRT}$ of the ST-CIRT. Observe in Figure 5.23 that the $\sigma^2_{ST-CIRT}$ difference between the normalized Doppler frequencies of $f_D = 0.001$ and $f_D = 0.0005$ is smaller, when the $q = 2$-bit channel quantizer is used. This indicates that the quantization error of the ST-CIRT limited the performance of the pilot assisted channel prediction even when it operated in a slow fading environment. Figure 5.24 shows that at the normalized Doppler frequency of $f_D = 0.001$, a loss of about 1.5 dB has to be tolerated in comparison to $f_D = 0.005$, when the KSD-CS detector using $N_{cand} = 16$ was employed in both cases.

In Figure 5.25 we set the target BER to 10^{-5} and recorded the required SNR for the LDC-MUT assisted DL-SDMA system using pilot assisted channel prediction based on $q = 2$-bit ST-CIRT feedback. The Log-MAP detector was applied in all scenarios, in order to arrive at a fair comparison. The systems were configured to use their minimum required number of iterative decoding steps to

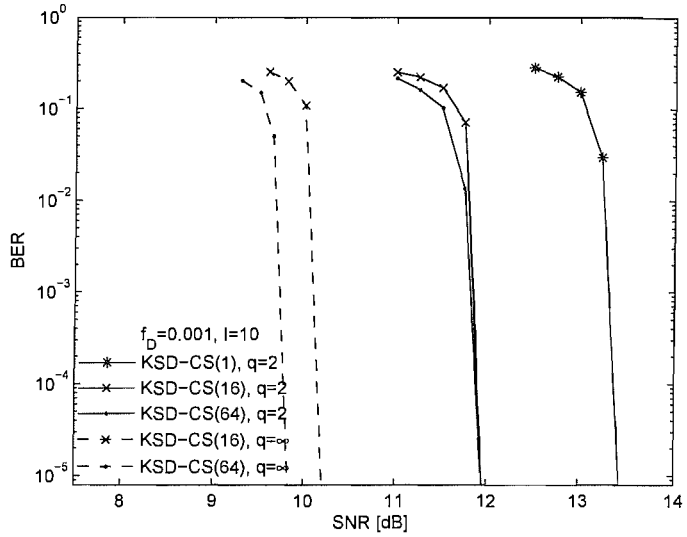

Figure 5.22: BER performance of the LDC-MUT aided DL-SDMA system of Figure 5.3 using pilot assisted channel prediction. The systems invoking different detectors are investigated. The normalized Doppler frequency is $f_D = 0.001$. The other system parameters are listed in Table 5.8.

reach the target BER of 10^{-5}. Different values of Q, such as $3, 4, 5$ and 6 were used, which resulted in the loading ratios of $\Gamma_o = [3/6, 4/6, 5/6, 6/6]$, as defined in Equation 5.15. Observe in Figure 5.25 that lower values of Γ_o required lower SNRs, indicating that a lower system load Γ_o results in a reduced SNR requirement at a given BER. For example, for the faster fading scenario of $f_D = 0.001$, the required SNR is about 8 dB lower, when Γ_o is reduced from $4/6(0.667)$ to $3/6(0.5)$. For the slower fading scenario of $f_D = 0.0005$, the required SNR is about 2.5 dB lower, when Γ_o is reduced from $4/6(0.667)$ to $3/6(0.5)$. In conclusion, there is a trade-off between having a low SNR requirement for achieving the target BER and supporting a high system load Γ_o, especially in the presence of severely contaminated ST-CIRTs, which was induced by using $0.02\%(1/50)$ pilot overhead and very low feedback rate of a $q = 2$-bit channel quantizer. On the other hand, the high diversity gain provided by the LDC-MUT assisted DL-SDMA system is associated with a reduced system load Γ_o, which hence results in a low BER performance (BER $< 10^{-5}$), even in the presence of severely contaminated ST-CIRTs.

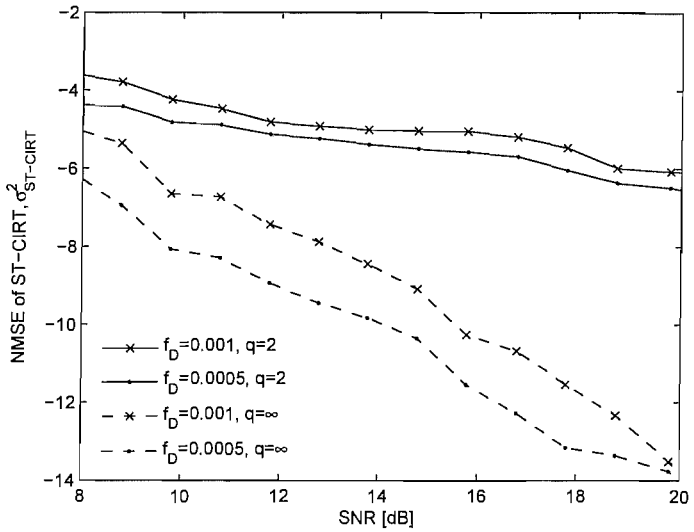

Figure 5.23: NMSE $\sigma^2_{ST-CIRT}$ of the ST-CIRT for pilot assisted channel prediction at the normalized Doppler frequencies of $f_D = 0.001$ and $f_D = 0.0005$. A $q = 2$-bit ST-CIRT feedback was employed. Channel prediction based on the perfectly quantized ST-CIRT ($q = \infty$) was used as a benchmarker. The other system parameters are listed in Table 5.8.

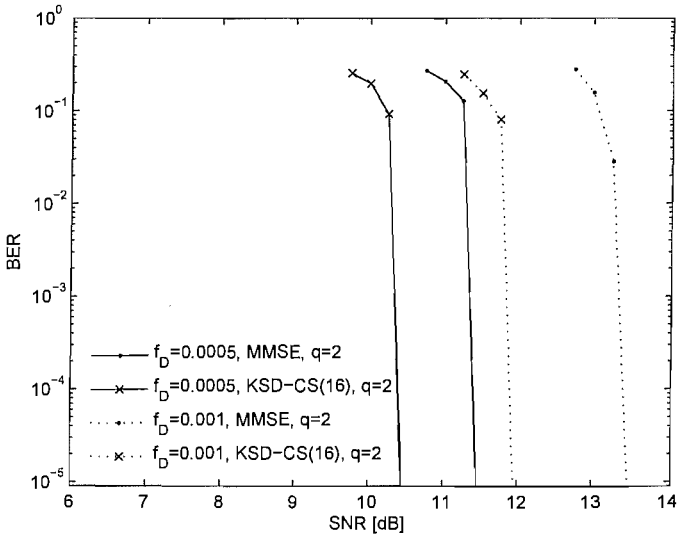

Figure 5.24: BER performance of the LDC-MUT aided DL-SDMA system of Figure 5.3 using pilot assisted channel prediction in different normalized Doppler frequency settings ($f_D = 0.001$ and $f_D = 0.0005$). The other system parameters are listed in Table 5.8.

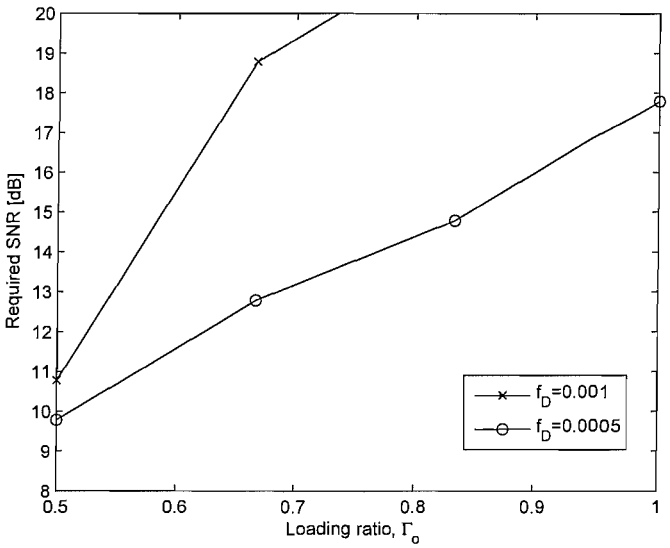

Figure 5.25: The required SNR of the LDC-MUT aided DL-SDMA system of Figure 5.3 using pilot assisted channel prediction based on q = 2-bit ST-CIRT feedback. The system operated at $Q = 3,4,5$ and 6, which results in the loading ratios of $\Gamma_o = [3/6, 4/6, 5/6, 6/6]$. The other system parameters are listed in Table 5.8.

5.4 Summary and Conclusions

In Section 5.1, we introduced the LDC-MUT aided DL-SDMA system using linear dispersion codes. The capacity of the LDC MUT aided DL-SDMA system characterized in Figure 5.6(a) was summarized in Table 5.3. In addition, observe in Figure 5.7(b) that upon increasing the value of T, the achievable diversity gain improves, which in turn enhances the BER performance, as evidenced by Table 5.4.

In Section 5.2, we introduced the novel KSD-CS scheme, which is capable of approaching the performance of the ML detector at a reduced complexity. In Section 5.2.3 we proposed LDC aided MUT DL-SDMA systems invoking the IrSD-CS detector, which has the potential of reducing the complexity of the iterative decoder employed. Table 5.7 summarized the complexity of the different detectors and concluded that the IrSD-CS scheme imposes a lower complexity than all the other detectors.

In Section 5.3, we characterized the attainable performance of the LDC-MUT aided DL-SDMA systems using imperfect ST-CIRTs, which was induced by a combination of the pilot interval's ST-CIRT estimation error, quantization error, feedback latency and the BS's ST-CIRT prediction error. Although there is trade-off between the low SNR required for achieving the target BER and the system load Γ_o that may be supported, especially in the presence of severely contaminated ST-CIRTs. We found in Figure 5.25 that the high diversity gain provided by the LDC-MUT assisted DL-SDMA system was achieved at the cost of reducing the system load Γ_o, when a low BER has to be maintained, even in the presence of imperfect ST-CIRT.

Chapter 6

Conclusions and Future Work

6.1 Summary of Results

In this thesis we characterized DL-SDMA communicating over MIMO Rayleigh-fading channels with the aid of MUT techniques, iterative detection and decoding. We also considered the impact of imperfect channel knowledge.

More specifically, we reported the following major findings:

- Firstly, in Chapter 2 we investigated a MUT aided DL-SDMA system and found that SVD based MUT has the advantages of high capacity and supports a high variety of system configurations, when compared to both MMSE and ZF aided MUT schemes.
- In Chapter 3 we studied an iterative detection aided DL-SDMA system and improved its convergence behaviour. In addition, we compensated the impact of imperfect channel knowledge on the iterative DL-SDMA system by using IRCCs.
- In Chapter 4 we proposed the concept of IrGD for maintaining a high integrity by the iterative DL-SDMA systems. In addition, we proposed the philosophy of an EXIT-chart optimized CSI quantizer (ECO-CQ) to reduce the feedback overhead of iterative DL-SDMA systems.
- In Chapter 5 we improved the achievable capacity of iterative DL-SDMA systems by invoking LDCs and proposed the concept of irregular sphere detection, which was created by extending the IrGD philosophy of Chapter 4. Furthermore, we reduce the complexity imposed by the joint iterative detection and decoding of the LDC aided iterative DL-SDMA system.

In the forthcoming sections, we will summarize some of the major conclusions of this study and propose promising directions for future work.

6.1.1 Multi-User Transmission Technique

In Section 2.1, we investigated the benefits of MUT aided DL-SDMA systems, where the system employed a linear spatio-temporal preprocessor (STP) at the BS's transmitter in order to mitigate the multi-user interference (MUI) imposed on the received signals of the MSs and to facilitate multi-stream/multi-user transmissions. In Section 2.1.2, we introduced a MUT-STP designed by using the classic zero-forcing (ZF) technique, the minimum mean square error criterion (MMSE) and singular value decomposition (SVD) aided MUT. In Section 2.1.3, we studied the achievable capacity of the system employing the above three MUT-STPs. In Figures 2.2 and 2.3 we observed that the achievable capacity of the DL-SDMA system employing the SVD-assisted MUT-STP scheme is higher than that of the system employing the other two MUT-STP schemes across most of the SNR region. In addition, in Table 2.1 we reported that the SVD-MUT is capable of operating in diverse system configurations, namely in lightly-loaded, fully-loaded and rank-deficient scenarios, while the MMSE-MUT and the ZF-MUT are unable to operate in rank-deficient scenarios. We repeat Table 2.1 in Table 6.1 for the reader's convenience.

	SVD-MUT	MMSE-MUT	ZF-MUT
Rank-deficient ($M > N$, $L_k > N_k$)	$\surd$	$\times$	$\times$
Fully-loded ($M = N$, $L_k = N_k$)	$\surd$	$\surd$	$\surd$
Lightly-loded ($M < N$, $L_k < N_k$)	$\surd$	$\surd$	$\times$

Table 6.1: System configurations supported by the different linear MUT-STP schemes

In conclusion, compared to the MMSE-MUT and ZF-MUT schemes we found that the SVD-MUT scheme has the advantages of maintaining a high capacity and supporting a high variety of system configurations in different channel conditions in the context of the DL-SDMA system.

6.1.2 Iterative Detection and Decoding

In Chapter 2, we investigated the DL-SDMA system employing non-iterative detection schemes. More specifically, in Section 2.2 we evaluated the DL-SDMA system employing both linear and nonlinear detection techniques, when each user's received signal imposes multi-stream interference

(MSI), where the MUI has been mitigated by our SVD-MUT scheme. Firstly, we defined the normalized system load in Section 2.2.1, which characterized different system configuration scenarios, namely the lightly-loaded, full-loaded and rank-deficient scenario. Then, in Figure 2.8 we compared the E_b/N_0 required by the DL-SDMA systems for maintaining a target BER of 10^{-4} associated with different normalized system loads using linear detectors, such as the MMSE and nonlinear detectors, such as the Log-MAP detector. In Figure 2.8 we demonstrated that linear detectors, such as the MMSE detector, were not ideal for the DL-SDMA system operating in the rank-deficient scenario. On the other hand, nonlinear detectors, such as the Log-MAP detector, are capable of operating even in rank-deficient scenarios, albeit they may impose an excessive complexity, as documented in Figure 2.8. Therefore, we advocated the DL-SDMA system invoking a near-ML detector, which employed the optimum hierarchically reduced search algorithm (OHRSA) [20] of Section 2.2.2 to reduce the ML detector's complexity, while maintaining a near-ML performance. In Figure 2.7, we showed that the DL-SDMA system employing the OHRSA aided ML detector has a near-Log-MAP BER performance and it is suitable for operating in rank-deficient scenarios, while maintaining a low complexity, as seen in Figure 2.6.

In Chapters 3 and 4 we designed an iterative detection aided DL-SDMA system. In Section 3.2 we first derived an iterative near-ML detection aided DL-SDMA system, where the extrinsic information was exchanged between the OHRSA detector and the channel decoder, as illustrated for the iterative scheme (1) of Figure 6.1(b). Furthermore, we designed the iterative DL-SDMA system with the aid of EXIT charts and employed a unity-rate precoder (URC) to improve the decoding convergence behavior, where the extrinsic information was exchanged between the URC and the channel decoder as seen for the iterative scheme (2) of Figure 6.1(b). Similarly, in Section 4.2.2 we designed a three-stage iterative DL-SDMA system exchanging the extrinsic information between the detector, the URC and the channel decoder, as shown for the iterative scheme (3) of Figure 6.1(b). In Figure 6.1(a) we compared the required E_b/N_0 of the non-iterative DL-SDMA systems with their corresponding iteratively detected counterparts outlined in Figure 6.1(b). As seen in Figure 6.1(a), the iterative DL-SDMA scheme (3) of Figure 6.1(b) attains the target BER of 10^{-5} at the lowest E_b/N_0 requirement. However, the three-stage iterative scheme of Figure 6.1(b) imposes the highest complexity.

In Section 4.2 we proposed an irregular generic detection (IrGD) scheme, which may reduce the complexity imposed by the iterative DL-SDMA system employing scheme (1) of Figure 6.1(b), while maintaining an infinitesimally low BER at the target E_b/N_0. We introduced the design principle of IrGD in Section 4.2.1 and optimized the constituent detectors' duty-cycles in Section 4.2.4. In Figures 4.6 and 4.7 we compared the complexity imposed by the iterative IrGD aided DL-SDMA

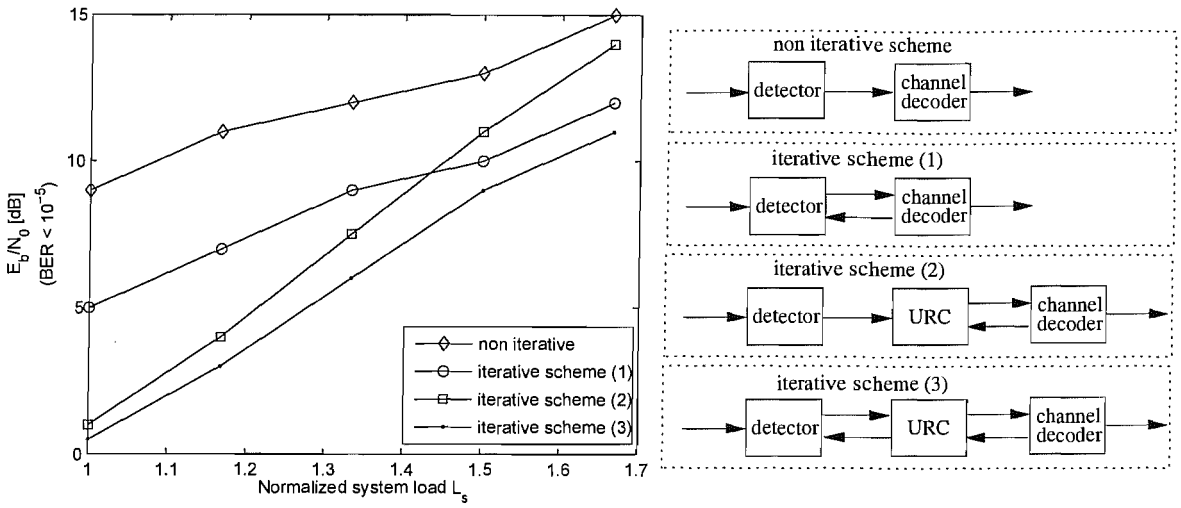

(a) (b)

Figure 6.1: Comparison of the iterative DL-SDMA systems employing different receiver schemes and supporting different normalized system loads. (a) shows the required E_b / N_0 in order to achieve a BER of 10^{-5} for the iterative schemes (1), (2) and (3). The normalized system load L_s corresponded to the system configurations of $(M, L) = [(6,2)(7,3)(8,4)(9,5)(10,6)]$ seen in TABLE 3.1. The system supports $K = 3$ users and each MS is equipped with $N = 2$ receive antennas. (b) illustrates the iterative receiver schemes.

system to those of the other detectors. We concluded that by switching amongst the constituent detectors according to the appropriately designed duty-cycle, the system may be expected to operate at the lowest possible iterative decoding complexity. Quantitatively, we exemplified the complexity reduction by summarizing the complexity ratio of IrGD aided DL-SDMA systems using 4QAM and 16QAM in Tables 4.4 and 4.5, which we repeated in Table 6.2 and 6.3.

6.1.3 The Impact of Imperfect Channel Knowledge

In Section 2.2.5 we investigated the impact of imperfect channel impulse response (CIR) knowledge on the DL-SDMA system. As illustrated in Figure 2.12, the imperfect ST-CIRT imposes a higher BER degradation on the DL-SDMA system than imperfect ST-CIRR does. In this thesis, we focused our attention on the investigation of imperfect ST-CIRT, while assuming that the receivers have perfect ST-CIRR.

In Section 3.3 we analyzed the iterative DL-SDMA system having imperfect ST-CIRT, which may be imposed by the combination of quantization errors and channel prediction error. As a first step,

Table 6.2: Comparison of the complexity ratio of iterative DL-SDMA systems using different detectors (extracted from Figure 4.6)

E_b/N_0 [dB]	1.7	2.2	2.7	3.2
Log-MAP	1	1	1	1
OHRSA	0.64	0.4167	0.4000	0.3750
MMSE	0.41	0.2056	0.2056	0.2056
IrGD	0.36	0.2056	0.1967	0.1752

Table 6.3: Comparison of the complexity ratio of iterative DL-SDMA systems using different detectors (extracted from Figure 4.7)

E_b/N_0 [dB]	4	4.5	5	5.5	6
Log-MAP	1	1	1	1	1
OHRSA	N/A	0.0101	0.0097	0.0095	0.0091
MMSE	N/A	N/A	N/A	0.0003	0.0003
IrGD	N/A	0.0037	0.0028	0.0003	0.0003

the inaccuracy of ST-CIRT was modeled by using Gaussian noise. In Section 3.3.3, we characterized impact of imperfect ST-CIRT on the iterative DL-SDMA system using EXIT charts which was similar to the effects of reducing the SNR of the iterative DL-SDMA system. We proposed to redesign the outer EXIT curve of the channel decoder by employing IRCCs [69] in order to maintain an open EXIT-tunnel, which may be expected to lead to an infinitesimally low BER.

In Section 4.3 we assumed that the iterative DL-SDMA had a limited ST-CIRT feedback and investigated the impact of the resultant imperfect ST-CIRT on the system. By striking a trade-off between maintaining a low BER and a low feedback overhead, we proposed the concept of EXIT-chart optimized CSI quantizer (ECO-CQ), which assisted us in potentially reducing the overhead required for maintaining an open EXIT-tunnel. In conclusion, our iterative DL-SDMA system employing ECO-CQ may require a lower feedback overhead than its counterpart employing a conventional CQ. Quantitatively, Table 4.10 exemplified the reduced feedback overhead of the ECO-CQ aided iterative DL-SDMA systems compared to that of the conventional CQ, which is repeated here in Table 6.4 as follows.

Table 6.4: Reduced feedback rate of the ECO-CQ aided iterative DL-SDMA systems (extracted from Figure 4.20)

	E_b/N_0 [dB]	3	3.5	4	4.5	5	6
Conventional CQ	Minimum required q-bit	4	3	3	3	3	3
	Normalized overhead Λ	0.024	0.018	0.018	0.018	0.018	0.018
ECO-CQ	Minimum required q-bit	4	3	2.9	2.8	2.7	2.6
	Normalized overhead Λ	0.024	0.018	0.0174	0.0168	0.0162	0.0156
Normalized overhead reduction ratio R_Λ		0	0	0.033	0.067	0.1	0.13

6.1.4 Approaching Channel Capacity

In Chapter 5, we upgraded the basic MUT-aided DL-SDMA system discussed in Chapter 2, 3 and 4 to the LDC-MUT aided DL-SDMA system, which potentially benefits from a higher achievable capacity and from a high degree of diversity. More specifically, in Figure 5.6(a) we showed that the achievable sum capacity of the LDC-MUT aided DL-SDMA system may be approached at a lower SNR than that of the basic MUT aided DL-SDMA system, as described in Section 5.1.3. We summarized the SNR gains of the LDC-MUT aided DL-SDMA system in Table 6.5. In Figure 5.7(b) we showed that the LDC-MUT aided DL-SDMA system may benefit from a high grade of diversity gain by increasing the LDC's symbol interval T. Table 6.6 summarized the SNR gain of LDC-MUT aided SDMA system in three different modes. In the case of $T = 1$ the system was equivalent to the DL-SDMA system employing the basic MUT scheme of Figure 5.2.

Although our LDC aided MUT scheme may assist the DL-SDMA system in achieving a high degree of diversity order and a high throughput by jointly exploiting the spatial- and time-domain dimensions, it imposed a higher complexity. Therefore, in Section 5.2 we proposed an irregular sphere detection for reducing the complexity imposed by joint iterative detection and decoding. Firstly, in Section 5.2.2 we derived the center-shifting aided K-best sphere detection (KSD-CS) concept, which may allow us to control the detection complexity by using different number of SD candidates N_{cand}. By contrast, the complexity of the OHRSA detector of Section 2.2.2 depends on the channel SNR [20]. Hence, by extending the previously proposed irregular generic detection scheme of Section 4.2, we derived the irregular SD philosophy in Section 5.2.3. Compared to IrGD, IrSD has a more wide variety of constituent detectors by simply using different values of N_{cand}. In Figure 5.18 we

Table 6.5: Required SNR of the LDC aided MUT DL-SDMA system at the specific target sum capacity (extracted from Figure 5.6(a))

Sum capacity (bits/s/Hz)	Basic MUT of Figure 5.2 (SNR [dB])	LDC aided MUT of Figure 5.3 (SNR [dB])	single-user MIMO (SNR [dB])
5	4.9	4.9	4.6
6	6.2	6.1	5.9
7	7.6	7.4	7.0
8	9.0	8.8	8.0
9	10.5	10.1	8.9
10	12.1	11.5	9.8
11	14.6	13.5	10.6

Table 6.6: Required SNR of the DL-SDMA system using the LDC aided MUT scheme at the target BER performance of 10^{-3} (extracted from Figure 5.7(b))

Schematic	LDC-MUT $[M, N, L, Q]$	The interval of the LDC symbol T	Γ_o	SNR [dB]
Figure 5.8	[7,2,3,2]	3	1/3	7.7
	[7,2,3,2]	2	1/2	9.2
	[7,2,3,2]	1	1	13.9
Figure 5.5	[6,2,2,2]	3	1/3	7.4
	[6,2,2,2]	2	1/2	8.8
	[6,2,2,2]	1	1	13.7
Figure 5.9	[5,2,1,2]	3	1/3	7.0
	[5,2,1,2]	2	1/2	8.5
	[5,2,1,2]	1	1	∞

Table 6.7: Comparison of the complexity ratio of the DL-SDMA system using IrSD and KSD-CS for different values of N_{cand} (extracted from Figure 5.18)

SNR [dB]	3	4	5	6
KSD-CS, N_{cand}=4096	1	1	1	1
KSD-CS, N_{cand}=256	N/A	0.1567	0.1671	0.1879
KSD-CS, N_{cand}=64	N/A	0.0239	0.0266	0.0319
KSD-CS, N_{cand}=32	N/A	0.0143	0.0163	0.0204
KSD-CS, N_{cand}=1	N/ A	N/A	0.0098	0.0054
IrSD	0.6989	0.0057	0.00233	0.0011

compared the complexity of the IrSD to that of other detectors in the context of LDC-MUT aided DL-SDMA systems. In Table 6.7 we concluded that IrSD had the lowest complexity.

6.2 Future Work

6.2.1 Design for Realistic Channel Conditions

In this thesis we assumed spatially uncorrelated MIMO channels. In our future work we may consider more realistic channel conditions by modelling the spatial correlation [89] of MIMO channels. When the MIMO channels are spatially correlated, the potential issues to be considered are: 1) When the MSs are close to each other, their spatial correlation may induce a higher multi-user interferences because their channel impulse responses are similar. 2) The multiple receive antennas of each user may experience similar fading owing to the limited size of the MS, which may induce an increased multi-stream interference. The potential solutions for these scenarios are High-Speed Downlink Packet Access (HSDPA)-style adaptive modulation [90] or cooperative virtual antenna arrays.

Furthermore, we may develop our solutions further for MIMO channels experiencing frequency selective fading, since we designed the iterative DL-SDMA system for flat-fading MIMO channels in this thesis.

6.2.2 Generalization of the IrGD and IrSD

The IrGD and IrSD schemes proposed in Chapters 4 and 5 were based on an off-line design. We may further develop the IrGD and IrSD schemes to near-instantaneously adaptive on-line-optimized arrangements, which are capable of taking into account the time-variant channel conditions and other system parameters, such as different SNRs, different modulation schemes, a different interleaver lengths, etc.

6.2.3 Joint Channel Estimation and Detection

In this thesis, we did not include the investigation of channel estimation. In our future research we may study the design of suitable channel estimation techniques for the iterative DL-SDMA system. It has been shown in the literature that joint channel estimation and detection may increase the integrity of the resultant systems [91–95] under diverse channel conditions [96].

6.2.4 Noncoherent DL-SDMA Systems

In this thesis, we studied coherently detected DL-SDMA systems, which require accurate channel estimation. Achieving accurate channel estimation for fast-fading channels is challenging. On the other hand, differentially encoded modulation schemes [97] are capable of providing a low-complexity alternative solution at the cost of a 3 dB performance degradation.

6.2.5 Non-linear MUT

In Figure 2.4 of Section 2.1.3, we quantified the difference between the achievable capacity of DL-SDMA and the channel capacity. We may further approach the channel capacity with the aid of non-linear MUT schemes designed based on Dirty paper coding [36].

6.2.6 Cross-layer Design of DL-SDMA Systems

In [98], we embarked on a cross-layer design by amalgamating the iterative DL-SDMA system with Luby-transform coding [98], which may be further improved by using soft-decision aided Luby-transform coding [99].

Appendix A

The search of the weighting-coefficient vector α

Lemma A.1:

When the general solution α of a linear equation $\mathbf{C} = \alpha\mathbf{d}$ is given by

$$\alpha = \alpha_p + \mathbf{N}_C \cdot \beta, \tag{A.1}$$

where α_p is a particular solution of the equation, $\mathbf{N}_C$ is the nullspace of $\mathbf{C}$, and β is an arbitrary vector, the last $(N_\alpha - r_c)$ elements of α are directly constituted by β, provided that the following conditions are met:

1. $\mathbf{N}_C$ is obtained from the Row Reduced Echelon Form [100] of $\mathbf{C}$.
2. The rank of $\mathbf{C}$, denoted as r_c, is smaller than the length N_α of α.
3. α_p is chosen by letting the last $(N_\alpha - r_c)$ elements be zeros.

Note 1: Observe that Lemma A.1 shows that β directly constitutes α. According to the constraint of Equation 4.1, we have $\alpha_j \in [0, 1], \forall j$. Therefore we have $\beta_j \in [0, 1], \forall j$. This observation assists us in narrowing down the search for each element of the vector β, from $\mathbb{R}$ to $[0, 1]$. Given that a low number of detectors are used, the length of β is low and hence the full search becomes computational feasible, when we set the search-step-size a to a moderate value when searching for values of $\beta_j \in [0, 1], \forall j$. For example, in our system, we have $N_{det} = 3$, hence we found that $a = 0.1$ is sufficiently low for obtaining an adequate value α for creating an attractive design. In the example of $N_{det} = 4$, the length of β becomes $N_{det} - r_c = 4 - 2 = 2$. Hence we require only 10×10-time search-steps to

step through all the candidates $\alpha \in \mathcal{C}$. This weighting factor search procedure may be termed as an offline design and hence it will not contribute to the complexity of the system.

Proof of Lemma A.1: Let $\mathbf{R}$ be the Row Reduced Echelon Form of $\mathbf{C}$, which is given by

$$\mathbf{R} = [\mathbf{I}|\mathbf{G}], \tag{A.2}$$

where $\mathbf{I}$ is a $(r_c \times r_c)$-element identity matrix, and $\mathbf{G}$ is a $(r_c \times (N_\alpha - r_c))$-element matrix. The nullspace of $\mathbf{C}$, $\mathbf{N}_C$, is then constructed as

$$\mathbf{N}_C = \begin{bmatrix} \mathbf{G} \\ \mathbf{I} \end{bmatrix}. \tag{A.3}$$

Therefore, we have

$$\alpha = \alpha_p + \mathbf{N}_C\beta = \alpha_p + \begin{bmatrix} \mathbf{G} \\ \mathbf{I} \end{bmatrix} \beta = \begin{bmatrix} \alpha_p(1, r_c) + G\beta \\ \beta \end{bmatrix}, \tag{A.4}$$

where $\alpha_p(1, r_c)$ represents a subvector of α_p containing are the elements $[1, \cdots, r_c]$. Based on Equation A.4, it becomes explicit that the last $(N_\alpha - r_c)$ elements of α are constituted by β.

Appendix B

The LDC matrix employed

- The LDC matrix χ employed for the DL-SDMA system using the system parameters $[M, N, L, Q, T] = [6, 2, 2, 4, 2]$ as seen in Figure 5.6.

$$\chi = \begin{bmatrix} -0.365504 - 0.076468i & 0.236904 + 0.381938i & -0.240679 - 0.261350i & 0.118783 - 0.134981i \\ 0.243718 - 0.230448i & -0.187326 + 0.108061i & -0.340004 + 0.163364i & -0.169758 - 0.411848i \\ 0.162237 - 0.378655i & 0.229401 - 0.187959i & -0.316700 - 0.028397i & 0.107380 + 0.360153i \\ 0.036713 - 0.277500i & 0.326753 - 0.237721i & 0.329306 - 0.148095i & -0.017642 - 0.357326i \end{bmatrix}. \tag{B.1}$$

- The LDC matrix χ employed for the DL-SDMA system using the system parameters $[M, N, L, Q, T] = [6, 2, 2, 5, 2]$ as seen in Figure 5.6.

$$\chi = \begin{bmatrix} -0.364657 + 0.437156i & 0.111442 - 0.163i & -0.100193 - 0.490698i & -0.120364 - 0.157433i & 0.338015 + 0.482267i \\ -0.359146 + 0.314798i & -0.526392 - 0.25344i & 0.338136 + 0.0768587i & -0.180814 + 0.481895i & -0.122457 - 0.17447i \\ -0.0697556 - 0.540973i & -0.169708 + 0.232321i & 0.181819 - 0.20386i & 0.0320995 + 0.337909i & 0.654063 + 0.0456086i \\ -0.364225 - 0.0927279i & -0.480867 + 0.232824i & -0.502131 + 0.420185i & 0.155626 - 0.158151i & 7.36269e - 05 + 0.308836i \end{bmatrix}. \tag{B.2}$$

- The LDC matrix χ employed for the DL-SDMA system using the system parameters $[M, N, L, Q, T] = [6, 2, 2, 6, 2]$ as seen in Figure 5.6.

$$\chi = \begin{bmatrix} -0.0440919 - 0.428357i & -0.078833 + 0.106539i & -0.320444 + 0.175787i & 0.488498 - 0.225926i & 0.236483 - 0.534793i & -0.0791616 + 0.159836i \\ 0.682253 + 0.0152345i & -0.240226 - 0.0163081i & -0.316124 - 0.0331736i & -0.400621 - 0.305126i & -0.105959 - 0.176117i & 0.280853 + 0.0238348i \\ -0.0842056 - 0.00696569i & 0.25341 + 0.0093214i & -0.574617 + 0.250999i & -0.100184 - 0.158024i & 0.0298448 + 0.543083i & -0.192414 + 0.409282i \\ -0.240327 - 0.0308184i & 0.15447 - 0.689107i & -0.425431 - 0.0555653i & -0.0072809 + 0.0465028i & -0.0622881 - 0.0967451i & 0.186853 - 0.456197i \end{bmatrix} \tag{B.3}$$

- The LDC matrix χ employed for the DL-SDMA system using the system parameters $[M, N, L, Q, T] =$

$[7,2,3,2,3]$ as seen in Figure 5.8 and 5.7.

$$\chi = \begin{bmatrix} -0.629903 - 0.622921i & -0.133503 + 0.3674i \\ 0.507698 - 0.97614i & -0.287397 - 0.0359928i \\ 0.0225052 - 0.439087i & 0.938598 + 0.0654208i \\ -0.6518 + 0.176313i & -0.803655 + 0.161508i \\ -0.143949 - 0.823714i & 0.417149 + 0.258973i \\ 0.752175 - 0.000294448i & 0.16617 - 0.00961248i \\ -0.438565 + 0.531933i & -0.0959144 + 0.440403i \\ 0.145084 - 0.258644i & -0.769565 + 0.623698i \\ 0.138341 + 0.0893382i & -1.1138 + 0.111333i \end{bmatrix}. \quad \text{(B.4)}$$

- The LDC matrix χ employed for the DL-SDMA system using the system parameters $[M, N, L, Q, T] = [7,2,3,2,2]$ as seen in Figure 5.8 and 5.7.

$$\chi = \begin{bmatrix} -0.408923 + 0.117148i & -0.706372 - 0.923294i \\ 0.0763814 + 0.269614i & -0.407563 + 0.383128i \\ 0.269889 - 0.135087i & -0.00374318 - 0.635666i \\ -1.0508 + 0.468835i & 0.291083 + 0.187959i \\ -0.674004 - 0.214244i & -0.648255 - 0.0452135i \\ 0.298715 - 0.857931i & -0.189487 + 0.594428i \end{bmatrix}. \quad \text{(B.5)}$$

- The LDC matrix χ employed for the LDC-MUT aided DL-SDMA system using the system parameters $[M, N, L, Q, T] = [6,2,2,2,3]$ as seen in Figure 5.5 and 5.7.

$$\chi = \begin{bmatrix} -0.482495 + 0.203925i & 0.00353892 - 0.962946i \\ -0.0123285 - 0.061417i & -0.422575 - 1.16584i \\ 0.0620071 + 0.823024i & -0.0435254 + 0.322053i \\ -1.27365 + 0.460496i & 0.176064 + 0.38129i \\ 0.10419 + 0.0664627i & 0.323222 + 0.171i \\ -0.431801 + 0.0671743i & 0.28895 - 0.189153i \end{bmatrix}. \quad \text{(B.6)}$$

- The LDC matrix χ employed for the LDC-MUT aided DL-SDMA system using the system parameters $[M, N, L, Q, T] = [6,2,2,2,2]$ as seen in Figure 5.5 and 5.7.

$$\chi = \begin{bmatrix} -0.270698 - 0.588709i & -0.705028 + 0.701468i \\ -0.318851 + 0.390749i & -0.774812 + 0.184033i \\ -0.993415 + 0.509296i & -0.192848 - 0.321879i \\ -0.276347 + 0.0562931i & 0.472979 + 0.110318i \end{bmatrix}. \quad \text{(B.7)}$$

- The LDC matrix χ employed for the LDC-MUT aided DL-SDMA system using the system parameters $[M, N, L, Q, T] = [5,2,1,2,3]$ as seen in Figure 5.9 and 5.7.

$$\chi = \begin{bmatrix} -0.7615 + 0.0357084i & 0.416281 - 0.7728i \\ 0.3301 - 0.0671739i & -0.233187 - 0.567409i \\ 0.449499 - 0.776734i & -0.143463 - 0.576697i \end{bmatrix}. \quad \text{(B.8)}$$

- The LDC matrix χ employed for the LDC-MUT aided DL-SDMA system using the system parameters $[M, N, L, Q, T] = [5, 2, 1, 2, 2]$ as seen in Figure 5.9 and 5.7.

$$\chi = \begin{bmatrix} -0.0520544 - 0.666864i & -0.592056 + 0.449502i \\ -0.224486 + 0.708652i & -0.645596 + 0.174994i \end{bmatrix}. \tag{B.9}$$

- The LDC matrix χ employed for the LDC-MUT aided DL-SDMA system using the system parameters $[M, N, L, Q, T] = [7, 2, 3, 6, 2]$ as seen in Table 5.5.

$$\chi = \begin{bmatrix} -0.043322 + 0.348318i & 0.304732 + 0.025573i & -0.023573 + 0.115284i & -0.169037 + 0.128196i & -0.159138 - 0.154316i & 0.062855 + 0.068358i \\ 0.058011 - 0.233308i & -0.116555 + 0.097088i & -0.138989 - 0.018661i & -0.166884 + 0.389783i & -0.025041 - 0.129054i & 0.187272 + 0.026913i \\ 0.031429 + 0.078267i & -0.087741 + 0.185898i & -0.020794 + 0.147883i & -0.153971 + 0.166647i & -0.023753 + 0.320414i & -0.324489 - 0.040747i \\ 0.001902 + 0.012817i & -0.026987 - 0.071990i & 0.232984 + 0.232990i & -0.111220 + 0.050639i & 0.278650 - 0.162422i & -0.001761 - 0.315792i \\ 0.108748 - 0.063507i & 0.109532 + 0.327422i & 0.296142 - 0.115826i & -0.078892 - 0.097321i & -0.107906 + 0.123211i & 0.211046 - 0.100478i \\ -0.180652 + 0.310737i & -0.220804 - 0.026124i & 0.078831 - 0.248241i & 0.037441 + 0.158224i & 0.131502 + 0.124658i & 0.164161 - 0.025454i \end{bmatrix}. \tag{B.10}$$

Glossary

AWGN	Additive White Gaussian Noise
BD	Block Diagonalization
CDMA	Code Division Multiple Access
CIRs	Channel Impulse Responses
CS	Centre-Shifting
CSD	Complex Sphere Decoding
CSD	Complex-valued Sphere Decoding
CSI	Channel State Information
DL	Downlink
DL-SDMA	DownLink of Space Division Multiple Access
DPC	Dirty Paper Coding
ECO-CQ	EXIT-Chart Optimized CSI Quantizer
EXIT	Extrinsic Information Transfer
GA	Genetic Algorithm
HSDPA	High-Speed Downlink Packet Access
ICI	Inter-Channel Interference

IDMA	Interleaver Division Multiple Access
IRCC	IrRegular Convolutional Codes
IrGD	Irregular Generic Detection
IrSD	Irregular Sphere Detection
KSD-CS	Center-Shifting aided K-best Sphere Detector
LTE	Long-Term-Evolution
MCMC	Markov Chain Monte Carlo
MIMO	Multiple Input and Multiple Output
ML	Maximum-Likelihood
MMSE	Minimum Mean Squared Error
MMSE-MUT	Minimum Mean Squared Error aided Multi-User Transmission
MSE	Mean Squared Error
MUD	Multi-User Detector
MUI	Multi-User Interference
MUT	Multi-User Transmission
NML	Near-Maximum-Likelihood
OFDM	Orthogonal Frequency Division Multiplexing
OHRSA	Optimized Hierarchy aided Reduced Search Algorithm
PDF	Probability Density Function
PI-DL-SDMA	Precoder aided Iterative DL-SDMA
PIC	Parallel Interference Cancellation
RSC	Recursive Systematic Convolutional
SD	Sphere Decoding
SDMA	Space Division Multiple Access
SIC	Successive Interference Cancellation

SISO	Soft-In Soft-Ouput
SNR	Signal to Noise Ratio
ST-CIRR	Spatio-Temporal Channel Impulse Response at the Receivers
ST-CIRT	Spatio-Temporal Channel Impulse Response available at the Transmitters
STP	Spatio-Temporal Pre-processing
SVD	Singular Value Decomposition
SVD-MUT	Singular Value Decomposition based Multi-User Transmission
UL	Uplink
V-BLAST	Vertical Bell Laboratories Layered Space-Time Architecture
ZF	Zero-Forcing
ZF-MUT	Zero Forcing aided Multi-User Transmission

Bibliography

[1] A. Paulraj, D. Gore, R. Nabar, and H. Bolcskei, "An overview of MIMO communications - a key to gigabit wireless," in *Proceedings of the IEEE*, vol. 92, pp. 198–218, February 2004.

[2] H. Ekstrom, A. Furuskar, J. Karlsson, M. Meyer, S. Parkvall, J. Torsner, and M. Wahlqvist, "Technical solutions for the 3G long-term evolution," *IEEE Communications Magazine*, vol. 44, pp. 38–45, March 2006.

[3] Y. Xiao, "IEEE 802.11n: enhancements for higher throughput in wireless LANs," *IEEE Wireless Communications*, vol. 12, pp. 82–91, December 2005.

[4] A. Goldsmith, S. Jafar, N. Jindal, and S. Vishwanath, "Fundamental capacity of MIMO channels," *IEEE Journal on Selected Areas in Communications*, vol. 21, pp. 684–702, June 2003.

[5] L. Hanzo and M. Münster and B-J. Choi and T. Keller, *OFDM and MC-CDMA for broadband multi-user communications, WLANs and Broadcasting*. John Wiley and IEEE press, 2003.

[6] C. Berrou, A. Glavieux, and P. Thitimajshima, "Near shannon limit error correcting coding and decoding: Turbo-codes ," in *Proceedings of IEEE International Conference on Communications*, pp. 1064–1070, May 1993.

[7] J. Blogh and L. Hanzo, *3G systems and intelligent networking*. John Wiley and IEEE Press, 2002. (For detailed contents, please refer to http://www-mobile.ecs.soton.ac.uk.).

[8] G. Stuber, J. Barry, S. McLaughlin, Y. Li, M. Ingram, and T. Pratt, "Broadband MIMO-OFDM wireless communications," *Proceedings of the IEEE*, vol. 92, pp. 271 – 294, 2004.

[9] V. Tarokh, H. Jafarkhani, and A. Calderbank, "Space-time block codes from orthogonal designs," *IEEE Transactions on Information Theory*, vol. 45, pp. 1456–1467, May 1999.

[10] V. Tarokh, N. Seshadri, and A. Calderbank, "Space-time codes for high data rate wireless communication:performance criterion and code construction," *IEEE Transactions on Information Theory*, vol. 44, pp. 744–765, March 1998.

[11] A. van Zelst, R. van Nee, and G. Awater, "Space division multiplexing (SDM) for OFDM systems," in *Proceedings of IEEE Vehicular Technology Conference, VTC 2000-Spring*, vol. 2, pp. 1070–1074, 2000.

[12] P. Wolniansky, G. Foschini, G. Golden, and R. Valenzuela, "V-BLAST: an architecture for realizing very high data rates overthe rich-scattering wireless channel," in *Proceedings of the International Symposium on Signals, Systems, and Electronics*, pp. 295–300, 1998.

[13] P. Vandenameele, L. van der Perre, and M. Engels, *Space division multiple access for wireless local area networks*. Kluwer, 2001.

[14] A. van Zelst, "Physical Interpretation of MIMO Transmissions," in *Proceedings Symposium IEEE Benelux Chapter on Communications and Vehicular Technology*, 2003.

[15] M. Damen, H. Gamal, and G.Caier, "On maximum-likelihood detection and the search for closest lattice point," *IEEE Transactions on Information Theory*, vol. 49, pp. 2389–2402, October 2003.

[16] B. Hochwald and S. ten Brink, "Achieving near-capacity on a multiple-antenna channel," *IEEE Transactions on Communications*, vol. 51, pp. 389–399, March 2003.

[17] D. Pham, K. Pattipati, P. Willet, and J. Luo, "An improved complex sphere decoder for V-BLAST systems," *IEEE Signal Processing Letters*, vol. 11, pp. 748–751, 2004.

[18] J. Akhtman, A. Wolfgang, S. Chen, and L. Hanzo, "An optimized-hierarchy-aided approximate log-MAP detector for MIMO systems," *IEEE Transactions on Wireless Communications*, vol. 6, pp. 1900–1909, May 2007.

[19] M. Jiang, J. Akhtman, and L. Hanzo, "Soft-information assisted near-optimum nonlinear detection for BLAST-type space division multiplexing OFDM systems," *IEEE Transactions on Wireless Communications*, vol. 6, pp. 1230–1234, April 2007.

[20] L. Hanzo and T. Keller, *OFDM and MC-CDMA: a primer*. John Wiley and IEEE press, 2006.

[21] H. Zhu, B. Farhang-Boroujeny, and R.-R. Chen, "On performance of sphere decoding and markov chain monte carlo detection methods," *IEEE Signal Processing Letters*, vol. 12, pp. 669–672, October 2005.

[22] L. Hanzo, T. Liew, and B. Yeap, *Turbo coding, turbo equalisation and space-time coding*. John Wiley and IEEE Press, 2002.

[23] J. Akhtman and L. Hanzo, "Advanced channel estimation for MIMO-OFDM in realistic channel conditions," in *Proceedings of the IEEE International Conference on Communications*, pp. 2528–2533, June 2007.

[24] C. Berrou, J. Hagenauer, M. Luise, C. Schlegel, and L. Vandendorpe, "Special issue on Turbo-Information processing: algorithms, implementations & applications," *Proceedings of the IEEE*, vol. 95, pp. 1146–1149, June 2007.

[25] X. Wang and H. Poor, "Iterative (turbo) soft interference cancellation and decoding for coded CDMA," *IEEE Transactions on Communications*, vol. 47, pp. 1046–1061, July 1999.

[26] A. van Zelst, R. van Nee, and G. Awater, "Turbo-BLAST and its performance," in *Proceedings of the IEEE Vehicular Technology Conference, VTC 2001-Spring*, vol. 2, pp. 1282–1286, 2001.

[27] H. Vikalo, B. Hassibi, and T. Kailath, "Iterative decoding for MIMO channels via modified sphere decoding," *IEEE Transactions on Wireless Communications*, vol. 3, pp. 2299–2311, November 2004.

[28] A. Wolfgang, J. Akhtman, S. Chen, and L. Hanzo, "Iterative MIMO detection for rank-deficient systems," *IEEE Signal Processing Letters*, vol. 13, pp. 699–702, November 2006.

[29] K.-K. Wong and A. Paulraj, "On the decoding order of MIMO maximum-likelihood sphere decoder: linear and non-linear receivers," in *IEEE Vehicular Technology Conference, VTC 2004-Spring.*, vol. 2, pp. 698–702, May 2004.

[30] K.-K. Wong, A. Paulraj, and R. D. Murch, "Efficient high-performance decoding for overloaded MIMO antenna systems," *IEEE Transactions on Wireless Communications*, vol. 6, pp. 1833–1843, May 2007.

[31] T. Cui and C. Tellambura, "Approximate ML detection for MIMO systems using multistage sphere decoding," in *Conference Record of the Thirty-Eighth Asilomar Conference on Signals, Systems and Computers*, vol. 1, pp. 1054–1056, Nov. 2004.

[32] T. Cui and C. Tellambura, "Approximate ML detection for MIMO systems using multistage sphere decoding," *IEEE Signal Processing Letters*, vol. 12, pp. 222–225, Mar. 2005.

[33] M. Tuchler, A. C. Singer, and R. Koetter, "Minimum mean squared error equalization using a priori information," *IEEE Transactions on Signal Processing*, vol. 50, pp. 673–683, March 2002.

[34] Q. Spencer, A. Swindlehurst, and M. Haardt, "Zero-forcing methods for downlink spatial multiplexing in multiuser MIMO channels," *IEEE Transactions on Signal Processing*, vol. 52, pp. 461–471, February 2004.

[35] L.-U. Choi and R. Murch, "A transmit preprocessing technique for multiuser MIMO systems using a decomposition approach," *IEEE Transactions on Wireless Communications*, vol. 3, no. 1, pp. 20 – 24, 2004.

[36] M. Costa, "Writing on dirty paper," *IEEE Transactions on Information Theory*, vol. 29, pp. 439–441, May 1983.

[37] Q. Spencer, C. Peel, A. Swindlehurst, and M. Haardt, "An introduction to the multi-user MIMO downlink," *IEEE Communications Magazine*, vol. 42, pp. 60–67, October 2004.

[38] C. Peel, B. Hochwald, and A. Swindlehurst, "A vector-perturbation technique for near-capacity multiantenna multiuser communication-part I: channel inversion and regularization," *IEEE Transactions on Communications*, vol. 53, pp. 195–202, January 2005.

[39] B. Hochwald, C. Peel, and A. Swindlehurst, "A vector-perturbation technique for near-capacity multiantenna multiuser communication-part II: perturbation," *IEEE Transactions on Communications*, vol. 53, pp. 537–544, March 2005.

[40] K.-K. Wong, R. Murch, and K. B. Letaief, "A joint-channel diagonalization for multiuser MIMO antenna systems," *IEEE Transactions on Wireless Communications*, vol. 2, pp. 773–786, July 2003.

[41] A. Tenenbaum and R. Adve, "Joint multiuser transmit-receive optimization using linear processing," in *IEEE International Conference on Communications*, vol. 1, pp. 588–592, June 2004.

[42] J. Akhtman, C.-Y. Wei, and L. Hanzo, "Reduced-complexity maximum-likelihood detection in downlink SDMA systems," in *Proceedings of the IEEE Vehicular Technology Conference, VTC 2006-Fall*, pp. 1834 – 1838, 2006.

[43] C.-Y. Wei, J. Akhtman, S. X. Ng, and L. Hanzo, "Iterative near-maximum-likelihood detection in rank-deficient downlink SDMA systems," *IEEE Transactions on Vehicular Technology*, vol. 57, pp. 653 – 657, January 2008.

[44] C.-Y. Wei, J. Wang, and L. Hanzo, "EXIT chart aided irregular convolutional code design for iterative downlink SDMA systems using imperfect channel state information," in *Proceedings of the IEEE Workshop on Signal Processing Systems*, pp. 105–110, October 2007.

[45] C.-Y. Wei and L. Hanzo, "Irregular generic detection aided iterative downlink SDMA systems," in *Proceedings of the IEEE Vehicular Technology Conference, VTC 2008-Spring*, 2008 (accepted).

[46] C.-Y. Wei, D. Yang, L. Yang, and L. Hanzo, "Iterative detection aided downlink SDMA systems using quantized channel impulse response," in *Proceedings of the IEEE Vehicular Technology Conference, VTC 2008-Fall*, submitted in February 2008.

[47] R. J. Heath and A. Paulraj, "Linear dispersion codes for MIMO systems based on frame theory," *IEEE Transactions on Signal Processing*, vol. 50, pp. 2429–2441, October 2002.

[48] C.-Y. Wei, L. Wang, and L. Hanzo, "Irregular sphere detection in full-diversity and high-rate downlink SDMA systems," *IEEE Transactions on Vehicular Technology*, submitted in March 2008.

[49] C.-Y. Wei, L. Wang, and L. Hanzo, "Irregular sphere detection aided downlink SDMA systems using linear dispersion codes," in *Proceedings of the IEEE Global Telecommunications Conference*, submitted in March 2008.

[50] J. Winters, "Smart antennas for wireless systems," *IEEE Personal Communications*, vol. 5, pp. 23–27, February 1998.

[51] R. Narasimhan, "Spatial multiplexing with transmit antenna and constellation selection for correlated MIMO fading channels," *IEEE Transactions on Signal Processing*, vol. 51, pp. 2829–2838, November 2003.

[52] K. Li, X. Wang, and L. Ping, "Analysis and optimization of interleave-division multiple-access communication systems," *IEEE Transactions on Wireless Communications*, vol. 6, pp. 1973–1983, May 2007.

[53] Z. Luo, H. Gao, Y. Liu, and J. Gao, "Robust pilot-symbol-aided mimo channel estimation and prediction," *Proceedings of the IEEE Global Telecommunications Conferenc*, vol. 6, pp. 3646–3650, 2004.

[54] A. Duel-Hallen, S. Hu, and H. Hallen, "Long-range prediction of fading signals," *IEEE Signal Processing Magazine*, vol. 17, pp. 62–75, 2000.

[55] S. X. Ng and L. Hanzo, "On the MIMO channel capacity of multidimensional signal sets," *IEEE Transactions on Vehicular Technology*, vol. 55, pp. 528– 536, 2006.

[56] D. Tse, P. Viswanath, and L. Zheng, "Diversity-multiplexing tradeoff in multiple-access channels," *IEEE Transactions on Information Theory*, vol. 50, pp. 1859– 1874, 2004.

[57] R. Irmer, *Multiuser Transmission in Code Division Multiple Access Mobile Communications Systems*. PhD thesis, Technische Universitat Dresden, 2005.

[58] R. L.-U. Choi and R. Murch, "New transmit schemes and simplified receivers for MIMO wireless communication systems," *IEEE Transactions on Wireless Communications*, vol. 2, no. 6, pp. 1217 – 1230, 2003.

[59] J. Zhang, Y. Wu, S. Zhou, and J. Wang, "Joint linear transmitter and receiver design for the downlink of multiuser MIMO systems," *IEEE Communications Letters*, vol. 9, pp. 991–993, November 2005.

[60] T. Moon and W. Stirling, *Mathematical Methods and Algorithms for Signal Processing*. Prentice Hall, 2000.

[61] J. E. Gentle, *Numerical linear algebra for applications in statistics*. Springer-Verlag, 1998.

[62] J. Ha, A. Mody, J. Sung, J. Barry, S. McLaughlin, and G. Stuber, "LDPC coded OFDM with Alamouti/SVD diversity technique," *Wireless Personal Communications*, vol. 23, pp. 183–194, 2002.

[63] C. E. Shannon, *Mathematical Theory of Communication*. University of Illinois Press, 1963.

[64] J. Proakis, *Digital communications*. McGraw-Hill, 1995.

[65] Z. Shen, R. Chen, J. G. Andrews, R. W. Heath, and B. L. Evans, "Sum capacity of multiuser MIMO broadcast channels with block diagonalization," in *Proceedings of the IEEE International Symposium on Information Theory*, pp. 886–890, July 2006.

[66] B. Suard, G. Xu, H. Liu, and T. Kailath, "Uplink channel capacity of space-division-multiple-access schemes," *IEEE Transactions on Information Theory*, vol. 44, pp. 1468–1476, July 1998.

[67] K. Dawui and D. Slock, "Multiuser-MIMO downlink TX-RX design based on SVD channel diagonalization and multiuser diversity," in *Conference Record of the Thirty-Ninth Asilomar Conference on Signals, Systems and Computers*, pp. 1493–1497, October 2005.

[68] S. ten Brink, "Designing iterative decoding schemes with the extrinsic information transfer chart," *AEÜ International Journal of Electronics Communications*, vol. 55, pp. 389 – 398, 2000.

[69] M. Tüchler and J. Hagenauer, "EXIT charts of irregular codes," in *Proceedings of Conference Information Sciences and Systems*, March 2002.

[70] D. Divsalar, S. Dolinar, and F. Pollara, "Serial turbo trellis coded modulation with rate-1 inner code," in *IEEE Global Telecommunications Conference*, vol. 2, pp. 777 – 782, 2000.

[71] I. Land, P. Hoeher, and S. Gligorevic, "Computation of symbol-wise mutual information in transmission systems with logAPP decoders and application to EXIT charts," in *Proceedings of the International Conference on Source and Channel Coding*, pp. 195 – 202, 2004.

[72] M. Tüchler, "Design of serially concatenated systems depending on the block length," *IEEE Transactions on Communications*, vol. 52, pp. 209– 218, 2004.

[73] L. Hanzo, L.-L. Yang, E.-L. Kuan, and K. Yen, *Single- and Multi-Carrier DS-CDMA*. John Wiley and IEEE Press, 2003.

[74] T. Richardson, M. Shokrollahi, and R. Urbanke, "Design of capacity-approaching irregular low-density parity-check codes," *IEEE Transactions on Information Theory*, vol. 47, pp. 619–637, 2001.

[75] B. J. Frey and D. J. C. MacKay, "Irregular turbo-like codes," in *Proceedings of International Symposium on Turbo Codes and Related Topics*, pp. 67–72, 2000.

[76] H. Jin, A. Khandekar, and R. McEliece, "Irregular repeat-accumulate codes," in *Proceedings 2nd International Symposium on Turbo codes and Related Topics*, pp. 1–8, 2000.

[77] I. Land, P. A. Hoeher, and J. Huber, "Analytical derivation of EXIT charts for simple block codes and for LDPC codes using information combining," in *Proceedings of European Signal Processing Conference*, pp. 1561–1564, 2004.

[78] S. Zhou and G. B. Giannakis, "How accurate channel prediction needs to be for transmit-beamforming with adaptive modulation over Rayleigh MIMO channels?," *IEEE Transactions on Wireless Communications*, vol. 3, pp. 1285–1294, July 2004.

[79] A. Gersho and R. M. Gray, *Vector Quantization and Signal Compression.* Kluwer Academic Publishers, 1991.

[80] L. Hanzo, F. Somerville, and J. Woodard, *Voice and Audio Compression for Wireless Communications.* IEEE Press and John Wiley, 2007.

[81] B. Hassibi and B. Hochwald, "High-rate codes that are linear in space and time," *IEEE Transactions on Information Theory*, vol. 48, pp. 1804–1824, July 2002.

[82] X. Wang, V. Krishnamurthy, and J. Wang, "Stochastic gradient algorithms for design of minimum error-rate linear dispersion codes in MIMO wireless systems," *IEEE Transactions on Signal Processing*, vol. 54, pp. 1242–1255, April 2006.

[83] F. Oggier, G. Rekaya, J. C. Belfiore, and E. Viterbo, "Perfect space - time block codes," *IEEE Transactions on Information Theory*, vol. 52, pp. 3885–3902, Sept. 2006.

[84] S. Yang, J.-C. Belfiore, G. Rekaya, and B. Othman, "Perfect space-time block codes for parallel MIMO channels," in *Information Theory, 2006 IEEE International Symposium on*, pp. 1949–1953, July 2006.

[85] G. Golub and C. van Loan, *Matrix Computations.* North Oxford Academic, 1983.

[86] K.-W. Wong, C.-Y. Tsui, R. Cheng, and W.-H. Mow, "A VLSI architecture of a K-best lattice decoding algorithm for MIMO channels," in *IEEE International Symposium on Circuits and Systems*, vol. 3, pp. 273–276, 2002.

[87] S. Hara and R. Prasad, "Overview of multicarrier CDMA," *IEEE Communications Magazine*, vol. 35, pp. 126–133, December 1997.

[88] S. Haykin, *Adaptive Filter Theory.* Prentice-Hall, 1996.

[89] N. M. Khan, M. T. Simsim, and P. B. Rapajic, "A generalized model for the spatial characteristics of the cellular mobile channel," *IEEE Transactions on Vehicular Technology*, vol. 57, pp. 22–37, January 2008.

[90] L. Hanzo, J. Blogh, and S. Ni, *3G, HSPDA and FDD Versus TDD Networking: Smart Antennas and Adaptive Modulation.* IEEE Press and John Wiley, 2008.

[91] M. Jiang, J. Akhtman, and L. Hanzo, "Iterative joint channel estimation and multi-user detection for multiple-antenna aided OFDM systems," *IEEE Transactions on Wireless Communications*, vol. 6, pp. 2904–2914, August 2007.

[92] J. Akhtman and L. Hanzo, "Decision directed channel estimation aided OFDM employing sample-spaced and fractionally-spaced CIR estimators," *IEEE Transactions on Wireless Communications*, vol. 6, pp. 1171–1175, April 2007.

[93] A. Wolfgang, S. Chen, and L. Hanzo, "Parallel interference cancellation based turbo space-time equalization in the SDMA uplink," *IEEE Transactions on Wireless Communications*, vol. 6, pp. 609–616, February 2007.

[94] J. Kim, G. L. Stuber, and Y. G. Li, "Iterative channel estimators in V-BLAST OFDM systems," *IEEE Transactions on Wireless Communications*, vol. 7, pp. 65–71, January 2008.

[95] S. Talakoub and B. Shahrrava, "Joint iterative multiuser detection and channel estimation for differentially coded asynchronous CDMA systems," *IEEE Transactions on Vehicular Technology*, vol. 57, pp. 380–392, January 2008.

[96] S. Ahmed, T. Ratnarajah, M. Sellathurai, and C. Cowan, "Reduced-complexity iterative equalization for severe time-dispersive MIMO channels," *IEEE Transactions on Vehicular Technology*, vol. 57, pp. 594–600, January 2008.

[97] M. El-Hajjar, B. Hu, L.-L. Yang, and L. Hanzo, "Coherent and differential downlink space-time steering aided generalised multicarrier DS-CDMA," *IEEE Transactions on Wireless Communications*, vol. 6, pp. 3857–3863, November 2007.

[98] M. Luby, "LT codes," in *Proceedings of the IEEE Symposium on Foundations of Computer Science*, pp. 271–282, November 2002.

[99] T. D. Nguyen, L. L. Yang, and L. Hanzo, "Systematic luby transform codes and their soft decoding," in *IEEE Workshop on Signal Processing Systems*, pp. 67–72, October 2007.

[100] L. Mirsky, *An Introduction to Linear Algebra.* Dover Publications, 1990.

Author Index

I

J

K

L

M

Z